# Quasiprobability methods in quantum interferometry of ultracold matter

Bogdan Opanchuk

Submitted in total fulfilment of the requirements
of the degree of Doctor of Philosophy.


Centre for Atom Optics and Ultrafast Spectroscopy
Swinburne University of Technology • Melbourne, Australia

January 2014

# Abstract

A method of simulating the full quantum field dynamics of multimode, multi-component Bose-Einstein condensates is developed. The truncated Wigner representation is used to obtain a probabilistic theory. The representation is extended to to use a functional calculus and can be applied to quantum fields in the arbitrary number of dimensions.

Detailed proofs of the corresponding theorems are given. This approach produces c-number stochastic equations which may be solved using conventional stochastic integration methods, with the limitation that it is only valid for large mode occupation numbers. The equations describe the spatial evolution of spinor components and properly account for nonlinear interactions and losses. The method is further used to model several experiments where quantum effects are significant, and cannot be calculated with simpler approximations. It is shown to describe leading quantum corrections accurately, including effects such as phase noise, quantum squeezing, entanglement, and interactions with engineered nonlinear reservoirs. In addition to this approach, other positive phase-space methods are also analysed for sampling highly nonclassical states.

In conclusion, the phase-space representations developed in this thesis provide a relatively fast and accurate method of simulating dynamics of large nonlinear quantum systems, such as trapped Bose-Einstein condensates. The required stochastic equations are easily and scalably integrated in parallel. Algorithms for efficient computation on modern graphical processing unit hardware are presented.

# Acknowledgements

I would like to thank both of my supervisors, Prof. Peter D. Drummond and Prof. Andrei I. Sidorov, for many helpful discussions.

My primary supervisor, Peter Drummond, provided a fundamental outlook on the methods that I developed and used, employing both mathematical arguments and physical considerations. He could always give a piece of practical advice on the application of numerical methods to various problems. Besides that, I appreciate him encouraging me to venture into the field of parallel computing, which turned out to be perfectly suited to solve the problems we were investigating.

My secondary supervisor, Andrei Sidorov, supplied expertise in the experimental side of my research, explaining where and how the theoretical models I used clash with reality.

I thank my fellow theorists: Rodney Polkinghorne, Dr Qiong-Yi He, Dr Laura Rosales-Zárate, who gave me advice on tricky problems I was facing, and with whom I enjoyed co-authoring papers. I also thank Dr Michael Egorov and Dr Valentine Ivannikov from the experimental part of our research group, who had a hands-on expertise on the atom interferometry experiments in Swinburne, and who supplied me with data necessary to test my models.

# Declaration

This is to certify that this thesis

- contains no material which has been accepted for the award to me of any other degree or diploma, except where due reference is made in the text,
- to the best of my knowledge contains no material previously published or written by another person except where due reference is made in the text, and
- where the work is based on joint research or publications, discloses the relative contributions of the respective workers or authors.

Bogdan Opanchuk _____

Date _____

# Publications of the author

1. M. Egorov, R. P. Anderson, V. Ivannikov, B. Opanchuk, P. D. Drummond, B. V. Hall, and A. I. Sidorov, *Long-lived periodic revivals of coherence in an interacting Bose-Einstein condensate*, Phys. Rev. A **84(2)**, 021605(R) (2011)

2. Q.-Y. He, M. D. Reid, B. Opanchuk, R. Polkinghorne, L. E. C. Rosales-Zárate, and P. D. Drummond, *Quantum dynamics in ultracold atomic physics*, Front. Phys. **7(1)**, 16–30 (2012)

3. B. Opanchuk, M. Egorov, S. E. Hoffmann, A. I. Sidorov, and P. D. Drummond, *Quantum noise in three-dimensional BEC interferometry*, Europhys. Lett. **97(5)**, 50003 (2012)

4. B. Opanchuk, Q.-Y. He, M. D. Reid, and P. D. Drummond, *Dynamical preparation of Einstein-Podolsky-Rosen entanglement in two-well Bose-Einstein condensates*, Phys. Rev. A **86(2)**, 023625 (2012)

5. B. Ramachandhran, B. Opanchuk, X.-J. Liu, H. Pu, P. D. Drummond, and H. Hu, *Half-quantum vortex state in a spin-orbit-coupled Bose-Einstein condensate*, Phys. Rev. A **85(2)**, 023606 (2012)

6. B. Opanchuk, and P. D. Drummond, *Functional Wigner representation of quantum dynamics of Bose-Einstein condensate*, J. Math. Phys. **54(4)**, 042107 (2013)

7. M. Egorov, B. Opanchuk, P. D. Drummond, B. V. Hall, P. Hannaford, and A. I. Sidorov, *Measurement of s-wave scattering lengths in a two-component Bose-Einstein condensate*, Phys. Rev. A **87**, 053614 (2013)

8. B. Opanchuk, R. Polkinghorne, O. Fialko, J. Brand, and P. D. Drummond, *Quantum simulations of the early universe*, Ann. Phys. **525(10–11)**, 866–876 (2013)

Published as preprints:

1. B. Opanchuk, L. Rosales-Zárate, M. D. Reid, and P. D. Drummond, *Probabilistic simulation of mesoscopic quantum paradoxes*, arXiv:1301.6305 (2013)

2. P. D. Drummond, B. Opanchuk, L. Rosales-Zárate, and M. D. Reid, *Simulating Bell violations without quantum computers*, arXiv:1310.0668 (2013)

# Contents

# List of Figures

# Chapter 1.

# Introduction

The problem of calculating the dynamics of quantum systems has been around since the dawn of quantum mechanics itself. In most cases, the exact simulation of such systems is intractable or at least extremely slow due to the exponential growth of the system's Hilbert space with particle number. The continuing increase of the available computational power has made it possible to solve the time-dependent many-boson Schrödinger equation almost exactly for one-dimensional systems with as many as 100 particles [1].

Meanwhile, mesoscopic quantum systems gain in popularity. The most prominent of such systems, a Bose-Einstein condensate (BEC), has been first observed by Cornell, Wieman *et al* [2], and Ketterle *et al* [3] 70 years after its theoretical description by Bose [4] and Einstein [5, 6]. A BEC can be easily observed with macroscopic detectors and is, in fact, almost large enough to be seen with a naked eye. Its properties can be varied in a wide range (even during an experiment) with an application of external electromagnetic fields. On the other hand, it is able to exhibit inherent non-classical properties such as entanglement, formation of quantised vortices or destructive interference. This unique combination makes BECs a convenient model for various physical phenomena.

BECs are marcoscopic quantum systems exhibiting inherent quantum mechanical properties, which makes them extremely sensitive to properties of surrounding environment. Because of this, BECs are used as detectors for precise measurements of time or gravity. The precision of these measurements is limited by signal-to-noise ratio and can be significantly improved by manipulating the quantum state of a BEC, in particular by reducing the uncertainty of a measurable parameter ("spin squeezing"). But planning such changes and

explaining the results of corresponding experiments requires an accurate model of BEC dynamics. Such model must properly account for the effect of strong nonlinear elastic and inelastic interactions on the quantum state, all of which can affect the evolution of a condensate significantly.

However, developing a quantitative model of a BEC proved out to be difficult. At the time of the writing, mesoscopic systems in two or three dimensions remain unreachable for exact simulation approaches. In theory, quantum computers can solve this problem, and Feynman speculated as early as 1982 [7] that they are the most perspective way to simulate quantum systems efficiently. Unfortunately, even today quantum computers of any useable size are not readily available, and estimates about the speed of their development seem rather slow. At the moment of writing, the largest universal quantum computer operates with 6 qubits [8]. If one restricts himself to a particular algorithm, somewhat larger numbers are available (8 qubits for quantum factorisation, for instance [9]). Among the problems current quantum computers are facing today are decoherence, circuit errors, and speed. A more subtle problem is that an exponentially growing number of measurements (and, consequently, experiments) are needed to perform in order to get the complete result of a computation. Therefore, even despite a number of recent developments in the field, it will require a major breakthrough for quantum computers to overcome classical ones in the near future.

That is why, in order to handle existing quantum dynamics problems, approximations of varying accuracy have been developed in parallel with the quantum computing research. This thesis is dedicated to one of such approaches — quasiprobabilities.

## 1.1. Rationale

The essence of the quasiprobability methods is representing the system's density matrix in the form of a probability distribution, or at least a probability distribution-like function. This function can then be propagated in time (directly or by means of a Monte-Carlo approach) and used to obtain required observables. The first quasiprobability representations, the Wigner function [10–12] and the Husimi Q-function [13], were introduced as early as the first half of the 20th century. They were followed by the Glauber-Sudarshan P-representation [14–16] and its improved version by Drummond, Gardiner and Walls,

the positive-P representation [17, 18]. These representations circumvent Feynman's claim (based on the Bell's theorem [19]) about the impossibility of simulating quantum systems probabilistically [7]. They use a complex phase space, have a domain larger than the values of observables predicted by quantum mechanics, and only give correct values of those observables on average [20, 21].

This thesis has arisen from the task of simulating non-classical effects in BEC experiments and is focused primarily on this area. Since different representations may perform better or worse depending on the system in question, we picked one that was best suited for our problem.

The Q-function is usually difficult to propagate in time, although it can be extremely efficient for the sampling of static states (it will make a brief appearance in Chapter 9). The positive-P representation is exact, but is often characterised by sampling errors that grow in time. This can be in some cases handled by exploiting its non-uniqueness and tailoring the exact form of the function for the task, resulting in the gauge-P representation [22]. Alternatively, one may project the distribution on the required part of Hilbert space, thus preventing it from venturing into "useless" states, which will cancel out during measurement, yet still affect the total error.

The Wigner distribution is, in general, not positive, which presents problems when simulating systems with a small number of particles. Fortunately, assuming that the number of particles is large enough (as in our case), one can make certain approximations (see Section 5.4 for details), under which the Wigner function can be truncated, making it strictly positive. This turns it into a probability distribution, thus providing a way to reduce the initial master equation to a set of stochastic differential equations (SDEs), for which an extensive set of numerical integration methods exists. Of course, it is not the only method for this type of the system. A very useful group of two-mode variational methods has been used by different research groups [23–25], but these have some difficulties handling nonlinear losses in BECs, and the approximation starts to break down in the presence of many populated modes. The Wigner method allows us to treat a large number of independent field modes, thus taking into account degrees of freedom that are excited due to collisional and nonlinear losses [26, 27].

This combination of features made the truncated Wigner representation the best choice for the task of simulating the dynamics of bosonic quantum fields, including optical

fields [28–31] and BECs. For BEC systems, the representation has been successfully used to describe fragmentation [32–34], dissipative atom transport [35], dynamically unstable lattice dynamics [36], dark solitons [37, 38], turbulence [26, 39], quantum noise and decoherence [40–42], squeezing [43] and entanglement [44]. The truncated Wigner method is especially effective in low-dimensional and trap environments, where it was successfully used to predict quantum squeezing and phase-diffusion effects, in good agreement with dynamical experiments in photonic quantum soliton propagation [31, 45].

The comparison of the results of the truncated Wigner method with analytical predictions has generally shown an excellent agreement [27, 30]. Other quasiprobability representations, such as the positive-P are known to work better near the threshold of applicability of the truncation condition [27, 46]. There are studies that compare the truncated Wigner method with the exact positive-P method [28, 47, 48]. We perform a simple comparison of the multimode Wigner representation with an exact expansion in number states in Chapter 6. The typical outcome of such comparisons is that the truncated Wigner method gives correct results out to a characteristic break time. After this, the accumulated errors are high enough to give large discrepancies in calculated correlations. The method thus performs badly in modeling nonlinear quantum tunneling [49, 50], which depends on both long time dynamics and quantum correlations. The overall picture of how this method is related to other techniques for quantum dynamics has been recently reviewed [51].

Although the Wigner representation was initially formulated for a single-mode system, the definition and associated methods were later extended to operate on field operators and wave functions, which facilitates the phase-space treatment of multimode problems. The first such description was produced by Graham [52, 53], followed by its usage in various other works [33, 37, 39–41, 54, 55] without a formal introduction of corresponding definitions and accompanying theorems. A more detailed description was given by Polkovnikov [56] in his review paper of phase-space methods.

Direct numerical integration of the partial differential equation resulting from the application of the Wigner transformation is, in general, very cumbersome. One has to truncate third-order derivative terms [28, 40, 57] and apply projection to remove modes with low population. This adds to the complexity of the formal description of the method. Moreover, nonlinear inelastic interactions, which were not approached

methodically before, are important in BEC experiments. Accordingly, much of the mathematical derivation of these techniques is not readily available. This thesis intends to provide a rigorous formal description of the functional truncated Wigner method for simulating the dynamics of multimode BECs, along with examples of its application to existing experiments. The core of the theory described in this thesis has been published separately [58].

## 1.2. Thesis structure

This thesis is laid out in the mathematical tradition, with the formalism preceding its application. Supplementary information, methods, and parts of the formalism that are not directly connected to quantum mechanics can be found in the Appendices.

The first three chapters contain the foundation for the functional Wigner transformation. Chapter 2 introduces the Wigner transformation. In this chapter we also extend it to work with sets of single-mode operators. This chapter contains proofs of known properties of the transformation and presents the single-mode transformation in a way facilitating further extension into the functional domain. Chapter 3 introduces the functional calculus, restricted basis formalism and their application to bosonic field operators. We then define the functional Wigner transformation and prove several central theorems that govern the transformation of field operators and the measurement of their moments. Finally, Chapter 4 uses these theorems to derive general identities which can be used to transform different terms of the initial master equation describing a BEC. This chapter focuses especially on the terms related to nonlinear damping. This is a dominant relaxation mechanism in BEC systems, and it is often ignored or incorrectly approximated using linear loss terms.

Chapter 5 applies the formalism from the previous chapters to reduce a master equation for bosonic field operators describing a BEC to a system of SDEs, which have significantly lower computational complexity. We discuss the truncation approximation, which is essentially a $1/\sqrt{N}$ expansion, and the question of sampling initial states for the simulation. We also give an example of usage of the formalism for a single-component multimode BEC.

The next three chapters describe several applications of the truncated Wigner formalism.

In Chapter 6, we use a simple single-well two-mode system to compare the predictions for the degree of spin squeezing obtained from the multimode truncated Wigner method and an exact quantum mechanical solution. We also investigate the behavior of sampling and systematic errors of the truncated Wigner method for varying mode populations and numbers of trajectories. Chapter 7 is dedicated to the theoretical description of the quantum interferometry experiments performed in Swinburne University. It shows how the truncated Wigner method can predict the visibility dynamics (including its decay) in the experiment, along with the growth of phase noise. Chapter 8 illustrates how the truncated Wigner method can be used to calculate the degree of spin squeezing in interferometry experiments with complex dynamics.

Chapter 9 treats a topic of future significance. It investigates some basic properties of positive quasiprobability representations, namely their ability to simulate the violation of Bell inequalities. In contrast to the previous chapters, it mostly makes use of the probabilistic positive-P and the SU(2)-Q representations. These are used to sample cooperative photon states and the "Schrödinger cat" state, and demonstrate the violation of the corresponding inequalities. We also investigate the growth of the sampling error in these simulations.

Finally, Chapter 10 summarizes the thesis and discusses some possible directions of development in the field of quasiprobability representations.

The thesis includes several Appendices, which deal with auxiliary topics. Appendix A briefly describes the relaxed complex (Wirtinger) differentiation and associated integration, which are commonly used in the field of quasiprobabilities. Appendix B applies these differentiation rules to define the similar formalism for functionals. Appendix C contains several theorems, which describe the equivalence correspondence between a Fokker-Planck equation (FPE) and a set of SDEs, expressed using complex variables and functional operators. Appendix E outlines numerical methods used for the simulations described in the thesis. We also provide links to the programs and libraries used to perform these simulations, including those developed by us.

# Chapter 2.

# Multimode Wigner transformation

The single-mode Wigner representation was introduced as early as 1932 [10] and later extended by Dirac [11] and Moyal [12]. It has been described in textbooks multiple times and widely used by researchers. A detailed description of the single-mode Wigner function, analogous to the one provided in this thesis, was given by Moyal [12] or, using a notation close to the one in this thesis, by later authors [59–61]. Nevertheless, before diving into the functional Wigner formalism, it is still advantageous to go through a derivation of the single-mode and multimode Wigner transformations. Firsty, this chapter will help to familiarise the reader with the notation used in the functional case of the tranformation. Secondly, the proof structure used here will repeat itself in Chapter 3, and it is grasped easier when applied to a simpler mathematical object.

This chapter will use the Wirtinger calculus for differentials of complex-valued functions. Details of this calculus are described in Appendix A.

## 2.1. Single-mode transformation

In this section we will work with a single-mode bosonic system with the standard creation and annihilation operators

$$\begin{aligned} [\hat{a}, \hat{a}] = [\hat{a}^\dagger, \hat{a}^\dagger] = 0, \\ [\hat{a}, \hat{a}^\dagger] = 1. \end{aligned} \tag{2.1}$$

An essential part of the Wigner function definition is the displacement operator. This was first introduced by Weyl [62] and thoroughly described by Cahill and Glauber [59]:

**Definition 2.1.** *The displacement operator is the operator-valued function of a complex variable*

$$\hat{D}(\lambda) = \exp(\lambda\hat{a}^\dagger - \lambda^*\hat{a}).$$

We will need the differentials of this operator with respect to $\lambda$ and $\lambda^*$. In order to calculate these, we separate commuting terms in the exponent using the Baker-Hausdorff theorem for operators $\hat{A} \equiv \lambda\hat{a}^\dagger$ and $\hat{B} \equiv -\lambda^*\hat{a}$. In our case $[\hat{A}, [\hat{A}, \hat{B}]] = [\hat{B}, [\hat{A}, \hat{B}]] = 0$, so the theorem gives

$$\exp(\lambda\hat{a}^\dagger - \lambda^*\hat{a}) = \exp(-|\lambda|^2/2)\exp(\lambda\hat{a}^\dagger)\exp(-\lambda^*\hat{a}). \tag{2.2}$$

This can be easily differentiated (minding the ordering of factors with $\hat{a}^\dagger$ and $\hat{a}$) as

$$\frac{\partial}{\partial\lambda}\hat{D}(\lambda) = (\hat{a}^\dagger - \frac{1}{2}\lambda^*)\hat{D}(\lambda). \tag{2.3}$$

Similarly, for $\partial/\partial\lambda^*$ and for two different orderings of operator factors we find that

$$\begin{aligned} \frac{\partial}{\partial\lambda}\hat{D}(\lambda) &= \hat{D}(\lambda)(\hat{a}^\dagger + \frac{1}{2}\lambda^*) = (\hat{a}^\dagger - \frac{1}{2}\lambda^*)\hat{D}(\lambda), \\ -\frac{\partial}{\partial\lambda^*}\hat{D}(\lambda) &= \hat{D}(\lambda)(\hat{a} + \frac{1}{2}\lambda) = (\hat{a} - \frac{1}{2}\lambda)\hat{D}(\lambda). \end{aligned} \tag{2.4}$$

Using the displacement operator we can define the Wigner transformation:

**Definition 2.2.** *The Wigner transformation converts an operator $\hat{A}$ on a Hilbert space to a complex-valued function $\mathcal{W}[\hat{A}](\alpha)$ on phase space:*

$$\mathcal{W}\left[\hat{A}\right] = \frac{1}{\pi^2}\int \mathrm{d}^2\lambda \exp(-\lambda\alpha^* + \lambda^*\alpha)\,\mathrm{Tr}\left\{\hat{A}\hat{D}(\lambda)\right\}.$$

*The backward transformation (called the Weyl transformation) restores the operator:*

$$\mathcal{W}^{-1}[f] = \frac{1}{\pi}\int \mathrm{d}^2\xi\hat{D}^\dagger(\xi)\int \mathrm{d}^2\eta \exp(-\eta\xi^* + \eta^*\xi)f(\eta).$$

It is easy to demonstrate that Wigner and Weyl transformations define a bijection $\mathbb{H} \leftrightarrow (\mathbb{C} \to \mathbb{C})$ for Hilbert-Schmidt operators and square-integrable functions. Let us assume $\hat{A} \equiv \mathcal{W}^{-1}[f]$. Then, using the fact that $\operatorname{Tr}\left\{\hat{D}^\dagger(\xi)\hat{D}(\lambda)\right\} = \pi\delta(\operatorname{Re}\xi - \operatorname{Re}\lambda)\delta(\operatorname{Im}\xi - \operatorname{Im}\lambda)$ [59]:

$$\begin{aligned}\mathcal{W}[\hat{A}] &= \frac{1}{\pi^3}\int \mathrm{d}^2\lambda \exp(-\lambda\alpha^* + \lambda^*\alpha) \\ &\quad \times \operatorname{Tr}\left\{\int \mathrm{d}^2\xi \hat{D}^\dagger(\xi)\int \mathrm{d}^2\eta \exp(-\eta\xi^* + \eta^*\xi) f(\eta)\hat{D}(\lambda)\right\} \\ &= \frac{1}{\pi^2}\int \mathrm{d}^2\lambda \int \mathrm{d}^2\eta \exp(-\lambda\alpha^* + \lambda^*\alpha)\exp(-\eta\lambda^* + \eta^*\lambda) f(\eta).\end{aligned} \tag{2.5}$$

Applying Lemma A.1 to integrate over $\lambda$:

$$\begin{aligned}\mathcal{W}[\hat{A}] &= \frac{1}{\pi^2}\int \mathrm{d}^2\eta \int \mathrm{d}^2\lambda \exp(-\lambda(\alpha^* - \eta^*) + \lambda^*(\alpha - \eta)) f(\eta) \\ &= \int \mathrm{d}^2\eta\delta(\operatorname{Re}\alpha - \operatorname{Re}\eta)\delta(\operatorname{Im}\alpha - \operatorname{Im}\eta) f(\eta) \\ &= f(\alpha).\end{aligned} \tag{2.6}$$

The proof for the other direction looks the same.

Although, in general, the result of the Wigner transformation is a complex-valued function, for Hermitian operators, which are of the main interest for us, it can be proved to always be real-valued.

**Theorem 2.1.** *If an operator $\hat{A}$ is Hermitian, its Wigner transformation $W[\hat{A}]$ is a real-valued function.*

*Proof.* Let us calculate the conjugate of $W[\hat{A}]$:

$$(W[\hat{A}])^* = \frac{1}{\pi^2}\int \mathrm{d}^2\lambda \exp(-\lambda^*\alpha + \lambda\alpha^*)(\operatorname{Tr}\left\{\hat{A}\exp(\lambda\hat{a}^\dagger - \lambda^*\hat{a})\right\})^*. \tag{2.7}$$

Changing variables as $\lambda \to -\lambda$ and using the fact that $(\operatorname{Tr}\hat{B})^* = \operatorname{Tr}\hat{B}^\dagger$:

$$\begin{aligned}(W[\hat{A}])^* &= \frac{1}{\pi^2}\int \mathrm{d}^2\lambda \exp(\lambda^*\alpha - \lambda\alpha^*)\operatorname{Tr}\left\{\hat{A}^\dagger\exp(-\lambda^*\hat{a} + \lambda\hat{a}^\dagger)\right\} \\ &= W[\hat{A}^\dagger].\end{aligned} \tag{2.8}$$

Therefore, if $\hat{A} = \hat{A}^\dagger$, the conjugate of $W[\hat{A}]$ is equal to itself and, therefore, is real. □

Earlier in this section we have defined the Wigner transformation for arbitrary operators, but the most often occurring and the most important case is the transformation of a

density matrix.

**Definition 2.3.** *The Wigner function is the Wigner transformation of a density matrix:*

$$W(\alpha) \equiv \mathcal{W}[\hat{\rho}].$$

The Wigner function always exists for any density matrix [61]. Note also that since any density matrix is Hermitian, according to Theorem 2.1 $W(\alpha)$ is a real-valued function.

In some cases, it will be convenient to use the Wigner function in the form

$$W(\alpha) = \frac{1}{\pi^2} \int \mathrm{d}^2\lambda \exp(-\lambda\alpha^* + \lambda^*\alpha)\chi_W(\lambda), \tag{2.9}$$

where $\chi_W(\lambda)$ is the characteristic function

$$\chi_W(\lambda) = \mathrm{Tr}\left\{\hat{\rho}\hat{D}(\lambda)\right\}. \tag{2.10}$$

We will finish this section with the proofs of two central theorems which are required for any practical application of the Wigner function. The first theorem provides a way to transform any master equation written in terms of creation and annihilation operators to a partial differential equation for the Wigner function.

**Theorem 2.2** (operator correspondences)**.** *For any Hilbert-Schmidt operator* $\hat{A}$

$$\mathcal{W}[\hat{a}\hat{A}] = \left(\alpha + \frac{1}{2}\frac{\partial}{\partial\alpha^*}\right)\mathcal{W}[\hat{A}], \quad \mathcal{W}[\hat{a}^\dagger\hat{A}] = \left(\alpha^* - \frac{1}{2}\frac{\partial}{\partial\alpha}\right)\mathcal{W}[\hat{A}],$$
$$\mathcal{W}[\hat{A}\hat{a}] = \left(\alpha - \frac{1}{2}\frac{\partial}{\partial\alpha^*}\right)\mathcal{W}[\hat{A}], \quad \mathcal{W}[\hat{A}\hat{a}^\dagger] = \left(\alpha^* + \frac{1}{2}\frac{\partial}{\partial\alpha}\right)\mathcal{W}[\hat{A}].$$

*Proof.* We will prove the first correspondence. First, let us transform the trace using (2.4):

$$\mathrm{Tr}\left\{\hat{a}\hat{A}\hat{D}\right\} = \mathrm{Tr}\left\{\hat{A}\hat{D}\hat{a}\right\} = \left(-\frac{\partial}{\partial\lambda^*} - \frac{1}{2}\lambda\right)\mathrm{Tr}\left\{\hat{A}\hat{D}\right\}. \tag{2.11}$$

Substituting this into the definition of the Wigner transformation:

$$\begin{aligned}\mathcal{W}[\hat{a}\hat{A}] &= \frac{1}{\pi^2}\int \mathrm{d}^2\lambda \exp(-\lambda\alpha^* + \lambda^*\alpha)\,\mathrm{Tr}\left\{\hat{a}\hat{A}\hat{D}(\lambda)\right\} \\ &= \frac{1}{\pi^2}\int \mathrm{d}^2\lambda \exp(-\lambda\alpha^* + \lambda^*\alpha)\left(-\frac{\partial}{\partial\lambda^*} - \frac{1}{2}\lambda\right)\mathrm{Tr}\left\{\hat{A}\hat{D}(\lambda)\right\} \\ &= \frac{1}{2}\frac{\partial}{\partial\alpha^*}\mathcal{W}[\hat{A}] - \frac{1}{\pi^2}\int \mathrm{d}^2\lambda \exp(-\lambda\alpha^* + \lambda^*\alpha)\frac{\partial}{\partial\lambda^*}\mathrm{Tr}\left\{\hat{A}\hat{D}(\lambda)\right\}.\end{aligned} \tag{2.12}$$

The second term is almost the definition of the Wigner function, except for the derivative over $\lambda^*$. Here we can use Lemma A.2 since $\hat{A}$ is a Hilbert-Schmidt operator, which means that $\mathrm{Tr}\left\{\hat{A}\hat{D}\right\}$ is square-integrable [59]. This implies that we can use integration by parts with vanishing boundary terms, so

$$\begin{aligned}\mathcal{W}[\hat{a}\hat{A}] &= \frac{1}{2}\frac{\partial}{\partial\alpha^*}\mathcal{W}[\hat{A}] + \frac{1}{\pi^2}\int \mathrm{d}^2\lambda\left(\frac{\partial}{\partial\lambda^*}\exp(-\lambda\alpha^* + \lambda^*\alpha)\right)\mathrm{Tr}\left\{\hat{A}\hat{D}(\lambda)\right\} \\ &= \left(\alpha + \frac{1}{2}\frac{\partial}{\partial\alpha^*}\right)\mathcal{W}[\hat{A}].\end{aligned}$$

□

This theorem is paired with the second theorem, which helps to extract observables (again, expressed in terms of creation and annihilation operators) from a known Wigner function. We will start by proving an auxiliary lemma which connects the expectation of an operator product with a derivative of the characteristic function.

**Lemma 2.1.** *For a system with a density matrix $\hat{\rho}$ and a corresponding characteristic function $\chi_W$:*

$$\langle\left\{\hat{a}^r(\hat{a}^\dagger)^s\right\}_{\mathrm{sym}}\rangle = \left(\frac{\partial}{\partial\lambda}\right)^s\left(-\frac{\partial}{\partial\lambda^*}\right)^r\chi_W(\lambda)\Big|_{\lambda=0}.$$

*Proof.* The exponent in the expression for $\chi_W$ can be expanded as

$$\exp(\lambda\hat{a}^\dagger - \lambda^*\hat{a}) = \sum_{j,k}\frac{(-\lambda^*)^j\lambda^k}{j!\,k!}\left\{\hat{a}^j(\hat{a}^\dagger)^k\right\}_{\mathrm{sym}}. \tag{2.13}$$

Thus,

$$\begin{aligned}\chi_W(\lambda) &= \sum_{j,k}\frac{(-\lambda^*)^j\lambda^k}{j!\,k!}\,\mathrm{Tr}\left\{\hat{\rho}\left\{\hat{a}^j(\hat{a}^\dagger)^k\right\}_{\mathrm{sym}}\right\} \\ &= \sum_{j,k}\frac{(-\lambda^*)^j\lambda^k}{j!\,k!}\langle\left\{\hat{a}^j(\hat{a}^\dagger)^k\right\}_{\mathrm{sym}}\rangle.\end{aligned} \tag{2.14}$$

Clearly, the application of $(\partial/\partial\lambda)^s$ and $(-\partial/\partial\lambda^*)^r$ will eliminate all moments with $j < r$ and $k < s$, and setting $\lambda = 0$ afterwards will eliminate all moments with $j > r$ and $k > s$, leaving only the term with $\left\{\hat{a}^r(\hat{a}^\dagger)^s\right\}_{\text{sym}}$:

$$\begin{aligned}\left(\frac{\partial}{\partial\lambda}\right)^s\left(-\frac{\partial}{\partial\lambda^*}\right)^r\chi_W(\lambda)\Big|_{\lambda=0} &= r!\,s!\,\frac{1}{r!\,s!}\langle\left\{\hat{a}^r(\hat{a}^\dagger)^s\right\}_{\text{sym}}\rangle \\ &= \langle\left\{\hat{a}^r(\hat{a}^\dagger)^s\right\}_{\text{sym}}\rangle.\end{aligned}$$ □

Using this lemma we can now prove the main theorem which connects expectations of observables with moments of the Wigner function.

**Theorem 2.3.** *For a system with a density matrix $\rho$ and a corresponding Wigner function $W(\alpha)$, given any non-negative integers $r$, $s$:*

$$\langle\left\{\hat{a}^r(\hat{a}^\dagger)^s\right\}_{\text{sym}}\rangle = \int \mathrm{d}^2\alpha\,\alpha^r(\alpha^*)^s W(\alpha).$$

*Proof.* By definition of the Wigner function:

$$\int \mathrm{d}^2\alpha\,\alpha^r(\alpha^*)^s W(\alpha) = \frac{1}{\pi^2}\int \mathrm{d}^2\alpha\,\alpha^r(\alpha^*)^s \int \mathrm{d}^2\lambda \exp(-\lambda\alpha^* + \lambda^*\alpha)\chi_W(\lambda). \tag{2.15}$$

Integrating over $\alpha$ using Lemma A.1:

$$\int \mathrm{d}^2\alpha\,\alpha^r(\alpha^*)^s W(\alpha) = \int \mathrm{d}^2\lambda \left(\left(\frac{\partial}{\partial\lambda}\right)^s\left(-\frac{\partial}{\partial\lambda^*}\right)^r \delta(\operatorname{Re}\lambda)\delta(\operatorname{Im}\lambda)\right)\chi_W(\lambda). \tag{2.16}$$

Integrating by parts and eliminating terms which fit Lemma A.3:

$$\begin{aligned}\int \mathrm{d}^2\alpha\,\alpha^r(\alpha^*)^s W(\alpha) &= \int \mathrm{d}^2\lambda\delta(\operatorname{Re}\lambda)\delta(\operatorname{Im}\lambda)\left(\frac{\partial}{\partial\lambda}\right)^s\left(-\frac{\partial}{\partial\lambda^*}\right)^r\chi_W(\lambda) \\ &= \left(\frac{\partial}{\partial\lambda}\right)^s\left(-\frac{\partial}{\partial\lambda^*}\right)^r\chi_W(\lambda)\Big|_{\lambda=0}.\end{aligned} \tag{2.17}$$

Now, recognising the final expression as a part of Lemma 2.1, we immediately get the statement of the theorem. □

With the help of Theorem 2.2 and Theorem 2.3 one can straightforwardly transform any master equation written in terms of creation and annihilation operators $\hat{a}^\dagger$ and $\hat{a}$ to an ordinary differential equation, and use its solution to get expectations of any observables.

## 2.2. Multimode transformation

The single-mode definition of the Wigner transformation can be extended to a case of many modes, where mode operators $\hat{a}_{\mathbf{n}}$, $\mathbf{n} \in \mathbb{M}$ obey bosonic commutation relations:

$$\begin{aligned} [\hat{a}_{\mathbf{m}}, \hat{a}_{\mathbf{n}}] &= [\hat{a}^\dagger_{\mathbf{m}}, \hat{a}^\dagger_{\mathbf{n}}] = 0, \\ [\hat{a}_{\mathbf{m}}, \hat{a}^\dagger_{\mathbf{n}}] &= \delta_{\mathbf{m},\mathbf{n}}. \end{aligned} \tag{2.18}$$

**Definition 2.4.** *Let $\boldsymbol{\lambda}$ and $\boldsymbol{\alpha}$ be vectors of complex elements $\lambda_{\mathbf{n}}$ and $\alpha_{\mathbf{n}}$ respectively. The multimode Wigner transformation is*

$$W[\hat{A}] = \frac{1}{\pi^{2|\mathbb{M}|}} \int \mathrm{d}^2\boldsymbol{\lambda} \left( \prod_{\mathbf{n}\in\mathbb{M}} \exp(-\lambda_{\mathbf{n}}\alpha^*_{\mathbf{n}} + \lambda^*_{\mathbf{n}}\alpha_{\mathbf{n}}) \right) \mathrm{Tr}\left\{ \hat{A} \prod_{\mathbf{n}\in\mathbb{M}} \hat{D}_{\mathbf{n}}(\lambda_{\mathbf{n}}) \right\},$$

*where $\hat{D}_{\mathbf{n}}(\lambda_{\mathbf{n}}) = \exp(\lambda_{\mathbf{n}}\hat{a}^\dagger_{\mathbf{n}} - \lambda^*_{\mathbf{n}}\hat{a}_{\mathbf{n}})$, $\int \mathrm{d}^2\boldsymbol{\lambda} \equiv \int \prod_{\mathbf{n}\in\mathbb{M}} \mathrm{d}\lambda_{\mathbf{n}}$, and $|\mathbb{M}|$ stands for the cardinality of $\mathbb{M}$. The multi-component Weyl transformation is, correspondingly,*

$$W^{-1}[f] = \frac{1}{\pi^{|\mathbb{M}|}} \int \mathrm{d}^2\boldsymbol{\xi} \left( \prod_{\mathbf{n}\in\mathbb{M}} \hat{D}^\dagger_{\mathbf{n}}(\xi_{\mathbf{n}}) \right) \int \mathrm{d}^2\boldsymbol{\eta} \left( \prod_{\mathbf{n}\in\mathbb{M}} \exp(-\eta_{\mathbf{n}}\xi^*_{\mathbf{n}} + \eta^*_{\mathbf{n}}\xi_{\mathbf{n}}) \right) f(\boldsymbol{\eta}).$$

It can be proved, as in Theorem 2.1 for the single-mode case, that $W[\hat{A}]$ is real if $\hat{A}$ is Hermitian. The equality $\mathcal{W}[\mathcal{W}^{-1}1[f]] \equiv f$ is proved analogously to the single-mode case as well.

Corresponding definitions of the multimode characteristic and Wigner functions are, therefore,

$$\chi_W(\boldsymbol{\lambda}) = \mathrm{Tr}\left\{ \hat{\rho} \prod_{\mathbf{n}\in\mathbb{M}} \hat{D}_{\mathbf{n}}(\lambda_{\mathbf{n}}) \right\}, \tag{2.19}$$

and

$$W(\boldsymbol{\alpha}) \equiv \mathcal{W}[\hat{\rho}] = \frac{1}{\pi^{2|\mathbb{M}|}} \int \mathrm{d}^2\boldsymbol{\lambda} \left( \prod_{\mathbf{n}\in\mathbb{M}} \exp(-\lambda_{\mathbf{n}}\alpha^*_{\mathbf{n}} + \lambda^*_{\mathbf{n}}\alpha_{\mathbf{n}}) \right) \chi_W(\boldsymbol{\lambda}). \tag{2.20}$$

Following the single-mode scheme, we can formulate two theorems that govern the transformation of a master equation and the subsequent calculation of observables.

**Theorem 2.4** (multimode extension of Theorem 2.2)**.** *For any Hilbert-Schmidt operator* $\hat{A}$

$$\mathcal{W}[\hat{a}_{\mathbf{n}}\hat{A}] = \left(\alpha_{\mathbf{n}} + \frac{1}{2}\frac{\partial}{\partial\alpha^*_{\mathbf{n}}}\right)\mathcal{W}[\hat{A}], \quad \mathcal{W}[\hat{a}^\dagger_{\mathbf{n}}\hat{A}] = \left(\alpha^*_{\mathbf{n}} - \frac{1}{2}\frac{\partial}{\partial\alpha_{\mathbf{n}}}\right)\mathcal{W}[\hat{A}],$$
$$\mathcal{W}[\hat{A}\hat{a}_{\mathbf{n}}] = \left(\alpha_{\mathbf{n}} - \frac{1}{2}\frac{\partial}{\partial\alpha^*_{\mathbf{n}}}\right)\mathcal{W}[\hat{A}], \quad \mathcal{W}[\hat{A}\hat{a}^\dagger_{\mathbf{n}}] = \left(\alpha^*_{\mathbf{n}} + \frac{1}{2}\frac{\partial}{\partial\alpha_{\mathbf{n}}}\right)\mathcal{W}[\hat{A}].$$

*Proof.* The procedure is the same as in Theorem 2.2. □

**Lemma 2.2** (multimode extension of Lemma 2.1)**.** *For a system with a density matrix* $\rho$ *and a corresponding characteristic function* $\chi_W$*:*

$$\left\langle \left\{ \prod_{\mathbf{n}\in\mathbb{M}} \hat{a}^{r_{\mathbf{n}}}_{\mathbf{n}} (\hat{a}^\dagger_{\mathbf{n}})^{s_{\mathbf{n}}} \right\}_{\mathrm{sym}} \right\rangle = \left( \prod_{\mathbf{n}\in\mathbb{M}} \left(\frac{\partial}{\partial\lambda_{\mathbf{n}}}\right)^{s_{\mathbf{n}}} \left(-\frac{\partial}{\partial\lambda^*_{\mathbf{n}}}\right)^{r_{\mathbf{n}}} \right) \chi_W(\boldsymbol{\lambda}) \Big|_{\boldsymbol{\lambda}=0}.$$

*Proof.* Mode operators with different indices commute, so

$$\begin{aligned}
\chi_W(\boldsymbol{\lambda}) &= \mathrm{Tr}\left\{ \hat{\rho} \prod_{\mathbf{n}\in\mathbb{M}} \exp(\lambda_{\mathbf{n}}\hat{a}^\dagger_{\mathbf{n}} - \lambda^*_{\mathbf{n}}\hat{a}_{\mathbf{n}}) \right\} \\
&= \mathrm{Tr}\left\{ \hat{\rho} \prod_{\mathbf{n}\in\mathbb{M}} \sum_{j_{\mathbf{n}}\in\mathbb{M},k_{\mathbf{n}}\in\mathbb{M}} \frac{(-\lambda^*_{\mathbf{n}})^{j_{\mathbf{n}}}\lambda^{k_{\mathbf{n}}}_{\mathbf{n}}}{j_{\mathbf{n}}!\,k_{\mathbf{n}}!} \left\{ \hat{a}^{j_{\mathbf{n}}}_{\mathbf{n}} (\hat{a}^\dagger_{\mathbf{n}})^{k_{\mathbf{n}}} \right\}_{\mathrm{sym}} \right\} \\
&= \mathrm{Tr}\left\{ \hat{\rho} \left( \prod_{\mathbf{n}\in\mathbb{M}} \sum_{j_{\mathbf{n}},k_{\mathbf{n}}} \right) \left( \prod_{\mathbf{n}\in\mathbb{M}} \frac{(-\lambda^*_{\mathbf{n}})^{j_{\mathbf{n}}}\lambda^{k_{\mathbf{n}}}_{\mathbf{n}}}{j_{\mathbf{n}}!\,k_{\mathbf{n}}!} \left\{ \hat{a}^{j_{\mathbf{n}}}_{\mathbf{n}} (\hat{a}^\dagger_{\mathbf{n}})^{k_{\mathbf{n}}} \right\}_{\mathrm{sym}} \right) \right\},
\end{aligned} \tag{2.21}$$

where we have used $\left(\prod_{\mathbf{n}\in\mathbb{M}} \sum_{j_{\mathbf{n}},k_{\mathbf{n}}}\right)$ in the sense of the sequence of summations $\ldots \sum_{j_{\mathbf{n}},k_{\mathbf{n}}} \ldots$ for all values of $\mathbf{n} \in \mathbb{M}$. Separating operator and scalar parts:

$$\begin{aligned}
\chi_W(\boldsymbol{\lambda}) &= \mathrm{Tr}\left\{ \left( \prod_{\mathbf{n}\in\mathbb{M}} \sum_{j_{\mathbf{n}},k_{\mathbf{n}}} \right) \left( \prod_{\mathbf{n}\in\mathbb{M}} \frac{(-\lambda^*_{\mathbf{n}})^{j_{\mathbf{n}}}\lambda^{k_{\mathbf{n}}}_{\mathbf{n}}}{j_{\mathbf{n}}!\,k_{\mathbf{n}}!} \right) \hat{\rho} \left\{ \prod_{\mathbf{n}\in\mathbb{M}} \hat{a}^{j_{\mathbf{n}}}_{\mathbf{n}} (\hat{a}^\dagger_{\mathbf{n}})^{k_{\mathbf{n}}} \right\}_{\mathrm{sym}} \right\} \\
&= \left( \prod_{\mathbf{n}\in\mathbb{M}} \sum_{j_{\mathbf{n}},k_{\mathbf{n}}} \right) \left( \prod_{\mathbf{n}\in\mathbb{M}} \frac{(-\lambda^*_{\mathbf{n}})^{j_{\mathbf{n}}}\lambda^{k_{\mathbf{n}}}_{\mathbf{n}}}{j_{\mathbf{n}}!\,k_{\mathbf{n}}!} \right) \left\langle \left\{ \prod_{\mathbf{n}\in\mathbb{M}} \hat{a}^{j_{\mathbf{n}}}_{\mathbf{n}} (\hat{a}^\dagger_{\mathbf{n}})^{k_{\mathbf{n}}} \right\}_{\mathrm{sym}} \right\rangle.
\end{aligned} \tag{2.22}$$

As in Lemma 2.1, differentiating the resulting expression and setting $\boldsymbol{\lambda} = 0$ will leave only the term with required $j_{\mathbf{n}} = r_{\mathbf{n}}$ and $k_{\mathbf{n}} = s_{\mathbf{n}}$. □

Moments of the multimode Wigner function correspond to averages of symmetrically ordered products in the same way as for the single-mode case.

**Theorem 2.5** (multimode extension of Theorem 2.3)**.** *For a system with a density matrix $\rho$ and a corresponding Wigner function $W(\boldsymbol{\alpha})$, given any non-negative integers $r$, $s$:*

$$\left\langle \left\{ \prod_{\mathbf{n}\in\mathbb{M}} \hat{a}_{\mathbf{n}}^{r_{\mathbf{n}}} (\hat{a}_{\mathbf{n}}^{\dagger})^{s_{\mathbf{n}}} \right\}_{\mathrm{sym}} \right\rangle = \int \mathrm{d}^2\boldsymbol{\alpha} \left( \prod_{\mathbf{n}\in\mathbb{M}} \alpha_{\mathbf{n}}^{r_{\mathbf{n}}} (\alpha_{\mathbf{n}}^{*})^{s_{\mathbf{n}}} \right) W(\boldsymbol{\alpha}).$$

*Proof.* The proof is carried out similarly to Theorem 2.3: integrals over $\alpha_{\mathbf{n}}$ are eliminated one by one using Lemma A.1, and the resulting integrals over $\lambda_{\mathbf{n}}$ are dealt with using integration by parts and Lemma A.3, until we get the right-hand part of Lemma 2.2. □

# Chapter 3.

# Functional Wigner transformation

While single-mode and multimode Wigner transformations proved to be quite useful in a multitude of applications, in multidimensional cases with nonlinear evolution and losses it is much more convenient to operate on a higher level, using field operators and wave functions. Of course, it is possible to use single-mode creation and annihilation operators exclusively, but similarly to how vectors and matrices encapsulate summations and facilitate operations with sets of values, the field operator calculus simplifies multimode master equations and corresponding differential equations.

The main thrust of this chapter is to introduce mappings that allow one to replace non-commuting field operators $\hat{\Psi}$ and $\hat{\Psi}^{\dagger}$ by classical fields for computational purposes in later chapters.

## 3.1. Field operator calculus

Field operators can simplify both the analysis of a master equation and its transformation to an FPE using phase-space methods, which is the main topic of this thesis. In this section we are going to outline the field operator calculus. It is quite similar to the calculus of functional operators, described in Appendix B. The similarity and interconnection of field operators and functional operators will become even more evident during the description of the functional Wigner transformation in Chapter 3.

A multimode field of a $C$-component BEC in $D$ effective dimensions is described by

field operators $\hat{\Psi}_j^\dagger(\mathbf{x})$ and $\hat{\Psi}_j(\mathbf{x})$, where $\hat{\Psi}_j^\dagger$ creates a bosonic atom of spin $j$, $j = 1 \dots C$ at a location defined by a $D$-component coordinate vector $\mathbf{x}$, and $\hat{\Psi}_j$ destroys one. We will use the same scheme as with functions of coordinates in Appendix B, abbreviating $\hat{\Psi}_j \equiv \hat{\Psi}_j(\mathbf{x})$ and $\hat{\Psi}'_j \equiv \hat{\Psi}_j(\mathbf{x}')$.

The field operators obey standard bosonic commutation relations

$$\begin{aligned} [\hat{\Psi}_j, \hat{\Psi}'_k] = [\hat{\Psi}_j^\dagger, \hat{\Psi}'^\dagger_k] = 0, \\ [\hat{\Psi}_j, \hat{\Psi}'^\dagger_k] = \delta_{jk}\delta(\mathbf{x}' - \mathbf{x}). \end{aligned} \tag{3.1}$$

Field operators have type $\hat{\Psi}_j \in (\mathbb{R}^D \to \mathbb{H}_j) \equiv \mathbb{F}\mathbb{H}_j$, where the component Hilbert spaces $\mathbb{H}_j$ constitute the system Hilbert space $\mathbb{H} = \bigotimes_{j=1}^{C} \mathbb{H}_j$. Field operators can be decomposed using a single-particle orthonormal basis (see (B.1) for details):

$$\hat{\Psi}_j(\mathbf{x}) = \sum_{\mathbf{n}\in\mathbb{B}_j} \phi_{j,\mathbf{n}}(\mathbf{x})\hat{a}_{j,\mathbf{n}}. \tag{3.2}$$

Note that each component can have its own basis. Single mode operators $\hat{a}_{j,\mathbf{n}}$ obey commutation relations (2.18), with the pair $j, \mathbf{n}$ serving as a mode identifier. From now on, we drop the coordinate argument of mode functions $\phi(\mathbf{x})$.

In practice, one cannot use an infinitely sized basis in numerical calculations; some subset of modes is always chosen. In order to take this into account, we will restrict ourselves to a subset of modes from the full basis for each component: $\mathbb{M}_j \subset \mathbb{B}_j$. The new restricted field operators are

$$\tilde{\Psi}_j = \sum_{\mathbf{n}\in\mathbb{M}_j} \phi_{j,\mathbf{n}}\hat{a}_{j,\mathbf{n}}. \tag{3.3}$$

These map coordinates to restricted Hilbert subspaces: $\tilde{\Psi}_j \in (\mathbb{R} \to \mathbb{H}_{\mathbb{M}_j}) = \mathbb{F}\mathbb{H}_{\mathbb{M}_j}$. Because of the restricted nature of these operators, the commutation relations (3.1) no longer apply. The following ones must be used instead:

$$\begin{aligned} \left[\tilde{\Psi}_j, \tilde{\Psi}'_k\right] = \left[\tilde{\Psi}_j^\dagger, \tilde{\Psi}'^\dagger_k\right] = 0, \\ \left[\tilde{\Psi}_j, \tilde{\Psi}'^\dagger_k\right] = \delta_{jk}\delta_{\mathbb{M}_j}(\mathbf{x}', \mathbf{x}), \end{aligned} \tag{3.4}$$

where $\delta_{\mathbb{M}_j}$ is the restricted delta function introduced in Appendix B, Definition B.4.

Let us now find the expression for high-order commutators of restricted field operators,

analogous to the one for single-mode operators, which can be found in the book by Louisell [63]. For simplicity we will consider the case of a single component and, consequently, omit the component subscript of field operators in the following two lemmas.

**Lemma 3.1.** *For* $\tilde{\Psi} \in \mathbb{F}\mathbb{H}_{\mathbb{M}}$,

$$\begin{aligned}\left[\tilde{\Psi}, (\tilde{\Psi}'^{\dagger})^l\right] &= l\delta_{\mathbb{M}}(\mathbf{x}', \mathbf{x})(\tilde{\Psi}'^{\dagger})^{l-1},\\ \left[\tilde{\Psi}^{\dagger}, (\tilde{\Psi}')^l\right] &= -l\delta^*_{\mathbb{M}}(\mathbf{x}', \mathbf{x})(\tilde{\Psi}')^{l-1}.\end{aligned}$$

*Proof.* Proved by induction. Given that we know the expression for $\left[\tilde{\Psi}, (\tilde{\Psi}'^{\dagger})^{l-1}\right]$, the commutator of higher order can be expanded as

$$\begin{aligned}\left[\tilde{\Psi}, (\tilde{\Psi}'^{\dagger})^l\right] &= \tilde{\Psi}(\tilde{\Psi}'^{\dagger})^l - (\tilde{\Psi}'^{\dagger})^l\tilde{\Psi}\\ &= (\delta_{\mathbb{M}}(\mathbf{x}', \mathbf{x}) + \tilde{\Psi}'^{\dagger}\tilde{\Psi})(\tilde{\Psi}'^{\dagger})^{l-1} - (\tilde{\Psi}'^{\dagger})^l\tilde{\Psi}\\ &= \delta_{\mathbb{M}}(\mathbf{x}', \mathbf{x})(\tilde{\Psi}'^{\dagger})^{l-1} + \tilde{\Psi}'^{\dagger}(\tilde{\Psi}(\tilde{\Psi}'^{\dagger})^{l-1} - (\tilde{\Psi}'^{\dagger})^{l-1}\tilde{\Psi})\\ &= \delta_{\mathbb{M}}(\mathbf{x}', \mathbf{x})(\tilde{\Psi}'^{\dagger})^{l-1} + \tilde{\Psi}'^{\dagger}[\tilde{\Psi}, (\tilde{\Psi}'^{\dagger})^{l-1}].\end{aligned} \tag{3.5}$$

A similar result holds for the second relation, on conjugating the first one. Now we can get the commutator of any order starting from the known relation (3.4). □

A further generalisation of these relations is

**Lemma 3.2.** *For* $\tilde{\Psi} \in \mathbb{F}\mathbb{H}_{\mathbb{M}}$,

$$\begin{aligned}\left[\tilde{\Psi}, f(\tilde{\Psi}', \tilde{\Psi}'^{\dagger})\right] &= \delta_{\mathbb{M}}(\mathbf{x}', \mathbf{x})\frac{\partial f}{\partial \tilde{\Psi}'^{\dagger}},\\ \left[\tilde{\Psi}^{\dagger}, f(\tilde{\Psi}', \tilde{\Psi}'^{\dagger})\right] &= -\delta^*_{\mathbb{M}}(\mathbf{x}', \mathbf{x})\frac{\partial f}{\partial \tilde{\Psi}'},\end{aligned}$$

*where* $f(x, y)$ *is a function that can be expanded in the power series of* $x$ *and* $y$.

*Proof.* Let us prove the first relation. The procedure for the second one is the same. Without loss of generality, we can assume that $f(\tilde{\Psi}', \tilde{\Psi}'^{\dagger})$ can be expanded in the power series of normally ordered operators (otherwise we can just use the commutation rela-

tions). Thus,

$$\begin{aligned}\left[\tilde{\Psi}, f(\tilde{\Psi}', \tilde{\Psi}'^{\dagger})\right] &= \sum_{r,s} f_{rs}[\tilde{\Psi}, (\tilde{\Psi}'^{\dagger})^r (\tilde{\Psi}')^s] \\ &= \sum_{r,s} f_{rs}[\tilde{\Psi}, (\tilde{\Psi}'^{\dagger})^r](\tilde{\Psi}')^s \\ &= \sum_{r,s} f_{rs} r \delta_P(\mathbf{x}', \mathbf{x})(\tilde{\Psi}'^{\dagger})^{r-1}(\tilde{\Psi}')^s \\ &= \delta_P(\mathbf{x}', \mathbf{x}) \frac{\partial f}{\partial \tilde{\Psi}'^{\dagger}}.\end{aligned}$$

□

## 3.2. Functional transformation

Now we have all the tools we need to work with the functional Wigner representation. The notation for multidimensional integral follows that given in Appendix B. First, we will define a functional analogue of the displacement operator (2.1):

**Definition 3.1.** *The functional displacement operator* $\hat{D} \in \mathbb{F}_{\mathbb{M}} \to \mathbb{H}_{\mathbb{M}}$ *is defined as*

$$\hat{D}[\Lambda] = \exp \int \mathrm{d}\mathbf{x} \left(\Lambda(\mathbf{x})\tilde{\Psi}^{\dagger}(\mathbf{x}) - \Lambda^*(\mathbf{x})\tilde{\Psi}(\mathbf{x})\right). \tag{3.6}$$

From now on we drop the coordinate argument of functions and field operators for brevity. It can be shown that the displacement operator has properties similar to (2.4).

**Lemma 3.3.** *Derivatives of the functional displacement operator are*

$$\begin{aligned}\frac{\delta}{\delta\Lambda'}\hat{D}[\Lambda] &= \hat{D}[\Lambda](\tilde{\Psi}'^{\dagger} + \frac{1}{2}\Lambda'^*) = (\tilde{\Psi}'^{\dagger} - \frac{1}{2}\Lambda'^*)\hat{D}[\Lambda], \\ -\frac{\delta}{\delta\Lambda'^*}\hat{D}[\Lambda] &= \hat{D}[\Lambda](\tilde{\Psi}' + \frac{1}{2}\Lambda') = (\tilde{\Psi}' - \frac{1}{2}\Lambda')\hat{D}[\Lambda].\end{aligned}$$

*Proof.* We will prove the second part of the first equation. Using the Baker-Hausdorff theorem, the functional displacement operator can be rewritten as

$$\hat{D}[\Lambda] = \exp\left(\int \mathrm{d}\mathbf{x}\Lambda\tilde{\Psi}^{\dagger}\right)\exp\left(-\int \mathrm{d}\mathbf{x}\Lambda^*\tilde{\Psi}\right)\exp\frac{1}{2}\left[\int \mathrm{d}\mathbf{x}'\Lambda'\tilde{\Psi}'^{\dagger}, \int \mathrm{d}\mathbf{x}\Lambda^*\tilde{\Psi}\right]. \tag{3.7}$$

Recognising the commutator of field operators, we can simplify

$$\begin{aligned}\left[\int \mathrm{d}\mathbf{x}'\Lambda'\tilde{\Psi}'^{\dagger}, \int \mathrm{d}\mathbf{x}\Lambda^{*}\tilde{\Psi}\right] &= \iint \mathrm{d}\mathbf{x}\,\mathrm{d}\mathbf{x}'\Lambda'\Lambda^{*}\delta_{\mathbb{M}}(\mathbf{x}',\mathbf{x}) \\ &= \int \mathrm{d}\mathbf{x}\Lambda\Lambda^{*},\end{aligned} \tag{3.8}$$

resulting in the expression for the displacement operator

$$\hat{D}[\Lambda] = \exp\left(\int \mathrm{d}\mathbf{x}\Lambda\tilde{\Psi}^{\dagger}\right)\exp\left(-\int \mathrm{d}\mathbf{x}\Lambda^{*}\tilde{\Psi}\right)\exp\left(-\frac{1}{2}\int \mathrm{d}\mathbf{x}\Lambda\Lambda^{*}\right). \tag{3.9}$$

Thus, differentiation of the displacement operator gives

$$\frac{\delta}{\delta\Lambda'}\hat{D}[\Lambda] = \left(\int \mathrm{d}\mathbf{x}\tilde{\Psi}^{\dagger}\delta_{\mathbb{M}}(\mathbf{x}',\mathbf{x}) - \frac{1}{2}\int \mathrm{d}\mathbf{x}\Lambda^{*}\delta_{\mathbb{M}}(\mathbf{x}',\mathbf{x})\right)\hat{D}[\Lambda]. \tag{3.10}$$

Expanding $\Lambda^{*}$ into modes and using the Definition B.4 of the restricted delta function, it is easy to show that

$$\begin{aligned}\int \mathrm{d}\mathbf{x}\Lambda^{*}\delta_{\mathbb{M}}(\mathbf{x}',\mathbf{x}) &= \sum_{\mathbf{m},\mathbf{n}\in\mathbb{M}}\int \mathrm{d}\mathbf{x}\phi^{*}_{\mathbf{m}}\lambda^{*}_{\mathbf{m}}\phi'^{*}_{\mathbf{n}}\phi_{\mathbf{n}} \\ &= \sum_{\mathbf{n}\in\mathbb{M}}\phi'^{*}_{\mathbf{n}}\lambda^{*}_{\mathbf{m}} \equiv \Lambda'^{*},\end{aligned} \tag{3.11}$$

and similarly that

$$\int \mathrm{d}\mathbf{x}\tilde{\Psi}^{\dagger}\delta_{\mathbb{M}}(\mathbf{x}',\mathbf{x}) = \tilde{\Psi}'^{\dagger}. \tag{3.12}$$

This results in the final expression for the differential

$$\frac{\delta}{\delta\Lambda'}\hat{D}[\Lambda] = (\tilde{\Psi}'^{\dagger} - \frac{1}{2}\Lambda'^{*})\hat{D}[\Lambda]. \tag{3.13}$$

The remaining equations from the statement are proved analogously. □

Similar to the single-mode Wigner transformation from Definition 2.2, the functional Wigner transformation is the Fourier transform of a trace, but expressed in functional terms.

**Definition 3.2.** *The functional Wigner transformation* $\mathcal{W} \in \mathbb{F}\mathbb{H}_{\mathbb{M}} \to \mathbb{F}_{\mathbb{M}}$ *is defined as*

$$\mathcal{W}[\hat{A}] = \frac{1}{\pi^{2|\mathbb{M}|}}\int \delta^{2}\Lambda\, D[\Lambda,\Psi]\,\mathrm{Tr}\left\{\hat{A}\hat{D}[\Lambda]\right\}.$$

*It transforms an operator $\hat{A}$ on a restricted subset of a Hilbert space to a functional $(\mathcal{W}[\hat{A}])[\Psi]$. The corresponding functional Weyl transformation is:*

$$\mathcal{W}^{-1}[F] = \frac{1}{\pi^{|\mathbb{M}|}} \int \delta^2\Xi\, \hat{D}^\dagger[\Xi] \int \delta^2\Phi\, D[\Phi,\Xi]F[\Phi].$$

*Here $\Psi \equiv \Psi(\mathbf{x})$ is a complex-valued classical field, unlike the operator-valued field $\tilde{\Psi}$ introduced earlier in this chapter.*

It can be proved, as in Theorem 2.1 for the single-mode case, that $\mathcal{W}[\hat{A}]$ is real if $\hat{A}$ is Hermitian, and $\mathcal{W}[\mathcal{W}^{-1}[F]] \equiv F$ (by mode expansion). Following the single-mode and the multimode cases we define the characteristic functional $\chi_W[\Lambda] \in \mathbb{F}_{\mathbb{M}} \to \mathbb{C}$

$$\chi_W[\Lambda] = \mathrm{Tr}\left\{\hat{\rho}\hat{D}[\Lambda]\right\}, \tag{3.14}$$

and the Wigner functional $W \in \mathbb{F}_{\mathbb{M}} \to \mathbb{R}$

$$W[\Psi] \equiv \mathcal{W}[\hat{\rho}] = \frac{1}{\pi^{2|\mathbb{M}|}} \int \delta^2\Lambda\, D[\Lambda,\Psi]\chi_W[\Lambda]. \tag{3.15}$$

Correspondence relations and the moment extraction theorem have the same form as in the single-mode case.

**Theorem 3.1** (functional extension of Theorem 2.2)**.** *For any Hilbert-Schmidt operator $\hat{A}$,*

$$\begin{aligned}
\mathcal{W}[\tilde{\Psi}\hat{A}] &= \left(\Psi + \frac{1}{2}\frac{\delta}{\delta\Psi^*}\right)\mathcal{W}[\hat{A}], \quad \mathcal{W}[\tilde{\Psi}^\dagger\hat{A}] = \left(\Psi^* - \frac{1}{2}\frac{\delta}{\delta\Psi}\right)\mathcal{W}[\hat{A}], \\
\mathcal{W}[\hat{A}\tilde{\Psi}] &= \left(\Psi - \frac{1}{2}\frac{\delta}{\delta\Psi^*}\right)\mathcal{W}[\hat{A}], \quad \mathcal{W}[\hat{A}\tilde{\Psi}^\dagger] = \left(\Psi^* + \frac{1}{2}\frac{\delta}{\delta\Psi}\right)\mathcal{W}[\hat{A}].
\end{aligned}$$

*Proof.* We will prove the first correspondence. First, let us transform the trace using Lemma 3.3:

$$\begin{aligned}
\mathrm{Tr}\left\{\tilde{\Psi}\hat{A}\hat{D}\right\} = \mathrm{Tr}\left\{\hat{A}\hat{D}\tilde{\Psi}\right\} &= \mathrm{Tr}\left\{\hat{A}\left(-\frac{\delta}{\delta\Lambda^*} - \frac{1}{2}\Lambda\right)\hat{D}\right\} \\
&= \left(-\frac{\delta}{\delta\Lambda^*} - \frac{1}{2}\Lambda\right)\mathrm{Tr}\left\{\hat{A}\hat{D}\right\}.
\end{aligned} \tag{3.16}$$

Moving the additional multiplier to the outside of the integral:

$$\begin{aligned}\mathcal{W}[\hat{\Psi}\hat{A}] &= \frac{1}{\pi^{2|\mathbb{M}|}}\int \delta^2\Lambda \left(\exp\int \mathrm{d}\mathbf{x}\,(-\Lambda\Psi^* + \Lambda^*\Psi)\right)\mathrm{Tr}\left\{\tilde{\Psi}\hat{A}\hat{D}[\Lambda]\right\}\\ &= \frac{1}{\pi^{2|\mathbb{M}|}}\int \delta^2\Lambda \left(\exp\int \mathrm{d}\mathbf{x}\,(-\Lambda\Psi^* + \Lambda^*\Psi)\right)\left(-\frac{\delta}{\delta\Lambda^*} - \frac{1}{2}\Lambda\right)\mathrm{Tr}\left\{\hat{A}\hat{D}[\Lambda]\right\}\\ &= \frac{1}{2}\frac{\delta}{\delta\Psi^*}\mathcal{W}[\hat{A}] - \frac{1}{\pi^{2|\mathbb{M}|}}\int \delta^2\Lambda \left(\exp\int \mathrm{d}\mathbf{x}\,(-\Lambda\Psi^* + \Lambda^*\Psi)\right)\frac{\delta}{\delta\Lambda^*}\mathrm{Tr}\left\{\hat{A}\hat{D}[\Lambda]\right\}.\end{aligned} \tag{3.17}$$

Using Lemma B.2 to move the partial derivative over $\Lambda^*$ ($\hat{D}[\Lambda]$ equals a product of single-mode displacement operators, which makes the operator in the trace Hilbert-Schmidt, and the trace itself bounded):

$$\begin{aligned}\mathcal{W}[\hat{\Psi}\hat{A}] &= \frac{1}{2}\frac{\delta}{\delta\Psi^*}\mathcal{W}[\hat{A}] + \frac{1}{\pi^{2|\mathbb{M}|}}\int \delta^2\Lambda\left(\frac{\delta}{\delta\Lambda^*}\exp\int \mathrm{d}\mathbf{x}\,(-\Lambda\Psi^* + \Lambda^*\Psi)\right)\mathrm{Tr}\left\{\hat{A}\hat{D}[\Lambda]\right\}\\ &= \left(\Psi + \frac{1}{2}\frac{\delta}{\delta\Psi^*}\right)\mathcal{W}[\hat{A}].\end{aligned}$$

□

**Lemma 3.4** (functional extension of Lemma 2.1)**.** *For a system with a density matrix $\hat{\rho}$ and a corresponding characteristic function $\chi_W$:*

$$\langle\left\{(\tilde{\Psi}')^r(\tilde{\Psi}'^\dagger)^s\right\}_{\mathrm{sym}}\rangle = \left(\frac{\delta}{\delta\Lambda'}\right)^s\left(-\frac{\delta}{\delta\Lambda'^*}\right)^r\chi_W[\Lambda]\Big|_{\Lambda\equiv 0}.$$

*Proof.* The proof follows the same general scheme as in the single-mode case. The exponent in the expression for $\chi_W$ can be expanded as

$$\exp(\int \mathrm{d}\mathbf{x}\Lambda\tilde{\Psi}^\dagger - \int \mathrm{d}\mathbf{x}\Lambda^*\tilde{\Psi}) = \sum_{r,s}\frac{\left\{\left(\int \mathrm{d}\mathbf{x}\Lambda\tilde{\Psi}^\dagger\right)^r\left(-\int \mathrm{d}\mathbf{x}\Lambda^*\tilde{\Psi}\right)^s\right\}_{\mathrm{sym}}}{r!\,s!}. \tag{3.18}$$

We can swap a functional derivative with both integration and multiplication by an independent function, so:

$$\begin{aligned}\frac{\delta}{\delta\Lambda'}\left(\int \mathrm{d}\mathbf{x}\Lambda\tilde{\Psi}^\dagger\right)^r &= r\int \mathrm{d}\mathbf{x}\frac{\delta\Lambda}{\delta\Lambda'}\tilde{\Psi}^\dagger\left(\int \mathrm{d}\mathbf{x}\Lambda\tilde{\Psi}^\dagger\right)^{r-1}\\ &= r\int \mathrm{d}\mathbf{x}\,\delta_{\mathbb{M}}(\mathbf{x}',\mathbf{x})\tilde{\Psi}^\dagger\left(\int \mathrm{d}\mathbf{x}\,\Lambda\tilde{\Psi}^\dagger\right)^{r-1}\\ &= r\tilde{\Psi}'^\dagger\left(\int \mathrm{d}\mathbf{x}\,\Lambda\tilde{\Psi}^\dagger\right)^{r-1}.\end{aligned} \tag{3.19}$$

A multiple application of the differential then gives us

$$\left(\frac{\delta}{\delta\Lambda'}\right)^r \left(\int \mathrm{d}\mathbf{x}\, \Lambda\tilde{\Psi}^\dagger\right)^r = r!\,(\tilde{\Psi}'^\dagger)^r. \tag{3.20}$$

Similarly, for the other differential:

$$\left(-\frac{\delta}{\delta\Lambda'^*}\right)^s \left(-\int \mathrm{d}\mathbf{x}\, \Lambda\tilde{\Psi}^\dagger\right)^s = s!\,(\tilde{\Psi}'^\dagger)^s. \tag{3.21}$$

Thus, as in the single-mode case, the differentiation will eliminate all lower order terms in the expansion, and all higher order terms will be eliminated by setting $\Lambda \equiv 0$, leaving only one operator product with the required order:

$$\begin{aligned}\left(\frac{\delta}{\delta\Lambda'}\right)^s \left(-\frac{\delta}{\delta\Lambda'^*}\right)^r \chi_W[\Lambda]\Big|_{\Lambda\equiv 0} &= r!\,s!\,\frac{1}{r!\,s!}\langle\left\{(\tilde{\Psi}')^r(\tilde{\Psi}'^\dagger)^s\right\}_{\mathrm{sym}}\rangle \\ &= \langle\left\{(\tilde{\Psi}')^r(\tilde{\Psi}'^\dagger)^s\right\}_{\mathrm{sym}}\rangle. \qquad \square\end{aligned}$$

**Theorem 3.2** (functional extension of Theorem 2.3)**.** *For a system with a density matrix $\hat{\rho}$ and a corresponding Wigner functional $W[\Psi]$, given any non-negative integers $r$, $s$:*

$$\langle\left\{\tilde{\Psi}^r(\tilde{\Psi}^\dagger)^s\right\}_{\mathrm{sym}}\rangle = \int \delta^2\Psi\, \Psi^r(\Psi^*)^s W[\Psi].$$

*Proof.* By definition of the Wigner functional:

$$\int \delta^2\Psi\, \Psi^r(\Psi^*)^s W[\Psi] = \frac{1}{\pi^{2|\mathbb{M}|}} \mathrm{Tr}\left\{\hat{\rho}\int \delta^2\Psi\, \Psi^r(\Psi^*)^s \int \delta^2\Lambda \exp(-\Lambda\Psi^* + \Lambda^*\Psi)\hat{D}[\Lambda]\right\} \tag{3.22}$$

Evaluating the integral over $\Psi$ using Lemma B.1:

$$\int \delta^2\Psi\, \Psi^r(\Psi^*)^s W[\Psi] = \int \delta^2\Lambda \left(\left(\frac{\delta}{\delta\Lambda}\right)^s \left(-\frac{\delta}{\delta\Lambda^*}\right)^r \Delta_{\mathbb{M}}[\Lambda]\right) \mathrm{Tr}\left\{\hat{\rho}\hat{D}[\Lambda]\right\}. \tag{3.23}$$

Integrating by parts and eliminating the terms that fit Lemma B.3:

$$\begin{aligned}\int \delta^2\Psi\, \Psi^r(\Psi^*)^s W[\Psi] &= \int \delta^2\Lambda\, \Delta_{\mathbb{M}}[\Lambda] \left(\frac{\delta}{\delta\Lambda}\right)^s \left(-\frac{\delta}{\delta\Lambda^*}\right)^r \mathrm{Tr}\left\{\hat{\rho}\hat{D}[\Lambda]\right\} \\ &= \left(\frac{\delta}{\delta\Lambda}\right)^s \left(-\frac{\delta}{\delta\Lambda^*}\right)^r \chi_W[\Lambda]\Big|_{\Lambda\equiv 0}.\end{aligned} \tag{3.24}$$

Now, recognising the final expression as a part of Lemma 3.4, we immediately get the statement of the theorem. □

## 3.3. Multi-component functional transformation

Many experiments with BECs involve several interacting components, so it is useful to extend the definition of the functional Wigner transformation from the previous section, along with Theorem 3.1 and Theorem 3.2, to the case of several components.

First, definitions of the displacement operator and the Wigner functional are extended to the case multiple components.

**Definition 3.3.** *The functional displacement operator* $\hat{D}_j \in \mathbb{F}_{\mathbb{M}_j} \to \mathbb{H}_{\mathbb{M}_j}$ *for the component* $j$ *is defined as*

$$\hat{D}_j[\Lambda, \Lambda^*] = \exp \int \mathrm{d}\mathbf{x} \left( \Lambda \tilde{\Psi}_j^\dagger - \Lambda^* \tilde{\Psi}_j \right),$$

*where* $\tilde{\Psi}_j^\dagger$ *and* $\tilde{\Psi}_j$ *are creation and annihilation field operators for this component.*

**Definition 3.4.** *The multi-component functional Wigner transformation* $\mathcal{W}$ *is defined as*

$$\mathcal{W} \in \left( \mathbb{R}^D \to \prod_{j=1}^{C} \mathbb{H}_{\mathbb{M}_j} \right) \to \prod_{j=1}^{C} \mathbb{F}_{\mathbb{M}_j} \to \mathbb{C}$$
$$\mathcal{W}[\hat{A}] = \frac{1}{\pi^{2 \sum |\mathbb{M}_j|}} \int \delta^2 \mathbf{\Lambda} \left( \prod_{j=1}^{C} D[\Lambda_j, \Psi_j] \right) \mathrm{Tr} \left\{ \hat{A} \prod_{j=1}^{C} \hat{D}_j[\Lambda_j] \right\},$$

*where* $\Lambda_j \in \mathbb{F}_{\mathbb{M}_j}$, *and* $\int \delta^2 \mathbf{\Lambda} \equiv \int \delta^2 \Lambda_1 \ldots \int \delta^2 \Lambda_C$. *This transforms an operator* $\hat{A}$ *on a restricted subset of the Hilbert space to a functional* $(\mathcal{W}[\hat{A}])[\mathbf{\Psi}]$. *The corresponding Weyl transformation is*

$$\mathcal{W}^{-1}[F] = \frac{1}{\pi^{\sum |\mathbb{M}_j|}} \int \delta^2 \mathbf{\Xi} \left( \prod_{j=1}^{C} \hat{D}_j^\dagger[\Xi_j] \right) \int \delta^2 \mathbf{\Phi} \left( \prod_{j=1}^{C} D[\Phi_j, \Xi_j] \right) F[\mathbf{\Phi}].$$

**Definition 3.5.** *The Wigner functional* $W \in \prod_{j=1}^{C} \mathbb{F}_{\mathbb{M}_j} \to \mathbb{R}$ *is defined as*

$$W[\mathbf{\Psi}] \equiv \mathcal{W}[\hat{\rho}] = \frac{1}{\pi^{2 \sum |\mathbb{M}_j|}} \int \delta^2 \mathbf{\Lambda} \left( \prod_{j=1}^{C} D[\Lambda_j, \Psi_j] \right) \chi_W[\mathbf{\Lambda}],$$

*where* $\chi_W[\mathbf{\Lambda}] \in \prod_{j=1}^{C} \mathbb{F}_{\mathbb{M}_j} \to \mathbb{C}$ *is the characteristic functional*

$$\chi_W[\mathbf{\Lambda}] = \mathrm{Tr}\left\{\hat{\rho}\prod_{j=1}^{C}\hat{D}_j[\Lambda_j]\right\}.$$

The two central theorems for the single-component functional Wigner transformation can be straightforwardly reformulated for multiple components.

**Theorem 3.3** (multi-component extension of Theorem 3.1)**.** *For any Hilbert-Schmidt operator* $\hat{A}$*,*

$$\mathcal{W}[\tilde{\Psi}_j\hat{A}] = \left(\Psi_j + \frac{1}{2}\frac{\delta}{\delta\Psi_j^*}\right)\mathcal{W}[\hat{A}], \quad \mathcal{W}[\tilde{\Psi}_j^\dagger\hat{A}] = \left(\Psi_j^* - \frac{1}{2}\frac{\delta}{\delta\Psi_j}\right)\mathcal{W}[\hat{A}],$$
$$\mathcal{W}[\hat{A}\tilde{\Psi}_j] = \left(\Psi_j - \frac{1}{2}\frac{\delta}{\delta\Psi_j^*}\right)\mathcal{W}[\hat{A}], \quad \mathcal{W}[\hat{A}\tilde{\Psi}_j^\dagger] = \left(\Psi_j^* + \frac{1}{2}\frac{\delta}{\delta\Psi_j}\right)\mathcal{W}[\hat{A}].$$

*Proof.* Proved in the same way as Theorem 3.1. □

**Theorem 3.4** (multi-component extension of Theorem 3.2)**.** *For a system with a density matrix* $\hat{\rho}$ *and a corresponding Wigner functional* $W[\mathbf{\Psi}]$*, given any non-negative integers* $r$*,* $s$*:*

$$\left\langle\left\{\prod_{j=1}^{C}\tilde{\Psi}_j^{r_j}(\tilde{\Psi}_j^\dagger)^{s_j}\right\}_{\mathrm{sym}}\right\rangle = \int \delta^2\mathbf{\Psi}\left(\prod_{j=1}^{C}\Psi_j^{r_j}(\Psi_j^*)^{s_j}\right)W[\mathbf{\Psi}].$$

*Proof.* Proved in the same way as Theorem 3.2, processing each component successively. □

# Chapter 4.

# Transformation of the master equation

Although the functional correspondences from Theorem 3.3 are relatively straightforward, there is a certain amount of work required to apply them to actual master equations arising in real world problems. This chapter contains several theorems describing transformations of specific operator sequences, encountered in master equations describing BEC evolution. We will use these theorems in Chapter 5 to obtain a correspondence between operator evolution equations and functional derivatives of a classical field $\Psi$, which act on the Wigner functional instead of the quantum density matrix.

In order to give an idea about the form of expressions we are targeting, we will outline the master equation of interest. It will be described in more detail in Section 5.1 and Section 5.3. We are interested in transforming a master equation of the form

$$\frac{\mathrm{d}\hat{\rho}}{\mathrm{d}t} = -\frac{i}{\hbar}\left[\hat{H}, \hat{\rho}\right] + \sum_{\mathbf{l}\in L} \kappa_{\mathbf{l}} \int \mathrm{d}\mathbf{x} \mathcal{L}_{\mathbf{l}}\left[\hat{\rho}\right], \tag{4.1}$$

where $\hat{H}$ is the Hamiltonian of the system, and the $\mathcal{L}$ are nonlinear Liouville loss terms

$$\mathcal{L}_{\mathbf{l}}[\hat{A}] = 2\hat{O}_{\mathbf{l}}\hat{A}\hat{O}_{\mathbf{l}}^{\dagger} - \hat{O}_{\mathbf{l}}^{\dagger}\hat{O}_{\mathbf{l}}\hat{A} - \hat{A}\hat{O}_{\mathbf{l}}^{\dagger}\hat{O}_{\mathbf{l}}. \tag{4.2}$$

Here $\mathbf{l} = (l_1, \ldots, l_C)^T$ is the identifier of a loss process, with $l_j$ denoting the number of

particles of the component $j$ lost in the event, and

$$\hat{O}_{\mathbf{l}} \equiv \hat{O}_{\mathbf{l}}(\tilde{\mathbf{\Psi}}) = \prod_{j=1}^{C} \tilde{\Psi}_j^{l_j}(\mathbf{x}). \tag{4.3}$$

The Hamiltonian, in turn, has the general form

$$\hat{H} = \int \mathrm{d}\mathbf{x} \sum_{j=1}^{C}\sum_{k=1}^{C} \left\{ \tilde{\Psi}_j^\dagger K_{jk} \tilde{\Psi}_k + \frac{1}{2}\int \mathrm{d}\mathbf{x}' \tilde{\Psi}_j^\dagger \tilde{\Psi}_k'^\dagger U_{jk}(\mathbf{x}-\mathbf{x}')\tilde{\Psi}_j \tilde{\Psi}_k' \right\}, \tag{4.4}$$

where $K_{jk} = \alpha\nabla^2 + \beta(\mathbf{x}, t)$ is a linear operator that does not depend on $\tilde{\Psi}_j$, possibly containing a linear occurrence of a Laplacian.

## 4.1. Unitary evolution

The simplest non-trivial element of the Hamiltonian (4.4) is the second-order operator $\tilde{\Psi}_j^\dagger \tilde{\Psi}_k$, which may describe, for instance, a potential or a coupling field.

**Theorem 4.1.** *For a Hilbert-Schmidt operator $\hat{A}$ with a corresponding Wigner functional $\mathcal{W}[\hat{A}] \equiv (\mathcal{W}[\hat{A}])[\mathbf{\Psi}]$,*

$$\mathcal{W}\left[\left[\int \mathrm{d}\mathbf{x} \tilde{\Psi}_j^\dagger \tilde{\Psi}_k, \hat{A}\right]\right] = \int \mathrm{d}\mathbf{x} \left( -\frac{\delta}{\delta \Psi_j}\Psi_k + \frac{\delta}{\delta \Psi_k^*}\Psi_j^* \right) \mathcal{W}[\hat{A}].$$

*Proof.* Expanding the commutator and applying Theorem 3.3:

$$\begin{aligned}
\mathcal{W}\left[\left[\int \mathrm{d}\mathbf{x} \tilde{\Psi}_j^\dagger \tilde{\Psi}_k, \hat{A}\right]\right] = \int \mathrm{d}\mathbf{x} \Bigg( & \left(\Psi_j^* - \frac{1}{2}\frac{\delta}{\delta\Psi_j}\right)\left(\Psi_k + \frac{1}{2}\frac{\delta}{\delta\Psi_k^*}\right) \\
& - \left(\Psi_k - \frac{1}{2}\frac{\delta}{\delta\Psi_k^*}\right)\left(\Psi_j^* + \frac{1}{2}\frac{\delta}{\delta\Psi_j}\right)\Bigg)\mathcal{W}[\hat{A}] \\
= \frac{1}{2}\int \mathrm{d}\mathbf{x} & \left( -\frac{\delta}{\delta\Psi_j}\Psi_k + \Psi_j^*\frac{\delta}{\delta\Psi_k^*} + \frac{\delta}{\delta\Psi_k^*}\Psi_j^* - \Psi_k\frac{\delta}{\delta\Psi_j} \right)\mathcal{W}[\hat{A}].
\end{aligned} \tag{4.5}$$

Changing the order of derivatives and functions using the relation

$$\Psi_k \frac{\delta}{\delta\Psi_j}\mathcal{F} = \left( \frac{\delta}{\delta\Psi_j}\Psi_k - \delta_{jk}\delta_{\mathbb{M}_j}(\mathbf{x},\mathbf{x}) \right)\mathcal{F}, \tag{4.6}$$

we get

$$\mathcal{W}\left[\left[\int \mathrm{d}\mathbf{x}\tilde{\Psi}_j^\dagger\tilde{\Psi}_k, \hat{A}\right]\right] = \int \mathrm{d}\mathbf{x}\left(-\frac{\delta}{\delta\Psi_j}\Psi_k + \frac{\delta}{\delta\Psi_k^*}\Psi_j^*\right)\mathcal{W}[\hat{A}], \tag{4.7}$$

which is the statement of the theorem. □

Commutators with a Laplacian inside require special treatment, because the Laplacian acts on basis functions and, in general, cannot be treated like a constant. For our purposes, we only need the case where it occurs linearly in a Hamiltonian (referred to as the kinetic term). Fortunately, in this case the Laplacian does act like a constant.

**Theorem 4.2.** *For a Hilbert-Schmidt operator $\hat{A}$ with a corresponding Wigner functional $\mathcal{W}[\hat{A}] \equiv (\mathcal{W}[\hat{A}])[\boldsymbol{\Psi}]$,*

$$\mathcal{W}\left[\int \mathrm{d}\mathbf{x}[\tilde{\Psi}^\dagger(\mathbf{x})\nabla^2\tilde{\Psi}(\mathbf{x}), \hat{A}]\right] = \int \mathrm{d}\mathbf{x}\left(-\frac{\delta}{\delta\Psi}\nabla^2\Psi + \frac{\delta}{\delta\Psi^*}\nabla^2\Psi^*\right)\mathcal{W}[\hat{A}].$$

*Proof.* First, it is obvious from the linearity of the Wigner transformation that an integral or a derivative acting on coordinates can be moved in and out of the transformation:

$$\begin{aligned}\mathcal{W}\left[\int \mathrm{d}\mathbf{x}\hat{B}(\mathbf{x})\hat{A}\right] &= \int \mathrm{d}\mathbf{x}\mathcal{W}[\hat{B}(\mathbf{x})\hat{A}],\\ \mathcal{W}[\nabla^2\hat{B}(\mathbf{x})\hat{A}] &= \nabla^2\mathcal{W}[\hat{B}(\mathbf{x})\hat{A}].\end{aligned} \tag{4.8}$$

Let us now expand the commutator and apply the correspondences from Theorem 3.1:

$$\begin{aligned}&\mathcal{W}\left[\int \mathrm{d}\mathbf{x}[\tilde{\Psi}^\dagger(\mathbf{x})\nabla^2\tilde{\Psi}(\mathbf{x}), \hat{A}]\right]\\ &= \int \mathrm{d}\mathbf{x}\left(\Psi^* - \frac{1}{2}\frac{\delta}{\delta\Psi}\right)\left(\nabla^2\Psi + \frac{1}{2}\nabla^2\frac{\delta}{\delta\Psi^*}\right)\mathcal{W}[\hat{A}]\\ &\quad - \int \mathrm{d}\mathbf{x}\left(\nabla^2\Psi - \frac{1}{2}\nabla^2\frac{\delta}{\delta\Psi^*}\right)\left(\Psi^* + \frac{1}{2}\frac{\delta}{\delta\Psi}\right)\mathcal{W}[\hat{A}]\\ &= \frac{1}{2}\int \mathrm{d}\mathbf{x}\left(-\frac{\delta}{\delta\Psi}\nabla^2\Psi + \Psi^*\nabla^2\frac{\delta}{\delta\Psi^*} + \left(\nabla^2\frac{\delta}{\delta\Psi^*}\right)\Psi^* - \left(\nabla^2\Psi\right)\frac{\delta}{\delta\Psi}\right)\mathcal{W}[\hat{A}].\end{aligned} \tag{4.9}$$

Using the basis expansion, one can easily check that

$$\Psi^*\nabla^2\frac{\delta}{\delta\Psi^*}\mathcal{F}[\Psi] = \left(\nabla^2\frac{\delta}{\delta\Psi^*}\right)\Psi^*\mathcal{F}[\Psi] - \sum_{\mathbf{n}\in\mathbb{M}}\phi_{\mathbf{n}}^*\nabla^2\phi_{\mathbf{n}}\mathcal{F}[\Psi], \tag{4.10}$$

and

$$\left(\nabla^2\Psi\right)\frac{\delta}{\delta\Psi}\mathcal{F}[\Psi] = \frac{\delta}{\delta\Psi}\left(\nabla^2\Psi\right)\mathcal{F}[\Psi] - \sum_{\mathbf{n}\in\mathbb{M}}\phi^*_{\mathbf{n}}\nabla^2\phi_{\mathbf{n}}\mathcal{F}[\Psi]. \tag{4.11}$$

Therefore,

$$\begin{aligned}&\mathcal{W}\left[\int \mathrm{d}\mathbf{x}[\tilde{\Psi}^\dagger(\mathbf{x})\nabla^2\tilde{\Psi}(\mathbf{x}), \hat{A}]\right]\\ &= \frac{1}{2}\int \mathrm{d}\mathbf{x}\left(-\frac{\delta}{\delta\Psi}\nabla^2\Psi + \left(\nabla^2\frac{\delta}{\delta\Psi^*}\right)\Psi^* + \left(\nabla^2\frac{\delta}{\delta\Psi^*}\right)\Psi^* - \frac{\delta}{\delta\Psi}\nabla^2\Psi\right)\mathcal{W}[\hat{A}].\end{aligned} \tag{4.12}$$

Now, using Lemma B.4, we can get the final result:

$$\begin{aligned}&= \frac{1}{2}\int \mathrm{d}\mathbf{x}\left(-\frac{\delta}{\delta\Psi}\nabla^2\Psi + \frac{\delta}{\delta\Psi^*}\nabla^2\Psi^* + \frac{\delta}{\delta\Psi^*}\nabla^2\Psi^* - \frac{\delta}{\delta\Psi}\nabla^2\Psi\right)\mathcal{W}[\hat{A}]\\ &= \int \mathrm{d}\mathbf{x}\left(-\frac{\delta}{\delta\Psi}\nabla^2\Psi + \frac{\delta}{\delta\Psi^*}\nabla^2\Psi^*\right)\mathcal{W}[\hat{A}].\end{aligned}$$

□

The last of the terms in the Hamiltonian (4.4) is the fourth order nonlinear interaction term. We will provide a transformation for its general non-local form, which can be later simplified to a local one by integration with the delta function.

**Theorem 4.3.** *For a Hilbert-Schmidt operator $\hat{A}$ with a corresponding Wigner functional $\mathcal{W}[\hat{A}] \equiv (\mathcal{W}[\hat{A}])[\mathbf{\Psi}]$,*

$$\begin{aligned}&\mathcal{W}\left[\left[\iint \mathrm{d}\mathbf{x}\,\mathrm{d}\mathbf{x}'\tilde{\Psi}^\dagger_j\tilde{\Psi}'^\dagger_k\tilde{\Psi}_j\tilde{\Psi}'_k, \hat{A}\right]\right]\\ &= \iint \mathrm{d}\mathbf{x}\,\mathrm{d}\mathbf{x}'\left(-\frac{\delta}{\delta\Psi_j}\mathcal{Q}_{jk} + \frac{\delta}{\delta\Psi^*_j}\mathcal{Q}^*_{jk} - \frac{\delta}{\delta\Psi_k}\mathcal{Q}_{kj} + \frac{\delta}{\delta\Psi^*_k}\mathcal{Q}^*_{kj}\right.\\ &\quad\left. + \frac{\delta}{\delta\Psi^*_j}\frac{\delta}{\delta\Psi_j}\left(\frac{\delta}{\delta\Psi'_k}\frac{\Psi'_k}{4} - \frac{\delta}{\delta\Psi'^*_k}\frac{\Psi'^*_k}{4}\right) + \frac{\delta}{\delta\Psi^*_k}\frac{\delta}{\delta\Psi_k}\left(\frac{\delta}{\delta\Psi'_j}\frac{\Psi'_j}{4} - \frac{\delta}{\delta\Psi'^*_j}\frac{\Psi'^*_j}{4}\right)\right)\mathcal{W}[\hat{A}],\end{aligned}$$

*where we introduced*

$$\mathcal{Q}_{jk}[\mathbf{\Psi}](\mathbf{x},\mathbf{x}') = \Psi_j|\Psi'_k|^2 - \frac{1}{2}\Psi_j\delta_{\mathbb{M}_k}(\mathbf{x}',\mathbf{x}') - \frac{\delta_{jk}}{2}\Psi'_j\delta_{\mathbb{M}_k}(\mathbf{x}',\mathbf{x}).$$

*Proof.* Proved by a straightforward application of Theorem 3.3 and a simplification of the resulting expression, similarly to Theorem 4.1. □

## 4.2. Losses

In this section we will derive the theorem for transformation of the loss terms (4.2). Before approaching the main theorem we will need two auxiliary lemmas. The result of an application of Theorem 3.3 to the operator $\mathcal{L}$ will contain terms with mixed order of $\Psi_j$ and $\delta/\delta\Psi_j$, while we need all derivatives to be grouped in the beginning in order to apply Theorem C.3 to the resulting differential equation. The first lemma will provide a way to perform this rearrangement.

**Lemma 4.1.** *For a function $\Psi \in \mathbb{F}_{\mathbb{M}}$ and a functional operator $\mathcal{F} \in \mathbb{F}_{\mathbb{M}} \to \mathbb{F}$, and non-negative integers $a, b$*

$$\Psi^a \left(\frac{\delta}{\delta\Psi}\right)^b \mathcal{F}[\Psi] = \sum_{j=0}^{\min(a,b)} \binom{b}{j} \frac{(-1)^j a!}{(a-j)!} \delta^j_{\mathbb{M}}(\mathbf{x},\mathbf{x}) \left(\frac{\delta}{\delta\Psi}\right)^{b-j} \Psi^{a-j}\mathcal{F}[\Psi].$$

*Proof.* Proved by induction. Let us assume that the statement is correct for $b-1$, and prove it for $b$ (also assuming the non-trivial case of $a > 0$). Moving a single differential to the left:

$$\Psi^a \left(\frac{\delta}{\delta\Psi}\right)^b \mathcal{F} = \left(\frac{\delta}{\delta\Psi}\Psi^a - a\Psi^{a-1}\delta_{\mathbb{M}}(\mathbf{x},\mathbf{x})\right)\left(\frac{\delta}{\delta\Psi}\right)^{b-1} \mathcal{F}. \tag{4.13}$$

Using the known relation for $b-1$:

$$\begin{aligned}\Psi^a \left(\frac{\delta}{\delta\Psi}\right)^b \mathcal{F} = \frac{\delta}{\delta\Psi} &\sum_{j=0}^{\min(a,b-1)} \binom{b-1}{j} \frac{(-1)^j a!}{(a-j)!} \delta^j_{\mathbb{M}}(\mathbf{x},\mathbf{x}) \left(\frac{\delta}{\delta\Psi}\right)^{b-1-j} \Psi^{a-j}\mathcal{F} \\ &- a\delta_{\mathbb{M}}(\mathbf{x},\mathbf{x}) \sum_{j=0}^{\min(a-1,b-1)} \binom{b-1}{j} \frac{(-1)^j (a-1)!}{(a-1-j)!} \\ &\times \delta^j_{\mathbb{M}}(\mathbf{x},\mathbf{x}) \left(\frac{\delta}{\delta\Psi}\right)^{b-1-j} \Psi^{a-1-j}\mathcal{F}.\end{aligned} \tag{4.14}$$

Merging the coefficients in front of the sums into the internal expressions:

$$\begin{aligned}\Psi^a \left(\frac{\delta}{\delta\Psi}\right)^b \mathcal{F} = &\sum_{j=0}^{\min(a,b-1)} \binom{b-1}{j} \frac{(-1)^j a!}{(a-j)!} \delta^j_{\mathbb{M}}(\mathbf{x},\mathbf{x}) \left(\frac{\delta}{\delta\Psi}\right)^{b-j} \Psi^{a-j}\mathcal{F} \\ &+ \sum_{j=0}^{\min(a-1,b-1)} \binom{b-1}{j} \frac{(-1)^{j+1} a!}{(a-1-j)!} \delta^{j+1}_{\mathbb{M}}(\mathbf{x},\mathbf{x}) \left(\frac{\delta}{\delta\Psi}\right)^{b-1-j} \Psi^{a-1-j}\mathcal{F}.\end{aligned} \tag{4.15}$$

Shifting the counter in the second sum:

$$\begin{aligned}\Psi^a\left(\frac{\delta}{\delta\Psi}\right)^b\mathcal{F} = &\sum_{j=0}^{\min(a,b-1)}\binom{b-1}{j}\frac{(-1)^j a!}{(a-j)!}\delta^j_{\mathbb{M}}(\mathbf{x},\mathbf{x})\left(\frac{\delta}{\delta\Psi}\right)^{b-j}\Psi^{a-j}\mathcal{F}\\ &+\sum_{j=1}^{\min(a,b)}\binom{b-1}{j-1}\frac{(-1)^j a!}{(a-j)!}\delta^j_{\mathbb{M}}(\mathbf{x},\mathbf{x})\left(\frac{\delta}{\delta\Psi}\right)^{b-j}\Psi^{a-j}\mathcal{F}.\end{aligned} \tag{4.16}$$

Now we can merge the sums, noticing that $\binom{b-1}{j}+\binom{b-1}{j-1}=\binom{b}{j}$. There will be at most two leftover terms: first, the term for $j=0$ from the first sum, and, possibly, the term with $j=\min(a,b)$ from the second sum. The former term appears only if $\min(a,b)>\min(a,b-1)$, or, in other words, $a\geq b$ (which means that $\min(a,b)=b$ and $\min(a,b-1)=b-1$):

$$\begin{aligned}\Psi^a\left(\frac{\delta}{\delta\Psi}\right)^b\mathcal{F} = &\binom{b-1}{0}\frac{(-1)^0 a!}{(a-0)!}\delta^0_{\mathbb{M}}(\mathbf{x},\mathbf{x})\left(\frac{\delta}{\delta\Psi}\right)^{b-0}\Psi^{a-0}\mathcal{F}\\ &+\sum_{j=1}^{\min(a,b-1)}\binom{b}{j}\frac{(-1)^j a!}{(a-j)!}\delta^j_{\mathbb{M}}(\mathbf{x},\mathbf{x})\left(\frac{\delta}{\delta\Psi}\right)^{b-j}\Psi^{a-j}\mathcal{F}\\ &+H[a-b]\binom{b-1}{b-1}\frac{(-1)^j a!}{(a-b)!}\delta^b_{\mathbb{M}}(\mathbf{x},\mathbf{x})\left(\frac{\delta}{\delta\Psi}\right)^{b-b}\Psi^{a-b}\mathcal{F},\end{aligned} \tag{4.17}$$

where $H[n]$ is the discrete Heaviside step function. Now, since $\binom{b-1}{0}\equiv\binom{b}{0}$ and $\binom{b-1}{b-1}\equiv\binom{b}{b}$, we can attach the two leftover terms to the sum as well:

$$\Psi^a\left(\frac{\delta}{\delta\Psi}\right)^b\mathcal{F} = \sum_{j=0}^{\min(a,b)}\binom{b}{j}\frac{(-1)^j a!}{(a-j)!}\delta^j_{\mathbb{M}}(\mathbf{x},\mathbf{x})\left(\frac{\delta}{\delta\Psi}\right)^{b-j}\Psi^{a-j}\mathcal{F}, \tag{4.18}$$

obtaining the statement of the lemma. □

**Lemma 4.2** (sum rearrangement)**.** *For any non-negative integers $a$, $b$:*

$$\sum_{k=0}^{a}\sum_{m=0}^{\min(a-b,k)} f_{k-m}g_{k,m} = \sum_{v=0}^{a} f_v \sum_{m=0}^{a-\max(b,v)} g_{v+m,m}.$$

*Proof.* Clearly, the index $v=k-m$ of the factor $f$ can vary from 0 (when $m=k$) to $a$ (when $k=a$ and $m=0$). Therefore,

$$\sum_{k=0}^{a}\sum_{m=0}^{\min(a-b,k)} f_{k-m}g_{k,m} = \sum_{v=0}^{a} f_v \sum_{m\in K(a,b,v)} g_{v+m,m}, \tag{4.19}$$

where the set $K$ is defined as

$$\begin{aligned} K(a,b,v) &= \{m|0 \leq k \leq a \wedge 0 \leq m \leq \min(a-b,k) \wedge k - m = v\} \\ &= \{m|-v \leq m \leq a - v \wedge 0 \leq m \leq \min(a-b, v+m)\} \\ &= \{m|m \leq a - v \wedge 0 \leq m \leq \min(a-b, v+m)\}. \end{aligned} \tag{4.20}$$

It is convenient to consider the cases of $v \leq b$ and $v > b$ separately. For the former case,

$$K_{v\leq b} = \{m|m \leq a - v \wedge 0 \leq m \leq \min(a-b, m+v) \wedge v \leq b\}. \tag{4.21}$$

Since $v \leq b$, $m \leq a - v \leq a - b \leq \min(a-b, m+v)$ is always true, and the first inequation is redundant:

$$K_{v\leq b} = \{m|0 \leq m \leq \min(a-b, v+m) \wedge v \leq b\}. \tag{4.22}$$

Splitting it into two sets to get rid of the minimum function:

$$\begin{aligned} K_{v\leq b} &= \{m|v \leq b \wedge m \geq 0 \\ &\qquad \wedge ((m \leq a-b \wedge a-b < v+m) \vee (m \leq v+m \wedge a-b \geq v+m))\} \\ &= \{m|v \leq b \wedge m \geq 0 \wedge ((m \leq a-b \wedge m > a-b-v) \vee (m \leq a-b-v))\} \\ &= \{m|v \leq b \wedge m \geq 0 \wedge (m \leq a-b)\} \\ &= \{m|v \leq b \wedge 0 \leq m \leq a-b\}. \end{aligned} \tag{4.23}$$

For the latter case of $v < U$ we have

$$\begin{aligned} K_{v>b} &= \{m|m \leq a - v \wedge 0 \leq m \leq \min(a-b, m+v) \wedge v > b\} \\ &= \{m|v > b \wedge m \geq 0 \\ &\qquad \wedge ((m \leq a-v \wedge m \geq a-b-v) \vee (m \leq a-v \wedge m < a-b-v))\} \\ &= \{m|v > b \wedge 0 \leq m \leq a-v\}. \end{aligned} \tag{4.24}$$

The final result is a union of these two cases:

$$\begin{aligned} K &= K_{v\le b} \cup K_{v>b} \\ &= \{m|v \le b \wedge 0 \le m \le a-b\} \cup \{m|v > b \wedge 0 \le m \le a-v\} \\ &= \{m|0 \le m \le a - \max(b,v)\}, \end{aligned} \tag{4.25}$$

which gives us the statement of the lemma. □

With the help of these two lemmas, we can perform the Wigner transformation of the nonlinear loss operator.

**Theorem 4.4.** *The Wigner transformation of the loss operator $\mathcal{L}_\mathbf{l}$ of form (4.2) is*

$$\mathcal{W}\left[\mathcal{L}_\mathbf{l}[\hat{A}]\right] = \sum_{j_1=0}^{l_1}\sum_{k_1=0}^{l_1} \dots \sum_{j_C=0}^{l_C}\sum_{k_C=0}^{l_C} \left(\prod_{c=1}^{C}\left(\frac{\delta}{\delta\Psi_c^*}\right)^{j_c}\left(\frac{\delta}{\delta\Psi_c}\right)^{k_c}\right) Z_{\mathbf{l},\mathbf{j},\mathbf{k}}\mathcal{W}[\hat{A}],$$

*where*

$$\begin{aligned} Z_{\mathbf{l},\mathbf{j},\mathbf{k}} = &\left(2-(-1)^{\sum_c j_c}-(-1)^{\sum_c k_c}\right) \\ &\times\prod_{c=1}^{C}\left(\frac{1}{2^{j_c+k_c}}\binom{l_c}{j_c}\binom{l_c}{k_c}\exp\left(-\frac{\delta_{\mathbb{M}_c}(\mathbf{x},\mathbf{x})}{2}\frac{\partial^2}{\partial\Psi_c\partial\Psi_c^*}\right)\Psi_c^{l_c-j_c}(\Psi_c^*)^{l_c-k_c}\right). \end{aligned}$$

*Proof.* Let us perform the transformation for each term of the loss operator. For the first term we have

$$\begin{aligned} W_1 &\equiv \mathcal{W}[\hat{O}_\mathbf{l}\hat{A}\hat{O}_\mathbf{l}^\dagger] \\ &= \prod_{c=1}^{C}\left(\Psi_c+\frac{1}{2}\frac{\delta}{\delta\Psi_c^*}\right)^{l_c}\left(\Psi_c^*+\frac{1}{2}\frac{\delta}{\delta\Psi_c}\right)^{l_c}\mathcal{W}[\hat{A}] \\ &= \prod_{c=1}^{C}\left(\sum_{j=0}^{l_c}\binom{l_c}{j}\left(\frac{1}{2}\right)^j\left(\frac{\delta}{\delta\Psi_c^*}\right)^j\Psi_c^{l_c-j}\sum_{k=0}^{l_c}\binom{l_c}{k}\left(\frac{1}{2}\right)^k\left(\frac{\delta}{\delta\Psi_c}\right)^k(\Psi_c^*)^{l_c-k}\right)\mathcal{W}[\hat{A}] \\ &= \prod_{c=1}^{C}\left(\sum_{j=0}^{l_c}\sum_{k=0}^{l_c}\binom{l_c}{j}\binom{l_c}{k}\left(\frac{1}{2}\right)^{j+k}\left(\frac{\delta}{\delta\Psi_c^*}\right)^j\Psi_c^{l_c-j}\left(\frac{\delta}{\delta\Psi_c}\right)^k(\Psi_c^*)^{l_c-k}\right)\mathcal{W}[\hat{A}]. \end{aligned} \tag{4.26}$$

Using Lemma 4.1 to swap $\Psi_c$ and $\delta/\delta\Psi_c$:

$$W_1 = \prod_{c=1}^{C}\left(\sum_{j=0}^{l_c}\sum_{k=0}^{l_c}\binom{l_c}{j}\binom{l_c}{k}\left(\frac{1}{2}\right)^{j+k}\left(\frac{\delta}{\delta\Psi_c^*}\right)^j \times \sum_{m=0}^{\min(l_c-j,k)}\binom{k}{m}\frac{(-1)^m(l_c-j)!}{(l_c-j-m)!}\delta^m_{\mathbb{M}_c}(\mathbf{x},\mathbf{x})\left(\frac{\delta}{\delta\Psi_c}\right)^{k-m}\Psi_c^{l_c-j-m}(\Psi_c^*)^{l_c-k}\right)\mathcal{W}[\hat{A}]. \tag{4.27}$$

Using Lemma 4.2 with $a = l_c$ and $b = j$, and

$$\begin{aligned} f_{k-m} &= \left(\frac{\delta}{\delta\Psi_c}\right)^{k-m}, \\ g_{k,m} &= \binom{l_c}{j}\binom{l_c}{k}\left(\frac{1}{2}\right)^{j+k}\binom{k}{m}\frac{(-1)^m(l_c-j)!}{(l_c-j-m)!}\delta^m_{\mathbb{M}_c}(\mathbf{x},\mathbf{x})\Psi_c^{l_c-j-m}(\Psi_c^*)^{l_c-k}, \end{aligned} \tag{4.28}$$

we obtain

$$W_1 = \prod_{c=1}^{C}\left(\sum_{j=0}^{l_c}\sum_{k=0}^{l_c}\left(\frac{\delta}{\delta\Psi_c^*}\right)^j\left(\frac{\delta}{\delta\Psi_c}\right)^k \times \sum_{m=0}^{l_c-\max(j,k)} Q(l_c,j,k,m)\delta^m_{\mathbb{M}_c}(\mathbf{x},\mathbf{x})\Psi_c^{l_c-j-m}(\Psi_c^*)^{l_c-k-m}\right)\mathcal{W}[\hat{A}], \tag{4.29}$$

where

$$\begin{aligned} Q(l,j,k,m) &= \frac{1}{2^{j+k+m}}\binom{l}{j}\binom{l}{k+m}\binom{k+m}{m}\frac{(-1)^m(l-j)!}{(l-j-m)!} \\ &= \frac{(-1)^m m!}{2^{j+k+m}}\binom{l}{j}\binom{l}{k}\binom{l-k}{m}\binom{l-j}{m}. \end{aligned} \tag{4.30}$$

Similarly, for the second term:

$$\begin{aligned} W_2 &\equiv \mathcal{W}[\hat{O}_1^\dagger\hat{O}_1\hat{A}] \\ &= \prod_{c=1}^{C}\left(\sum_{j=0}^{l_c}\sum_{k=0}^{l_c}\left(\frac{\delta}{\delta\Psi_c^*}\right)^j\left(\frac{\delta}{\delta\Psi_c}\right)^k \times \sum_{m=0}^{l_c-\max(j,k)}(-1)^k Q(l_c,j,k,m)\delta^m_{\mathbb{M}_c}(\mathbf{x},\mathbf{x})\Psi_c^{l_c-j-m}(\Psi_c^*)^{l_c-k-m}\right)\mathcal{W}[\hat{A}], \end{aligned} \tag{4.31}$$

and for the third term:

$$\begin{aligned} W_3 &\equiv \mathcal{W}[\hat{A}\hat{O}_1^\dagger \hat{O}_1] \\ &= \prod_{c=1}^{C} \left( \sum_{j=0}^{l_c} \sum_{k=0}^{l_c} \left( \frac{\delta}{\delta \Psi_c^*} \right)^j \left( \frac{\delta}{\delta \Psi_c} \right)^k \right. \\ &\quad \left. \times \sum_{m=0}^{l_c - \max(j,k)} (-1)^j Q(l_c, j, k, m) \delta^m_{\mathbb{M}_c}(\mathbf{x}, \mathbf{x}) \Psi_c^{l_c - j - m} (\Psi_c^*)^{l_c - k - m} \right) \mathcal{W}[\hat{A}]. \end{aligned} \tag{4.32}$$

The full expression for the Wigner transformation of $\mathcal{L}_1$ is, therefore,

$$\mathcal{W}[\hat{\mathcal{L}}_1[\hat{A}]] = 2W_1 - W_2 - W_3, \tag{4.33}$$

The expressions for $W_1$, $W_2$ and $W_3$ can be simplified further using the formal differentiation notation

$$\begin{aligned} \frac{\partial \left( \Psi^{l_c - j} (\Psi^*)^{l_c - k} \right)}{\partial^m \Psi \partial^m \Psi^*} &\equiv H[l_c - j - m] H[l_c - k - m] \\ &\quad \times \binom{l_c - j}{m} \binom{l_c - k}{m} (m!)^2 \Psi^{l_c - j - m} (\Psi^*)^{l_c - k - m}, \end{aligned} \tag{4.34}$$

where $H[n]$ is the discrete Heaviside function, which equals 1 for $n \geq 0$, and 0 otherwise. With this in mind, the internal summation over $m$ can be rewritten as

$$\begin{aligned} &\sum_{m=0}^{l_c - \max(j,k)} Q(l_c, j, k, m) \delta^m_{\mathbb{M}_c}(\mathbf{x}, \mathbf{x}) \Psi_c^{l_c - j - m} (\Psi_c^*)^{l_c - k - m} \\ &= \sum_{m=0}^{l_c} \frac{(-1)^m}{2^{j+k+m} m!} \binom{l_c}{j} \binom{l_c}{k} \delta^m_{\mathbb{M}_c}(\mathbf{x}, \mathbf{x}) \frac{\partial \left( \Psi_c^{l_c - j} (\Psi_c^*)^{l_c - k} \right)}{\partial^m \Psi_c \partial^m \Psi_c^*}. \end{aligned} \tag{4.35}$$

Furthermore, we can extend the summation over $m$ from $l_c$ to $\infty$ since all the new terms will be equal to zero. This turns the expression into the power series for the exponential:

$$= \frac{1}{2^{j+k}} \binom{l_c}{j} \binom{l_c}{k} \exp\left( -\frac{\delta_{\mathbb{M}_c}(\mathbf{x}, \mathbf{x})}{2} \frac{\partial^2}{\partial \Psi_c \partial \Psi_c^*} \right) \Psi_c^{l_c - j} (\Psi_c^*)^{l_c - k}. \tag{4.36}$$

Substituting this into $W_1$, $W_2$ and $W_3$, and swapping the product and summations over $j_c$ and $k_c$, we get the statement of the lemma. □

This theorem is the most complex result needed in this thesis. It is essential for the treatment of nonlinear loss processes in a BEC using a master equation. In the next

chapters we will use these results to analyse realistic experiments, that often do involve nonlinear loss processes.

# Chapter 5.

# Wigner representation of BEC quantum dynamics

In this chapter we will apply the field operator calculus and the functional Wigner transformation from Chapter 3 along with the transformation theorems from Chapter 4 to the master equation of BEC dynamics. We will discuss the applicability of the truncation approximation, which is required to get rid of the possible negativity of the Wigner functional. Finally, we will employ the correspondences from Appendix C to derive stochastic equations which can be solved numerically.

## 5.1. Hamiltonian

The second-quantized Hamiltonian of a $C$-component BEC in $D$ effective dimensions is expressed using quantum field operators $\hat{\Psi}_j^\dagger(\mathbf{x})$ and $\hat{\Psi}_j(\mathbf{x})$ with the mode expansion (3.2) and the standard bosonic commutation relations (3.1):

$$\hat{H} = \int \mathrm{d}\mathbf{x} \sum_{j=1}^{C}\sum_{k=1}^{C}\left\{\hat{\Psi}_j^\dagger K_{jk}\hat{\Psi}_k + \frac{1}{2}\int \mathrm{d}\mathbf{x}'\hat{\Psi}_j^\dagger\hat{\Psi}_k'^\dagger U_{jk}(\mathbf{x}-\mathbf{x}')\hat{\Psi}_j\hat{\Psi}_k'\right\}. \tag{5.1}$$

Here $U_{jk}$ is a two-body scattering potential, and $K_{jk}$ is the single-particle Hamiltonian:

$$K_{jk} = \left(-\frac{\hbar^2}{2m}\nabla^2 + \hbar\omega_j + V_j(\mathbf{x})\right)\delta_{jk} + \hbar\tilde{\Omega}_{jk}(t), \tag{5.2}$$

where $V_j$ is the external trapping potential for the spin $j$, $\omega_j$ is the internal energy of spin $j$, and $\tilde{\Omega}_{jk}$ represents a time-dependent coupling that is used to rotate one spin projection

into another. For details about the physical source and the concrete form of this term see Section 7.2.

If we impose an energy cutoff $\epsilon_{\text{cut}}$ and only take into account low-energy modes of the field, the general scattering potential $U_{jk}(\mathbf{x}-\mathbf{x}')$ can be replaced by a contact potential $U_{jk}\delta(\mathbf{x}-\mathbf{x}')$ [64], giving the effective Hamiltonian

$$\hat{H} = \int \mathrm{d}\mathbf{x} \sum_{j=1}^{C}\sum_{k=1}^{C}\left\{\tilde{\Psi}_j^\dagger K_{jk}\tilde{\Psi}_k + \frac{U_{jk}}{2}\tilde{\Psi}_j^\dagger\tilde{\Psi}_k^\dagger\tilde{\Psi}_j\tilde{\Psi}_k\right\}, \tag{5.3}$$

where $\tilde{\Psi}_j^\dagger(\mathbf{x})$ and $\tilde{\Psi}_j(\mathbf{x})$ are restricted quantum field operators defined by (3.3), with the commutators (3.4).

For $s$-wave scattering in three dimensions the interaction coefficient is $U_{jk} = 4\pi\hbar^2 a_{jk}/m$, where $a_{jk}$ is the scattering length. Note that, in general, the coefficient must be renormalised depending on the grid [57, 65], but the change is small if $dx_i \gg a_{jk}$, where $dx_i$ is the grid step in dimension $i$.

## 5.2. Energy cutoff

As has been noted earlier, in order to use contact interactions, an energy cutoff has to be imposed. We use two different bases in numerical simulations, plane waves and harmonic oscillator modes (see Appendix D for details). Both have analytical expressions for modes and corresponding energies, which makes the selection of modes straightforward.

Besides being a requirement for using the contact interaction in the Hamiltonian, the energy cutoff has other important functions. First, it allows one to check for the convergence of integration with respect to decreasing cell size of the spatial grid. It effectively separates the propagation in momentum space (which remains constant) from the propagation of the nonlinear parts of the equation in coordinate space (which, hopefully, becomes more precise when the cell size is decreased). Alternatively, the energy cutoff can work in a different direction, lowering the amount of modes under consideration while keeping the spatial grid constant. This helps to satisfy the Wigner truncation condition (see Section 5.4 for details).

## 5.3. Master equation

The time evolution of the density matrix $\hat{\rho}$ of a multi-component BEC with particle losses can be written as a Markovian master equation [66]

$$\frac{\mathrm{d}\hat{\rho}}{\mathrm{d}t} = -\frac{i}{\hbar}\left[\hat{H},\hat{\rho}\right] + \sum_{\mathbf{l}\in L}\kappa_{\mathbf{l}}\int \mathrm{d}\mathbf{x}\mathcal{L}_{\mathbf{l}}\left[\hat{\rho}\right], \tag{5.4}$$

where $L$ is the set of all loss processes taken into account, and $\mathbf{l} = (l_1, l_2, \ldots, l_C)$ is a vector containing the number of particles of each component involved in the inelastic interaction causing the specific loss process (with $C$ being the number of components). The coefficients $\kappa_{\mathbf{l}}$ are strengths of the corresponding loss processes, whose connection to experimentally measurable population losses will be discussed later in Section 7.3 and is expressed by Eqn. (7.32). Here the local Liouville loss terms (introduced in Chapter 4) that describe $n$-body collisional losses in the Markovian approximation are

$$\mathcal{L}_{\mathbf{l}}\left[\hat{\rho}\right] = 2\hat{O}_{\mathbf{l}}\hat{\rho}\hat{O}_{\mathbf{l}}^{\dagger} - \hat{O}_{\mathbf{l}}^{\dagger}\hat{O}_{\mathbf{l}}\hat{\rho} - \hat{\rho}\hat{O}_{\mathbf{l}}^{\dagger}\hat{O}_{\mathbf{l}}. \tag{5.5}$$

The reservoir coupling operators $\hat{O}_{\mathbf{l}}$ are products of restricted field annihilation operators

$$\hat{O}_{\mathbf{l}} \equiv \hat{O}_{\mathbf{l}}(\tilde{\mathbf{\Psi}}) = \prod_{j=1}^{C}\tilde{\Psi}_j^{l_j}, \tag{5.6}$$

describing local $n = (\sum l_c)$-body collision losses. This definition assumes that $l_1, \ldots, l_C$ particles of internal states with quantum numbers $j = 1, \ldots C$ respectively all collide simultaneously within the volume corresponding to the inverse momentum cutoff, and are removed from the Bose gas.

This minimal model of particle loss assumes that the reservoir of "lost" particles does not interact with the original Bose gas. Its accuracy thus depends on the trapping mechanism since the "lost" particles are simply in a different quantum state (or are combined into molecules). The model is valid if the trap is state-selective, or the collision is highly exothermic, such that the resulting particles are able to move away rapidly. It is also possible to treat non-Markovian reservoirs within this formalism, by extending the Hamiltonian to include the detailed loss dynamics, but this is not treated in detail in this thesis.

The master equation allows us to derive an important property.

**Theorem 5.1.** *The time derivative of the expectation of the field operator whose evolution is described by the master equation (5.4) with the Hamiltonian (5.3) is*

$$\frac{\mathrm{d}}{\mathrm{d}t}\langle\tilde{\Psi}_j\rangle = \mathcal{P}_{\mathbb{M}_j}\left[\left\langle -\frac{i}{\hbar}\sum_{k=1}^{C}\left(K_{jk}\tilde{\Psi}_k + U_{jk}\tilde{\Psi}_k^\dagger\tilde{\Psi}_k\tilde{\Psi}_j\right) - \sum_{\mathrm{l}\in L}\kappa_\mathrm{l}\frac{\partial\hat{O}_\mathrm{l}^\dagger}{\partial\tilde{\Psi}_j^\dagger}\hat{O}_\mathrm{l}\right\rangle\right].$$

*Proof.* Rewriting the expectation as a trace, and substituting the right-hand part of (5.4):

$$\begin{aligned}\frac{\mathrm{d}}{\mathrm{d}t}\langle\tilde{\Psi}_j\rangle &= \frac{\mathrm{d}}{\mathrm{d}t}\operatorname{Tr}\left\{\hat{\rho}\tilde{\Psi}_j\right\} = \operatorname{Tr}\left\{\frac{\mathrm{d}\hat{\rho}}{\mathrm{d}t}\tilde{\Psi}_j\right\}\\ &= \int \mathrm{d}\mathbf{x}'\left(-\frac{i}{\hbar}\sum_{m=1}^{C}\sum_{k=1}^{C}\operatorname{Tr}\left\{\left[\tilde{\Psi}_m'^\dagger K'_{mk}\tilde{\Psi}'_k,\hat{\rho}\right]\tilde{\Psi}_j\right\}\right.\\ &\quad -\frac{i}{2\hbar}\sum_{m=1}^{C}\sum_{k=1}^{C}U_{mk}\operatorname{Tr}\left\{\left[\tilde{\Psi}_m'^\dagger\tilde{\Psi}_k'^\dagger\tilde{\Psi}'_m\tilde{\Psi}'_k,\hat{\rho}\right]\tilde{\Psi}_j\right\}\\ &\quad \left.+\sum_{\mathrm{l}\in L}\kappa_\mathrm{l}\operatorname{Tr}\left\{\mathcal{L}'_\mathrm{l}\left[\hat{\rho}\right]\tilde{\Psi}_j\right\}\right),\end{aligned} \tag{5.7}$$

where $K'_{mk}\equiv K_{mk}(\mathbf{x}')$, $\mathcal{L}'_\mathrm{l}\equiv\mathcal{L}(\tilde{\boldsymbol{\Psi}}')$.

Let us transform each term separately. Noticing that $K'_{mk}$ commutes with $\tilde{\Psi}_j$, and using Lemma 3.1, we can transform the first term as:

$$\begin{aligned}\operatorname{Tr}\left\{\left[\tilde{\Psi}_m'^\dagger K'_{mk}\tilde{\Psi}'_k,\hat{\rho}\right]\tilde{\Psi}_j\right\} &= \operatorname{Tr}\left\{\hat{\rho}\left(\tilde{\Psi}_j\tilde{\Psi}_m'^\dagger K'_{mk}\tilde{\Psi}'_k - \tilde{\Psi}_m'^\dagger K'_{mk}\tilde{\Psi}'_k\tilde{\Psi}_j\right)\right\}\\ &= \operatorname{Tr}\left\{\hat{\rho}\left[\tilde{\Psi}_j,\tilde{\Psi}_m'^\dagger\right]K'_{mk}\tilde{\Psi}'_k\right\}\\ &= \operatorname{Tr}\left\{\hat{\rho}\delta_{jm}\delta_{\mathbb{M}_j}(\mathbf{x}',\mathbf{x})K'_{mk}\tilde{\Psi}'_k\right\} = \delta_{jm}\delta_{\mathbb{M}_j}(\mathbf{x}',\mathbf{x})\langle K'_{mk}\tilde{\Psi}'_k\rangle.\end{aligned} \tag{5.8}$$

The second (nonlinear) term is transformed similarly:

$$\begin{aligned}\operatorname{Tr}\left\{\left[\tilde{\Psi}_m'^\dagger\tilde{\Psi}_k'^\dagger\tilde{\Psi}'_m\tilde{\Psi}'_k,\hat{\rho}\right]\tilde{\Psi}_j\right\} &= \operatorname{Tr}\left\{\hat{\rho}\left(\tilde{\Psi}_j\tilde{\Psi}_m'^\dagger\tilde{\Psi}_k'^\dagger\tilde{\Psi}'_m\tilde{\Psi}'_k - \tilde{\Psi}_m'^\dagger\tilde{\Psi}_k'^\dagger\tilde{\Psi}'_m\tilde{\Psi}'_k\tilde{\Psi}_j\right)\right\}\\ &= \operatorname{Tr}\left\{\hat{\rho}\left[\tilde{\Psi}_j,\tilde{\Psi}_m'^\dagger\tilde{\Psi}_k'^\dagger\right]\tilde{\Psi}'_m\tilde{\Psi}'_k\right\}\\ &= \operatorname{Tr}\left\{\hat{\rho}\delta_{\mathbb{M}_j}(\mathbf{x}',\mathbf{x})\left(\delta_{jm}\tilde{\Psi}_k'^\dagger + \delta_{jk}\tilde{\Psi}_m'^\dagger\right)\tilde{\Psi}'_m\tilde{\Psi}'_k\right\}.\end{aligned} \tag{5.9}$$

Swapping $m\leftrightarrow k$ in the term corresponding to the second Kronecker delta, and summing

over $m$:

$$\begin{aligned}\sum_{m=1}^{C} U_{mk} \operatorname{Tr}\left\{\left[\tilde{\Psi}'^{\dagger}_m \tilde{\Psi}'^{\dagger}_k \tilde{\Psi}'_m \tilde{\Psi}'_k, \hat{\rho}\right] \tilde{\Psi}_j\right\} &= 2U_{jk}\delta_{\mathbb{M}_j}(\mathbf{x}', \mathbf{x}) \operatorname{Tr}\left\{\hat{\rho}\tilde{\Psi}'^{\dagger}_k \tilde{\Psi}'_k \tilde{\Psi}'_j\right\} \\ &= 2U_{jk}\delta_{\mathbb{M}_j}(\mathbf{x}', \mathbf{x})\langle \tilde{\Psi}'^{\dagger}_k \tilde{\Psi}'_k \tilde{\Psi}'_j\rangle.\end{aligned} \tag{5.10}$$

Finally, for the third term we notice that $\hat{O}'_1$ commutes with $\tilde{\Psi}_j$ since it is just a product of annihilation operators itself:

$$\begin{aligned}\operatorname{Tr}\left\{\mathcal{L}'_1[\hat{\rho}]\tilde{\Psi}_j\right\} &= \operatorname{Tr}\left\{\hat{\rho}\hat{O}'^{\dagger}_1\hat{O}'_1\tilde{\Psi}_j + \hat{\rho}\hat{O}'^{\dagger}_1\tilde{\Psi}_j\hat{O}'_1 - \hat{\rho}\tilde{\Psi}_j\hat{O}'^{\dagger}_1\hat{O}'_1 - \hat{\rho}\hat{O}'^{\dagger}_1\hat{O}'_1\tilde{\Psi}_j\right\} \\ &= \operatorname{Tr}\left\{\hat{\rho}\left[\hat{O}'^{\dagger}_1, \tilde{\Psi}_j\right]\hat{O}'_1\right\}.\end{aligned} \tag{5.11}$$

Representing the commutator as a formal derivative of the coupling operator according to Lemma 3.2:

$$\begin{aligned}\operatorname{Tr}\left\{\mathcal{L}'_1[\hat{\rho}]\tilde{\Psi}_j\right\} &= -\delta_{\mathbb{M}_j}(\mathbf{x}', \mathbf{x}) \operatorname{Tr}\left\{\hat{\rho}\frac{\partial \hat{O}'^{\dagger}_1}{\partial \tilde{\Psi}'^{\dagger}_j}\hat{O}'_1\right\} \\ &= -\delta_{\mathbb{M}_j}(\mathbf{x}', \mathbf{x})\left\langle\frac{\partial \hat{O}'^{\dagger}_1}{\partial \tilde{\Psi}'^{\dagger}_j}\hat{O}'_1\right\rangle.\end{aligned} \tag{5.12}$$

Thus, the full relation is

$$\frac{d}{dt}\langle\tilde{\Psi}_j\rangle = \int \mathrm{d}\mathbf{x}'\,\delta_{\mathbb{M}_j}(\mathbf{x}', \mathbf{x})\left(-\frac{i}{\hbar}\sum_{k=1}^{C}\left(\langle K'_{jk}\tilde{\Psi}'_k\rangle + U_{jk}\langle\tilde{\Psi}'^{\dagger}_k\tilde{\Psi}'_k\tilde{\Psi}'_j\rangle\right) - \sum_{1}\kappa_1\left\langle\frac{\partial \hat{O}'^{\dagger}_1}{\partial \tilde{\Psi}'^{\dagger}_j}\hat{O}'_1\right\rangle\right), \tag{5.13}$$

which is equivalent to the statement of the theorem after replacing the integration with the restricted delta by a projector according to (B.4). □

The same method can be applied to calculating the time derivative of the per-component population.

**Theorem 5.2.** *For a system whose evolution is described by the master equation (5.4) with the Hamiltonian (5.3), the time derivative of the population of the component $j$ is*

$$\frac{d}{dt}\int \mathrm{d}\mathbf{x}\langle\tilde{\Psi}^{\dagger}_j\tilde{\Psi}_j\rangle = -2\sum_{1}\kappa_1\int \mathrm{d}\mathbf{x}\left\langle\tilde{\Psi}^{\dagger}_j\mathcal{P}_{\mathbb{M}_j}\left[\frac{\partial \hat{O}^{\dagger}_1}{\partial \tilde{\Psi}^{\dagger}_j}\hat{O}_1\right]\right\rangle.$$

*Proof.* Starting from the master equation, and ignoring the unitary evolution (which,

obviously, will not contribute to the total population change):

$$\frac{d}{dt}\int \mathrm{d}\mathbf{x}\langle\tilde{\Psi}_j^\dagger\tilde{\Psi}_j\rangle = \sum_{\mathrm{l}\in L}\kappa_\mathrm{l}\int \mathrm{d}\mathbf{x}\,\mathrm{d}\mathbf{x}'\,\mathrm{Tr}\left\{\mathcal{L}'_\mathrm{l}\left[\hat{\rho}\right]\tilde{\Psi}_j^\dagger\tilde{\Psi}_j\right\}. \tag{5.14}$$

Expanding the loss operator:

$$\begin{aligned}\frac{d}{dt}\langle\tilde{\Psi}_j^\dagger\tilde{\Psi}_j\rangle &= \sum_{\mathrm{l}\in L}\kappa_\mathrm{l}\iint \mathrm{d}\mathbf{x}\,\mathrm{d}\mathbf{x}'\,\mathrm{Tr}\left\{\hat{\rho}\left(2\hat{O}_\mathrm{l}'^\dagger\tilde{\Psi}_j^\dagger\tilde{\Psi}_j\hat{O}'_\mathrm{l}-\tilde{\Psi}_j^\dagger\tilde{\Psi}_j\hat{O}_\mathrm{l}'^\dagger\hat{O}'_\mathrm{l}-\hat{O}_\mathrm{l}'^\dagger\hat{O}'_\mathrm{l}\tilde{\Psi}_j^\dagger\tilde{\Psi}_j\right)\right\}\\ &= \sum_{\mathrm{l}\in L}\kappa_\mathrm{l}\iint \mathrm{d}\mathbf{x}\,\mathrm{d}\mathbf{x}'\langle\tilde{\Psi}_j^\dagger\left[\hat{O}_\mathrm{l}'^\dagger\hat{O}'_\mathrm{l},\tilde{\Psi}_j\right]+\left[\tilde{\Psi}_j^\dagger,\hat{O}_\mathrm{l}'^\dagger\hat{O}'_\mathrm{l}\right]\tilde{\Psi}_j\rangle\\ &= \sum_{\mathrm{l}\in L}\kappa_\mathrm{l}\iint \mathrm{d}\mathbf{x}\,\mathrm{d}\mathbf{x}'2\,\mathrm{Re}\langle\tilde{\Psi}_j^\dagger\left[\hat{O}_\mathrm{l}'^\dagger\hat{O}'_\mathrm{l},\tilde{\Psi}_j\right]\rangle.\end{aligned} \tag{5.15}$$

Applying Lemma 3.2 to transform the commutator and using (B.4) to integrate over $\mathbf{x}'$:

$$\begin{aligned}\frac{d}{dt}\int \mathrm{d}\mathbf{x}\langle\tilde{\Psi}_j^\dagger\tilde{\Psi}_j\rangle &= -2\sum_{\mathrm{l}\in L}\kappa_\mathrm{l}\iint \mathrm{d}\mathbf{x}\,\mathrm{d}\mathbf{x}'\,\mathrm{Re}\left\langle\tilde{\Psi}_j^\dagger\delta_{\mathbb{M}_j}(\mathbf{x}',\mathbf{x})\frac{\partial\left(\hat{O}_\mathrm{l}'^\dagger\hat{O}'_\mathrm{l}\right)}{\partial\tilde{\Psi}_j'^\dagger}\right\rangle\\ &= -2\sum_{\mathrm{l}\in L}\kappa_\mathrm{l}\int \mathrm{d}\mathbf{x}\left\langle\tilde{\Psi}_j^\dagger\mathcal{P}_{\mathbb{M}_j}\left[\frac{\partial\hat{O}_\mathrm{l}^\dagger}{\partial\tilde{\Psi}_j^\dagger}\hat{O}_\mathrm{l}\right]\right\rangle.\end{aligned} \tag{5.16}$$

□

## 5.4. Wigner truncation

In order to solve the operator equation (5.4) with the Hamiltonian (5.3) numerically, we will transform it to an ordinary differential equation using the Wigner transformation from Definition 3.4.

The term with $K_{jk}$ is transformed using Theorem 4.1 and Theorem 4.2 (since $K_{jk}$ is basically a sum of the Laplacian operator and functions of coordinates):

$$\mathcal{W}\left[\left[\int \mathrm{d}\mathbf{x}\tilde{\Psi}_j^\dagger K_{jk}\tilde{\Psi}_k,\hat{\rho}\right]\right] = \int \mathrm{d}\mathbf{x}\left(-\frac{\delta}{\delta\Psi_j}K_{jk}\Psi_k+\frac{\delta}{\delta\Psi_k^*}K_{jk}\Psi_j^*\right)W, \tag{5.17}$$

where the Wigner function is $W = \mathcal{W}[\hat{\rho}]$. The nonlinear term is transformed with

Theorem 4.3 (assuming the locality of the interaction, and $U_{kj} = U_{jk}$):

$$\mathcal{W}\left[\left[\int \mathrm{d}\mathbf{x}\frac{U_{jk}}{2}\tilde{\Psi}_j^\dagger\tilde{\Psi}_k^\dagger\tilde{\Psi}_j\tilde{\Psi}_k,\hat{\rho}\right]\right] = \int \mathrm{d}\mathbf{x}U_{jk}\left(\frac{\delta}{\delta\Psi_j}\left(-\Psi_j\Psi_k\Psi_k^* + \frac{\delta_{\mathbb{M}_k}(\mathbf{x},\mathbf{x})}{2}(\delta_{jk}\Psi_k + \Psi_j)\right)\right.$$
$$+\frac{\delta}{\delta\Psi_j^*}\left(\Psi_j^*\Psi_k\Psi_k^* - \frac{\delta_{\mathbb{M}_k}(\mathbf{x},\mathbf{x})}{2}(\delta_{jk}\Psi_k^* + \Psi_j^*)\right)$$
$$\left.+\frac{\delta}{\delta\Psi_j}\frac{\delta}{\delta\Psi_j^*}\frac{\delta}{\delta\Psi_k}\frac{1}{4}\Psi_k - \frac{\delta}{\delta\Psi_j}\frac{\delta}{\delta\Psi_j^*}\frac{\delta}{\delta\Psi_k^*}\frac{1}{4}\Psi_k^*\right)W. \tag{5.18}$$

Loss operator terms are transformed with Theorem 4.4 and result in similar expressions, with a finite number of differential terms up to order $2n$ for $n$-body collisional losses.

Assuming that $K_{jk}$, $U_{jk}$, and $\kappa_1$ are real-valued, all the transformations described above result in a partial differential equation for $W$ of the form

$$\frac{\mathrm{d}W}{\mathrm{d}t} = \int \mathrm{d}\mathbf{x}\left\{-\sum_{j=1}^{C}\frac{\delta}{\delta\Psi_j}\mathcal{A}_j - \sum_{j=1}^{C}\frac{\delta}{\delta\Psi_j^*}\mathcal{A}_j^* + \sum_{j=1}^{C}\sum_{k=1}^{C}\frac{\delta^2}{\delta\Psi_j^*\delta\Psi_k}\mathcal{D}_{jk} + \mathcal{O}\left[\frac{\delta^3}{\delta\Psi_j^3}\right]\right\}W. \tag{5.19}$$

The terms of order higher than 2 are produced both by the nonlinear term in the Hamiltonian, and loss terms. Such an equation could be solved perturbatively if there were only orders up to 3 (which means an absence of nonlinear losses) [67], but in most cases all terms except for first- and second-order ones are truncated. In order to justify this truncation in a consistent way, we develop an order-by-order expansion in $1/\sqrt{\tilde{N}_j}$, where $\tilde{N}_j$ is a characteristic particle number in a physical interaction volume, and truncate terms of formal order $1/\tilde{N}_j^{3/2}$. This is achieved by use of the formal definition of a scaled Wigner function $W^\psi$ [28], satisfying a scaled equation in terms of dimensionless scaled fields $\psi$, with:

$$\begin{aligned}
\tau &= t/t_c, \\
\psi_j &= \Psi_j\sqrt{\ell_c/\tilde{N}_j}, \\
\mathcal{A}_j^\psi &= t_c\sqrt{\ell_c/\tilde{N}_j}\mathcal{A}_j + \mathcal{O}\left(1/\tilde{N}_j^2\right), \\
\mathcal{D}_{jk}^\psi &= t_c\left(\ell_c/\tilde{N}_j\right)\mathcal{D}_{jk} + \mathcal{O}\left(1/\tilde{N}_j^2\right).
\end{aligned} \tag{5.20}$$

Here $t_c$ is a characteristic interaction time, and $\ell_c$ is a characteristic interaction length.

These would normally be chosen as the healing time and healing length respectively in a BEC calculation. Typically the cell size is chosen to be proportional to the healing length, for optimum accuracy in resolving spatial detail. Using this expansion, a consistent order-by-order expansion in $1/\sqrt{\tilde{N}_j}$ can be obtained, of form:

$$\frac{\mathrm{d}W^{\psi}}{\mathrm{d}\tau} = \int \mathrm{d}\mathbf{x} \left\{ -\sum_{j=1}^{C} \frac{\delta}{\delta\psi_j} \mathcal{A}_j^{\psi} - \sum_{j=1}^{C} \frac{\delta}{\delta\psi_j^*} \mathcal{A}_j^{\psi *} + \sum_{j=1}^{C} \sum_{k=1}^{C} \frac{\delta^2}{\delta\psi_j^* \delta\psi_k} \mathcal{D}_{jk}^{\psi} + \mathcal{O}\left[ \frac{1}{\tilde{N}_j^{3/2}} \right] \right\} W^{\psi}. \tag{5.21}$$

With the assumption of the state being coherent, the simple condition for truncation — that is, omitting terms of the order $\mathcal{O}(1/\tilde{N}_j^{3/2})$ — can be shown to be [57]

$$N_j \gg |\mathbb{M}_j|, \tag{5.22}$$

where $N_j$ is the total number of atoms of the component $j$. The inclusion of the mode factor is caused by the fact that the number of additional terms increases as the number of modes increases, which may be needed to treat convergence of the method for large momentum cutoff. We see immediately that there are subtleties involved if one wishes to include larger numbers of high-momentum modes, since this increases the mode number while leaving the numbers unchanged. In other words, the truncation technique is inherently restricted in its ability to resolve fine spatial details in the high-momentum cutoff limit. The truncation condition (5.22) has a stronger form expressed in terms of component density [39]

$$\delta_{\mathbb{M}_j}(\mathbf{x}, \mathbf{x}) \ll |\Psi_j|^2. \tag{5.23}$$

The coherency assumption does not, of course, encompass all possible states that can be produced during evolution, which means that the condition above is more of a guide than a restriction. For certain systems, the truncation was shown to work even when (5.23) is violated [35]. The validity may also depend on the simulation time [68], and other physically relevant factors.

A common example of such relevant factors is that there can be a large difference in the size of the original parameters. To illustrate this issue, one may have a situation where $\kappa_1 \approx \kappa_2 \tilde{N}_j$ even though $\tilde{N}_j \gg 1$. Under these conditions, it is essential to include

a scaling of the parameters in calculating the formal order so that the scaled parameters have comparable sizes. This allows one to identify correctly which terms are negligible in a given physical problem, and which terms must be included.

In general, one can estimate the validity of truncation for the particular problem and the particular observable by calculating the quantum correction [56]. Other techniques for estimating validity include comparison with the exact positive-P simulation method [28], and examining results for unphysical behavior such as negative occupation numbers [27].

The use of this Wigner truncation allows us to simplify the results of Theorem 4.3 and Theorem 4.4. Wigner truncation is an expansion up to the order $1/\tilde{N}_j$, so during the simplification, along with the higher order derivatives, we drop all components with $\delta_{\mathbb{M}_j}$ of order higher than 1 in the drift terms, and of order higher than 0 in the diffusion terms.

**Theorem 5.3.** *Assuming the conditions for the Wigner truncation are satisfied, the result of the Wigner transformation of the nonlinear term of a Hamiltonian is*

$$\mathcal{W}\left[\left[\int \mathrm{d}\mathbf{x}\frac{U_{jk}}{2}\tilde{\Psi}_j^\dagger\tilde{\Psi}_k^\dagger\tilde{\Psi}_j\tilde{\Psi}_k,\hat{\rho}\right]\right] \approx \int \mathrm{d}\mathbf{x}U_{jk}\left(\frac{\delta}{\delta\Psi_j}\left(-\Psi_j\Psi_k\Psi_k^* + \frac{\delta_{\mathbb{M}_k}(\mathbf{x},\mathbf{x})}{2}(\delta_{jk}\Psi_k+\Psi_j)\right)\right.$$
$$\left.+\frac{\delta}{\delta\Psi_j^*}\left(\Psi_j^*\Psi_k\Psi_k^* - \frac{\delta_{\mathbb{M}_k}(\mathbf{x},\mathbf{x})}{2}(\delta_{jk}\Psi_k^*+\Psi_j^*)\right)\right)W.$$

*Proof.* A straightforward result of neglecting the high-order terms in (5.18). □

**Theorem 5.4.** *Assuming the conditions for the Wigner truncation are satisfied, the result of the Wigner transformation of the loss term is*

$$\mathcal{W}[\mathcal{L}_\mathrm{l}[\hat{\rho}]] \approx \left(\sum_{m=1}^{C}\frac{\delta}{\delta\Psi_m^*}\left(\frac{\partial O_\mathrm{l}}{\partial\Psi_m}O_\mathrm{l}^* - \frac{1}{2}\sum_{n=1}^{C}\delta_{\mathbb{M}_n}(\mathbf{x},\mathbf{x})\frac{\partial^2 O_\mathrm{l}}{\partial\Psi_m\partial\Psi_n}\frac{\partial O_\mathrm{l}^*}{\partial\Psi_n^*}\right)\right.$$
$$+\sum_{m=1}^{C}\frac{\delta}{\delta\Psi_m}\left(\frac{\partial O_\mathrm{l}^*}{\partial\Psi_m^*}O_\mathrm{l} - \frac{1}{2}\sum_{n=1}^{C}\delta_{\mathbb{M}_n}(\mathbf{x},\mathbf{x})\frac{\partial^2 O_\mathrm{l}^*}{\partial\Psi_m^*\partial\Psi_n^*}\frac{\partial O_\mathrm{l}}{\partial\Psi_n}\right)$$
$$\left.+\sum_{m=1}^{C}\sum_{n=1}^{C}\frac{\delta^2}{\delta\Psi_m^*\delta\Psi_n}\frac{\partial O_\mathrm{l}}{\partial\Psi_m}\frac{\partial O_\mathrm{l}^*}{\partial\Psi_n^*}\right)W,$$

*where the coupling functionals* $O_\mathrm{l} \equiv O_\mathrm{l}[\boldsymbol{\Psi}] = \prod_{c=1}^{C}\Psi_c^{l_c}$.

*Proof.* The proof is basically a simplification of the result of Theorem 4.4 under two conditions following from neglecting the terms smaller than $1/N$. First, we are dropping all terms with high order differentials, which can be expressed as limiting $\sum j_c + \sum k_c \leq 2$. Second, we are only considering the terms with the restricted delta function of up to first

order in the drift part (containing functional differentials of order 1), and terms with no restricted delta functions in the diffusion part (containing functional differentials of order 2).

The only combinations of $j_c$ and $k_c$ for which $Z_{\mathbf{l},\mathbf{j},\mathbf{k}}$ is not zero are thus $\{j_c = \delta_{cm}, k_c = 0, m \in [1,C]\}$, $\{j_c = 0, k_c = \delta_{cm}, m \in [1,C]\}$ and $\{j_c = \delta_{cm}, k_c = \delta_{cn}, m \in [1,C], n \in [1,C]\}$. These combinations produce terms with $\delta/\delta\Psi^*_n$, $\delta/\delta\Psi_n$ and $\delta^2/\delta\Psi_p\delta\Psi^*_n$, respectively:

$$\begin{aligned}\mathcal{W}[\mathcal{L}_{\mathbf{l}}[\hat{\rho}]] \approx \Bigg( &\sum_{m=1}^{C} \frac{\delta}{\delta\Psi^*_m} H[l_m - 1] Z_{\mathbf{l},\mathbf{e}_m,\mathbf{0}} + \sum_{m=1}^{C} \frac{\delta}{\delta\Psi_m} H[l_m - 1] Z_{\mathbf{l},\mathbf{0},\mathbf{e}_m} \\ &+ \sum_{m=1}^{C}\sum_{n=1}^{C} \frac{\delta^2}{\delta\Psi^*_m\delta\Psi^*_n} H[l_m - 1] H[l_n - 1] Z_{\mathbf{l},\mathbf{e}_m,\mathbf{e}_n} \Bigg) W,\end{aligned} \tag{5.24}$$

where $\mathbf{e}_n$ is a vector consisting of zeros and a single 1 at the $n$-th position, and $H[n]$ is the discrete Heavyside function.

Evaluating the partially parametrised $Z$ function in the first term using the expression in Theorem 4.4:

$$Z_{\mathbf{l},\mathbf{e}_m,\mathbf{0}} = l_m \prod_{c=1}^{C} \exp\left( -\frac{\delta_{\mathbb{M}_c}(\mathbf{x},\mathbf{x})}{2} \frac{\partial^2}{\partial\Psi_c\partial\Psi^*_c} \right) \Psi_c^{l_c - \delta_{cm}} (\Psi^*_c)^{l_c}. \tag{5.25}$$

Expanding the exponent in series and discarding the terms with more than one restricted delta function, we obtain:

$$Z_{\mathbf{l},\mathbf{e}_m,\mathbf{0}} \approx l_m \left( \prod_{c=1}^{C} \Psi_c^{l_c - \delta_{cm}} (\Psi^*_c)^{l_c} - \frac{1}{2} \sum_{n=1}^{C} \delta_{\mathbb{M}_n}(\mathbf{x},\mathbf{x}) \frac{\partial^2}{\partial\Psi_n\partial\Psi^*_p} \prod_{c=1}^{C} \Psi_c^{l_c - \delta_{cm}} (\Psi^*_c)^{l_c} \right). \tag{5.26}$$

Multiplied by the Heavyside function, this can be expressed using derivatives of the coupling functional $O_{\mathbf{l}}$:

$$H[l_m - 1] Z_{\mathbf{l},\mathbf{e}_m,\mathbf{0}} \approx \frac{\partial O_{\mathbf{l}}}{\partial\Psi_m} O^*_{\mathbf{l}} - \frac{1}{2} \sum_{n=1}^{C} \delta_{\mathbb{M}_n}(\mathbf{x},\mathbf{x}) \frac{\partial^2 O_{\mathbf{l}}}{\partial\Psi_m\partial\Psi_n} \frac{\partial O^*_{\mathbf{l}}}{\partial\Psi^*_n}. \tag{5.27}$$

Analogously, for the second term in (5.24) we get

$$H[l_m - 1] Z_{\mathbf{l},\mathbf{0},\mathbf{e}_m} \approx \frac{\partial O^*_{\mathbf{l}}}{\partial\Psi^*_m} O_{\mathbf{l}} - \frac{1}{2} \sum_{n=1}^{C} \delta_{\mathbb{M}_n}(\mathbf{x},\mathbf{x}) \frac{\partial^2 O^*_{\mathbf{l}}}{\partial\Psi^*_m\partial\Psi^*_n} \frac{\partial O_{\mathbf{l}}}{\partial\Psi_n}, \tag{5.28}$$

and for the third term (discarding all terms with the restricted delta function in the

expansion of the exponent):

$$H[l_m - 1]H[l_n - 1]Z_{\mathbf{l},\mathbf{e}_m,\mathbf{e}_n} \approx \frac{\partial O_\mathbf{l}}{\partial \Psi_m}\frac{\partial O_\mathbf{l}^*}{\partial \Psi_n^*}. \tag{5.29}$$

Substituting these expressions back into (5.24), we get the statement of the theorem. □

## 5.5. Fokker-Planck equation for the BEC

With the Wigner truncation applied, we can remove the third- and higher-order functional derivatives in (5.19). Under the reasonable assumption of $K_{jk}$, $U_{jk}$ and $\kappa_\mathbf{l}$ being real-valued, this results in the functional equation

$$\frac{\mathrm{d}W}{\mathrm{d}t} = \int \mathrm{d}\mathbf{x}\left(-\sum_{j=1}^{C}\frac{\delta}{\delta\Psi_j}\mathcal{A}_j - \sum_{j=1}^{C}\frac{\delta}{\delta\Psi_j^*}\mathcal{A}_j^* + \sum_{j=1}^{C}\sum_{k=1}^{C}\frac{\delta^2}{\delta\Psi_j^*\delta\Psi_k}\mathcal{D}_{jk}\right)W, \tag{5.30}$$

with drift terms

$$\begin{aligned}\mathcal{A}_j = &-\frac{i}{\hbar}\left(\sum_{k=1}^{C}K_{jk}\Psi_k + \Psi_j\sum_{k=1}^{C}U_{jk}\left(|\Psi_k|^2 - \frac{\delta_{jk}+1}{2}\delta_{\mathbb{M}_k}(\mathbf{x},\mathbf{x})\right)\right)\\ &-\sum_{\mathbf{l}\in L}\kappa_\mathbf{l}\left(\frac{\partial O_\mathbf{l}^*}{\partial\Psi_j^*}O_\mathbf{l} - \frac{1}{2}\sum_{k=1}^{C}\delta_{\mathbb{M}_k}(\mathbf{x},\mathbf{x})\frac{\partial^2 O_\mathbf{l}^*}{\partial\Psi_j^*\partial\Psi_k^*}\frac{\partial O_\mathbf{l}}{\partial\Psi_k}\right),\end{aligned} \tag{5.31}$$

and diffusion matrix

$$\mathcal{D}_{jk} = \sum_{\mathbf{l}\in L}\kappa_\mathbf{l}\frac{\partial O_\mathbf{l}}{\partial\Psi_j}\frac{\partial O_\mathbf{l}^*}{\partial\Psi_k^*}. \tag{5.32}$$

It can be shown (see Appendix C for details) that this truncated equation has a positive-definite diffusion matrix $\mathcal{D}$ and is, therefore, a Fokker-Planck equation (FPE), with its solution $W(t)$ being a probability distribution (provided that $W(0)$ was a probability distribution). This differs from the original Wigner function(al), which can be negative, and is the result of the truncation. Thus, the solution of this equation may not be equivalent to the solution of the original master equation (5.4), if the corresponding density matrices have non-positive Wigner functions. If the truncation condition is satisfied, the difference is small (see Chapter 6 for a simple comparison, and references therein).

A direct solution of the above FPE is generally impractical, and a Monte Carlo or a sampled calculation is called for. The equation can be further transformed to an equivalent

set of stochastic differential equations (SDEs) using Theorem C.3 with

$$\mathcal{B}_{j\mathbf{l}} = \sqrt{\kappa_{\mathbf{l}}}\frac{\partial O_{\mathbf{l}}^*}{\partial \Psi_j^*}. \tag{5.33}$$

This results in the set of functional SDEs in the Itô form

$$\mathrm{d}\Psi_j = \mathcal{P}_{\mathbb{M}_j}\left[\mathcal{A}_j \mathrm{d}t + \sum_{\mathbf{l}\in L}\mathcal{B}_{j\mathbf{l}}\mathrm{d}Q_{\mathbf{l}}\right], \tag{5.34}$$

or, alternatively, in the Stratonovich form

$$\mathrm{d}\Psi_j = \mathcal{P}_{\mathbb{M}_j}\left[(\mathcal{A}_j - \mathcal{S}_j)\mathrm{d}t + \sum_{\mathbf{l}\in L}\mathcal{B}_{j\mathbf{l}}\mathrm{d}Q_{\mathbf{l}}\right], \tag{5.35}$$

where the Stratonovich term is

$$\begin{aligned}\mathcal{S}_j &= \frac{1}{2}\sum_{k=1}^{C}\sum_{\mathbf{l}\in L}\mathcal{B}_{k\mathbf{l}}^*\frac{\delta}{\delta\Psi_k^*}\mathcal{B}_{j\mathbf{l}} \\ &= \frac{1}{2}\sum_{k=1}^{C}\sum_{\mathbf{l}\in L}\delta_{\mathbb{M}_k}(\mathbf{x},\mathbf{x})\frac{\partial^2 O_{\mathbf{l}}^*}{\partial\Psi_k^*\partial\Psi_j^*}\frac{\partial O_{\mathbf{l}}}{\partial\Psi_k}.\end{aligned} \tag{5.36}$$

Note that the Stratonovich term is exactly equal to the correction proportional to $\delta_{\mathbb{M}_k}$ in the loss-induced part of the drift term (5.31). This means that in the Stratonovich form the SDEs are actually simpler. Physically, this corresponds to the fact that the Stratonovich form is the broad-band limit of a finite bandwidth noise equation. Hence, one expects this to occur as the most natural equation in the Markovian master equation limit of damping.

The equations (5.34) can be solved by conventional integration methods for SDEs (see Appendix E for details). The required expectations of symmetrically ordered operator products can be obtained by averaging results from multiple independent integration trajectories according to Theorem 3.4, since the truncated Wigner functional is a probability distribution:

$$\begin{aligned}\left\langle\left\{\prod_{j=1}^{C}\tilde{\Psi}_j^{r_j}(\tilde{\Psi}_j^\dagger)^{s_j}\right\}_{\mathrm{sym}}\right\rangle &= \int \delta^2\boldsymbol{\Psi}\left(\prod_{j=1}^{C}\Psi_j^{r_j}(\Psi_j^*)^{s_j}\right)W[\boldsymbol{\Psi}] \\ &\approx \left\langle\prod_{j=1}^{C}\Psi_j^{r_j}(\Psi_j^*)^{s_j}\right\rangle_{\mathrm{traj}},\end{aligned} \tag{5.37}$$

where $\{r_j\}$ and $\{s_j\}$ are some sets of non-negative integers. The second approximate equality becomes exact in the limit of the infinite number of integration trajectories.

## 5.6. Integral averages

It is interesting to derive an expression for the time dependence of some simple observables using SDEs (5.34) and Itô's formula (Theorem C.6). Namely, we are interested in the population $N_i = \int \mathrm{d}\mathbf{x} \langle \tilde{\Psi}_i^\dagger \tilde{\Psi}_i \rangle$. We will first prove a general theorem which is valid for any drift and diffusion terms, and then apply it to the concrete expressions (5.31) and (5.32).

**Theorem 5.5.** *In a BEC with the evolution governed by the set of SDEs (5.34), the population changes in time as*

$$\frac{\mathrm{d}N_i}{\mathrm{d}t} = \int \mathrm{d}\mathbf{x} \left\langle \mathcal{A}_i \Psi_i^* + \mathcal{A}_i^* \Psi_i + \sum_{\mathbf{l}\in L} \mathcal{B}_{i\mathbf{l}} \mathcal{B}_{i\mathbf{l}}^* \delta_{\mathbb{M}_i}(\mathbf{x},\mathbf{x}) \right\rangle_{\mathrm{traj}} .$$

*Proof.* Let us apply Theorem C.6 with $f_j \equiv \Psi_j$ to $\mathcal{F} \equiv \Psi_i^* \Psi_i$. Since, in the end, we are interested in the average of $\mathcal{F}$, and $\langle dQ_{\mathbf{l}} \rangle_{\mathrm{traj}} \equiv 0$, we can discard the third term in the Itô formula. The resulting expression for the differential is

$$\begin{aligned} \mathrm{d}(\Psi_i^* \Psi_i) = \int \mathrm{d}\mathbf{x}' \Bigg( & \sum_{j=1}^{C} \mathcal{A}'_j \frac{\delta(\Psi_i^* \Psi_i)}{\delta \Psi'_j} + \sum_{j=1}^{C} \mathcal{A}'^*_j \frac{\delta(\Psi_i^* \Psi_i)}{\delta \Psi'^*_j} \\ & + \sum_{j=1}^{C} \sum_{k=1}^{C} \sum_{\mathbf{l}\in L} \mathcal{B}'_{j\mathbf{l}} \mathcal{B}'^*_{k\mathbf{l}} \frac{\delta^2(\Psi_i^* \Psi_i)}{\delta \Psi'_j \delta \Psi'^*_k} \Bigg) \mathrm{d}t. \end{aligned} \tag{5.38}$$

The derivatives are evaluated as

$$\begin{aligned} \frac{\delta(\Psi_i^* \Psi_i)}{\delta \Psi'_j} &= \delta_{ij} \Psi_i^* \delta_{\mathbb{M}_i}(\mathbf{x}',\mathbf{x}), \\ \frac{\delta(\Psi_i^* \Psi_i)}{\delta \Psi'^*_j} &= \delta_{ij} \Psi_i \delta^*_{\mathbb{M}_i}(\mathbf{x}',\mathbf{x}), \\ \frac{\delta^2(\Psi_i^* \Psi_i)}{\delta \Psi'_j \delta \Psi'^*_k} &= \delta_{ij}\delta_{ik} \delta_{\mathbb{M}_i}(\mathbf{x}',\mathbf{x}) \delta^*_{\mathbb{M}_i}(\mathbf{x}',\mathbf{x}). \end{aligned} \tag{5.39}$$

From (5.37), it follows that

$$\begin{aligned}\frac{\mathrm{d}N_i}{\mathrm{d}t} &= \int \mathrm{d}\mathbf{x}\frac{\mathrm{d}\langle\tilde{\Psi}_i^*\tilde{\Psi}_i\rangle}{\mathrm{d}t} \\ &\approx \int \mathrm{d}\mathbf{x}\frac{\mathrm{d}(\langle\Psi_i^*\Psi_i\rangle_{\text{traj}} - \frac{1}{2}\delta_{\mathbb{M}_i}(\mathbf{x},\mathbf{x}))}{\mathrm{d}t} = \int \mathrm{d}\mathbf{x}\left\langle\frac{\mathrm{d}(\Psi_i^*\Psi_i)}{\mathrm{d}t}\right\rangle_{\text{traj}}.\end{aligned} \tag{5.40}$$

Substituting the expression for the differential of $\Psi_i^*\Psi_i$, we get

$$\begin{aligned}\frac{\mathrm{d}N_i}{\mathrm{d}t} = \iint \mathrm{d}\mathbf{x}\,\mathrm{d}\mathbf{x}' \Big\langle &\mathcal{A}_i'\Psi_i^*\delta_{\mathbb{M}_i}(\mathbf{x}',\mathbf{x}) + \mathcal{A}_i'^*\Psi_i\delta_{\mathbb{M}_i}^*(\mathbf{x}',\mathbf{x}) \\ &+ \sum_{\mathbf{l}\in L}\mathcal{B}_{i\mathbf{l}}'\mathcal{B}_{i\mathbf{l}}'^*\delta_{\mathbb{M}_i}(\mathbf{x}',\mathbf{x})\delta_{\mathbb{M}_i}^*(\mathbf{x}',\mathbf{x})\Big\rangle_{\text{traj}},\end{aligned} \tag{5.41}$$

where we were able to move the integral over $\mathbf{x}$ since the drift and diffusion terms depend on $\mathbf{x}'$. Integrating by $\mathbf{x}$, and expanding $\Psi_i$ and restricted delta functions:

$$\begin{aligned}\iint \mathrm{d}\mathbf{x}\,\mathrm{d}\mathbf{x}'\mathcal{A}_i'\Psi_i^*\delta_{\mathbb{M}_i}(\mathbf{x}',\mathbf{x}) &= \iint \mathrm{d}\mathbf{x}\,\mathrm{d}\mathbf{x}'\mathcal{A}_i'\sum_{\mathbf{n}\in\mathbb{M}_i}\phi_{i,\mathbf{n}}^*\alpha_{i,\mathbf{n}}^*\sum_{\mathbf{m}\in\mathbb{M}_i}\phi_{i,\mathbf{m}}\phi_{i,\mathbf{m}}'^* \\ &= \int \mathrm{d}\mathbf{x}'\mathcal{A}_i'\sum_{\mathbf{m}\in\mathbb{M}_i}\alpha_{i,\mathbf{n}}^*\phi_{i,\mathbf{n}}'^* \\ &= \int \mathrm{d}\mathbf{x}\mathcal{A}_i\Psi_i^*.\end{aligned} \tag{5.42}$$

Similarly,

$$\iint \mathrm{d}\mathbf{x}\,\mathrm{d}\mathbf{x}'\mathcal{A}_i'^*\Psi_i\delta_{\mathbb{M}_i}^*(\mathbf{x}',\mathbf{x}) = \int \mathrm{d}\mathbf{x}\mathcal{A}_i^*\Psi_i, \tag{5.43}$$

and

$$\iint \mathrm{d}\mathbf{x}\,\mathrm{d}\mathbf{x}'\mathcal{B}_{i\mathbf{l}}'\mathcal{B}_{i\mathbf{l}}'^*\delta_{\mathbb{M}_i}(\mathbf{x}',\mathbf{x})\delta_{\mathbb{M}_i}^*(\mathbf{x}',\mathbf{x}) = \int \mathrm{d}\mathbf{x}\mathcal{B}_{i\mathbf{l}}\mathcal{B}_{i\mathbf{l}}^*\delta_{\mathbb{M}_i}(\mathbf{x},\mathbf{x}). \tag{5.44}$$

The integration of the equation (5.41) over $\mathbf{x}$ thus gives us the statement of the theorem.

□

Now we can substitute the known expressions for drift terms (5.31) and diffusion terms (5.32) in the equation given by the theorem. We will consider the case with with the absence of a population transfer between components (i.e., $K_{jk} \equiv 0$ if $j \neq k$), which would unnecessarily complicate the resulting equation. From the form of the expression $\mathcal{A}_i\Psi_i^* + \mathcal{A}_i^*\Psi_i$ it is clear that the unitary evolution part of the drift term does not contribute

to the population change rate (which agrees with the intuition). Thus, the drift terms can be safely simplified to

$$\mathcal{A}_i^{(\mathrm{loss})} = -\sum_{\mathrm{l}\in L} \kappa_{\mathrm{l}} \left( \frac{\partial O_{\mathrm{l}}^*}{\partial \Psi_i^*} O_{\mathrm{l}} - \frac{1}{2} \sum_{k=1}^{C} \delta_{\mathbb{M}_k}(\mathbf{x},\mathbf{x}) \frac{\partial^2 O_{\mathrm{l}}^*}{\partial \Psi_i^* \partial \Psi_k^*} \frac{\partial O_{\mathrm{l}}}{\partial \Psi_k} \right), \tag{5.45}$$

which gives the population change rate

$$\begin{aligned} \frac{\mathrm{d}N_i}{\mathrm{d}t} = -\sum_{\mathrm{l}\in L} \kappa_{\mathrm{l}} \int \mathrm{d}\mathbf{x} \Bigg\langle & 2\frac{\partial O_{\mathrm{l}}^*}{\partial \Psi_i^*} O_{\mathrm{l}} \Psi_i^* - \sum_{k=1}^{C} \delta_{\mathbb{M}_k}(\mathbf{x},\mathbf{x}) \frac{\partial^2 O_{\mathrm{l}}^*}{\partial \Psi_i^* \partial \Psi_k^*} \frac{\partial O_{\mathrm{l}}}{\partial \Psi_k} \Psi_i^* \\ & - \frac{\partial O_{\mathrm{l}}}{\partial \Psi_i} \frac{\partial O_{\mathrm{l}}^*}{\partial \Psi_i^*} \delta_{\mathbb{M}_i}(\mathbf{x},\mathbf{x}) \Bigg\rangle_{\mathrm{traj}}, \end{aligned} \tag{5.46}$$

where we have used the fact that the coupling functional $O_{\mathrm{l}}$ are products of integer powers of $\Psi_j$, which makes $\mathcal{A}_i^{(\mathrm{loss})} \Psi_j^* \equiv (\mathcal{A}_i^{(\mathrm{loss})})^* \Psi_j$.

In practice, it is more convenient to express the above equation using more intuitive quantities, namely real component densities $n_i = \langle \tilde{\Psi}_i^\dagger \tilde{\Psi}_i \rangle$. To do that, we have to rewrite the resulting path averages of the moments of $\Psi_j$ as averages of symmetric products of $\tilde{\Psi}_j$, transform them to the normal order using the analogue of the ordering transformation formula [59] for field operators

$$\left\{ (\tilde{\Psi}_j^\dagger)^r \tilde{\Psi}_j^s \right\}_{\mathrm{sym}} = \sum_{k=0}^{\min(r,s)} \frac{k!}{2^k} \binom{r}{k} \binom{s}{k} (\tilde{\Psi}^\dagger)^{r-k} \tilde{\Psi}^{s-k} \delta_{\mathbb{M}_j}^k, \tag{5.47}$$

and simplify the resulting averages of normally ordered operators using correlation factors $g^{(k)} = \langle (\tilde{\Psi}^\dagger)^k \tilde{\Psi}^k \rangle / \langle \tilde{\Psi}^\dagger \tilde{\Psi} \rangle$. In other words, the coefficients $g^{(k)}$ define the degree of high-order correlations. In the ideal condensate, these are equal to 1, and increase with the temperature (the so called photon bunching, or atom bunching). For example, the theoretical maximum value for $g_{(3)}$ is $3! = 6$ [69], which has been confirmed experimentally [70].

## 5.7. Usage example

General theorems from the previous sections may seem complicated, so in this section we will look into a simple example of how they can be applied to real systems.

We will consider a simple case of a single-component BEC with a 3-body loss process

and no unitary evolution (the same as described by Norrie *et al* [41]). The master equation for this system is

$$\begin{aligned}\frac{\mathrm{d}\hat{\rho}}{\mathrm{d}t} &= \frac{\gamma}{6}\int \mathrm{d}\mathbf{x}\mathcal{L}_{111}[\hat{\rho}] \\ &\equiv \frac{\gamma}{6}\int \mathrm{d}\mathbf{x}\left(2\tilde{\Psi}^3\hat{\rho}(\tilde{\Psi}^\dagger)^3 - (\tilde{\Psi}^\dagger)^3\tilde{\Psi}^3\hat{\rho} - \hat{\rho}(\tilde{\Psi}^\dagger)^3\tilde{\Psi}^3\right),\end{aligned} \tag{5.48}$$

so we have $K \equiv 0$, $U \equiv 0$ and a single source of losses with $\mathbf{l} = (1,1,1)$ and $\hat{O}_{111} = \tilde{\Psi}^3$ (and, consequently, $O_{111} = \Psi^3$). The coefficient $\gamma = 6\kappa_{111}$ corresponds to the "experimental" normalization of loss rates; see (7.31) and the surrounding paragraph for details. The FPE for this system is, therefore,

$$\begin{aligned}\frac{\mathrm{d}W}{\mathrm{d}t} = &-\frac{\delta}{\delta\Psi}\left(-\frac{\gamma}{2}|\Psi|^4\Psi + \frac{3\gamma}{2}|\Psi|^2\Psi\delta_{\mathbb{M}}(\mathbf{x},\mathbf{x}) - \frac{3\gamma}{4}\Psi\delta^2_{\mathbb{M}}(\mathbf{x},\mathbf{x})\right) \\ &-\frac{\delta}{\delta\Psi^*}\left(-\frac{\gamma}{2}|\Psi|^4\Psi^* + \frac{3\gamma}{2}|\Psi|^2\Psi^*\delta_{\mathbb{M}}(\mathbf{x},\mathbf{x}) - \frac{3\gamma}{4}\Psi^*\delta^2_{\mathbb{M}}(\mathbf{x},\mathbf{x})\right) \\ &+\frac{\delta^2}{\delta\Psi^*\delta\Psi}\left(\frac{3\gamma}{2}|\Psi|^4 - 3\gamma|\Psi|^2\delta_{\mathbb{M}}(\mathbf{x},\mathbf{x}) + \frac{3\gamma}{4}\delta^2_{\mathbb{M}}(\mathbf{x},\mathbf{x})\right) \\ &+\frac{\delta^3}{\delta\Psi^*\delta\Psi^2}\left(\frac{3\gamma}{8}|\Psi|^2\Psi - \frac{3\gamma}{8}\Psi\delta_{\mathbb{M}}(\mathbf{x},\mathbf{x})\right) \\ &+\frac{\delta^3}{\delta(\Psi^*)^2\delta\Psi}\left(\frac{3\gamma}{8}|\Psi|^2\Psi^* - \frac{3\gamma}{8}\Psi^*\delta_{\mathbb{M}}(\mathbf{x},\mathbf{x})\right) \\ &+\frac{\delta}{\delta\Psi^3}\left(\frac{\gamma}{24}\Psi^3\right) + \frac{\delta^3}{\delta(\Psi^*)^3}\left(\frac{\gamma}{24}(\Psi^*)^3\right) + \mathcal{O}\left[\frac{1}{N^4}\right].\end{aligned} \tag{5.49}$$

After truncation, the resulting stochastic equation describing the system is

$$\begin{aligned}\mathrm{d}\Psi &= \mathcal{P}_{\mathbb{M}}\left[-\frac{\gamma}{6}\left(\frac{\partial O^*}{\partial\Psi^*}O - \frac{1}{2}\delta_{\mathbb{M}}(\mathbf{x},\mathbf{x})\frac{\partial^2 O^*}{\partial(\Psi^*)^2}\frac{\partial O}{\partial\Psi}\right)\mathrm{d}t + \sqrt{\frac{\gamma}{6}}\frac{\partial O^*}{\partial\Psi^*}\mathrm{d}Q(\mathbf{x},t)\right] \\ &= \mathcal{P}_{\mathbb{M}}\left[-\left(\frac{\gamma}{2}|\Psi|^4\Psi - \frac{3\gamma}{2}\delta_{\mathbb{M}}(\mathbf{x},\mathbf{x})|\Psi|^2\Psi\right)\mathrm{d}t + \sqrt{\frac{3\gamma}{2}}(\Psi^*)^2\mathrm{d}Q(\mathbf{x},t)\right].\end{aligned} \tag{5.50}$$

The equation above coincides with the one given by Norrie *et al*, except for the additional correction to the drift term, which is of order $1/N$ and, therefore, cannot be omitted.

If we calculate the rate population change over time using Theorem 5.5 and its corollary (5.46), we obtain

$$\frac{\mathrm{d}N}{\mathrm{d}t} = -\gamma\int \mathrm{d}\mathbf{x}\left(\langle|\Psi|^6\rangle_{\mathrm{traj}} - \frac{9}{2}\delta_{\mathbb{M}}(\mathbf{x},\mathbf{x})\langle|\Psi|^4\rangle_{\mathrm{traj}}\right). \tag{5.51}$$

This can be transformed further to a more conventional form. Using the equivalence (5.37)

and the ordering transformation formula (5.47) for field operators, we get

$$\begin{aligned}\langle|\Psi|^4\rangle_{\text{traj}} &= g^{(2)}n^2 + 2\delta_{\mathbb{M}}(\mathbf{x},\mathbf{x})n + \frac{1}{2}\delta^2_{\mathbb{M}}(\mathbf{x},\mathbf{x}),\\ \langle|\Psi|^6\rangle_{\text{traj}} &= g^{(3)}n^3 + \frac{9}{2}\delta_{\mathbb{M}}(\mathbf{x},\mathbf{x})g^{(2)}n^2 + \frac{9}{2}\delta^2_{\mathbb{M}}(\mathbf{x},\mathbf{x})n + \frac{3}{4}\delta^3_{\mathbb{M}}(\mathbf{x},\mathbf{x}).\end{aligned} \tag{5.52}$$

Here $n = \langle\tilde{\Psi}^\dagger\tilde{\Psi}\rangle$ is the particle density, and $g^{(k)}$ are correlation factors. Substituting above expressions into the equation for the population change rate:

$$\frac{\mathrm{d}N}{\mathrm{d}t} = -\gamma\int \mathrm{d}\mathbf{x}\left(g^{(3)}n^3 - \frac{9}{2}\delta^2_{\mathbb{M}}(\mathbf{x},\mathbf{x})n - \frac{3}{2}\delta^3_{\mathbb{M}}(\mathbf{x},\mathbf{x})\right). \tag{5.53}$$

We see that the second highest term in the expression is canceled, which agrees with the expansion being correct up to the order $1/N$. If the quantum correction term to the drift is omitted, one finds that a physically incorrect quadratic nonlinear term proportional to $n^2$ is obtained, which is inconsistent with the exact short-time solution to the master equation [41]. The last two terms in this result are artefacts of the truncated Wigner method. They give rise to loss processes that occur even when $N = 0$, which, of course, is physically impossible.

## 5.8. Initial states

Before integrating the evolution equations (5.34) or (5.35), the initial value of $\Psi_j$ at $t = 0$ has to be sampled for each integration trajectory. The general procedure is to take the density matrix of the desired initial state and find its Wigner transformation using Definition 3.4. The resulting Wigner function is then sampled.

### 5.8.1. Coherent state

The simplest case of an initial state is a coherent state. It also serves as a good first approximation for most BEC interferometry experiments.

**Theorem 5.6.** *The Wigner distribution for a multimode coherent state with the expectation value* $\Psi^{(0)} \equiv \sum_{\mathbf{n}\in\mathbb{M}} \alpha^{(0)}_{\mathbf{n}}\phi_{\mathbf{n}}$ *is*

$$W_{\text{coh}}[\Psi] = \left(\frac{2}{\pi}\right)^{|\mathbb{M}|}\prod_{\mathbf{n}\in\mathbb{M}}\exp(-2|\alpha_{\mathbf{n}} - \alpha^{(0)}_{\mathbf{n}}|^2).$$

*Proof.* The density matrix of the state is

$$\hat{\rho} = |\alpha_{\mathbf{n}}^{(0)}, \mathbf{n} \in \mathbb{M}\rangle\langle\alpha_{\mathbf{n}}^{(0)}, \mathbf{n} \in \mathbb{M}| = \left(\prod_{\mathbf{n}\in\mathbb{M}} |\alpha_{\mathbf{n}}^{(0)}\rangle\right)\left(\prod_{\mathbf{n}\in\mathbb{M}} \langle\alpha_{\mathbf{n}}^{(0)}|\right). \tag{5.54}$$

Then the characteristic functional for this state can be expressed as

$$\begin{aligned}\chi_W[\Lambda] &= \mathrm{Tr}\left\{\left(\prod_{\mathbf{n}\in\mathbb{M}} |\alpha_{\mathbf{n}}^{(0)}\rangle\right)\left(\prod_{\mathbf{n}\in\mathbb{M}} \langle\alpha_{\mathbf{n}}^{(0)}|\right)\left(\prod_{\mathbf{n}\in\mathbb{M}} \hat{D}_{\mathbf{n}}(\lambda_{\mathbf{n}}, \lambda_{\mathbf{n}}^*)\right)\right\} \\ &= \prod_{\mathbf{n}\in\mathbb{M}} \langle\alpha_{\mathbf{n}}^{(0)}|\hat{D}_{\mathbf{n}}(\lambda_{\mathbf{n}}, \lambda_{\mathbf{n}}^*)|\alpha_{\mathbf{n}}^{(0)}\rangle,\end{aligned} \tag{5.55}$$

where $\Lambda = \sum_{\mathbf{n}\in\mathbb{M}} \lambda_{\mathbf{n}}\phi_{\mathbf{n}}$. Displacement operators obey the multiplication law [59]

$$\hat{D}(\lambda, \lambda^*)\hat{D}(\alpha, \alpha^*) = \hat{D}(\lambda + \alpha, \lambda^* + \alpha^*)\exp(\frac{1}{2}(\lambda\alpha^* - \lambda^*\alpha)), \tag{5.56}$$

and the scalar product of two coherent state is calculated as [59]

$$\langle\beta|\alpha\rangle = \exp(-\frac{1}{2}|\alpha|^2 - \frac{1}{2}|\beta|^2 + \beta^*\alpha). \tag{5.57}$$

Therefore,

$$\begin{aligned}\hat{D}(\lambda, \lambda^*)|\alpha\rangle &= \hat{D}(\lambda, \lambda^*)\hat{D}(\alpha, \alpha^*)|0\rangle \\ &= \exp(\frac{1}{2}(\lambda\alpha^* - \lambda^*\alpha))|\lambda + \alpha\rangle,\end{aligned} \tag{5.58}$$

and the characteristic functional can be simplified as:

$$\begin{aligned}\chi_W[\Lambda] &= \prod_{\mathbf{n}\in\mathbb{M}} \exp(\frac{1}{2}(\lambda_{\mathbf{n}}(\alpha_{\mathbf{n}}^{(0)})^* - \lambda_{\mathbf{n}}^*\alpha_{\mathbf{n}}^{(0)}))\langle\alpha_{\mathbf{n}}^{(0)}|\lambda_{\mathbf{n}} + \alpha_{\mathbf{n}}^{(0)}\rangle \\ &= \prod_{\mathbf{n}\in\mathbb{M}} \exp(-\lambda_{\mathbf{n}}^*\alpha_{\mathbf{n}}^{(0)} + \lambda_{\mathbf{n}}(\alpha_{\mathbf{n}}^{(0)})^* - \frac{1}{2}|\lambda|^2).\end{aligned} \tag{5.59}$$

Finally, the Wigner functional is

$$\begin{aligned}W_c[\Psi] &= \frac{1}{\pi^{2|\mathbb{M}|}}\prod_{\mathbf{n}\in\mathbb{M}}\left(\int \mathrm{d}^2\lambda_{\mathbf{n}} \exp(-\lambda_{\mathbf{n}}(\alpha_{\mathbf{n}}^* - (\alpha_{\mathbf{n}}^{(0)})^*) + \lambda_{\mathbf{n}}^*(\alpha_{\mathbf{n}} - \alpha_{\mathbf{n}}^{(0)}) - \frac{1}{2}|\lambda|^2)\right) \\ &= \left(\frac{2}{\pi}\right)^{|\mathbb{M}|}\prod_{\mathbf{n}\in\mathbb{M}} \exp(-2|\alpha_{\mathbf{n}} - \alpha_{\mathbf{n}}^{(0)}|^2).\end{aligned}$$

□

The resulting Wigner distribution is a product of independent complex-valued Gaussian

distributions for each mode, with an expectation value equal to the expectation value of the mode, and the variance equal to $\frac{1}{2}$. Therefore, the initial state can be sampled as

$$\alpha_{\mathbf{n}} = \alpha_{\mathbf{n}}^{(0)} + \frac{1}{\sqrt{2}}\eta_{\mathbf{n}}, \tag{5.60}$$

where $\eta_{\mathbf{n}}$ are normally distributed complex random numbers with zero mean, $\langle \eta_{\mathbf{m}} \eta_{\mathbf{n}} \rangle = 0$ and $\langle \eta_{\mathbf{m}} \eta_{\mathbf{n}}^* \rangle = \delta_{\mathbf{m},\mathbf{n}}$, or, in other words, with components distributed independently with variance $\frac{1}{2}$. Physically, this looks like adding half a "vacuum particle" to each mode. In the functional form, the coherent initial condition can be written as

$$\Psi_j(\mathbf{x}, 0) = \Psi_j^{(0)}(\mathbf{x}, 0) + \sum_{\mathbf{n}\in\mathbb{M}} \frac{\eta_{j,\mathbf{n}}}{\sqrt{2}} \phi_{\mathbf{n}}(\mathbf{x}), \tag{5.61}$$

where $\Psi_j^{(0)}(\mathbf{x}, 0)$ is the "classical" ground state of the system.

### 5.8.2. Other cases

While sampling the coherent state is computationally easy, it is not the best choice for multimode systems. More involved examples, including thermalized states and Bogoliubov states, are reviewed by Blakie *et al* [55], Olsen and Bradley [71], and Ruostekoski and Martin [72]. In particular, a numerically efficient way to sample a Wigner distribution for Bogoliubov states has been developed by Sinatra *et al* [57].

# Chapter 6.

# Comparison with an exact method

The first test for an approximate theory is usually a comparison with exact analytical predictions, when it is possible. For systems where the functional truncated Wigner method really shines — the ones with hundreds of thousands of particles and thousands of modes — no exact methods exist. However, one can perform such a comparison for the multimode truncated Wigner with only a few modes. While it does not demonstrate the full extent of the truncated Wigner's functionality, it can still give a general idea about the accuracy of the method. In this chapter we will investigate a simple two-level system, the dynamics of which can be described exactly using an expansion in number states, and simulate its evolution using the Wigner representation.

## 6.1. Two-mode BEC example

We consider a single-well two-mode BEC system with the Hamiltonian

$$\hat{H}/\hbar = \frac{1}{2}\sum_{i,j=1}^{2} g_{jk}\hat{a}_j^\dagger \hat{a}_k^\dagger \hat{a}_k \hat{a}_j, \tag{6.1}$$

which is a special case of the two-well four-mode system described elsewhere [44]. To simplify the equations, we use the dimensionless variables $\tilde{g}_{jk} = g_{jk}/(g_{11}N) \equiv a_{jk}/(a_{11}N)$, $\tau = g_{11}Nt$, where $a_{jk}$ is the $s$-wave scattering length for the interaction between modes $j$ and $k$:

$$\tilde{H} = \frac{1}{2}\sum_{i,j=1}^{2} \tilde{g}_{jk}\hat{a}_j^\dagger \hat{a}_k^\dagger \hat{a}_k \hat{a}_j. \tag{6.2}$$

The evolution starts from the coherent state

$$\Psi(0) = \left|\sqrt{N/2}\right\rangle_1 \left|\sqrt{N/2}\right\rangle_2, \tag{6.3}$$

where $N$ stands for the initial total number of atoms in the well.

In the Schrödinger picture, the evolution of the system is governed by the master equation

$$\frac{\mathrm{d}\hat{\rho}}{\mathrm{d}\tau} = -i\left[\tilde{H}, \hat{\rho}\right]. \tag{6.4}$$

After the transformation to an FPE form with Theorem 2.4, truncation, and further transformation with Theorem C.2, this equation turns into the equivalent system of ODEs

$$\mathrm{d}\begin{pmatrix}\alpha_1\\ \alpha_2\end{pmatrix} = -i\begin{pmatrix}\alpha_1\left(\tilde{g}_{11}\left(|\alpha_1|^2-1\right)+\tilde{g}_{12}\left(|\alpha_2|^2-\frac{1}{2}\right)\right)\\ \alpha_2\left(\tilde{g}_{22}\left(|\alpha_2|^2-1\right)+\tilde{g}_{12}\left(|\alpha_1|^2-\frac{1}{2}\right)\right)\end{pmatrix}\mathrm{d}\tau. \tag{6.5}$$

We note that in this exactly solvable example, there is only initial Wigner noise, as the damping is zero. These equations can be solved numerically using conventional integration methods, which in our case was done with XMDS (see Appendix E for details). Observables are obtained from the moments of $\alpha_1$ and $\alpha_2$ with the help of Theorem 2.5.

## 6.2. Exact solution

On the other hand, time-dependent values of any observables for this system can be obtained exactly using an expansion in number states [44]. Theoretical derivations for this method were provided by Q.-Y. He and R. Y. Teh.

In the Heisenberg picture, the equations of motion for the annihilation operators are

$$\frac{\mathrm{d}\hat{a}_i(\tau)}{\mathrm{d}\tau} = i\left[\hat{H}, \hat{a}_i(\tau)\right] = -i\sum_{j=1}^{2}\tilde{g}_{ij}\hat{N}_j\hat{a}_i(\tau), \tag{6.6}$$

and their solution is (since the population of each mode is conserved):

$$\hat{a}_i(\tau) = \exp\left(-i\sum_{j=1}^{2}g_{ij}\hat{N}_j\tau\right)\hat{a}_i. \tag{6.7}$$

The initial conditions (6.3) can be, in turn, expanded as

$$\begin{aligned}\Psi_a(0) &= e^{-|\alpha|^2/2}\sum_{m=0}^{\infty}\frac{\alpha^m}{\sqrt{m!}}|m\rangle_1 e^{-|\alpha|^2/2}\sum_{n=0}^{\infty}\frac{\alpha^n}{\sqrt{n!}}|n\rangle_2 \\ &= \sum_{m=0}^{\infty}C_m^{(1)}|m\rangle_1\sum_{n=0}^{\infty}C_n^{(2)}|n\rangle_2,\end{aligned} \tag{6.8}$$

and used to calculate any required moments $f(\hat{a}_1^\dagger,\hat{a}_1,\hat{a}_2^\dagger,\hat{a}_2)$ at a time $\tau$ as

$$\begin{aligned}\langle f(\hat{a}_1^\dagger,\hat{a}_1,\hat{a}_2^\dagger,\hat{a}_2)\rangle = &\sum_{k,l,m,n=0}^{\infty}C_k^{(1)}C_l^{(2)}C_m^{(1)}C_n^{(2)} \\ &\times\langle k|_1\langle l|_2 f(\hat{a}_1^\dagger(\tau),\hat{a}_1(\tau),\hat{a}_2^\dagger(\tau),\hat{a}_2(\tau))|m\rangle_1|n\rangle_2.\end{aligned} \tag{6.9}$$

For the purposes of comparison, we will take a basic quantity that has been calculated for the system in question [44], namely the degree of local spin squeezing. First we introduce phase-rotated Schwinger spin operator measurements in the well as

$$\begin{aligned}\hat{J}_X &= \frac{1}{2}\left(\hat{a}_2^\dagger\hat{a}_1e^{i\Delta\theta}+\hat{a}_1^\dagger\hat{a}_2e^{-i\Delta\theta}\right), \\ \hat{J}_Y &= \frac{1}{2i}\left(\hat{a}_2^\dagger\hat{a}_1e^{i\Delta\theta}-\hat{a}_1^\dagger\hat{a}_2e^{-i\Delta\theta}\right), \\ \hat{J}_Z &= \frac{1}{2}\left(\hat{a}_2^\dagger\hat{a}_2-\hat{a}_1^\dagger\hat{a}_1\right),\end{aligned} \tag{6.10}$$

where $\Delta\theta = \pi/2 - \arg\langle\hat{a}_2^\dagger\hat{a}_1\rangle$ is the phase difference between the two modes.

We consider all possible orthogonal pairs of spin operators $\hat{J}_\theta$, $\hat{J}_{\theta+\pi/2}$ in the plane orthogonal to $\hat{J}_Y$, where $\hat{J}_\theta$ is defined as

$$\hat{J}_\theta = \hat{J}_Z\cos\theta + \hat{J}_X\sin\theta. \tag{6.11}$$

These pairs obey the Heisenberg uncertainty relation

$$\Delta\hat{J}_\theta\Delta\hat{J}_{\theta+\pi/2} \geq |\langle\hat{J}_Y\rangle|/2. \tag{6.12}$$

Even with this limit on the pair, the variance of one of the spins in the pair can be reduced below the Heisenberg limit:

$$\Delta^2\hat{J}_\theta < |\langle\hat{J}_Y\rangle|/2, \tag{6.13}$$

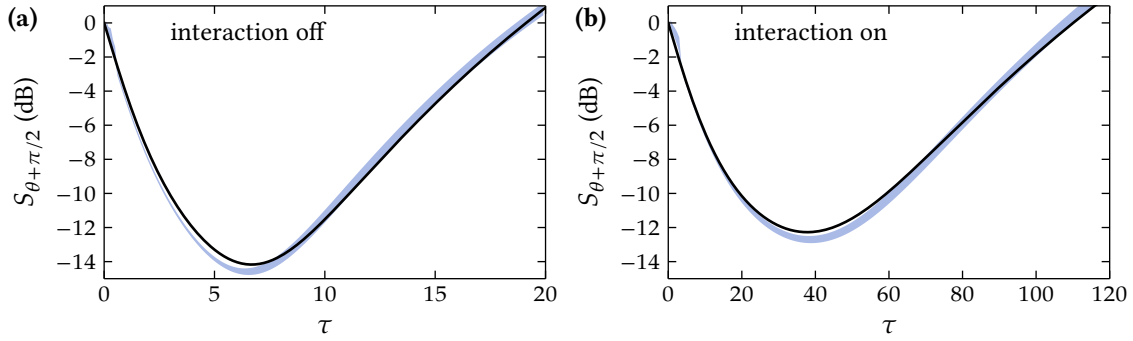


Figure 6.1.: Comparison of the Wigner simulated time-dependent spin squeezing (blue bands; the width corresponds to the estimated sampling error) against the exact results (black lines), plotted on the logarithmic scale. Trajectories used: 2,000. The plots correspond to **(a)** the case of no inter-component interaction ($\tilde{g}_{12} = 0$, $\tilde{g}_{11} = \tilde{g}_{22} = 1/N$), and **(b)** strong inter-component interaction ($\tilde{g}_{ij} = a_{ij}/(a_{11}N)$, where $a_{11} = 100.4$, $a_{12} = 80.8$ and $a_{22} = 95.5$). Here $N$ is the initial total number of atoms in the well (see (6.3)).

which is referred to as the "spin squeezed state".

It can be shown [44] that the optimal squeezing angle is

$$\theta = \frac{1}{2}\arctan\left(\frac{2\langle\hat{J}_Z,\hat{J}_X\rangle}{\Delta^2\hat{J}_Z - \Delta^2\hat{J}_X}\right), \tag{6.14}$$

and the degree of squeezing can be quantified as

$$S_{\theta,\theta+\pi/2} = \frac{\Delta^2\hat{J}_{\theta,\theta+\pi/2}}{|\langle\hat{J}_Y\rangle|/2}. \tag{6.15}$$

Here we denoted the pair correlation

$$\langle\hat{J}_Z,\hat{J}_X\rangle = \frac{1}{2}\left(\langle\hat{J}_Z\hat{J}_X\rangle + \langle\hat{J}_X\hat{J}_Z\rangle - 2\langle\hat{J}_Z\rangle\langle\hat{J}_X\rangle\right). \tag{6.16}$$

## 6.3. Comparisons of exact results and Wigner simulations

The expectations above can be expressed in terms of creation and annihilation operators, and calculated either in Wigner representation using Theorem 2.5, or with the number state expansion using (6.7) and (6.9). The results for $S_{\theta+\pi/2}$ are plotted in Fig. 6.1, using a low number of trajectories (2,000) for the truncated Wigner in order to make sampling errors more distinguishable. The Wigner method shows good agreement with the exact

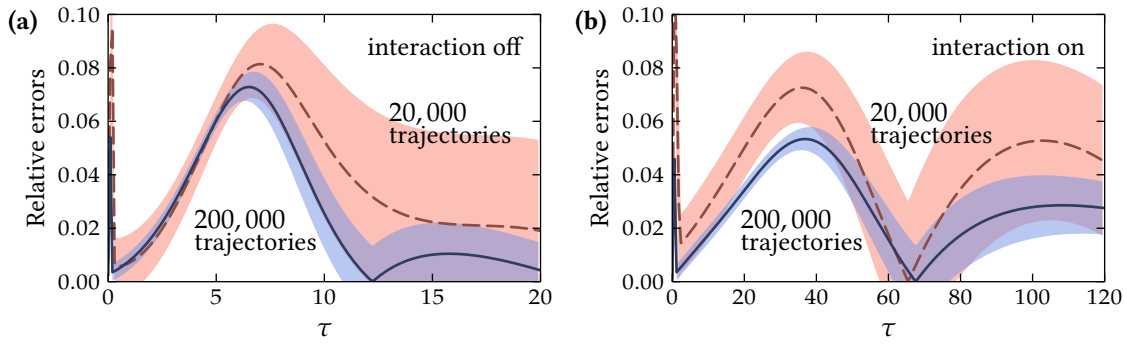


Figure 6.2.: Difference of the Wigner simulated spin squeezing $S_{\theta+\pi/2}$ and the exact results (lines) as compared to the sampling errors in Wigner simulations (bands), normalized by the exact results. The mean systematic errors for 20,000 trajectories (red dashed lines) and 200,000 trajectories (blue solid lines) are plotted. The plots correspond to **(a)** the case of no inter-component interaction, and **(b)** strong inter-component interaction (the interaction coefficients are the same as in Fig. 6.1).

results in the time range of interest; the growing sampling error can be reduced to a desirable extent by using more simulation trajectories.

The relative (normalized on the corresponding results from the exact method) sampling and systematic errors of the Wigner method are plotted in Fig. 6.2. The Wigner results show a systematic error several times bigger than the corresponding sampling error in the first half of the time interval, which is a sign of the failing truncation approximation. At other times, the difference with the exact results is within the sampling error range. The large oscillations of the systematic error at the start of the simulation can be explained by accumulating uncertainties in the denominator of (6.15).

It is also interesting to look how the systematic error changes with the mode population (Fig. 6.3). Since the time scale of the evolution varies with $N$, for this plot we normalized the time $\tau$ on the "characteristic time" $\tau_c(N)$, which corresponds to the time from the beginning of the evolution at which the squeezing $S_{\theta+\pi/2}$ rises back to 1. As expected, the larger is the population $N$, the smaller is the systematic error. This indirectly confirms the truncation condition (5.23).

It must be emphasized that, while relative systematic errors are noticeable (about 5% at the maximum), they correspond to the periods with low values of $S$ (see Fig. 6.1). Therefore, the absolute error is extremely low (of the order of tenths of decibel). On the other hand, the technical noise in spin squeezing experiments can reach 10 dB [73]. This means that the systematic errors in the truncated Wigner method are far from being

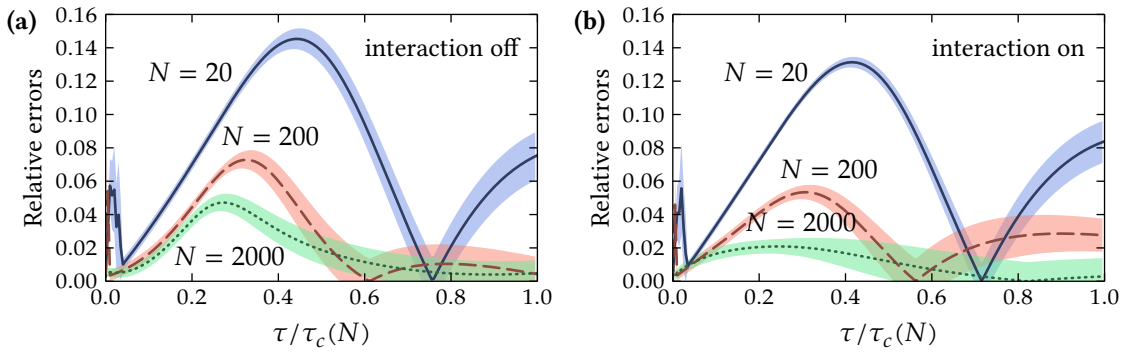


Figure 6.3.: Difference of the Wigner simulated spin squeezing $S_{\theta+\pi/2}$ and the exact results (lines) as compared to the sampling errors in Wigner simulations (bands), normalized on the exact results. The mean systematic errors for $N = 20$ (blue solid lines), $N = 200$ (red dashed lines) and $N = 2,000$ (green dotted lines) with $200,000$ trajectories are plotted. The plots correspond to **(a)** the case of no inter-component interaction, and **(b)** strong inter-component interaction (the interaction coefficients are the same as in Fig. 6.1).

detectable by current technology.

Note that, while in this particular example the exact method gives more accurate results at comparable or lower computational cost, it becomes unapplicable as soon as one wants to include tunneling and nonlinear losses into the model, while the Wigner method continues to perform with the same efficiency [44].

In conclusion, we have decisively shown that the truncated Wigner method gives accurate predictions for sophisticated compound observables (the squeezing (6.15) is calculated as a fourth order moment divided by a second order moment). The system used in this chapter was a very simple one; for more complex systems it is possible to perform comparisons with the exact (in the limit of infinite simulation trajectories) positive-P phase-space method [28, 47, 48]. A detailed study of the validity of the truncated Wigner method was carried out by Sinatra *et al* [57].

# Chapter 7.

# Quantum noise in BEC interferometry

BECs have macroscopic quantum states and can be potentially used as high precision interferometric detectors and sensors. Unlike photons, atoms can interact strongly, leading to loss of coherence and decreased interferometric contrast. An accurate quantitative model for these quantum many-body effects is essential for explaining the results of atom interferometry experiments and for planning future ones.

In this chapter we will apply the truncated Wigner method from Chapter 5 to the task of simulating the dynamics of such experiments. We will start from describing the mean-field approach leading to the conventional Gross-Pitaevskii equations (GPEs) [74]. We then extend it to include quantum effects, such as the noise from linear and nonlinear losses. The accurate description of nonlinear losses is especially important as their relative effect increases when atom numbers are increased to improve contrast.

We will compare the effect of quantum fluctuations and technical noise, such as imperfect measurements or coupling phase and amplitude uncertainty, on the interferometric contrast. We will also consider the experimental measurement of the contrast in detail and investigate the influence of quantum effects on the important characteristic of phase noise.

## 7.1. Two-component trapped BEC

The system we are interested in is an ultracold BEC harmonically trapped in 3 dimensions such as the one used in the experiments by Riedel *et al* [73] and Egorov *et al* [42, 75]. The BEC in question has two components (separate BECs consisting of atoms with different hyperfine states) with a significant nonlinear repulsive interaction (both inter- and intra-component), nonlinear losses and additional linear unitary effects, such as an electromagnetic coupling between components. The number of components is set to two in order to simplify the resulting equations for the experiments described in this chapter; it can be easily increased if necessary.

We assume that the BEC has $s$-wave interactions, which means the nonlinear interaction coefficients have the form

$$g_{jk} = \frac{4\pi\hbar^2 a_{jk}}{m}, \tag{7.1}$$

where $j$ and $k$ are the indices of the interacting components, $a_{jk}$ is the corresponding $s$-wave scattering length, and $m$ in this chapter stands for the mass of a $^{87}$Rb atom. Here we assume a momentum cutoff $k_d \ll 1/a_{jk}$ in the numerical simulations, otherwise the couplings must be renormalized [57].

The external harmonic trapping potential $V_j$ for the component $j$ (which can include a component-dependent shift along some of the axes) has the form

$$V_j = \frac{m}{2}\sum_{d=1}^{3} \omega_d^2 (x_d - l_d^{(j)})^2, \tag{7.2}$$

where $\omega_d$ are trapping frequencies, which will be specified later when the experiments are described.

In principle, the methods described in this chapter can be easily generalized to include an arbitrary potential shape, and possibly some different form of nonlinear interaction coefficients, but for the experiments to be described the equations above will apply.

## 7.2. Mean-field approximation

We will start from a classical model of a trapped BEC — the mean-field approximation. While it cannot predict quantum effects, it provides the basis for comparison with the truncated Wigner method, and can be also applied to calculate the ground state of a trapped BEC numerically.

We will use the combined model which includes linear coupling and losses, and later in Section 7.3, dedicated to the application of the truncated Wigner method we will show how we can get almost identical equations from the first principles.

### 7.2.1. Two-component condensate

In the mean-field approximation the two-component BEC is described by wavefunctions $\Psi_j$, which are normalized such that $\int |\Psi_j|^2 \mathrm{d}\mathbf{x} \equiv N_j$, where $N_j$ is the total population of the component $j$ (consequently, $|\Psi_j|^2 \equiv n_j$ is the component density). The evolution of the condensate is described by the system of coupled Gross-Pitaevskii equations (CGPEs) [74]

$$\begin{aligned} i\hbar\frac{\mathrm{d}\Psi_1}{\mathrm{d}t} &= \left(-\frac{\hbar^2\nabla^2}{2m} + V_1 + g_{11}|\Psi_1|^2 + g_{12}|\Psi_2|^2 - i\hbar\Gamma_1\right)\Psi_1 \\ &\quad + \frac{\hbar\Omega}{2}\left(e^{i(\omega t+\alpha)} + e^{-i(\omega t+\alpha)}\right)\Psi_2, \\ i\hbar\frac{\mathrm{d}\Psi_2}{\mathrm{d}t} &= \left(-\frac{\hbar^2\nabla^2}{2m} + V_2 + \hbar\omega_{hf} + g_{22}|\Psi_2|^2 + g_{12}|\Psi_1|^2 - i\hbar\Gamma_2\right)\Psi_2 \\ &\quad + \frac{\hbar\Omega}{2}\left(e^{i(\omega t+\alpha)} + e^{-i(\omega t+\alpha)}\right)\Psi_1. \end{aligned} \tag{7.3}$$

Here $V_j(\mathbf{x})$ are external potentials (7.2), $\omega_{hf}$ is the hyperfine splitting between components, $g_{jk}$ are nonlinear interaction coefficients (7.1), $\Gamma_j$ terms represent nonlinear losses for the component $j$, and $\Omega$ is the electromagnetic coupling strength (with $\omega$ being the frequency, and $\alpha$ the initial phase shift of the coupling). The CGPEs without loss or coupling terms were introduced by Zeng *et al* [76], and Ho and Shenoy [77]. The coupling terms were first included by Ballagh *et al* [78], and the loss terms by Yurovsky *et al* [79]. A detailed description of the mean-field approximation can be found in the book by Pitaevskii and Stringari [74].

The exact expressions for the loss parameters $\Gamma_j$ depend on the loss processes in a particular experiment. For example, the dominant three-body and two-body losses in a two-component $^{87}$Rb BEC with the components $|F = 1, m_F = -1\rangle$ and $|F = 2, m_F = +1\rangle$

result in [70, 80]

$$\begin{aligned}\Gamma_1 &= \left(\gamma_{111} n_1^2 + \gamma_{12} n_2\right)/2,\\ \Gamma_2 &= \left(\gamma_{12} n_1 + \gamma_{22} n_2\right)/2.\end{aligned} \tag{7.4}$$

These equations were obtained empirically, but we will see later in this chapter how the same expressions (to leading order) appear as a result of the application of the truncated Wigner method.

The coupling frequency $\omega$ is usually slightly detuned from the hyperfine frequency in the experiment: $\omega = \omega_{hf} + \delta$, where $\delta \ll \omega_{hf}$. It is convenient to use equations (7.3) in a rotating frame:

$$\begin{aligned}\Psi_1 &= \Psi_1^{(r)},\\ \Psi_2 &= \Psi_2^{(r)} e^{i\omega_{hf} t}.\end{aligned} \tag{7.5}$$

This transformation eliminates $\omega_{hf}$ from the equations and does not change single-time observable values. Dropping the rotating frame superscript for simplicity, we obtain the transformed equations

$$\begin{aligned}i\hbar\frac{\mathrm{d}\Psi_1}{\mathrm{d}t} &= \left(-\frac{\hbar^2\nabla^2}{2m} + V_1 + g_{11}|\Psi_1|^2 + g_{12}|\Psi_2|^2 - i\hbar\Gamma_1\right)\Psi_1\\ &\quad + \frac{\hbar\Omega}{2}\left(e^{i((\omega+\omega_{hf})t+\alpha)} + e^{-i(\delta t+\alpha)}\right)\Psi_2,\\ i\hbar\frac{\mathrm{d}\Psi_2}{\mathrm{d}t} &= \left(-\frac{\hbar^2\nabla^2}{2m} + V_2 + g_{22}|\Psi_2|^2 + g_{12}|\Psi_1|^2 - i\hbar\Gamma_2\right)\Psi_2\\ &\quad + \frac{\hbar\Omega}{2}\left(e^{i(\delta t+\alpha)} + e^{-i((\omega+\omega_{hf})t+\alpha)}\right)\Psi_1.\end{aligned} \tag{7.6}$$

Furthermore, in experiments the coupling field is typically applied for short periods of time $t_{\mathrm{pulse}}$, where $1/\omega \ll t_{\mathrm{pulse}} \ll 1/\delta$. This allows us to neglect the rapidly oscillating terms proportional to $e^{i(\omega+\omega_{hf})t}$ and come to CGPEs in the rotating frame:

$$\begin{aligned}i\hbar\frac{\mathrm{d}\Psi_1}{\mathrm{d}t} &= \left(-\frac{\hbar^2\nabla^2}{2m} + V_1 + g_{11}|\Psi_1|^2 + g_{12}|\Psi_2|^2 - i\hbar\Gamma_1\right)\Psi_1 + \frac{\hbar\Omega}{2}e^{-i(\delta t+\alpha)}\Psi_2,\\ i\hbar\frac{\mathrm{d}\Psi_2}{\mathrm{d}t} &= \left(-\frac{\hbar^2\nabla^2}{2m} + V_2 + g_{22}|\Psi_2|^2 + g_{12}|\Psi_1|^2 - i\hbar\Gamma_2\right)\Psi_2 + \frac{\hbar\Omega}{2}e^{i(\delta t+\alpha)}\Psi_1.\end{aligned} \tag{7.7}$$

When the pulse is applied twice using the same coupling field (which is the case for the

Ramsey interferometry), it is the same as just setting $\Omega$ to zero after the first pulse and then restoring its value for the time of the second pulse; therefore, $\alpha$ stays the same too. If one wants to apply pulse with the different detuning, the phase information is lost, and the value of $\alpha$ has to be regarded as random.

The application of the coupling field can be simplified when certain additional conditions are valid, namely:

- $\mu/\hbar \ll \Omega$, where $\mu$ is the chemical potential of the first component;
- $\delta \ll \Omega$;
- the characteristic time of the other terms in (7.3) is much greater than $t_{\text{pulse}}$.

This allows us to use an "instantaneous" pulse, multiplying the state vector by a rotation matrix:

$$\begin{pmatrix} \Psi_1' \\ \Psi_2' \end{pmatrix} = \begin{pmatrix} \cos\frac{\theta}{2} & -ie^{-i\phi}\sin\frac{\theta}{2} \\ -ie^{i\phi}\sin\frac{\theta}{2} & \cos\frac{\theta}{2} \end{pmatrix} \begin{pmatrix} \Psi_1 \\ \Psi_2 \end{pmatrix}, \tag{7.8}$$

where $\theta = \Omega t_{\text{pulse}}$, and $\phi = \delta t + \alpha$ is the total phase of the coupling field at the beginning of the pulse. In particular, for the two-pulse Ramsey scheme (Fig. 7.3, (a)) with the time $t_R$ between pulses, $\phi_2 = \phi_1 + \delta t_R$.

### 7.2.2. Ground state calculation

At the beginning of the simulation, the BEC is assumed to be in the ground state which has the lowest possible energy. The ground state is the solution of the stationary CGPEs

$$\begin{aligned} \mu_1\Psi_1 &= \left(-\frac{\hbar^2\nabla^2}{2m} + V_1 + g_{11}|\Psi_1|^2 + g_{12}|\Psi_2|^2\right)\Psi_1, \\ \mu_2\Psi_2 &= \left(-\frac{\hbar^2\nabla^2}{2m} + V_2 + g_{22}|\Psi_2|^2 + g_{12}|\Psi_1|^2\right)\Psi_2, \end{aligned} \tag{7.9}$$

where $\mu_1$ and $\mu_2$ are chemical potentials of the components.

The most common method of finding the mean-field ground state is the imaginary time propagation [81, 82]. The essence of the method is that the propagation of an arbitrary wavefunction using the time-dependent CGPEs, but with the substitution $t \to \tau = it$, lowers its energy; therefore, after the sufficient amount of time this propagation will lead

us arbitrarily close to the ground state. The actual equations to be propagated are (7.7) without the loss or coupling terms:

$$\begin{aligned} \hbar\frac{\mathrm{d}\Psi_1}{\mathrm{d}\tau} &= -\left(-\frac{\hbar^2\nabla^2}{2m} + V_1 + g_{11}|\Psi_1|^2 + g_{12}|\Psi_2|^2\right)\Psi_1, \\ \hbar\frac{\mathrm{d}\Psi_2}{\mathrm{d}\tau} &= -\left(-\frac{\hbar^2\nabla^2}{2m} + V_2 + g_{22}|\Psi_2|^2 + g_{12}|\Psi_1|^2\right)\Psi_2. \end{aligned} \tag{7.10}$$

The rigorous proof of this method was derived by Bao and Du [82]. The idea can be roughly illustrated by considering a one-component system with a linear Hamiltonian $\hat{K}$, whose eigenvalues are $\mu_1 < \mu_2 < \ldots$, where the lowest eigenvalue corresponds to ground state we want to find. The steady solution of the time-dependent GPE

$$i\hbar\frac{\mathrm{d}\Psi}{\mathrm{d}t} = \hat{K}\Psi \tag{7.11}$$

then looks like

$$\Psi(\mathbf{x}, t) = \sum_k e^{-\frac{i}{\hbar}\mu_k t} f_k(\mathbf{x}), \tag{7.12}$$

where $f_k$ are eigenfunctions of $\hat{K}$ corresponding to the eigenvalues $\mu_k$. After the substitution $t \to \tau = it$ the solution becomes fading, with higher-energy terms fading faster:

$$\Psi(\mathbf{x}, \tau) = \sum_k e^{-\frac{1}{\hbar}\mu_k \tau} f_k(\mathbf{x}). \tag{7.13}$$

Therefore, if we take some random initial solution and propagate it long enough in imaginary time using (7.10), the higher-energy terms will eventually die out (in comparison with the lowest-energy state) and leave us with the desired ground state. The state obtained from the Thomas-Fermi approximated GPE can be taken as the initial one since it is rather close to the desired one (and, therefore, higher-energy terms are already quite small).

Since the population will decrease exponentially after each step, and the precision of numerical calculations is limited, a renormalisation after each step will be required. The total number of atoms in the ground state serves best in this case (because we will have

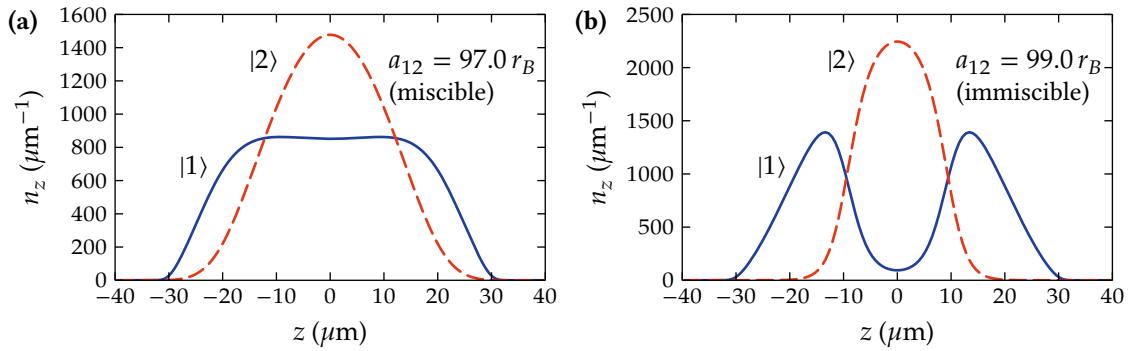


Figure 7.1.: Axial densities of two-component ground state for **(a)** a miscible and **(b)** an immiscible regime of $^{87}$Rb BEC with $N_1 = N_2 = 40,000$ atoms in a three-dimensional harmonic trap with the frequencies $f_x = f_y = 97.6\,\text{Hz}$, $f_z = 11.96\,\text{Hz}$. Blue solid lines and red dashed lines show the axial density of the first and the second component respectively. Intra-component scattering lengths are $a_{11} = 100.40\, r_B$, $a_{22} = 95.68\, r_B$, inter-component scattering length is **(a)** $a_{12} = 97.0\, r_B$ and **(b)** $a_{11} = 99.0\, r_B$, where $r_B$ is the Bohr radius.

to renormalise the final ground state anyway):

$$\int |\Psi(\tau, \mathbf{x})|^2 \mathrm{d}\mathbf{x} = N. \tag{7.14}$$

Propagation is terminated when the Gross-Pitaevskii energy of the state converges to the required precision (that is, only one eigenstate with the lowest energy is left out). The energy of the two-component condensate [74]

$$\begin{aligned} E[\boldsymbol{\Psi}] = \int \Bigg( & -\frac{\hbar^2 \Psi_1^* \nabla^2 \Psi_1}{2m} - \frac{\hbar^2 \Psi_2^* \nabla^2 \Psi_2}{2m} \\ & + (V_1 + \hbar\omega_1) n_1 + (V_2 + \hbar\omega_2) n_2 + \frac{g_{11}}{2} n_1^2 + \frac{g_{22}}{2} n_2^2 + g_{12} n_1 n_2 \Bigg) \mathrm{d}\mathbf{x} \end{aligned} \tag{7.15}$$

thus has to be calculated after each step and compared to the previous value, waiting for the desired precision to be reached.

As an example, Fig. 7.1 shows the axial density $n_z = \int n(\mathbf{x}) \mathrm{d}x\mathrm{d}y$ of the two-component ground state for an equal mix of two hyperfine states of $^{87}$Rb BEC. Two panes of the figure illustrate the difference between the miscible ($a_{12}^2 < a_{11} a_{22}$) and immiscible ($a_{12}^2 > a_{11} a_{22}$) regimes.

It should be emphasized that this ground state is not a true many-body ground state, but rather a type of mean-field (single-particle) approximation, since it omits quantum correlations.

### 7.2.3. Thomas-Fermi approximation

As was mentioned earlier in this section, the starting state for the imaginary time calculation can be set to the Thomas-Fermi approximate state to minimize the propagation time. Thomas-Fermi approximation consists of neglecting the kinetic term in the stationary equations (7.9). For a one-component state ($\Psi_2 \equiv 0$), the resulting equations can be easily solved analytically:

$$|\Psi_1(\mathbf{x})|^2 = \frac{1}{g_{11}} \max\left(\mu_1 - V_1(\mathbf{x}), 0\right). \tag{7.16}$$

In the $D$-dimensional harmonic trap potential

$$V_1(\mathbf{x}) = \frac{m}{2} \sum_{d=1}^{D} \omega_d^2 x_d^2, \tag{7.17}$$

this solution has the shape of an ellipsoid with radii $r_d = \sqrt{2\mu_1/(m\omega_d^2)}$.

The chemical potential $\mu_1$ is fixed by the normalisation condition $\int |\Psi_1|^2 \mathrm{d}\mathbf{x} = N_1$. For a three-dimensional trap it can be shown to be

$$\mu_1^{(3\mathrm{D})} = \left(\frac{15N_1}{8\pi}\right)^{\frac{2}{5}} \left(\frac{m\bar{\omega}^2}{2}\right)^{\frac{3}{5}} {g_{11}}^{\frac{2}{5}}, \tag{7.18}$$

where $\bar{\omega} = \sqrt[3]{\omega_x \omega_y \omega_z}$. For a one-dimensional trap it has the form

$$\mu_1^{(1\mathrm{D})} = \left(\frac{3g_{11}N_1}{4}\right)^{\frac{2}{3}} \left(\frac{m\omega_1^2}{2}\right)^{\frac{1}{3}}. \tag{7.19}$$

Now we can roughly estimate the conditions necessary to neglect the kinetic term from the equation. Substituting approximate solution (7.16) to (7.9) and comparing the kinetic term with the potential term, we get the following inequation:

$$\frac{\hbar^2}{2m}\left(\frac{m\sum_{d=1}^{D}\omega_d^2}{2} + \frac{m^2\sum_{d=1}^{D}\omega_d^4 x_d^2}{4\left(\mu_1 - V_1(\mathbf{x})\right)}\right) \ll \mu\left(\mu_1 - V_1(\mathbf{x})\right). \tag{7.20}$$

Near the centre of the condensate, this inequation simplifies to

$$\mu \gg \frac{\hbar}{2}|\boldsymbol{\omega}|, \tag{7.21}$$

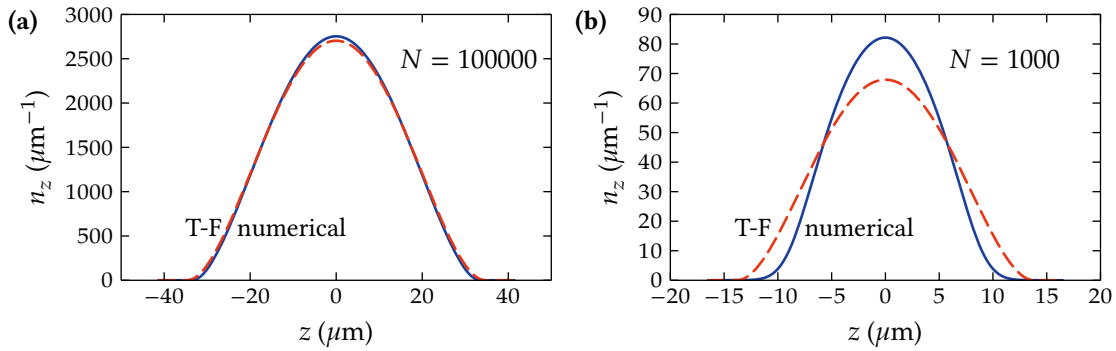


Figure 7.2.: Axial densities of numerically calculated (blue solid lines) and Thomas-Fermi approximated (red dashed lines) ground states for a one-component $^{87}$Rb BEC of **(a)** 100,000 atoms, and **(b)** 1,000 atoms.

where $\boldsymbol{\omega} \equiv (\omega_1, \ldots, \omega_D)^T$ is the vector of trap frequencies.

On the other hand, near the edges of the cloud the left-hand side of the inequation (7.20) diverges, while the right-hand side tends to zero. This means that near the edges the Thomas-Fermi approximation fails regardless of the conditions. Fortunately, the particle density there is low, so we can estimate the width $h$ of the "belt" where our first approximation of the state function is significantly incorrect. If it happens to be small as compared to the size of the condensate, the approximation can be considered valid.

The first term at the left-hand side of the inequation (7.20) is constant and can be dropped in the limit of $V_1(\mathbf{x}) \to \mu_1$. Then, for the sake of simplicity, we assume all but one of coordinates to be zero and the remaining one to be equal to $r_d - h_d$, where $r_d$ is the corresponding radius of the condensate. After replacing "$\ll$" by "$\approx$" and assuming $h_d$ to be small as compared to $r_d$, we obtain the conditions for each coordinate:

$$h_d \approx \sqrt{\frac{\hbar^2}{2\mu_1 m}}, \; d \in [1, \ldots, D]. \tag{7.22}$$

These have to be much smaller than the corresponding radii, which gives us

$$\mu_1 \gg \frac{1}{2}\hbar \max_{d \in [1,\ldots,D]} \omega_d. \tag{7.23}$$

This condition is less strict than the condition for the centre of the condensate. Therefore, we have only one condition justifying the application of the Thomas-Fermi approximation is (7.21).

Let us use some real-life experimental parameters and check how well the Thomas-Fermi

approximation works. For a three-dimensional trap with frequencies $f_x = f_y = 97.6\,\mathrm{Hz}$ and $f_z = 11.96\,\mathrm{Hz}$ and with $N_1 = 10^5$ $^{87}$Rb atoms (which have a scattering length of $a_{11} = 100.4 r_B$), we have $2\mu_1/(\hbar|\boldsymbol{\omega}|) \approx 10.68$. This means that the Thomas-Fermi approximation produces a solution which is close to the real one. However, for a lower amount of atoms, say $N_1 = 10^3$, we obtain $2\mu/(\hbar|\boldsymbol{\omega}|) \approx 1.69$, which is a sign that we are reaching the limit of the approximation's applicability. Fig. 7.2 shows the axial density for both cases: for 100,000 atoms the Thomas-Fermi approximation is very close to the numerically calculated ground state and for 1,000 atoms it differs significantly, as expected.

An extended discussion of the Thomas-Fermi approximation was given by Dalfovo *et al* [83]. It is possible to work out the Thomas-Fermi approximation for a two-component condensate, but it requires some non-trivial handling of various miscibility/immiscibility cases [84]. In this thesis we only consider single-component ground states, as these are the only ones used in the experiments we are simulating.

## 7.3. Quasiprobability approach

Having discussed the classical mean-field approach in the previous section, we will now apply the functional truncated Wigner method described in Chapter 5. While the mean-field approximation gives a fast way to obtain a qualitative picture of the BEC dynamics, it ignores many important effects that originate from the inherent quantum nature of the system, in particular, nonlinear quantum noise effects of quantum dynamics: phase diffusion, entanglement and spin squeezing. An initial satate uncertainty and noise terms do not occur in semi-classical CGPEs, which are unable to predict these effects.

We will see how an initial master equation produces a system of equations very similar to CGPEs (7.7) with loss terms resembling (7.4).

Since we assume that the BEC has $s$-wave interactions, we can use the effective Hamiltonian (5.3) expressed using restricted field creation and annihilation operators $\tilde{\Psi}_j^\dagger(\mathbf{x})$ and $\tilde{\Psi}_j(\mathbf{x})$:

$$\hat{H} = \int \mathrm{d}\mathbf{x} \sum_{j=1}^{2}\sum_{k=1}^{2} \left\{ \tilde{\Psi}_j^\dagger K_{jk} \tilde{\Psi}_k + \frac{g_{jk}}{2} \tilde{\Psi}_j^\dagger \tilde{\Psi}_k^\dagger \tilde{\Psi}_j \tilde{\Psi}_k \right\}, \tag{7.24}$$

where $g_{jk}$ are nonlinear interaction coefficients (7.1). The single-particle Hamiltonian $K_{jk}$ includes the electromagnetic coupling terms, added by analogy with the CGPEs (7.7):

$$K_{jk} = \left( -\frac{\hbar^2}{2m}\nabla^2 + V_j(\mathbf{x}) \right) \delta_{jk} + \hbar\tilde{\Omega}_{jk}(t). \tag{7.25}$$

Here, as in the classical CGPEs, $V_j(\mathbf{x})$ are external potentials (7.2), and $\tilde{\Omega}$ is the linear coupling matrix

$$\tilde{\Omega} = \frac{\hbar\Omega}{2} \begin{pmatrix} 0 & e^{-i(\delta t+\alpha)} \\ e^{i(\delta t+\alpha)} & 0 \end{pmatrix}. \tag{7.26}$$

Taking nonlinear losses into account, the evolution of the system's density matrix $\hat{\rho}$ is described by the Markovian master equation (5.4):

$$\frac{\mathrm{d}\hat{\rho}}{\mathrm{d}t} = -\frac{i}{\hbar}\left[\hat{H}, \hat{\rho}\right] + \sum_{\mathrm{l}\in L} \kappa_{\mathrm{l}} \int \mathrm{d}\mathbf{x} \mathcal{L}_{\mathrm{l}}\left[\hat{\rho}\right], \tag{7.27}$$

where $\mathcal{L}_{\mathrm{l}}$ are loss operators (5.5), and $L$ is the set of loss processes that are experimentally shown to affect the trapped $^{87}$Rb BEC [42, 80]:

- three-body recombination $\hat{O}_{111} = \tilde{\Psi}_1^3$,
- two-body inter-component loss $\hat{O}_{12} = \tilde{\Psi}_1\tilde{\Psi}_2$, and
- two-body intra-component loss $\hat{O}_{22} = \tilde{\Psi}_2^2$,

with the coefficients depending on the components used in a particular experiment.

Applying the general formulas from Chapter 5, we can transform the master equation (7.24) to an FPE for the truncated Wigner functional, and further to a set of SDEs in the Stratonovich form (5.35):

$$\begin{aligned} \mathrm{d}\Psi_1 &= \mathcal{P}_{\mathbb{M}_1}\left[\mathcal{A}_1^{(s)}\mathrm{d}t + \sum_{\mathrm{l}\in L}\mathcal{B}_{1,\mathrm{l}}\mathrm{d}Q_{\mathrm{l}}\right], \\ \mathrm{d}\Psi_2 &= \mathcal{P}_{\mathbb{M}_2}\left[\mathcal{A}_2^{(s)}\mathrm{d}t + \sum_{\mathrm{l}\in L}\mathcal{B}_{2,\mathrm{l}}\mathrm{d}Q_{\mathrm{l}}\right] \end{aligned} \tag{7.28}$$

with drift terms

$$\begin{aligned}\mathcal{A}_1^{(s)} = & -\frac{i}{\hbar}\left(\sum_{k=1}^{2} K_{1k}\Psi_k + \Psi_1 \sum_{k=1}^{2} g_{1k}\left(|\Psi_k|^2 - \frac{\delta_{1k}+1}{2}\delta_{\mathbb{M}_k}(\mathbf{x},\mathbf{x})\right)\right) \\ & - 3\kappa_{111}|\Psi_1|^2|\Psi_1|^2\Psi_1 - \kappa_{12}|\Psi_2|^2\Psi_1, \\ \mathcal{A}_2^{(s)} = & -\frac{i}{\hbar}\left(\sum_{k=1}^{2} K_{2k}\Psi_k + \Psi_2 \sum_{k=1}^{2} g_{2k}\left(|\Psi_k|^2 - \frac{\delta_{2k}+1}{2}\delta_{\mathbb{M}_k}(\mathbf{x},\mathbf{x})\right)\right) \\ & - \kappa_{12}|\Psi_1|^2\Psi_2 - 2\kappa_{22}|\Psi_2|^2\Psi_2,\end{aligned} \tag{7.29}$$

and noise terms

$$\begin{aligned}\mathcal{B}_{1,111} = 3\sqrt{\kappa_{111}}\left(\Psi_1^*\right)^2, \quad \mathcal{B}_{1,12} = \sqrt{\kappa_{12}}\Psi_2^*, \quad \mathcal{B}_{1,22} = 0, \\ \mathcal{B}_{2,111} = 0, \quad \mathcal{B}_{2,12} = \sqrt{\kappa_{12}}\Psi_1^*, \quad \mathcal{B}_{2,22} = 2\sqrt{\kappa_{22}}\Psi_2^*.\end{aligned} \tag{7.30}$$

Note that the leading order of the loss components in the drift terms coincides with the phenomenological loss components of the CGPEs (7.3).

The drift coefficients (7.29) and the CGPEs (7.3) use sligtly different loss parameters. This is caused by the fact that the parameters $\kappa$ originate from the "natural theoretical" definition (a coefficient in front of the loss operator $\mathcal{L}$), and the parameters $\gamma$ correspond to the "natural experimental" definition based on observed atom number losses:

$$\frac{\mathrm{d}n_j}{\mathrm{d}t} = -\gamma_{j,1} n_1^{l_1} n_2^{l_2} \ldots, \tag{7.31}$$

where $n_j$ is the density of component $j$. The conversion between these two parameters can be carried out easily as

$$\gamma_{j,1} \equiv 2 l_j \kappa_1. \tag{7.32}$$

The choice of an initial state for the integration largely depends on the system in question. While the mean value of the initial Wigner functional is usually chosen as the classical ground state minimising the energy functional (7.15), the full distribution is a more subtle problem. For the interferometry experiments described in this thesis, it is sufficient to assume an initial coherent state which can be sampled as a set of Gaussian random numbers according to Theorem 5.6 since the temperature of the atomic ensemble is low. The main source of quantum noise is due to the beam-splitter rather than the

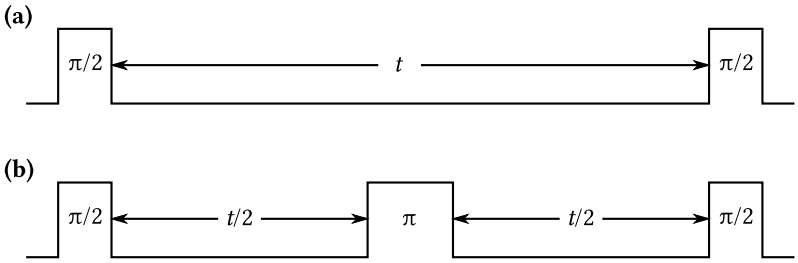


Figure 7.3.: Timeline of the experiment for **(a)** a regular Ramsey sequence, and **(b)** a Ramsey sequence with spin echo.

initial state, so this approximation is not a crucial one. In more complicated cases when the temperature cannot be neglected, one can use thermal Bogoliubov states [55, 72], for which there exists a numerically efficient sampling method [57]. The initial Wigner distribution may also include uncertainties of the ground state caused by "technical" reasons, for example, by a variation in the trap frequencies.

## 7.4. Fringe visibility

In this section we will apply the models from the previous sections to recent interferometry experiments involving a two-component $^{87}$Rb BEC with two components corresponding to the hyperfine states $|F = 1, m_F = -1\rangle$ and $|F = 2, m_F = +1\rangle$ [42] (the components are denoted $|1\rangle$ and $|2\rangle$ further in this section). In the following simulations, the intra- and inter-component scattering lengths for these states were taken to be $a_{11} = 100.4\, r_B$ [80, 85], $a_{12} = 98.0\, r_B$, $a_{22} = 95.44\, r_B$ [75], and the coefficients for the dominant loss processes are $\gamma_{111} = 5.4 \times 10^{-30}\,\mathrm{cm}^6/\mathrm{s}$ [80], $\gamma_{12} = 1.51 \times 10^{-14}\,\mathrm{cm}^3/\mathrm{s}$, and $\gamma_{22} = 8.1 \times 10^{-14}\,\mathrm{cm}^3/\mathrm{s}$ [75].

The experiment starts with $N = 55000$ atoms of the component $|1\rangle$ in the ground state in a cigar-shaped magnetic trap with the frequencies $f_x = 97.0\,\mathrm{Hz}$, $f_y = 99.91\,\mathrm{Hz}$ and $f_z = 11.69\,\mathrm{Hz}$ in a bias magnetic field of 3.23 G so that the magnetic field dephasing is mostly eliminated [86]. The experiment is then carried out using two protocols.

The first protocol is a regular Ramsey sequence, depicted schematically in Fig. 7.3, (a): a $\pi/2$-pulse is applied by an electromagnetic coupler, creating a non-equilibrium superposition of components $|1\rangle$ and $|2\rangle$. Mathematically, it means that coupling terms in (7.7) or in (7.25) are enabled for a period of time equal to $t_{\mathrm{pulse}} = \theta/\Omega$, where $\theta = \pi/2$, with the Rabi frequency of the oscillator in this experiment being $\Omega = 2\pi \times 350\,\mathrm{rad/s}$. Since this

pulse is short compared to the total evolution time, it was simulated via an application of the rotation matrix (7.8).

During the further evolution of the system the components experience complex dynamics, separating and merging periodically [80]. This, in turn, leads to periodic dephasing and self-rephasing of the BEC components. After some period of the free evolution, a second $\pi/2$-pulse is applied, transforming the phase difference between the two components in the superposition into a population difference which can be measured through imaging of both BEC components. Many such experiments are performed with different free evolution times, contributing one time-point each because the imaging effectively destroys the BEC. A more detailed description of the experiment can be found in the paper by Egorov *et al* [42], and in his PhD thesis [87]. The experimental points used in this and the next section are also courtesy of M. Egorov.

The integration was performed using a low-dissipation 4th-order Runge-Kutta algorithm (see Appendix E for details about the algorithm and convergence tests). Both GPE and truncated Wigner simulations in this section and Section 7.6 used 80,000 time steps for Fig. 7.7 and 200,000 time steps for Fig. 7.7). The resulting relative convergence error was lower than $10^{-3}$ in all cases. The truncated Wigner simulations used 128 trajectories, which lead to relative sampling errors lower than $10^{-3}$. Both of these sources of errors therefore would not be noticeable in the figures and have not been plotted.

The simulations in this chapter and Chapter 8 used the plane wave basis (see Appendix D for details) and a $8 \times 8 \times 64$ spatial grid. This grid choice was made to ensure that mode populations were high (in view of the truncation approximation inherent in our method) while making sure that the spatial resolution is sufficient to describe the required dynamics. More information about the spatial convergence tests performed can be found in Section 7.5.

Coherence of the interference signal can be characterised by a common quantity — the fringe contrast, or visibility:

$$\mathcal{V} = \frac{2\left|\int \langle \tilde{\Psi}_1^\dagger \tilde{\Psi}_2 \rangle \mathrm{d}\mathbf{x}\right|}{\int \langle \tilde{\Psi}_1^\dagger \tilde{\Psi}_1 + \tilde{\Psi}_2^\dagger \tilde{\Psi}_2 \rangle \mathrm{d}\mathbf{x}}, \tag{7.33}$$

where the denominator is just the total number of atoms in the system. This quantity can be shown to be the envelope curve of the population fringes produced by the second $\pi/2$-pulse in the experiment. In the mean-field approximation, the required correlations

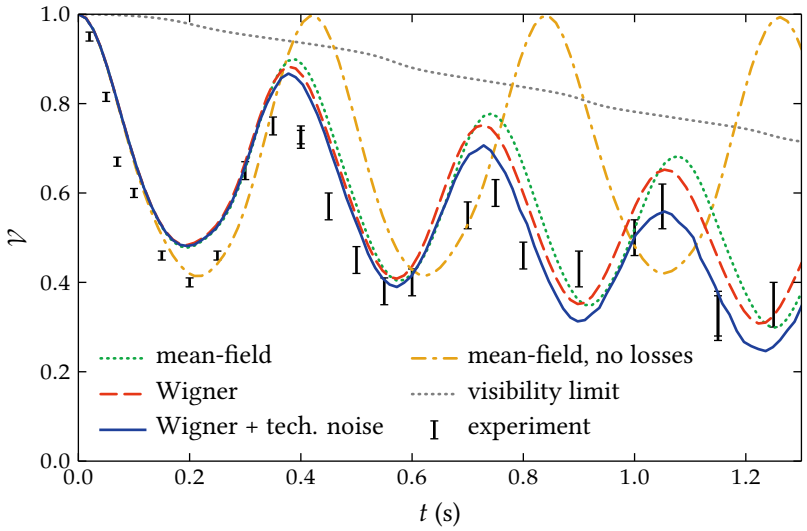


Figure 7.4.: Comparison of experimental and numerically simulated interferometric contrast at the end of a regular Ramsey sequence with the evolution time $t$. Experimental results (black bars) are shown in comparison with the results given by the mean-field approximation (green dotted line), the truncated Wigner method (red dashed line), and the truncated Wigner with technical noises included (blue solid line). The mean-field results with losses turned off (yellow dash-dotted line) and the population-dependent visibility limit (7.36) (grey dotted line) are included as a reference.

are calculated simply as

$$\begin{aligned} \tilde{n} &= \langle \tilde{\Psi}_1^\dagger \tilde{\Psi}_2 \rangle \approx \Psi_1^* \Psi_2, \\ n_j &= \langle \tilde{\Psi}_j^\dagger \tilde{\Psi}_j \rangle \approx \Psi_j^* \Psi_j. \end{aligned} \tag{7.34}$$

In the Wigner representation, we have to make the correlations symmetrically-ordered first, and then (5.37) gives us

$$\begin{aligned} \tilde{n} &= \langle \tilde{\Psi}_1^\dagger \tilde{\Psi}_2 \rangle = \langle \left\{ \tilde{\Psi}_1^\dagger \tilde{\Psi}_2 \right\}_{\text{sym}} \rangle \approx \left\langle \Psi_1^* \Psi_2 \right\rangle_{\text{traj}}, \\ n_j &= \langle \tilde{\Psi}_j^\dagger \tilde{\Psi}_j \rangle = \langle \left\{ \tilde{\Psi}_j^\dagger \tilde{\Psi}_j \right\}_{\text{sym}} - \frac{\delta_{\mathbb{M}_j}(\mathbf{x}, \mathbf{x})}{2} \rangle \approx \left\langle \Psi_j^* \Psi_j \right\rangle_{\text{traj}} - \frac{M}{2V}, \end{aligned} \tag{7.35}$$

where we have used the fact that $\delta_{\mathbb{M}_j}(\mathbf{x}, \mathbf{x}) \equiv M/V$ in the plane wave basis, where $M$ is the number of modes (for the grid we use $M = 64 \times 8 \times 8 = 4096$), and $V$ is the volume of the simulation area.

The visibility can serve as a good parameter of different effects (losses, quantum effects and technical noises) in the modelling of the experiment. The inclusion of these factors in the simulation of the Ramsey sequence is demonstrated in Fig. 7.4. The experimental

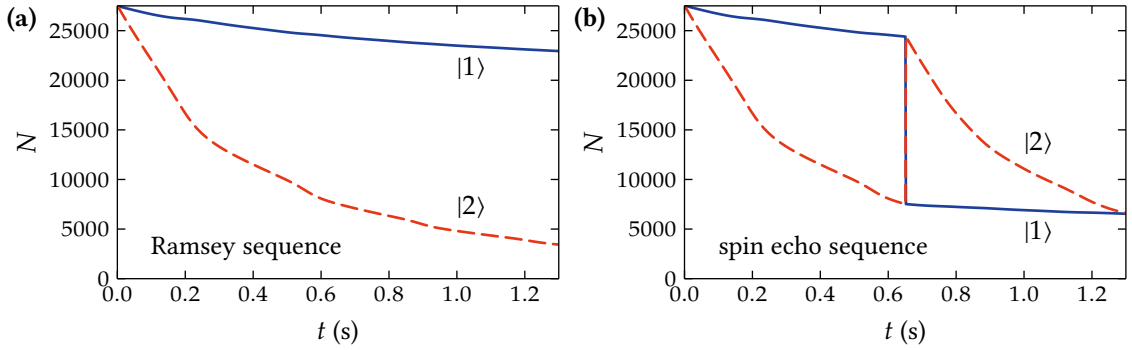


Figure 7.5.: Numerically simulated decay of the population of components $|1\rangle$ (blue solid lines) and $|2\rangle$ (red dashed lines) in **(a)** Ramsey and **(b)** spin echo sequences.

results and their uncertainties are shown as the black bars in the figure.

The simplest model — the mean-field CGPEs (7.7) with losses turned off — shows behavior that differs significantly from the experimental points: the visibility is completely restored during rephasings (yellow dash-dotted lines in the figure). This is to be expected as the theoretical limit of visibility

$$\mathcal{V}_{\max} = \frac{2\sqrt{N_1 N_2}}{N_1 + N_2}, \tag{7.36}$$

where $N_1$ and $N_2$ are populations before the second $\pi/2$-pulse, equals to 1 in this case, and there are no other limiting factors.

However, in the experiment losses are present and are significantly asymmetrical as shown in Fig. 7.5, (a). With populations typical for the experiment (tens of thousands of atoms or less), the two-body loss process in $|2\rangle$ is significantly stronger than the three-body one in $|1\rangle$. This makes the theoretical limit (7.36) decrease with time, as the dotted grey line in Fig. 7.4 illustrates. The resulting mean-field prediction with the inclusion of nonlinear losses (green dotted lines) is much closer to the experimental data.

The application of the SDEs (7.28) obtained with the Wigner method (red dashed lines) has little effect on the short-time visibility (although it becomes more important at longer times as we will see later in Fig. 7.7). The Wigner results can be further adjusted to account for the noise introduced by the final measurement and non-ideal coupling (blue solid lines), which will be explained in detail in the next section.

The final agreement with the experiment is still not ideal, and the explanation of this difference is an open question. Potential unaccounted factors include finite temperature effects and interaction with the surrounding cloud of non-condensed atoms.

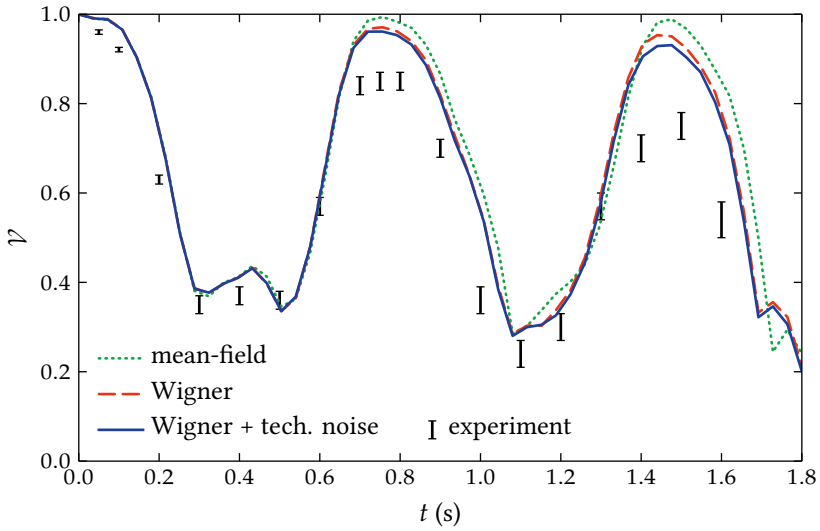


Figure 7.6.: Comparison of experimental and numerically simulated interferometric contrast at the end of a spin echo sequence with the evolution time $t$. Experimental results (black bars) show the final visibility value for a single spin echo sequence with the full evolution time $t$ as compared with the predictions from the mean-field approximation (green dotted line), the truncated Wigner method (red dashed line), and the truncated Wigner with technical noises included (blue solid line).

The asymmetricity introduced by the difference in loss rates can be compensated by periodically swapping the populations of the two components by a "spin echo" coupler pulse of the length $\pi$. The simplest, yet already very effective, variant is to apply the $\pi$-pulse in the middle of the evolution as illustrated by Fig. 7.3, (b). With this additional pulse, by the end of a single experimental sequence the populations of two components become equal again as shown in Fig. 7.5, (b), restoring the theoretical visibility limit (7.36) back to 1.

The mean-field approximation predicts the full recovery of the visibility even at long evolution times, which is inconsistent with the experiment as seen in Fig. 7.6. On the other hand, the quasiprobability model qualitatively predicts the decay of visibility with time. Just as in the case of the regular Ramsey sequence, the predictions of the simulation are improved by the inclusion of technical noise. Nevertheless, even after that the difference is still significant and is caused by initial atom number uncertainty, which will be discussed in the next section and in the conclusion. In the paper by Egorov *et al* [42] presenting the results of the experiment, the fit was improved by adding a phenomenological 10 s exponential decay to the visibility.

The simulations can be performed for longer times as shown in Fig. 7.7. The difference

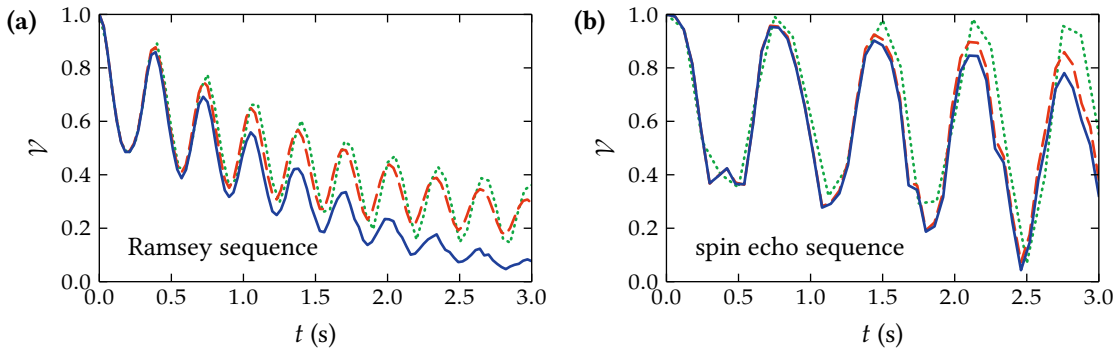


Figure 7.7.: Numerically simulated interferometric contrast for **(a)** a Ramsey sequence, and **(b)** a spin echo sequence at longer times. The results for the mean-field approximation (green dotted lines), the truncated Wigner method (red dashed lines) and the truncated Wigner with technical noises (blue solid lines) are plotted.

between the mean-field and the truncated Wigner approach becomes clearer in Fig. 7.7, (a), where the truncated Wigner predicts a significant decrease in the amplitude of the rephasing oscillations, caused by quantum noise. One must remember though that at such times the simulated atom densities become too low due to losses and violate the truncation validity criterion (5.23), thus making the predictions less reliable.

## 7.5. Choice of grid

In the previous section we mentioned that the spatial grid size for interferometry simulations was chosen to be $8 \times 8 \times 64$. This is the point of equilibrium for two conflicting requirements. First, the number of grid points (which corresponds to the number of modes) must be low enough to satisfy the Wigner truncation condition (5.22). To quantify this, we set the threshold $N > 10M$, where $N$ is the total population ($55,000$ atoms in our case) and $M$ is the number of grid points. Second, the number of grid points must be high enough (or, alternatively, the grid spacing must be low enough) to describe the dynamics of the condensate. As a quantitative threshold we will use the condition that the difference in the quantities of interest should be lower than 1% when the grid spacing is halved.

For our tests, we initially picked the grid

$$\mathbf{G}_{\text{ref}} \equiv G^x_{\text{ref}} \times G^y_{\text{ref}} \times G^z_{\text{ref}} = 8 \times 8 \times 64 \tag{7.37}$$

as the starting point for several reasons:

- it has 4096 points, which is just below the Wigner truncation threshold defined above;
- its shape corresponds to the shape of the trap (in other words, the spacings in every direction are close to each other);
- the number of points in each dimension is a power of 2, which is convenient for numerical calculations.

The box for this grid was set to be 1.2 times wider in all directions than the Thomas-Fermi ground state (7.16) for the target population. This resulted in the box with measures

$$\mathbf{B}_{\text{ref}} \equiv B^x_{\text{ref}} \times B^y_{\text{ref}} \times B^z_{\text{ref}} = 9.10\,\mu\text{m} \times 8.83\,\mu\text{m} \times 75.48\,\mu\text{m}, \tag{7.38}$$

which was used as the reference point along with the grid $\mathbf{G}_{\text{ref}}$.

The tests consisted of running the simulation for the Ramsey sequence with the time $t = 1.3\,\text{s}$ and comparing resulting vectors $\boldsymbol{\mathcal{V}}$, containing 100 sampled values of $\mathcal{V}(t)$ for times from 0 s to 1.3 s, as

$$\Delta\mathcal{V}_{\text{grid,box}} = \left\|\boldsymbol{\mathcal{V}}_{\text{grid,box}} - \boldsymbol{\mathcal{V}}_{G_{\text{ref}},B_{\text{ref}}}\right\|_2 / \left\|\boldsymbol{\mathcal{V}}_{G_{\text{ref}},B_{\text{ref}}}\right\|_2, \tag{7.39}$$

where $\|\ldots\|_2$ is the 2-norm.

In different runs we varied axial and radial grid spacing (box length divided by the number of points in the corresponding dimension) separately. Since the integration algorithm performed best with numbers of grid points being powers of 2, the required spacing was achieved by changing both box length and grid size (for example, the axial spacing 0.75 of the reference one was obtained by using $2G^z_{\text{ref}}$ grid points in the $z$ direction, and $1.5B^z_{\text{ref}}$ box length in that direction). To verify this approach we ran two additional tests with doubled box length and number of grid points in both directions, which resulted in two additional points for the relative spacing 1.0 in each pane of Fig. 7.8. These points are very close to the reference points (which have $y$-coordinate equal to zero), which proves that the $\Delta\mathcal{V}$ value is only sensitive to the grid spacing and not to the box or grid sizes separately.

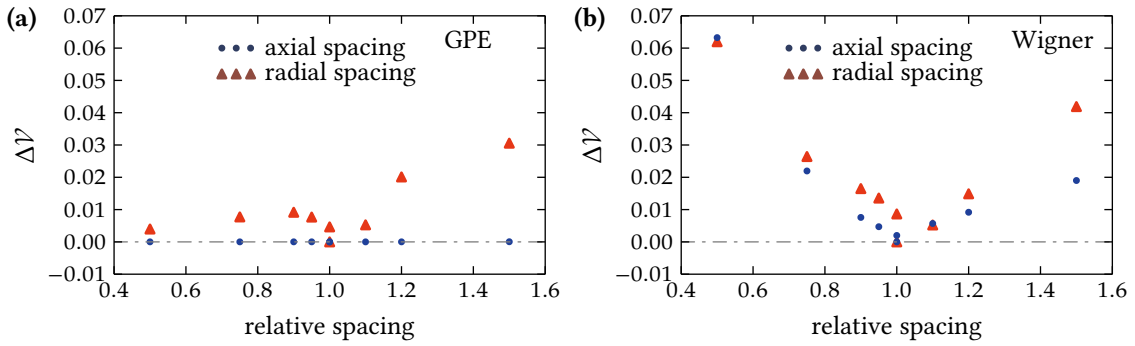


Figure 7.8.: Spatial convergence tests for the Ramsey sequence. The compound difference in visibility $\Delta\mathcal{V}$ is plotted against the axial (blue circles) and radial (red triangles) spacing, normalized by the spacing for the reference grid $\mathbf{G}_{\text{ref}}$ and box $\mathbf{B}_{\text{ref}}$. Simulation parameters are the same as in Fig. 7.4. All points were obtained with 160,000 time steps, the truncated Wigner simulations were run with 64 trajectories.

In order to check only the effect of spatial resolution without being influenced by changing number of modes, we performed a batch of tests for CGPEs (7.7) in addition to the truncated Wigner SDEs (7.28). The results for CGPEs are plotted in Fig. 7.8, (a). It is evident that further decrease of spacing after the reference point both in radial and axial directions does not change the results much. The change caused by decreased radial spacing is less than our 1% threshold, and the effect of axial spacing is too small to be noticeable in the plot. On the other hand, when the radial spacing is increased, $\Delta\mathcal{V}$ starts to grow. This means that the reference grid $G_{\text{ref}}$ provides enough spatial resolution for our purposes.

For the truncated Wigner SDEs, Fig. 7.8, (b) shows that the decrease of radial or axial spacing as compared to the reference values still changes the results significantly. But since it is not observed in CGPEs case, we must conclude that this is the result of the criterion (5.22) being violated. Even at $t = 0\,\text{s}$ the number of modes for the reference grid is only ten times smaller than $N = 55,000$, and at $t = 1.3\,\text{s}$ the total population becomes 2 times smaller due to losses (see Fig. 7.6, (a)). Therefore, the further increase of the number of grid points and, correspondingly, modes, makes the truncated Wigner results unreliable.

In view of the results described in this section, we have chosen the grid $\mathbf{G}_{\text{ref}}$ and the box $\mathbf{B}_{\text{ref}}$ for all the interferometry simulations in Chapter 7 and Chapter 8. The only exception to this is Section 8.2, where we used the same grid, but the box size was scaled down according to the lower total number of atoms (we used the same criterion of 1.2

times the size of the Thomas-Fermi ground state).

It must be noted that it is possible to decouple the grid size and the number of modes by applying the projector in (7.28) explicitly instead of relying on the implicit cutoff enforced by the grid. This requires grid padding to avoid aliasing [39], and thus significantly increases simulation time. On the other hand it does not give much in terms of spatial resolution, since, with higher frequency modes being projected out in mode space, the corresponding fine details in the coordinate space disappear. Therefore in this thesis we have settled with using only the implicit cutoff, except for Section 8.2, where the low number of atoms made the truncation approximation invalid otherwise.

## 7.6. Phase noise

Another important characteristic of a BEC interferometry experiment is phase noise, which is connected to the visibility. We will explain it by the example of the same experiment [42, 87] as in the previous section.

While in the simulation we can measure the visibility (7.33) simply by calculating a second-order moment, experimentalists do not have the luxury of knowing the wave-functions of the components. Instead, multiple runs of the Ramsey sequence with the same evolution time are performed, with the second $\pi/2$-pulse having a different phase lag $\phi$ each time. The quantity that can be measured in the experiment is the normalized atom difference

$$P_z = \frac{N_2' - N_1'}{N_1' + N_2'}, \tag{7.40}$$

where $N_1'$ and $N_2'$ are populations of the components obtained by imaging after the second $\pi/2$-pulse. Using the rotation matrix (7.8) it can be shown that $P_z$ can be expressed in terms of wave operators before the second $\pi/2$-pulse as

$$P_z(\phi) = -\frac{2}{N_1 + N_2} \operatorname{Im}\left(e^{-i\phi} \int \langle \tilde{\Psi}_1^\dagger \Psi_2 \rangle \mathrm{d}\mathbf{x}\right). \tag{7.41}$$

One can notice that the integral of the second order moment in this expression is the same as in (7.33) and is also normalized on the total population. Therefore if we vary $\phi$ in the experiment, the resulting $P_z(\phi)$ can be fitted with a sine function, and its amplitude

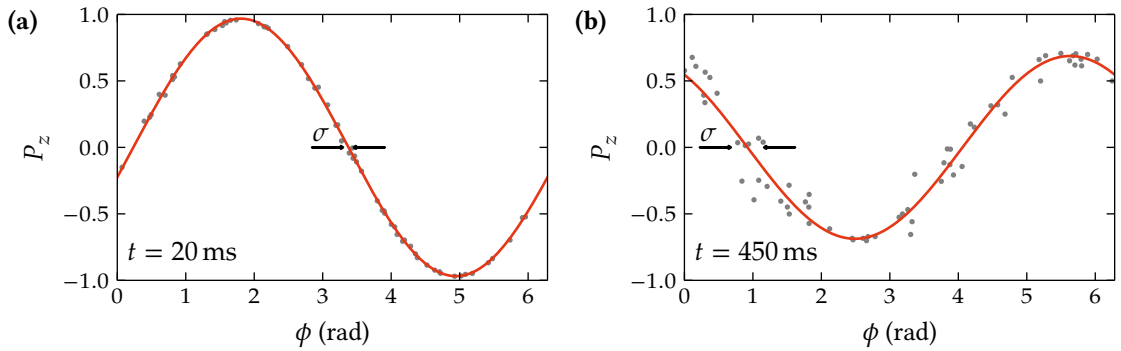


Figure 7.9.: Phase noise in experimental measurements of visibility at **(a)** $t = 20\,\mathrm{ms}$ and **(b)** $t = 450\,\mathrm{ms}$. Black dots illustrate possible results obtained in a single run of the Ramsey interferometry experiment.

will give us the visibility $\mathcal{V}$.

In practice, naturally, the measurement of $P_z$ is affected by various sources of technical noise. As a result, the measured points are displaced from the ideal curve. In the experiment in question, three such noise sources were identified. First, the length of $\pi/2$-pulses varied throughout the experimental runs with an estimated standard deviation of $\Delta\theta = 0.02\,\mathrm{rad}$ (caused by the drift of the Rabi frequency $\Omega$). The phase of the coupler also had an uncertainty caused by the microwave frequency instability of the oscillator used for coupling, that grew with time as $\Delta\phi/t = 0.5\,\mathrm{rad/s}$. Finally, the imaging technique used to measure populations $N_1'$ and $N_2'$ resulted in an uncertainty of $\Delta N/N = 0.023$. These factors can be trivially added to the simulations: the first two at the moment of the application of the rotation matrix (7.8), by adding a random factor to the length $\theta$ and the phase $\phi$, and the third one by adding a random factor to the populations $N_1$ and $N_2$ produced by integrating the corresponding moments of wavefunctions.

The result is illustrated in Fig. 7.9, with the "experimental" points emulated this way plotted against a sine fit, for two different evolution times. The base simulation is the truncated Wigner one for the regular Ramsey sequence from the previous section. The standard deviation $\sigma$ of the horizontal distance from the fitting curve for the experimental results is called the phase noise. The amplitude of the curve, in turn, is taken to be the predicted visibility accounting for the technical noises (see Fig. 7.4 and Fig. 7.6 in the previous section).

A comparison of the phase noise with the experimental data for the regular Ramsey sequence is shown in Fig. 7.10. The experimental parameters are the same as in the

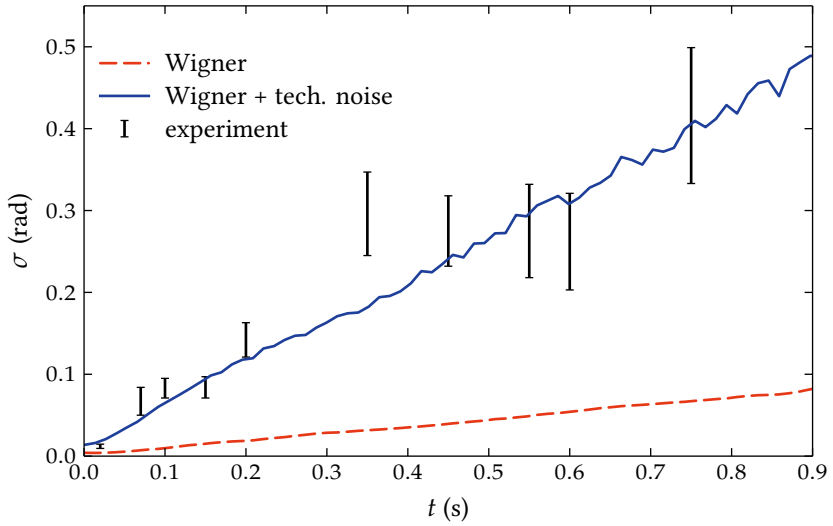


Figure 7.10.: Comparison of experimental (black bars) and numerically simulated phase noise at the end of a Ramsey sequence with evolution time $t$. The truncated Wigner predictions with (blue solid line) and without (red dashed line) the inclusion of technical noise is shown.

previous section. The effect of quantum noise (red dashed line) is noticeable, but not very large as compared to the compound effect of the technical noises (blue solid line). There seems to be a lot of room for the improvement of the apparatus until the measurements hit the "hard" limit of quantum noise.

Phase noise in a spin echo sequence can be estimated in the same way. The reported MW frequency instability for this experiment was $\Delta\phi/t = 0.125\,\mathrm{rad/s}$. As Fig. 7.11 shows, even after the inclusion of the technical noise, there is some disagreement with the experimental data. This may be caused by systematic error introduced by the Wigner truncation, or possibly by some additional source of technical noise.

The total noise shown in Fig. 7.10 and Fig. 7.11 is lower than the one reported by Egorov *et al* [42, 87]. The reason for this is that in this thesis we have not taken into account the uncertainty in the prepared atom number, which can be quite significant. If each of the experiments starts from a different atom number, each of the measured $P_z$ points in Fig. 7.9 belongs to a different family of results (since the frequency of Ramsey fringes has a non-trivial dependence on the atom number), so they cannot be fitted with a single curve. The initial atom number in each of the experiments can be inferred based on the measured final $N_1$ and $N_2$, and the adjustment to phase noise can be made. This adjustment grows in time as the inference becomes less accurate. Additional phase noise caused by this factor is comparable to that from the other sources [87] and accounts for

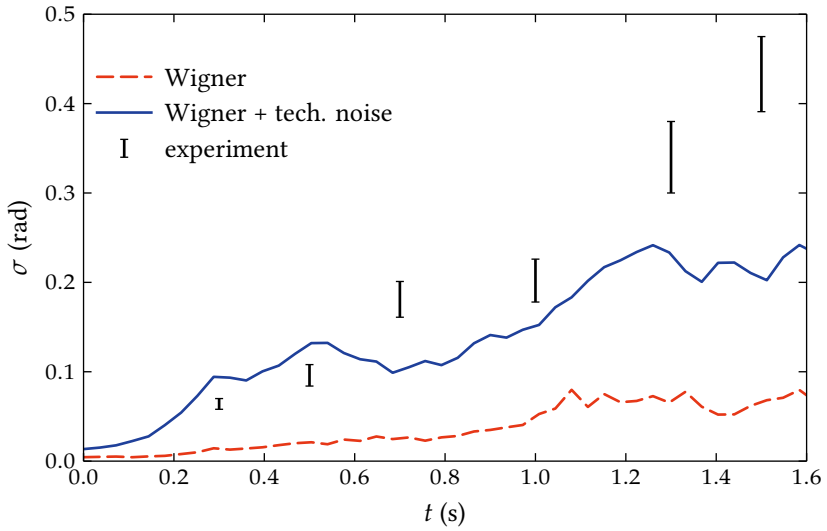


Figure 7.11.: Comparison of experimental (black bars) and numerically simulated phase noise at the end of a spin echo sequence with evolution time $t$. The truncated Wigner predictions with (blue solid line) and without (red dashed line) the inclusion of technical noise is shown.

the difference in presented results.

## 7.7. Conclusion

The examples in this chapter demonstrate that the truncated Wigner approach gives long-time predictions of quantum effects for the system comprised of a large number of atoms. Both of these features, large atom numbers and long time-scales, are essential to accurate interferometric measurements.

We show that current experiments are limited primarily by technical noise, and an accurate inclusion of these factors in the simulations can improve the predictions significantly. The uncertainty in the initial atom number has a large effect on phase noise and accounts for part of the difference of our simulations with the experimental results. A quantitative estimation of its effect on visibility requires it to be formally included in the model and remains for future work.

Another possible source of discrepancies are finite temperature effects. These can be included in the model by using an initial thermalized state (see the end of Section 5.8 for references). This factor may account for the noticeable difference in the minimum of the first visibility fringe (Fig. 7.4), which cannot be explained by technical noise.

# Chapter 8.

# Squeezing in BEC interferometry

As we have seen in the previous chapters, the truncated Wigner method provides significant corrections to such important experimental observables as visibility or phase noise. While they do establish the theoretical limits for these quantities, real measurements are still mostly limited by technical noise, which do not require quasiprobability methods to account for.

In this chapter we will consider a property of BEC interferometry experiments which cannot be obtained from the mean-field approximation. This property is the degree of spin squeezing, which allows to reduce the minimum uncertainty of the collective spin of a two-component BEC below the shot noise limit. A state with a high degree of coherence between the two components, the coherent spin state [88], has equal uncertainty in any direction. Further evolution and nonlinear interactions can redistribute quantum noise, making it possible to achieve an uncertainty lower than the shot noise along one direction (at the price of the increased uncertainty in other directions, to preserve the Heisenberg inequality). Spin squeezing has been theoretically introduced by Kitagawa and Ueda [88], and by Wineland *et al* [89], and later observed experimentally [90, 91]. It allows an outcome of interferometry experiments to be measured with uncertainty beyond the standard shot noise limit [73, 92] and can serve as a measure of entanglement in a two-component BEC [93, 94].

In this chapter we will derive an expression that will allow us to obtain the degree of squeezing from the moments of wavefunctions in the truncated Wigner method, and apply it to a recent spin squeezing experiment. We will also consider another possible experiment with a BEC near a Feshbach resonance where spin squeezing can be observed

and discuss the complications caused by nonlinear losses.

## 8.1. Spin squeezing in the Wigner representation

Following Sørensen *et al* [93] and Li *et al* [24], we define the components of the collective spin vector $\hat{\mathbf{S}} \equiv (\hat{S}_x, \hat{S}_y, \hat{S}_z)$ in terms of field operators as

$$\begin{aligned}
\hat{S}_x &= \frac{1}{2}\int \mathrm{d}\mathbf{x}\left(\tilde{\Psi}_2^\dagger\tilde{\Psi}_1 + \tilde{\Psi}_1^\dagger\tilde{\Psi}_2\right), \\
\hat{S}_y &= \frac{i}{2}\int \mathrm{d}\mathbf{x}\left(\tilde{\Psi}_2^\dagger\tilde{\Psi}_1 - \tilde{\Psi}_1^\dagger\tilde{\Psi}_2\right), \\
\hat{S}_z &= \frac{1}{2}\int \mathrm{d}\mathbf{x}\left(\tilde{\Psi}_1^\dagger\tilde{\Psi}_1 - \tilde{\Psi}_2^\dagger\tilde{\Psi}_2\right).
\end{aligned} \tag{8.1}$$

The degree of squeezing is then

$$\xi^2 = \frac{N \min_{\vec{n}\perp\langle\hat{\mathbf{S}}\rangle} \Delta\hat{S}^2_{\vec{n}}}{\langle\hat{\mathbf{S}}\rangle^2}, \tag{8.2}$$

where $\Delta\hat{S}^2_{\vec{n}}$ is the variance of the total spin along the direction $\vec{n}$, and $N$ is the total number of atoms. This quantity can serve as an entanglement criterion, indicating its occurrence when $\xi^2 < 1$ [93]. Note that in this thesis we only consider the squeezing along the direction orthogonal to the total spin, as was originally introduced, but other definitions are also possible [95].

A straightforward way of finding the $\xi^2$ is to shift the coordinate frame to the end of the vector $\langle\hat{\mathbf{S}}\rangle$, and rotate it so that one of the axes is aligned along it. The minimum variance can then be found by varying the angle of rotation of the other two axes and calculating the variance along one of them (in fact, this is how it is usually done in the experiment). The direct approach consists of expressing the desirable minimum variance in terms of variances of the components of the spin vector in the original coordinates [24]. We denote the polar and the azimuthal angle of $\langle\hat{\mathbf{S}}\rangle$ as $\nu$ and $\phi$ respectively, meaning that

$$\nu = \arccos\frac{\langle\hat{S}_z\rangle}{\langle\hat{\mathbf{S}}\rangle}, \quad \phi = \arg\langle\hat{S}_x + \hat{S}_z\rangle. \tag{8.3}$$

The minimum uncertainty is then expressed as

$$\begin{aligned}\min_{\vec{n}\perp\langle\hat{\mathbf{S}}\rangle}\Delta\hat{S}^2_{\vec{n}} = &\frac{1}{2}\left(\cos^2\nu\cos^2\phi+\sin^2\phi\right)\Delta_{xx}+\frac{1}{2}\left(\cos^2\nu\sin^2\phi+\cos^2\phi\right)\Delta_{yy}\\ &+\frac{1}{2}\sin^2\nu\,\Delta_{zz}-\frac{1}{2}\sin^2\nu\sin 2\phi\,\Delta_{xy}-\frac{1}{2}\sin 2\nu\cos\phi\,\Delta_{xz}\\ &-\frac{1}{2}\sin 2\nu\sin\phi\,\Delta_{yz}-\frac{1}{2}\sqrt{\tilde{A}^2+\tilde{B}^2},\end{aligned} \tag{8.4}$$

where

$$\begin{aligned}\tilde{A} = &\left(\sin^2\phi-\cos^2\nu\cos^2\phi\right)\Delta_{xx}+\left(\cos^2\phi-\cos^2\nu\sin^2\phi\right)\Delta_{yy}\\ &-\sin^2\nu\,\Delta_{zz}-\left(1+\cos^2\nu\right)\sin 2\phi\,\Delta_{xy}\\ &+\sin 2\nu\cos\phi\,\Delta_{xz}+\sin 2\nu\sin\phi\,\Delta_{yz},\end{aligned} \tag{8.5}$$

and

$$\begin{aligned}\tilde{B} = &\cos\nu\sin 2\phi\left(\Delta_{xx}-\Delta_{yy}\right)-2\cos\nu\cos 2\phi\,\Delta_{xy}\\ &-2\sin\nu\sin\phi\,\Delta_{xz}+2\sin\nu\cos\phi\,\Delta_{yz}.\end{aligned} \tag{8.6}$$

The spin correlations $\Delta_{ij}$ are defined as

$$\Delta_{ij}=\frac{1}{2}\langle\hat{S}_i\hat{S}_j+\hat{S}_j\hat{S}_i\rangle-\langle\hat{S}_i\rangle\langle\hat{S}_j\rangle,\quad i,j=x,y,z. \tag{8.7}$$

Averages of the total spin vector components and their pairwise moments can be expressed calculated using moments of the Wigner functional according to (5.37). The averages are calculated straightforwardly if we remember that the field operators of different components commute:

$$\begin{aligned}\langle\hat{S}_x\rangle &= \left\langle\mathrm{Re}\int\Psi_1^*\Psi_2\mathrm{d}\mathbf{x}\right\rangle_{\mathrm{traj}}\equiv\langle\mathrm{Re}\,I\rangle_{\mathrm{traj}}\equiv\left\langle S_x\right\rangle_{\mathrm{traj}},\\ \langle\hat{S}_y\rangle &= \left\langle\mathrm{Im}\int\Psi_1^*\Psi_2\mathrm{d}\mathbf{x}\right\rangle_{\mathrm{traj}}\equiv\langle\mathrm{Im}\,I\rangle_{\mathrm{traj}}\equiv\left\langle S_y\right\rangle_{\mathrm{traj}},\\ \langle\hat{S}_z\rangle &= \frac{1}{2}\left\langle\int\Psi_1^*\Psi_1\mathrm{d}\mathbf{x}-\int\Psi_2^*\Psi_2\mathrm{d}\mathbf{x}\right\rangle_{\mathrm{traj}}\equiv\left\langle(N_1-N_2)/2\right\rangle_{\mathrm{traj}}\equiv\left\langle S_z\right\rangle_{\mathrm{traj}},\end{aligned} \tag{8.8}$$

where we have introduced the functionals of wavefunctions in a single simulation path $I\equiv S_x+iS_y$ and $(N_1-N_2)/2\equiv S_z$.

The second-order moments of the spin operators are obtained by transforming normally ordered field operator products to symmetrically ordered ones, substituting path averages

of wavefunction moments and grouping terms. Starting with $\langle \hat{S}_x^2 \rangle$, we can express it in terms of symmetrically ordered operator products as

$$\begin{aligned}\langle \hat{S}_x^2 \rangle &= \frac{1}{4}\left\langle \iint \left(\tilde{\Psi}_2^\dagger \tilde{\Psi}_1 + \tilde{\Psi}_1^\dagger \tilde{\Psi}_2\right)\left(\tilde{\Psi}_2'^\dagger \tilde{\Psi}_1' + \tilde{\Psi}_1'^\dagger \tilde{\Psi}_2'\right) \mathrm{d}\mathbf{x}\,\mathrm{d}\mathbf{x}' \right\rangle \\ &= \frac{1}{4}\left\langle \iint \left( \left\{\tilde{\Psi}_2^\dagger \tilde{\Psi}_1 \tilde{\Psi}_2'^\dagger \tilde{\Psi}_1'\right\}_{\mathrm{sym}} + \left\{\tilde{\Psi}_1^\dagger \tilde{\Psi}_2 \tilde{\Psi}_2'^\dagger \tilde{\Psi}_1'\right\}_{\mathrm{sym}} \right.\right. \\ &\quad + \left\{\tilde{\Psi}_1^\dagger \tilde{\Psi}_2 \tilde{\Psi}_1'^\dagger \tilde{\Psi}_2'\right\}_{\mathrm{sym}} + \left\{\tilde{\Psi}_2^\dagger \tilde{\Psi}_1 \tilde{\Psi}_1'^\dagger \tilde{\Psi}_2'\right\}_{\mathrm{sym}} \\ &\quad \left.\left. -\frac{1}{2}\,\mathrm{Re}\left(\delta_{\mathbb{M}_1}(\mathbf{x},\mathbf{x}')\delta_{\mathbb{M}_2}(\mathbf{x}',\mathbf{x})\right)\right) \mathrm{d}\mathbf{x}\,\mathrm{d}\mathbf{x}' \right\rangle.\end{aligned} \tag{8.9}$$

In general, basis sets of the first and the second component are different, and the last term in the above equation cannot be simplified any further. However, in the numerical simulations in this chapter we use the same set $\mathbb{M}_1 = \mathbb{M}_2 = \mathbb{M}$ for both components, which allows us to transform it to a more convenient form

$$\begin{aligned}\iint \mathrm{Re}\left(\delta_{\mathbb{M}}(\mathbf{x},\mathbf{x}')\delta_{\mathbb{M}}(\mathbf{x}',\mathbf{x})\right) \mathrm{d}\mathbf{x}\,\mathrm{d}\mathbf{x}' &= \frac{1}{2}\iint \left(\sum_{\mathbf{m}\in\mathbb{M}} \phi_{\mathbf{m}}'\phi_{\mathbf{m}}^* \sum_{\mathbf{n}\in\mathbb{M}} \phi_{\mathbf{n}}\phi_{\mathbf{n}}'^* + \mathrm{c.c.}\right) \mathrm{d}\mathbf{x}\,\mathrm{d}\mathbf{x}' \\ &= \frac{1}{2}\sum_{\mathbf{m}\in\mathbb{M}}\sum_{\mathbf{n}\in\mathbb{M}} \left(\delta_{\mathbf{m},\mathbf{n}}\delta_{\mathbf{m},\mathbf{n}} + \delta_{\mathbf{m},\mathbf{n}}\delta_{\mathbf{m},\mathbf{n}}\right) \\ &= |\mathbb{M}|,\end{aligned} \tag{8.10}$$

where we have expanded the restricted delta functions using the expression from Definition B.4. Applying (5.37) to the full expression for $\langle \hat{S}_x^2 \rangle$, we rewrite it in terms of wavefunctions in the Wigner representation:

$$\begin{aligned}\langle \hat{S}_x^2 \rangle &= \frac{1}{4}\left\langle \int \Psi_2^*\Psi_1 \mathrm{d}\mathbf{x} \int \Psi_2^*\Psi_1 \mathrm{d}\mathbf{x} + \int \Psi_1^*\Psi_2 \mathrm{d}\mathbf{x} \int \Psi_2^*\Psi_1 \mathrm{d}\mathbf{x} \right. \\ &\quad \left. + \int \Psi_1^*\Psi_2 \mathrm{d}\mathbf{x} \int \Psi_1^*\Psi_2 \mathrm{d}\mathbf{x} + \int \Psi_2^*\Psi_1 \mathrm{d}\mathbf{x} \int \Psi_1^*\Psi_2 \mathrm{d}\mathbf{x} - \frac{|\mathbb{M}|}{2} \right\rangle_{\mathrm{traj}} \\ &= \frac{1}{4}\left\langle (I^*)^2 + II^* + I^2 + I^*I \right\rangle_{\mathrm{traj}} - \frac{|\mathbb{M}|}{8} \\ &= \left\langle (\mathrm{Re}\, I)^2 \right\rangle_{\mathrm{traj}} - \frac{|\mathbb{M}|}{8} = \left\langle S_x^2 \right\rangle_{\mathrm{traj}} - \frac{|\mathbb{M}|}{8}.\end{aligned} \tag{8.11}$$

Using the same procedure, we find the expectations for other pairwise moments of the

spin operators:

$$\begin{aligned}
\langle \hat{S}_y^2 \rangle &= \left\langle S_y^2 \right\rangle_{\text{traj}} - \frac{|\mathbb{M}|}{8}, \\
\langle \hat{S}_z^2 \rangle &= \langle S_z^2 \rangle_{\text{traj}} - \frac{|\mathbb{M}|}{8}, \\
\frac{1}{2}\langle \hat{S}_x \hat{S}_y + \hat{S}_y \hat{S}_x \rangle &= \left\langle S_x S_y \right\rangle_{\text{traj}}, \\
\frac{1}{2}\langle \hat{S}_x \hat{S}_z + \hat{S}_z \hat{S}_x \rangle &= \langle S_x S_z \rangle_{\text{traj}}, \\
\frac{1}{2}\langle \hat{S}_y \hat{S}_z + \hat{S}_z \hat{S}_y \rangle &= \left\langle S_y S_z \right\rangle_{\text{traj}}.
\end{aligned} \tag{8.12}$$

Now we have all the required expectations to calculate the spin correlations $\Delta_{ij}$ and, consequently, the degree of squeezing $\xi^2$. Note that if we neglect the term $|\mathbb{M}|/8$ in the equations for $\langle \hat{S}_i^2 \rangle$ (which is small as compared to $S_i^2$ when the Wigner truncation condition (5.23) applies), the spin correlations behave "classically". This means that they behave as if we had a "cloud" of spin vectors, where each vector corresponds to a separate simulation path, and the correlations are classical correlations of different vector components in this cloud. Consequently, without giving up too much accuracy we can informally illustrate the total spin uncertainty by plotting the distribution of the total spin vector $(S_x, S_y, S_z)$ over the integration trajectories.

## 8.2. Squeezing by component separation

As an example of measurement of the degree of squeezing in a real two-component BEC system, we will consider a recent experiment [73], in which multi-particle entanglement and resulting spin squeezing was achieved by controlling nonlinear interaction using a component-dependent potential.

The experiment essentially consisted of the same regular Ramsey sequence as depicted in Fig. 7.3, (a) performed for 1250 $^{87}$Rb atoms in the hyperfine state $|F = 1, m_F = -1\rangle$ in a cigar-shaped trap with $f_x = f_y = 109\,\text{Hz}, f_z = 500\,\text{Hz}$. The experiment started with an application of a $\pi/2$-pulse using an oscillator with the Rabi frequency $\Omega = 2\pi \times 2.1 \times 10^3\,\text{rad/s}$, creating an equal superposition of two hyperfine states $|F = 1, m_F = -1\rangle$ and $|F = 2, m_F = +1\rangle$. The second pulse had a varied length allowing a measurement of the spin along the angle $\theta$: $\hat{S}_\theta = \hat{S}_z \cos\theta - \hat{S}_y \sin\theta$ (spin tomography).

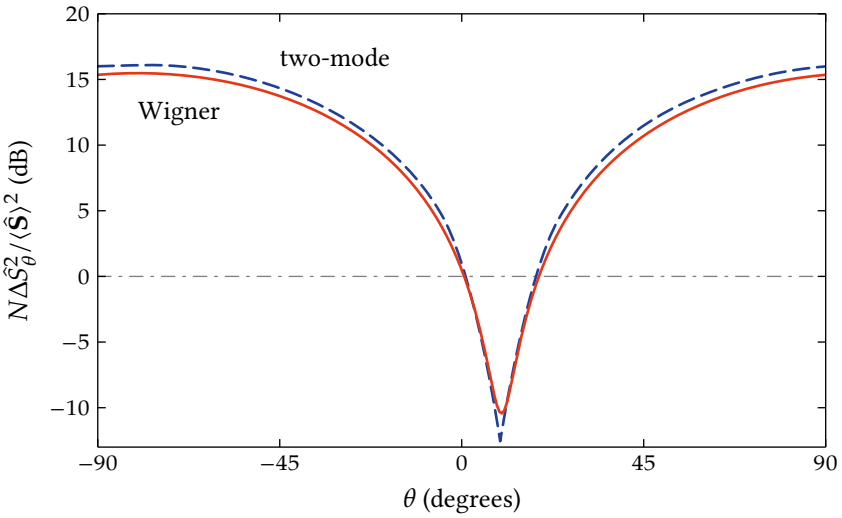


Figure 8.1.: Dependence of the normalized variance of the total spin in the orthogonal plane on the rotation angle $\theta$ for the Wigner method (red solid line) and the two-mode variational method (dashed blue line, data taken from Riedel *et al* [73]).

The important difference was an addition of the component-dependent longitudinal shift to the potential $l_z^{(1,2)} = \pm 0.26\,\mu\text{m}$ right after the first pulse (as described by (7.2)), persisting the whole time of the evolution until the second oscillator pulse. This effectively reduced the component overlap and provided a way of enabling the nonlinearity only at a chosen "best squeezing" time according to the one-axis twisting Hamiltonian model [88].

The truncated Wigner approach is applied straightforwardly to this system and allows us to measure the degree of squeezing $\xi^2$ according to the formula (8.2), calculating the required spin correlations using the expressions derived in Section 8.1. Furthermore, we can simulate the observations closer to those used in the experiment, and collect the spin tomography results, as shown in Fig. 8.1. The maximum degree of squeezing and the corresponding rotation angle corresponds to the minimum of the graph. The simulation used a $16 \times 16 \times 128$ spatial grid, $20,000$ time steps and $12,800$ stochastic trajectories (to collect more data for Fig. 8.2; the estimation of the optimum squeezing would require much less than that). We used the energy cutoff $\epsilon_{\text{cut}} = 5000\hbar$ (chosen to produce the safe padded momentum space [39]) which reduced the number of effective modes to 70.

The Wigner method shows good agreement with the two-mode variational method [24], which was used by the experimental team, and also includes the effect of particle losses. The two-mode method predictions were taken from [73] and plotted in Fig. 8.1 for the sake of comparison. The figure demonstrates that the predictions of the two methods for

the maximum squeezing angle are nearly identical, and the predictions of the degree of squeezing are close, yet noticeably different ($-10.73 \pm 0.05$ dB from the Wigner method as compared with $-12.8$ dB from the two-mode method). We believe that this is caused by the Wigner method being a more systematic type of quantum noise treatment, and, consequently, more suitable for such complex calculations.

This prediction is hard to verify experimentally as the technical noise greatly reduces the degree of squeezing (down to $-3.7$ dB), moving it far from the theoretical limit. The technical noise was not included in the simulations in this thesis, although it can be done similarly to Chapter 7 (since the technical noise in this experiment has similar nature). On the other hand, the maximum "unsqueezing" (the maximums of the plot in Fig. 8.1), while being irrelevant for practical purposes, can serve as a good experimental check for the two-mode and Wigner methods, as it is much less affected by the technical noise. The difference of 1 dB in the maximum unsqueezing between the two methods should be possible to distinguish. We see that while the variational approach is adequate for current experiments, the more precise method used here will be needed in future.

It should be noted that because of the large number fluctuations, the squeezing definition used in the experiment actually corresponds to the one introduced by He *et al* [94], with variable particle number.

We can go further and reconstruct the spin noise distribution using per-path values of the total spin components, as explained in the end of Section 8.1. The projections of the resulting probability distribution on three orthogonal planes are shown in Fig. 8.2. The projection on the $yz$ plane is similar to the one obtained experimentally [73], and it is clearly seen that the direction used to measure the squeezing in the experiment is indeed the best one, as the cloud is much wider in other directions. The $yz$ pane illustrates the physical meaning of the best squeezing angle: it is chosen so that the standard deviation of the total spin distribution in the orthogonal direction is minimal.

## 8.3. Squeezing near a Feshbach resonance

In the previous section we have discussed an experiment with component-dependent potentials, which helped to reduce the inter-component interaction for the majority of time and thus avoid "oversqueezing". A similar effect can be achieved differently — by

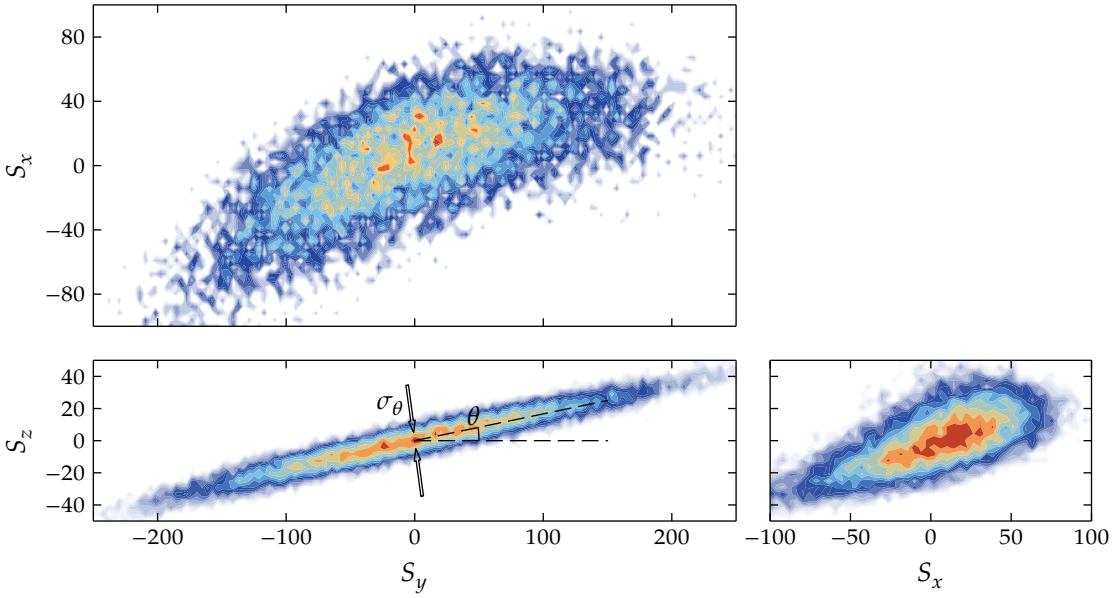


Figure 8.2.: Reconstructed probability distribution for the components of the total spin vector in $xy$ (top), $yz$ (bottom left) and $xz$ (bottom right) planes. The $yz$ plane illustrates the spin squeezing achieved in the experiment: the variance $\Delta^2 \hat{S}_\theta$ is the variance of the distribution in the direction $\theta$ (shown with two arrows): $\Delta^2 \hat{S}_\theta \equiv \sigma_\theta^2$.

manipulating the external magnetic field near a Feshbach resonance for a chosen pair of hyperfine states [92]. This allows one to vary the interaction in a wide range with relative ease. The downside of this approach is a significant increase of the inter-component nonlinear loss rate accompanying the change in the interaction strength. This results in the destruction of the squeezing as the two components interfere with each other and lose coherence.

The truncated Wigner approach allows us to investigate the combined effect of a reduced interaction strength and increased losses. In this section we will consider a hypothetical interferometry experiment with two hyperfine states of $^{87}$Rb and demonstrate how with the help of the Wigner method we can pick the optimal value of the magnetic field that leads to the maximum squeezing.

The experiment follows the general scheme used in this and the previous chapters. We start from a BEC of $N = 55000$ $^{87}$Rb atoms in the hyperfine state $|F = 1, m_F = +1\rangle$ in a cigar-shaped trap with the frequencies $f_x = f_y = 97.0\,\text{Hz}$ and $f_z = 11.69\,\text{Hz}$. The first $\pi/2$-pulse creates an equal superposition of two states, $|F = 1, m_F = +1\rangle$ and $|F = 2, m_F = -1\rangle$. The external magnetic field of strength $B \approx B_0$ is applied, where

$B_0 = 9.1047\,\mathrm{G}$ corresponds to the Feshbach resonance for the two hyperfine states used [96]. We then investigate the time dependence of the maximum degree of spin squeezing. Intra-component interaction strengths do not depend on the external magnetic field, and are taken to be $a_{11} = 100.4\,r_B$ and $a_{22} = 95.44\,r_B$. The numerical simulations used a $8 \times 8 \times 64$ spatial grid, $20,000$ time steps and 2560 stochastic trajectories.

The dependence of the inter-component interaction and loss rate can be described with a single equation for the complex scattering length [96]

$$a(B) = a_{\mathrm{bg}}\left(1 - \frac{\Delta B}{(B - B_0) - i\gamma_B/2}\right), \tag{8.13}$$

where $a_{\mathrm{bg}}$ is the background scattering length, $\Delta B$ is the resonance width, and $\gamma_B$ is the decay width. For a given $B$, the real part of this value acts as the $s$-wave scattering length $a_{12}$ for the interaction coefficient in (7.1):

$$g_{12}(B) = \frac{4\pi\hbar^2 \operatorname{Re} a(B)}{m} = \frac{4\pi\hbar^2 a_{\mathrm{bg}}}{m}\left(1 - \frac{\Delta B(B - B_0)}{(B - B_0)^2 + \gamma_B^2/4}\right), \tag{8.14}$$

and the imaginary part can be connected to the loss rate by substituting it into (7.1) as well and comparing the resulting expression with the corresponding loss term in (7.7):

$$\gamma_{12}(B) = -\frac{8\pi\hbar \operatorname{Im} a(B)}{m} = \frac{4\pi\hbar a_{\mathrm{bg}} \Delta B \gamma_B}{m((B - B_0)^2 + \gamma_B^2/4)}. \tag{8.15}$$

For the Feshbach resonance we use the reported parameters are $\Delta B = 2 \times 10^{-3}\,\mathrm{G}$, $\gamma_B = 4.7 \times 10^{-3}\,\mathrm{G}$, and $a_{\mathrm{bg}} = 97.7\,r_B$ [96]. The behavior of the real and imaginary parts of $a(B)$ near the resonance is shown in Fig. 8.3. From the equations above, as well as from the figure, it is obvious that the minimum inter-species scattering length is achieved when $B - B_0 = 0.5\gamma_B$. Unfortunately, this value also corresponds to a relatively large value of the imaginary part, and, correspondingly, an unacceptable loss rate. Therefore, we pick values of $B$ further from the resonance, as displayed in the figure, where the inter-component interaction is somewhat stronger, but the loss rate is much

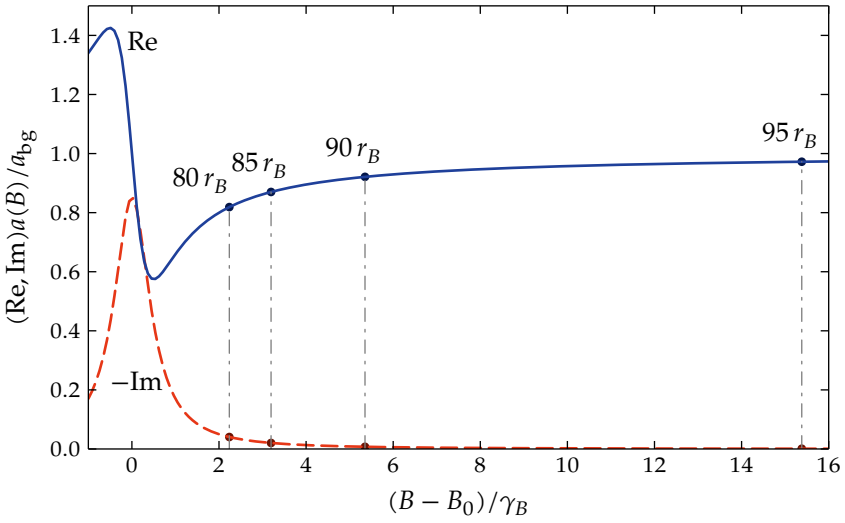


Figure 8.3.: Real (blue solid line) and imaginary (red dashed line, negated value is plotted for compactness) parts of the complex scattering length near the Feshbach resonance at $B_0 = 9.1047\,\mathrm{G}$. Four pairs of points show the distances from the resonance chosen for the simulation.

lower. Equations (8.14) and (8.15) give us the following values for the simulation:

$$\begin{aligned}
B - B_0 &= 2.24\gamma_B, \quad a_{12} = 80.0\,r_B, \quad \gamma_{12} = 3.85 \times 10^{-12}\,\mathrm{cm}^3/\mathrm{s}, \\
B - B_0 &= 3.20\gamma_B, \quad a_{12} = 85.0\,r_B, \quad \gamma_{12} = 1.93 \times 10^{-12}\,\mathrm{cm}^3/\mathrm{s}, \\
B - B_0 &= 5.35\gamma_B, \quad a_{12} = 90.0\,r_B, \quad \gamma_{12} = 7.00 \times 10^{-13}\,\mathrm{cm}^3/\mathrm{s}, \\
B - B_0 &= 15.4\gamma_B, \quad a_{12} = 95.0\,r_B, \quad \gamma_{12} = 8.53 \times 10^{-14}\,\mathrm{cm}^3/\mathrm{s}.
\end{aligned} \tag{8.16}$$

First, we run the simulations with $\gamma_{12}$ set to zero in order to test the squeezing in ideal conditions. As expected, the lower cross-term $a_{12}$ is, the stronger is the squeezing, as shown in Fig. 8.4, (a).

With the inclusion of inter-component losses, the picture is different. Feshbach tuning to $a_{12} = 90.0\,r_B$ ensures the best squeezing of the four variants (−12 dB at 60 ms), whereas long lasting squeezing is predicted for the variant with $a_{12} = 95.0\,r_B$ (Fig. 8.4, (b)). In practice, it is possible to run the simulation for other values of $B$, thus finding the ideal balance between the interaction strength and the loss rate which produces the maximum squeezing.

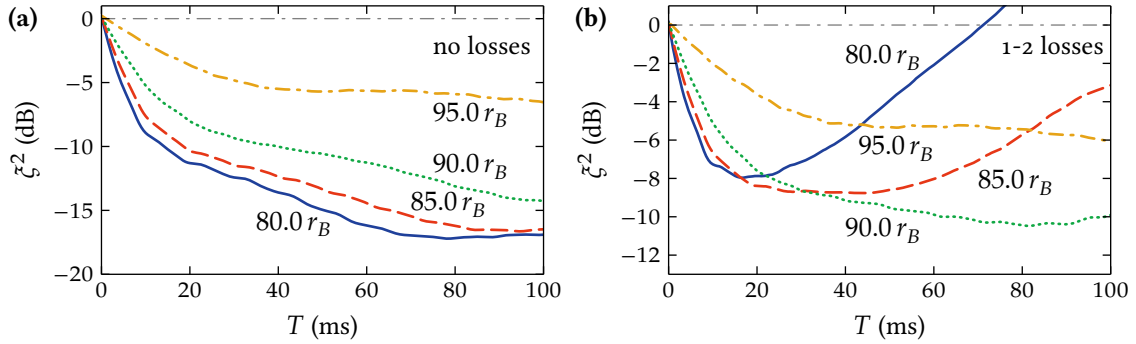


Figure 8.4.: Truncated Wigner simulations of the squeezing in the vicinity of the $B_0 = 9.1047\,\mathrm{G}$ Feshbach resonance in $^{87}$Rb with different values of the external magnetic field, with **(a)** losses turned off, and **(b)** inter-component 1, 2-losses turned on. Results corresponding to the scattering lengths $a_{12} = 80.0\,r_B$ (blue solid line), $a_{12} = 85.0\,r_B$ (red dashed line), $a_{12} = 90.0\,r_B$ (green dotted line), and $a_{12} = 95.0\,r_B$ (yellow dash-dotted line) are plotted. The same-colored bands show the estimated sampling error.

## 8.4. Conclusion

In this chapter we have demonstrated that the truncated Wigner approach can be successfully used to obtain correlations of higher orders from simulations without changing the simulations themselves, but only by processing the raw results. Nonlinear elastic and inelastic interactions, along with various sources of technical noises can be added to the model straightforwardly, without affecting the measurement of the required correlations. The simulations described in this chapter predict the degree of quantum noise-reduction, which is a technique that can be used to improve precision quantum interferometry. The quantum noise is initially reduced due to stretching and rotation of the quantum noise ellipsoid (see Fig. 8.2), similar to that found in quantum soliton squeezing [29, 45]. Importantly, these quantum squeezing calculations indicate conditions that will allow this macroscopic quantum effect to be experimentally observed in ultra-cold atomic BECs for much larger atom numbers than calculated previously.

# Chapter 9.

# Probabilistic representation of Bell inequalities violation

In this final chapter we will diverge from the central topic of this thesis — the Wigner representation — and briefly discuss other quasiprobability representations. In particular we will be interested in their ability to model such an inherent property of quantum systems as an entanglement [97], and a consequent violation of Bell inequalities [19]. The possibility of this is often discarded because of the famous Feynman's lecture [7], where he posed a question *"Can quantum systems be probabilistically simulated by a classical computer?"*, and his final answer was *"If ... there's no hocus-pocus, the answer is certainly, No!"*. His argument was based on the assertion that Bell violations cannot be modeled probabilistically [19].

However, it turns out that positive phase-space distributions of quantum optics [13, 17, 60, 61] are capable of such simulations, owing to extended range of the functions of phase-space variables corresponding to physical observables as compared to those considered by Bell. Namely, these functions can have a continuous range of values extending beyond the set of discrete expected values for the physical quantity, and, furthermore, their values can be complex [98]. The expectations of such observables correspond to physical quantities only when integrated with the phase-space distribution as a weight. This method of simulation is analogous to the weak measurement strategy, or POVM (positive operator valued measure) [99], which has been experimentally demonstrated recently [100].

The idea of computationally demonstrating the violation of Bell inequalities using

quasiprobability representations belongs to M. D. Reid.

## 9.1. Cooperative states

A Bell inequality sets a limit on observable correlations in a physical system that obeys a local hidden variable theory (LHV) [19, 101]. This is a classical theory where the results of the measurements are functions of local detector settings and a hidden parameter $\lambda$. Thus, values measured by two spatially separated observers, $A$ and $B$ (for Alice and Bob, as they are usually denoted), can be expressed as $A(a,\lambda)$ and $B(b,\lambda)$, where $a$ and $b$ are Alice's and Bob's detector settings. Possible correlations are defined probabilistically as

$$C(A,B) = \int_{\Lambda} A(a,\lambda)B(b,\lambda)P(\lambda)\mathrm{d}\lambda. \tag{9.1}$$

Experimental values $A$ and $B$ are usually encoded as either 1 or $-1$ in a binary experiment. The Bell theorem derives inequalities that any such correlations in a LHV theory must satisfy. Quantum mechanics violates these inequalities, thus ruling out LHV theories.

### 9.1.1. Quantum state

In this section we will consider Bell violations in cooperative states with $N$ photon pairs, similar to those demonstrated experimentally by Clauser [101], Aspect *et al* [102], and Zeilinger *et al* [103]. The quantum state in question is

$$|N\rangle = \frac{\left(\hat{a}^{\dagger}_{1+}\hat{a}^{\dagger}_{2+} + \hat{a}^{\dagger}_{1-}\hat{a}^{\dagger}_{2-}\right)^{N}|0\rangle}{N!\,(N+1)^{1/2}}, \tag{9.2}$$

where $N$ is the number of photon pairs, indices 1 and 2 denote the propagation direction, and $+$ and $-$ stand for the polarization direction. These states are generated in certain types of optical parametric down-conversion experiments, and it has proved difficult to obtain a direct, loophole free violation of a Bell inequality, owing to detector inefficiencies [104–106] (although this problem has been solved recently [107]). However, these issues are not significant for the simulations in this thesis since we are considering an ideal experiment.

We define the intensity correlations to be [108]

$$G^{IJ}(\gamma, N) = \langle N|\hat{A}^I(1, \hat{\mathbf{a}}_1)\hat{A}^J(\gamma, \hat{\mathbf{a}}_2)|N\rangle. \tag{9.3}$$

They are proportional (exactly for $I = J = N$ and in the first approximation for other variants) to the probability of observing $I$ "+"-polarized photons at detector 1 and $J$ "−"-polarized photons at detector 2. The linear combination parameter depends on the relative polarizer angle $\theta$ as $\gamma = \cos^2\theta$, and auxiliary functions are introduced so that:

$$\begin{aligned} \hat{A}^J(\gamma, \hat{\mathbf{a}}_k) &= \left(\sqrt{\gamma}\hat{a}^\dagger_{k-} + \sqrt{1-\gamma}\hat{a}^\dagger_{k+}\right)^J \left(\sqrt{\gamma}\hat{a}_{k-} + \sqrt{1-\gamma}\hat{a}_{k+}\right)^J, \\ \hat{A}^J(\infty, \hat{\mathbf{a}}_k) &= :\left(\hat{a}^\dagger_{k-}\hat{a}_{k-} + \hat{a}^\dagger_{k+}\hat{a}_{k+}\right)^J: . \end{aligned} \tag{9.4}$$

The "$\infty$" case and the corresponding $G^{IJ}(\infty, N)$ correlation stand for the same measurement as for $G^{IJ}(\gamma, N)$, but with no polarizer in the second detector.

For $N$ photon pairs, the Bell-type inequality is then known to be of the form [108]

$$\Delta^J_N(\theta) = 3g^J_N(\theta) - g^J_N(3\theta) - 2 \leq 0, \tag{9.5}$$

where

$$g^J_N(\theta) = G^{JJ}(\cos^2\theta, N)/G^{JJ}(\infty, N). \tag{9.6}$$

This expression generalizes the usual Clauser, Horne, Shimony and Holt (CHSH) [101] and Bell expressions to a multi-particle form. The quantum mechanical prediction for $g^J_N$ has especially simple form of $g^N_N(\theta) = \cos^{2N}\theta$ for the cases $J = N, N = 1, 2$ which we have simulated. This gives the violation of

$$\Delta_{1\text{ pair}}(\theta) \equiv \Delta^1_1(\theta) = 3\cos^2\theta - \cos^2 3\theta - 2 \tag{9.7}$$

for the two-particle case, which corresponds to the usual two-particle experiment originally proposed by Bell. For the four-particle case, the violation can be found to be

$$\Delta_{2\text{ pairs}}(\theta) \equiv \Delta^2_2(\theta) = 3\cos^4\theta - \cos^4 3\theta - 2. \tag{9.8}$$

### 9.1.2. Positive-P representation

We simulate the violation (9.5) using the positive-P representation [17, 61]. In essence, it is an exact expansion of an arbitrary density matrix of bosons with a positive probability distribution $P(\boldsymbol{\alpha}, \boldsymbol{\beta})$, such that the expectation of an observable $\hat{O}$ is

$$\langle \hat{O} \rangle = \int \mathrm{d}^2\boldsymbol{\alpha}\, \mathrm{d}^2\boldsymbol{\beta}\, P(\boldsymbol{\alpha}, \boldsymbol{\beta}) \langle \boldsymbol{\beta}^* | \hat{O} | \boldsymbol{\alpha} \rangle / \langle \boldsymbol{\beta}^* | \boldsymbol{\alpha} \rangle, \tag{9.9}$$

where $|\boldsymbol{\alpha}\rangle$ is a multimode coherent state. The positive P-representation, therefore, corresponds exactly to the definition of a physical weak measurement [99], with the initial state $|\boldsymbol{\alpha}\rangle$ and the final postselected state $|\boldsymbol{\beta}\rangle$ occurring with probability $P(\boldsymbol{\alpha}, \boldsymbol{\beta})$. The standard form we use is also known to be measurable using multiple beam-splitter operations [109].

The expression above looks very similar to (9.1), given by an LHV theory. The fundamental difference, which allows the correlations obtained from the positive-P distribution to violate Bell inequalities, is that the quantities being sampled can be complex numbers of any magnitude. Only after the weighted averaging with the probability distribution $P$ do they give the value of the observable.

For an arbitrary moment of creation and annihilation operators $\hat{O}(\mathbf{a}^\dagger, \mathbf{a})$, the expectation is calculated as

$$\langle \hat{O} \rangle = \int \mathrm{d}^2\boldsymbol{\alpha}\, \mathrm{d}^2\boldsymbol{\beta}\, P(\boldsymbol{\alpha}, \boldsymbol{\beta}) O(\boldsymbol{\beta}, \boldsymbol{\alpha}), \tag{9.10}$$

where $O$ is a function produced as a result of replacing any $\hat{a}_i$ with $\alpha_i$ and $\hat{a}_i^\dagger$ with $\beta_i$ in $\hat{O}$. For example, the mode population $\langle \hat{a}_i^\dagger \hat{a}_i \rangle$ corresponds to the moment $\beta_i \alpha_i$, which is, in general, complex, and only its expectation is real.

The quantum state (9.2) we are interested in corresponds to the positive-P distribution [108]

$$\begin{aligned} P(\boldsymbol{\alpha}, \boldsymbol{\beta}) = & \left\{ \frac{|(\beta_{1+} + \alpha_{1+}^*)(\beta_{2+} + \alpha_{2+}^*) + (\beta_{1-} + \alpha_{1-}^*)(\beta_{2-} + \alpha_{2-}^*)|^{2N}}{(2\pi)^8 (N+1)(N!)^2 2^{4N}} \right\} \\ & \times \exp\left( -\frac{|\boldsymbol{\alpha}|^2 + |\boldsymbol{\beta}|^2}{2} \right). \end{aligned} \tag{9.11}$$

This distribution exists and has a positive, probabilistic behavior for all values of $N$. Note that it is not unique, and it may be possible to find other expressions that correspond to

the same quantum state, but have better sampling properties.

### 9.1.3. Sampling

In order to illustrate our point better, we simulate the measurement of the operator (9.3) using the Monte-Carlo method: we sample the distribution (9.11) and calculate the weighted average (9.9).

We sample this distribution by transforming it to a form where we can use the well-known von Neumann rejection algorithm. Performing the variable change

$$\mu = \frac{\alpha - \beta^*}{2}, \quad \lambda = \frac{\alpha + \beta^*}{2}, \tag{9.12}$$

and grouping the components of $\lambda$ and $\mu$ as

$$\begin{aligned} \mathbf{A} &= [\lambda_{1+}, \lambda_{1-}], \quad \mathbf{B} = [\lambda_{2+}, \lambda_{2-}], \\ \delta\mathbf{A} &= [\mu_{1+}, \mu_{1-}], \quad \delta\mathbf{B} = [\mu_{2+}, \mu_{2-}], \end{aligned} \tag{9.13}$$

we can separate the positive-P function into independent parts as

$$P(\mathbf{A}, \mathbf{B}, \delta\mathbf{A}, \delta\mathbf{B}) = P'(\mathbf{A}, \mathbf{B}) G(\delta\mathbf{A}) G(\delta\mathbf{B}). \tag{9.14}$$

Here $G$ is a 4-component Gaussian distribution with the variance $\sigma^2 = 1/2$ in each real component

$$G(\delta\mathbf{A}) = \frac{1}{\pi^2} e^{-|\delta\mathbf{A}|^2}, \tag{9.15}$$

and $P'$ is the distribution core with a reduced number of variables

$$P'(\mathbf{A}, \mathbf{B}) = \left( \frac{|\mathbf{A} \cdot \mathbf{B}|^{2N}}{\pi^4 (N+1)(N!)^2} \right) e^{-|\mathbf{A}|^2 - |\mathbf{B}|^2}, \tag{9.16}$$

The Gaussian parts can be sampled exactly using conventional methods, while the distribution core requires requires an application of rejection sampling. Since $|\mathbf{A} \cdot \mathbf{B}| \leq |\mathbf{A}||\mathbf{B}|$, $P'$ can be bounded as

$$P'(\mathbf{A}, \mathbf{B}) \leq F(\mathbf{A}) F(\mathbf{B}), \tag{9.17}$$

where

$$F(\mathbf{A}) = \frac{|\mathbf{A}|^2 N}{\pi^2 \sqrt{N+1} N!} e^{-|\mathbf{A}|^2}. \tag{9.18}$$

The bounding function $F$ will be used as a probability distribution in the rejection sampling, so it must be normalised on 1. In order to do this, we notice that

$$\begin{aligned} \int |\mathbf{A}|^{2N} e^{-|\mathbf{A}|^2} \mathrm{d}^2\mathbf{A} &= S_{k-1}(1) \int_0^\infty r^{2N+k-1} \exp(-r^2) \mathrm{d}r \\ &= \frac{1}{2} \Gamma(N + k/2) S_{k-1}(1), \end{aligned} \tag{9.19}$$

where $k$ is the number of components in $\mathbf{A}$ (in our case $\mathbf{A}$ contains two complex numbers, so $k = 4$), and $S_{k-1}(R)$ is the surface area of a $k$-dimensional ball:

$$S_{k-1}(r) = \frac{2\pi^{k/2} r^{k-1}}{\Gamma(k/2)}. \tag{9.20}$$

Thus, the normalisation coefficient is

$$M = \int F(\mathbf{A}) \mathrm{d}^2\mathbf{A} = \frac{\Gamma(N+2)}{2\pi^2 \sqrt{N+1} N!} \times \frac{2\pi^2}{\Gamma(2)} = \sqrt{N+1}, \tag{9.21}$$

and $F(\mathbf{A}) = MF'(\mathbf{A})$, where $F'$ is a probability distribution

$$F'(\mathbf{A}) = \frac{|\mathbf{A}|^{2N}}{\pi^2 (N+1)!} e^{-|\mathbf{A}|^2}. \tag{9.22}$$

The distribution $F'$, in turn, can be represented as a product of two independent distributions [110]:

$$F'(\mathbf{A}) \equiv F'(r, \mathbf{n}) = S_{k-1}(r) g(r^2) U(\mathbf{n}) = R(r) U(\mathbf{n}), \tag{9.23}$$

where $r = |\mathbf{A}|$, $\mathbf{n}$ is a unit vector on a $k$-dimensional sphere, and $U = 1/S_{k-1}(1)$ is a uniform distribution of vector directions (or, in other words, a uniform distribution on the surface of a $k$-dimensional ball). The latter can be sampled using the Marsaglia algorithm [111] (sampling a vector of $k$ normally distributed random numbers and normalising it on 1). In order to sample the distribution $R$, we have to make another

variable change, $r^2 \to x$:

$$\begin{aligned} R(x) &= \frac{1}{2\sqrt{x}} S_{k-1}(\sqrt{x}) g(x) \\ &= \frac{1}{2\sqrt{x}} \frac{2\pi^{k/2} x^{(k-1)/2}}{\Gamma(k/2)} \frac{x^N}{\pi^2 (N+1)!} e^{-x} \\ &= \frac{x^{N+1}}{(N+1)!} e^{-x}. \end{aligned} \tag{9.24}$$

The result is exactly the gamma-distribution with the scale $\alpha = N + 2$, for which an efficient sampling method exists [112].

In summary, the rejection algorithm for sampling the probability distribution (9.11) consists of the following steps:

1. Sample two squared lengths $|\mathbf{A}|^2$ and $|\mathbf{B}|^2$ using the gamma distribution with the scale $N + 2$.
2. Sample two directions $\mathbf{n}_A$ and $\mathbf{n}_B$ using the Marsaglia algorithm.
3. Combine squared lengths and directions into $\mathbf{A}$ and $\mathbf{B}$.
4. Sample $u$ from the uniform distribution on $[0, 1)$.
5. If $u > P'(\mathbf{A}, \mathbf{B})/(M^2 F'(\mathbf{A}) F'(\mathbf{B}))$, reject the sample and start over.
6. Sample the real components of $\delta\mathbf{A}$ and $\delta\mathbf{B}$ independently using Gaussian distributions with the variance $1/2$ and combine them with $\mathbf{A}$ and $\mathbf{B}$ to get $\boldsymbol{\alpha}$ and $\boldsymbol{\beta}$ using (9.13) and (9.12).

The resulting phase-space coordinates $\boldsymbol{\alpha}$ and $\boldsymbol{\beta}$ can be now used to obtain a sample of any moment of creation and annihilation operators using the formula (9.10).

### 9.1.4. Results

Using the sampling method described in the previous subsection, we can now sample the positive-P distribution (9.11) and calculate the violation (9.5). We do this for the two-particle case $N = J = 1$, and also for the four-particle case $N = J = 2$, which has also been observed experimentally [113]. The results are plotted in Fig. 9.1, together with the analytical predictions (9.7) and (9.8). The second case requires significantly more samples to achieve a small enough sampling error, but it is clear that in both cases we

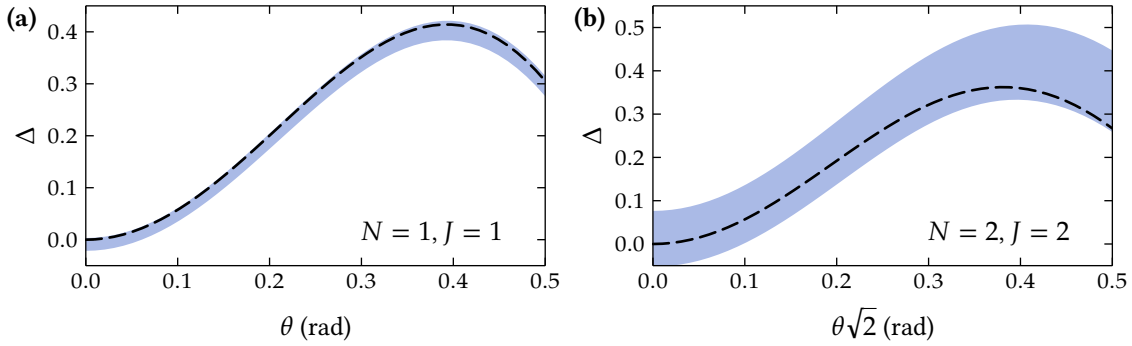


Figure 9.1.: Simulated Bell violation $\Delta_N^J$ as a function of the relative polarizer angle $\theta$ for **(a)** one, and **(b)** two photon pairs using the positive-P distribution with **(a)** $2^{21}$ and **(b)** $2^{25}$ samples. The filled area corresponds to the estimated sampling error around the mean of $\Delta_N^J(\theta)$ for the sampled state, while the dashed line is the exact quantum mechanical prediction of this value.

were able to demonstrate a violation which is beyond the sampling error range. This is a direct counterexample to Feynman's claim.

## 9.2. GHZM states

To understand the ultimate scaling properties of probabilistic sampling methods, we have also simulated higher order correlations that violate multipartite Bell inequalities. These are found in quantum states that display Bell violations with $M$ observers, not just two. The most well-known examples are the multimode entangled Greenberger-Horne-Zeilinger-Mermin (GHZM) states [114, 115], corresponding to "Schrödinger Cat" states. The GHZM states describe $M$ spin-$\frac{1}{2}$ particles or qubits:

$$|\Phi\rangle = \frac{1}{\sqrt{2}}\left(|\uparrow \ldots \uparrow\rangle + e^{i\phi}|\downarrow \ldots \downarrow\rangle\right). \tag{9.25}$$

Here $|\uparrow\rangle$ and $|\downarrow\rangle$ denote spin-up or spin-down particles in the $z$-direction. As well as being of deep significance in quantum physics, such mesoscopic states have been generated in recent ion-trap experiments [116–118].

Quantum paradoxes are obtained on measuring an operator $\hat{A}$ which is defined as a linear combination of $2^M$ distinct $M$-th order correlation functions:

$$\hat{A} = \prod_{j=1}^{M}\left(\hat{\sigma}_j^x + i\hat{\sigma}_j^y\right), \tag{9.26}$$

where $s_j \in -1, +1$, and $\hat{\sigma}_j^x$ and $\hat{\sigma}_j^y$ are the Pauli spin operators acting on the $j$-th qubit. We consider the constraints imposed by a LHV on the expectation $A_\lambda(\phi) \equiv \langle \Phi(\phi)|\hat{A}|\Phi(\phi)\rangle_\lambda$ (where $\langle\rangle_\lambda$ stands for the expectation under LHV assumptions) as compared to the predictions for these expectations given by quantum mechanics, $A_{\mathrm{QM}}(\phi) \equiv \langle \Phi(\phi)|\hat{A}|\Phi(\phi)\rangle$.

Mermin [115] originally proved that for the phase difference $\phi = \pi/2$, QM predicts that

$$\operatorname{Im} A_{\mathrm{QM}}(\pi/2) = 2^{M-1}, \tag{9.27}$$

while the LHV bounds are

$$\begin{aligned} \operatorname{Im} A_\lambda(\pi/2) &\leq 2^{M/2}, \qquad M \text{ is even}, \\ \operatorname{Im} A_\lambda(\pi/2) &\leq 2^{(M-1)/2}, \quad M \text{ is odd}. \end{aligned} \tag{9.28}$$

Ardehali [119] then proved that for $\phi = \pi$, the predictions are

$$-\operatorname{Re} A_{\mathrm{QM}}(\pi) = 2^{M-1}, \tag{9.29}$$

and

$$\begin{aligned} -\operatorname{Re} A_\lambda(\pi) &\leq 2^{(M-1)/2}, \quad M \text{ is even}, \\ -\operatorname{Re} A_\lambda(\pi) &\leq 2^{M/2}, \qquad M \text{ is odd}. \end{aligned} \tag{9.30}$$

Here we transformed the original expressions given by Ardehali to equivalent ones that use our definition of the target operator (9.26).

It is clear that the Mermin inequalities are stronger for the odd values of $M$, and the Ardehali ones are stronger for the even values of $M$ (in particular, for $M = 2$ the Mermin inequalities are not even violated by quantum mechanics). Therefore, for our sampling tests in this section we will use the strongest of two inequalities, and the corresponding phase difference in the GHZM state, for every $M$:

$$\begin{aligned} F &= -\operatorname{Re} A_\lambda(\pi), \quad M \text{ is even}, \\ F &= \operatorname{Im} A_\lambda(\pi/2), \quad M \text{ is odd}. \end{aligned} \tag{9.31}$$

Consequently, for QM and LHV predictions we get the uniform QM prediction $F_{\mathrm{QM}} =$

$2^{M-1}$ and the LHV limit

$$F_\lambda \leq 2^{(M-1)/2}. \tag{9.32}$$

The relative violation can thus be made arbitrarily large to compensate for any imperfections in the measurements.

### 9.2.1. Positive-P representation

One approach to the sampling of the state (9.25) is to use the the P-representation, the same as in the previous section. In general, spin-up and spin-down states are represented as $|\uparrow\rangle \equiv |10\rangle$ and $|\downarrow\rangle \equiv |01\rangle$, where $|0\rangle$ and $|1\rangle$ are number states, which allows for straightforward application of Pauli spin operators.

But for our particular choice of the target operator (9.26), we can choose a simplified representation, which will halve the dimensionality of the resulting phase space: $|\uparrow\rangle \equiv |0\rangle$ and $|\downarrow\rangle \equiv |1\rangle$. Since every term of $\hat{A}$ contains only one spin operator per qubit, it can be expressed in terms of creation and annihilation operators by replacing the spin operators with

$$\hat{\sigma}_j^x = \hat{a}_j + \hat{a}_j^\dagger, \quad \hat{\sigma}_j^y = \frac{1}{i}(\hat{a}_j - \hat{a}_j^\dagger), \tag{9.33}$$

from which the equivalent function of $\boldsymbol{\alpha}$ and $\boldsymbol{\beta}$ in P-representation immediately follows.

The P-representation of the target state is obtained with the canonical formula [17]

$$P[\hat{\rho}] = \left(\frac{1}{4\pi^2}\right)^M \exp\left(-\frac{|\boldsymbol{\alpha} - \boldsymbol{\beta}^*|^2}{4}\right) \left\langle \tfrac{1}{2}(\boldsymbol{\alpha} + \boldsymbol{\beta}^*)|\hat{\rho}|\tfrac{1}{2}(\boldsymbol{\alpha} + \boldsymbol{\beta}^*)\right\rangle, \tag{9.34}$$

which for $\rho \equiv |\Phi\rangle\langle\Phi|$ gives

$$P = \frac{1}{2\pi^{2M}} e^{-|\boldsymbol{\mu}|^2} e^{-|\boldsymbol{\lambda}^2|} \left|\prod_{j=1}^M \lambda_j + 1\right|^2, \tag{9.35}$$

where we have performed the variable change (9.12)

$$\boldsymbol{\mu} = \frac{\boldsymbol{\alpha} - \boldsymbol{\beta}^*}{2}, \quad \boldsymbol{\lambda} = \frac{\boldsymbol{\alpha} + \boldsymbol{\beta}^*}{2}. \tag{9.36}$$

The sampling is performed using the rejection method with bounding $P$ as

$$P \leq \frac{1}{2\pi^{2M}} e^{-|\boldsymbol{\mu}|^2} e^{-|\lambda^2|} \left( \prod_{j=1}^{M} |\lambda_j|^2 + 1 \right). \tag{9.37}$$

Therefore, $P$ can be sampled using a combination of independent samples from Gaussian and gamma distributions, and then conditionally rejecting samples, as described in the previous section.

The phase space in this representation has $4M$ dimensions. This can be further improved by using a specialized representation, allowing us to reduce the sampling error significantly, thus making the states with larger values of $M$ accessible for sampling. We will discuss this in the next subsection.

### 9.2.2. SU(2)-Q representation

The theoretical derivation of the SU(2)-Q representation has been performed by L. E. C. Rosales-Zárate. In this subsection we will briefly describe the framework of the representation, and apply it to our target state.

The positive-P representation does not impose any restrictions on the phase space, including the number states with population more than 1 in the calculation of moments. While it does not affect the calculated observable, it does increase the sampling error. For the cases when we know that the system consists of binary states, more suitable representations exist.

We will consider a Q-representation [13] for SU(2) coherent states [120, 121]:

$$\|\mathbf{z}\rangle = \prod_{j=1}^{M} \left( |\downarrow\rangle_j + z_j |\uparrow\rangle_j \right), \tag{9.38}$$

where $z_j$ are complex numbers. The SU(2)-Q function is the expectation value of the density operator over SU(2) coherent states and is defined explicitly in a normalized form as:

$$Q[\hat{\rho}] = \left( \prod_{j=1}^{M} \frac{2}{\pi(1 + |z_j|^2)^3} \right) \langle \mathbf{z} \| \hat{\rho} \| \mathbf{z} \rangle. \tag{9.39}$$

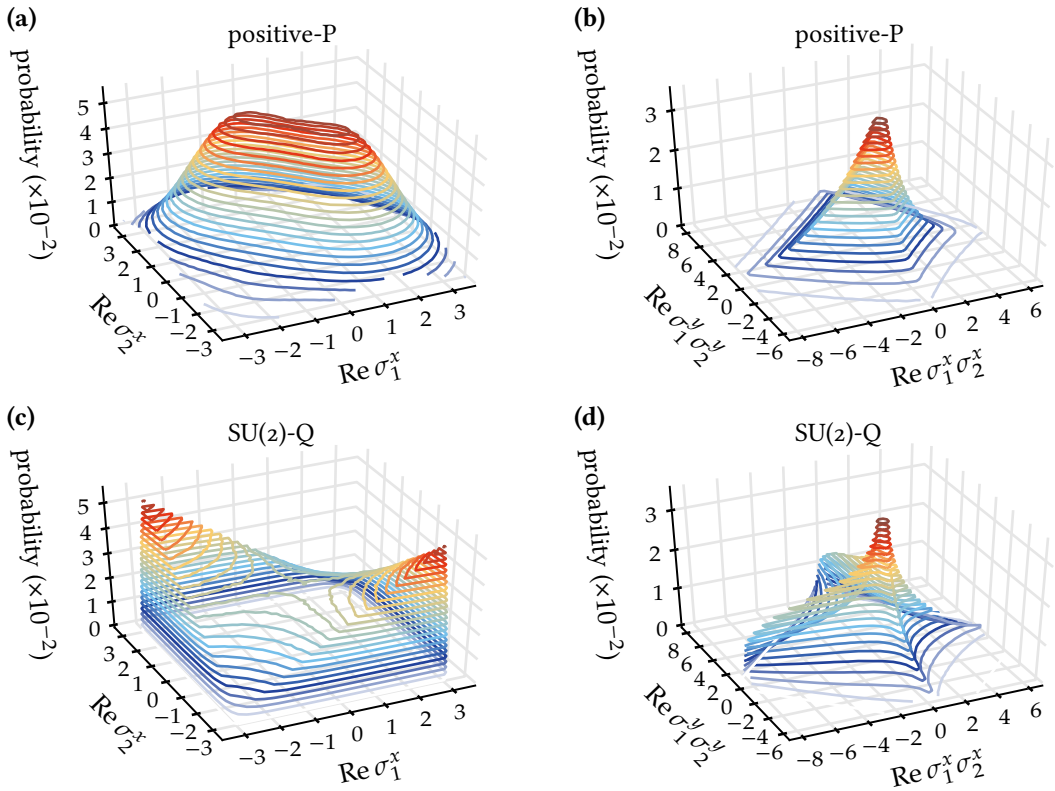


Figure 9.2.: Correlations for the different parts of the inequality (9.43), in case of **(a, b)** positive-P and **(c, d)** SU(2)-Q representations, $10^8$ samples.

For the target GHZM state (9.25), the function takes the form of a probability distribution

$$Q = \frac{1}{2}\prod_{j=1}^{M}\frac{2}{\pi(1+|z_j|^2)^3}\left|\prod_{j=1}^{M} z_j + e^{-i\phi}\right|^2 \tag{9.40}$$

The sampling is again performed using the rejection method with bounding $Q$ as

$$Q \leq \frac{1}{2}\prod_{j=1}^{M}\frac{2}{\pi(1+|z_j|^2)^3}\left(\prod_{j=1}^{M}|z_j|^2+1\right), \tag{9.41}$$

and using the inverse sampling on both terms. The expectation of $\hat{A}$ can be shown to be

$$A_{\mathrm{SU(2)-Q}} = \int 6^M \prod_{j=1}^{M}\frac{z_j^*}{1+|z_j|^2} Q(\mathbf{z})\mathrm{d}^2\mathbf{z}. \tag{9.42}$$

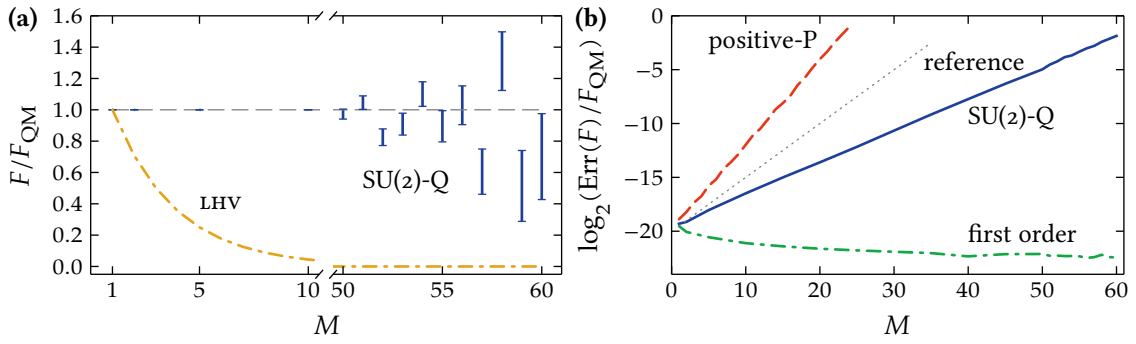


Figure 9.3.: Violations of the inequality (9.32) for multi-particle GHZM states. **(a)** Blue bars show the expectation $F$ simulated using the SU(2)-Q representation, with the length of the bars corresponding to the sampling error. The values of expectations and errors are normalized by the quantum mechanical prediction for the corresponding $M$. The horizontal grey dashed line gives the quantum prediction. The red dash-dotted line is the LHV prediction, which gives a Bell violation when the expectation $F$ is above this line. **(b)** Relative sampling errors for $F$ simulated using the positive-P (red dashed line) and SU(2)-Q (blue solid line) representations. Sampling errors for a first order correlation (total number of "spin-ups") in the SU(2)-Q representation are plotted as a green dashed line. The grey dotted reference line $\log_2$ error $\propto M/2$ shows the threshold at which the sampling errors would give scaling properties as slow as an experimental measurement.

### 9.2.3. Results

The difference between the positive-P and SU(2)-Q representations (and their difference from LHV theories) can be illustrated on the inequality (9.32) for $M = 2$:

$$-\langle\hat{\sigma}_1^x\hat{\sigma}_2^x\rangle_\lambda + \langle\hat{\sigma}_1^y\hat{\sigma}_2^y\rangle_\lambda \leq \sqrt{2}. \tag{9.43}$$

The real parts of the correlations in this expression for both representations used are plotted in Fig. 9.2.

The main feature of quasiprobability representations is apparent: neither of them limits the value of $\mathrm{Re}\,\sigma_1^x$ or $\mathrm{Re}\,\sigma_2^x$ to the range $[-1, 1]$ as would happen in a LHV theory. This means that the Bell theorem does not apply to these results because the sampled values differ from their physical equivalents. Moreover, the plots for the SU(2)-Q show that in this representation the correlations are more peaked, and also do not have exponential tails as the ones in the positive-P representation. This, in addition to the reduced phase space dimensionality, allows for more efficient sampling with SU(2)-Q representation for high values of $M$.

The results of such sampling are shown in Fig. 9.3. We used seven nVidia Tesla M2090 GPUs to generate $10^{12}$ samples of the distribution (9.40) and calculate the required correlation for the values of $M$ up to 60, and these samples were used to test the inequality (9.32). This corresponds to measurement of $10^{18}$ distinct sixtieth order correlation functions. As Fig. 9.3, (a) demonstrates, Bell violations were verified in all cases, although closer to $M = 60$ the sampling error grew almost enough to invalidate the results. Larger values of $M$ would require more samples.

We also investigated the growth of sampling errors for $F$ with the positive-P and SU(2)-Q representations, as shown in Fig. 9.3, (b). In order to have some reference for comparisons, we also plotted the sampling error for the total number of "spin-ups"

$$N = \langle \sum_{j=1}^{M} (\hat{\sigma}_j^z + 1)/2 \rangle. \tag{9.44}$$

This low-order spin correlation physically requires only a linearly growing amount of measurements in the experiment as compared to the exponentially growing amount for $F$. As the plot shows, the sampling error for $N$ slowly decreases as $M$ grows. This explains why low-order correlations could be efficiently sampled in previous work, for much larger Hilbert spaces than the ones studied here [28, 30, 31, 45].

On the other hand, high-order correlations showed exponentially growing sampling error. In the positive-P case the relative error scales as $2^{4M/5}$, which with the chosen number of samples, produces Bell violations only up to $M = 25$. The SU(2)-Q representation shows much better results with a relative error scaling of $2^{M/3}$, so the time taken by the simulation at constant error scales as $2^{2M/3}$. An experiment measuring the same quantity would take time proportional to $2^M$ since it would have to perform measurements for exponentially many settings. Thus, the probabilistic sampling of the SU(2)-Q function scales better than an analogous experiment for high-order correlations.

These results show that the probabilistic sampling is a viable technique both for low- and high-order correlations. Low-order correlations are the ones most commonly measured, and sampling errors in these are insensitive to scaling up to mesoscopic sizes. Correlations of the same order as the system size are still exponentially hard, but a carefully chosen quasiprobability representation can give an exponential advantage over the experimental scaling.

## 9.3. Conclusion

The results in this chapter show that probabilistic sampling can demonstrate the violation of Bell inequalities, due to the extended range of functions of phase-space variables in a quasiprobability representation. Generally, both low- and high-order correlations can be obtained. The low-order correlations are the simplest as the corresponding sampling error does not grow with the system size. Correlations with order comparable to the system size can also be simulated, but with exponentially large number of samples (although this does not imply exponentially large memory resources). Universal digital quantum computers, if sufficiently large, are expected to overcome these problems [122]. However, these are currently limited in size to 6 qubits or less [8]. Regardless of whether these are scalable to larger sizes, it is still useful to obtain theoretical predictions with methods that only require present technology.

Other examples of quantum correlations have been treated using phase-space methods, including quantum soliton dynamics [29], interacting quantum fields [27] equivalent to $\sim 10^6$ qubits and the Dicke superfluorescence model [123]. These simulated correlations are in general agreement with experimental observations [124], showing the range of potential applicability of these techniques.

# Chapter 10.

# Conclusion

In this thesis we formally introduced the functional Wigner transformation. We proved the required theorems from Wirtinger and functional calculi, and used them to derive the essential properties of the Wigner transformation: sequential transformation of operator products, and the correspondence between operator expectations and moments of the Wigner functional.

We then applied this framework to the exact operator equation governing the dynamics of a BEC and showed how to transform it into an equivalent partial differential equation. An approximation (Wigner truncation) was introduced, which allowed us to simplify this equation further, and turn it into a set of SDEs for trajectories in phase space. All of this was done while keeping the functional nature of the equations intact and retaining the inherent mode cutoff of field operators and wavefunctions, which is unavoidable in numerical simulations.

Thus, it allowed us to link the coefficients and terms in the master equation directly with those of SDEs, resulting in a simple method of numerical simulation of BEC dynamics. The method includes the effect of nonlinear losses in a natural way, is capable of producing any high-order correlations without changes to the initial state or the propagation, and is highly parallelisable. The latter is a huge advantage in the modern world of multi-core and multi-node computations and the recent advent of general calculations on GPUs. In particular, the use of modern GPUs allowed us to simulate the dynamics of hundreds of thousands of atoms with thousands of modes with a high degree of accuracy on a desktop in the order of hours.

As a simple test of the truncation accuracy, we applied the multimode form of the

Wigner representation to a two-mode system, for which an exact quantum mechanical description is possible. We have shown that the Wigner method gives correct results in the characteristic time frame for large squeezing, with systematic errors much lower than is testable in an experiment.

We then used the truncated Wigner method to model some recent BEC interferometry experiments, both local and reported by other experimental teams. The method showed reasonable agreement with the experimental results for such important observables as interferometric contrast (a second-order correlation), phase noise and degree of spin squeezing (fourth-order correlations). The method allows one to account for experimental imperfections (measurement and apparatus noises) naturally, which greatly increases the accuracy of predictions. There are clearly some currently unknown noise sources in these experiments.

In the last chapter we considered a more fundamental topic of the ability of phase space methods to simulate quantum mechanical systems that violate Bell inequalities, and their differences from LHV theories. We showed that, due to weaker restrictions on the range of the functions of phase-space variables that correspond to physical observables, such methods are indeed capable of demonstrating such essential quantum mechanical properties as the violation of Bell inequalities. We were able to calculate the correlations involving every particle in the system in highly entangled GHZM states for up to 60 particles. This result is far beyond the capabilities of current experimental techniques.

*
**

In conclusion, we have shown that the truncated Wigner method is a convenient and fast tool that can be used to plan future experiments, and to get better insight into existing ones. There is, of course, still room for further improvement.

First, we have only used coherent initial states and zero temperature for our simulations. While it is a reasonable first approximation, for some experiments this may not be acceptable. The obvious next step here is to include finite-temperature initial conditions using Bogoliubov modes [33, 35, 40, 55, 57]. During the simulation, the validity of the truncation needs to be estimated more accurately than by using the condition (5.23). This condition turns out to be, in fact, more of a guideline as there are examples of good agreement with the exact methods even when it is not satisfied. More accurate test can be performed by calculating the quantum correction [56].

For phase space methods in general, despite demonstrating excellent results in sampling static quantum states, these can struggle in simulating the quantum dynamics of these systems. In the extreme quantum limit, the positive-P method is known to display exponentially growing sampling error with time because of the redundant dimensions it uses. In some cases, this can be neutralized by using a gauge-P representation [22, 125], or adding a projection.

Finally, it is possible to make the Wigner representation positive in the same way it was done for the P representation [126]. The applicability of this "positive-Wigner" representation to various simulation problem is yet to be investigated.

# Appendix A.

# Wirtinger calculus

Formally, a function of complex variable has to be holomorphic in order to be complex differentiable. In many cases, however, it is enough to have less strict "physicists' " complex differentiation rules, which only require the function's real and imaginary part to be differentiable, without imposing additional constraints. Such rules were developed by Wirtinger [127]; further extension to vectors and matrices was performed by Hjørungnes and Gesbert [128]. A very good review and a thorough description of their application was made by Kreutz-Delgado [129]. This section will outline Wirtinger differentiation rules and provide some lemmas based on them, which, in turn, are going to be used in the further Appendices, and in the main body of the thesis.

## A.1. Differentiation

We will start from the definition of the differentiation:

**Definition A.1.** *For a complex variable* $z \equiv x + iy$*, and a function* $f(z) \equiv u(x,y) + iv(x,y)$

$$\frac{\partial f(z)}{\partial z} \equiv \frac{1}{2}\left(\frac{\mathrm{d}f}{\mathrm{d}x} - i\frac{\mathrm{d}f}{\mathrm{d}y}\right).$$

One can easily check that if $f(z)$ is holomorphic, this definition is equivalent to the standard complex differentiation. Wirtinger differentiation is quite intuitive in the sense that it obeys all the basic rules associated with a real-valued differentiation:

**Theorem A.1.** *For any* $f(z)$ *with differentiable real and imaginary parts, Wirtinger differentiation obeys sum, product, quotient, and chain differentiation rules. The chain differentiation*

*rule is applied as if the function $f(z)$ had two independent arguments $z$ and $z^*$:*

$$\frac{\partial f(g(z))}{\partial z} = \frac{\partial f}{\partial g}\frac{\partial g}{\partial z} + \frac{\partial f}{\partial g^*}\frac{\partial g^*}{\partial z}.$$

Some important functions we will encounter in this thesis are not holomorphic. Therefore, we will use Wirtinger differentiation unless explicitly stated otherwise, along with the notation $\partial f/\partial z$. Consequently, by "differentiability" we will mean the property used in the above theorem, namely the existence of partial derivatives of $\operatorname{Re} f$ and $\operatorname{Im} f$ over real and imaginary axes.

It is convenient to connect symbolic rules for Wirtinger differentiation with the rules for real-valued differentiation.

**Theorem A.2.** *If a function $f(z)$ can be expanded into the series of $z^n(z^*)^m$, then $\partial f/\partial z$ and $\partial f/\partial z^*$ can be calculated as partial derivatives of the function $f$ expressed in terms of $z$ and $z^*$, over $z$ and $z^*$ respectively:*

$$\frac{\partial f(z)}{\partial z} = \frac{\mathrm{d} f(z, z^*)}{\mathrm{d} z}, \quad \frac{\partial f(z)}{\partial z^*} = \frac{\mathrm{d} f(z, z^*)}{\mathrm{d} z^*}.$$

*Proof.* We will prove the first identity. Without loss of generality, we can consider $f(z) = z^r(z^*)^s$. First, one can easily prove (by transition to real variables) that $\partial(zz^*)/\partial z = z^*$ and $\partial(zz^*)/\partial z^* = z$. Let us assume that the identity is correct for some $r$ and $s$; then, using the product rule,

$$\begin{aligned}\frac{\partial}{\partial z}(z^{r+1}(z^*)^s) = \frac{\partial}{\partial z}(zz^r(z^*)^s) &= z^r(z^*)^s + z\frac{\partial}{\partial z}(z^r(z^*)^s) \\ &= z^r(z^*)^s + rzz^{r-1}(z^*)^s = (r+1)z^r(z^*)^s.\end{aligned} \tag{A.1}$$

By induction, the statement is correct for any natural $r$ and $s$, and it is obviously true if $r = 0$ or $s = 0$, which proves the theorem. □

The chain differentiation rule in Theorem A.1 and the above theorem give rise to the common notation used in conjunction with Wirtinger differentiation. In order to emphasize the "independent" behavior of $z$ and $z^*$, function arguments are sometimes written as $f(z, z^*)$, even though technically they are not independent. We will not use such notation in this thesis because it will create a lot of clutter later on.

## A.2. Integration

Wirtinger differentiation can be paired with the somewhat more common integration over the complex plane:

**Definition A.2.** *For a complex $z = x + iy$*

$$\int \mathrm{d}^2 z \equiv \int_{-\infty}^{\infty} \int_{-\infty}^{\infty} \mathrm{d}x\, \mathrm{d}y.$$

This definition allows us to prove an analogue of one of the properties of the Fourier transform expressed in terms of Wirtinger differentiation:

**Lemma A.1.** *For a complex $\beta$ and any non-negative integers $r$ and $s$*

$$\int \mathrm{d}^2\alpha\, \alpha^r (\alpha^*)^s \exp(-\beta\alpha^* + \beta^*\alpha) = \pi^2 \left(-\frac{\partial}{\partial \beta^*}\right)^r \left(\frac{\partial}{\partial \beta}\right)^s \delta(\operatorname{Re}\beta)\delta(\operatorname{Im}\beta).$$

*Proof.* First, by changing variables in the integral and using known Fourier transform relations, we can prove that for real $x$ and $v$, and a non-negative integer $n$

$$\int_{-\infty}^{\infty} \mathrm{d}v\, v^n \exp(\pm 2ixv) = \pi(\mp i/2)^n \delta^{(n)}(x). \tag{A.2}$$

Note that we have explicitly written the integration limits here; they are swapped when we change variables in the first integral.

Denoting $\alpha = u + iv$ and $\beta = x + iy$, we can expand the initial expression as

$$\begin{aligned}
&\int \mathrm{d}^2\alpha\, \alpha^r (\alpha^*)^s \exp(-\beta\alpha^* + \beta^*\alpha) \\
&= \int \mathrm{d}u\, \mathrm{d}v\, \exp(2ivx - 2iuy) \\
&\quad \times \sum_{m=0}^{r} \binom{r}{m} u^m (iv)^{r-m} \sum_{n=0}^{s} \binom{s}{n} u^n (-iv)^{s-n} \\
&= \sum_{m=0}^{r} \sum_{n=0}^{s} \binom{r}{m}\binom{s}{n} i^{r-m} (-i)^{s-n} \\
&\quad \times \int \mathrm{d}u\, u^{m+n} \exp(2ivx) \int \mathrm{d}v\, v^{r-m+s-n} \exp(-2iuy).
\end{aligned} \tag{A.3}$$

Applying (A.2) and grouping differentials:

$$\begin{aligned}
&= \pi^2 \sum_{m=0}^{r} \sum_{n=0}^{s} \binom{r}{m}\binom{s}{n} \\
&\quad \times i^{r-m}(-i)^{s-n}(-i/2)^{m+n}\delta^{(m+n)}(y)(i/2)^{r-m+s-n}\delta^{(r-m+s-n)}(x) \\
&= \pi^2 \sum_{m=0}^{r} \binom{r}{m}\frac{1}{2^r}(-i\mathrm{d}/\mathrm{d}y)^m(-\mathrm{d}/\mathrm{d}x)^{r-m} \\
&\quad \times \sum_{n=0}^{s} \binom{s}{n}\frac{1}{2^s}(-i\mathrm{d}/\mathrm{d}y)^n(\mathrm{d}/\mathrm{d}x)^{s-n}\delta(y)\delta(x).
\end{aligned} \tag{A.4}$$

Collapsing sums and recognising Definition A.1:

$$\begin{aligned}
&= \pi^2 \left(\frac{1}{2}(-i\mathrm{d}/\mathrm{d}y - \mathrm{d}/\mathrm{d}x)\right)^r \left(\frac{1}{2}(-i\mathrm{d}/\mathrm{d}y + \mathrm{d}/\mathrm{d}x)\right)^s \delta(y)\delta(x) \\
&= \pi^2 \left(-\frac{\partial}{\partial\beta^*}\right)^r \left(\frac{\partial}{\partial\beta}\right)^s \delta(\mathrm{Re}\,\beta)\delta(\mathrm{Im}\,\beta). \qquad \square
\end{aligned}$$

It can be proved by expansion in real variables that the formally written rule of integration by parts works for the integral from Definition A.2:

$$\int \mathrm{d}z f\frac{\partial g}{\partial z} = \int \mathrm{d}z \frac{\partial(fg)}{\partial z} - \int \mathrm{d}z \frac{\partial f}{\partial z} g. \tag{A.5}$$

Integration by parts will be used extensively in further proofs, and we will need two lemmas that will handle the first term in the right-hand part of the above expression.

**Lemma A.2.** *For a square-integrable $f(\beta)$ and a complex $\alpha$*

$$\int \mathrm{d}^2\beta \frac{\partial}{\partial\beta}\left(\exp(-\beta\alpha^* + \beta^*\alpha)f(\beta)\right) = 0,$$
$$\int \mathrm{d}^2\beta \frac{\partial}{\partial\beta^*}\left(\exp(-\beta\alpha^* + \beta^*\alpha)f(\beta)\right) = 0.$$

*Proof.* It follows from the square-integrability of $f$ that $\lim_{\mathrm{Re}\,\beta\to\infty} = 0$ and $\lim_{\mathrm{Im}\,\beta\to\infty} = 0$, so the statement of the lemma can be proved by transforming to real variables and integrating. $\square$

**Lemma A.3.** *For a bounded $f(z)$*

$$\int \mathrm{d}^2 z \frac{\partial}{\partial z} \left( f(z) \left( \frac{\partial}{\partial z} \right)^s \left( -\frac{\partial}{\partial z^*} \right)^r \delta(\operatorname{Re} z) \delta(\operatorname{Im} z) \right) = 0,$$
$$\int \mathrm{d}^2 z \frac{\partial}{\partial z^*} \left( f(z) \left( \frac{\partial}{\partial z} \right)^s \left( -\frac{\partial}{\partial z^*} \right)^r \delta(\operatorname{Re} z) \delta(\operatorname{Im} z) \right) = 0.$$

*Proof.* Proved straightforwardly by expanding integrals in real values, separating variables and integrating, using the fact that any derivative of the delta function is zero on the infinity. □

# Appendix B.

# Functional calculus

The definitions of differentiation and integration from Appendix A can be extended to operate on functions and functionals. This proved to be a useful tool in the derivation of the functional Wigner transformation and expressing accompanying results as it helps encapsulate bases and mode populations inside wave functions and field operators. It has been introduced (among other places) in most of the papers treating functional extensions of quasiprobability with varying level of detail. The most extensive description was made by Dalton [130]. Nevertheless, while these papers cover the foundations quite well, they are missing several important results which are essential for this thesis, and which will be, therefore, proved in this Appendix.

## B.1. Functional spaces and projections

We will assume that we are provided with an arbitrary orthonormal basis $\mathbb{B}$, consisting of functions $\phi_{\mathbf{n}}(\mathbf{x})$, where $\mathbf{x} \in \mathbb{R}^D$ is a $D$-dimensional coordinate vector, and $\mathbf{n} \in \mathbb{B}$ is a mode identifier. The exact nature of the mode identifier is irrelevant; we only require it to have an equivalence relation defined, and be enumerable. For example, for a three-dimensional harmonic potential, the mode identifier is a tuple $(k, l, m)$ of three non-negative integers.

The orthonormality and completeness conditions for basis functions are, respectively,

$$\int_A \phi^*_{\mathbf{n}}(\mathbf{x})\phi_{\mathbf{m}}(\mathbf{x})\mathrm{d}\mathbf{x} = \delta_{\mathbf{nm}}, \tag{B.1}$$

$$\sum_{\mathbf{n}\in\mathbb{B}} \phi^*_{\mathbf{n}}(\mathbf{x})\phi_{\mathbf{n}}(\mathbf{x}') = \delta(\mathbf{x}' - \mathbf{x}), \tag{B.2}$$

where the integration area $A$ depends on the basis set (for example, $A$ is the whole space for harmonic oscillator modes and a box for plane waves). From now on we assume that the integration $\int \mathrm{d}\mathbf{x}$ is always performed over $A$, unless explicitly stated otherwise. In addition, to avoid clutter, the argument list will be often omitted for functions of coordinates (e.g. $f(\mathbf{x}) \equiv f$ and $f(\mathbf{x}') \equiv f'$), except where it is necessary for clarity.

Various functions can be combined using all, or the certain subset, of basis modes by means of the composition:

**Definition B.1.** *For some subset of the full basis $\mathbb{M} \subseteq \mathbb{B}$, the composition transformation creates a function out of a vector of mode populations:*

$$\mathcal{C}_{\mathbb{M}}(\boldsymbol{\alpha}) = \sum_{\mathbf{n}\in\mathbb{M}} \phi_{\mathbf{n}}\alpha_{\mathbf{n}}.$$

*The decomposition transformation, correspondingly, creates a vector of populations out of a function:*

$$(\mathcal{C}_{\mathbb{M}}^{-1}[f])_{\mathbf{n}} = \int \mathrm{d}\mathbf{x}\phi_{\mathbf{n}}^{*}f, \quad \mathbf{n} \in \mathbb{M}.$$

For any subset of the full basis, there is a subspace of functions that can be obtained by composing modes from this subset only.

**Definition B.2.** *For some subset of the full basis $\mathbb{M} \subseteq \mathbb{B}$, $\mathbb{F}_{\mathbb{M}} \equiv (\mathbb{R}^D \to \mathbb{C})_{\mathbb{M}}$ is the space of all functions of coordinates that can be obtained using $\mathcal{C}_{\mathbb{M}}$. In other words, such functions consist only of the modes from $\mathbb{M}$. We denote $\mathbb{F}_{\mathbb{B}} \equiv \mathbb{F}$.*

With the help of this definition, the "type signatures" of the composition and decomposition transformations can be written as

$$\mathcal{C}_{\mathbb{M}} \in \mathbb{C}^{|\mathbb{M}|} \to \mathbb{F}_{\mathbb{M}}, \quad \mathcal{C}_{\mathbb{M}}^{-1} \in \mathbb{F} \to \mathbb{C}^{|\mathbb{M}|}. \tag{B.3}$$

Note also that, for any $f \in \mathbb{F}_{\mathbb{M}}$, the corresponding composition and decomposition transformations are reversible, that is $\mathcal{C}_{\mathbb{M}}(\mathcal{C}_{\mathbb{M}}^{-1}[f]) \equiv f$. We will call such functions "restricted".

The result of any nonlinear transformation of a function $f \in \mathbb{F}_{\mathbb{M}}$ is not guaranteed to belong to $\mathbb{F}_{\mathbb{M}}$ and requires an explicit projection to be used with other restricted functions

from the same subspace $\mathbb{F}_{\mathbb{M}}$:

**Definition B.3.** *An arbitrary function can be projected to $\mathbb{F}_{\mathbb{M}}$ using the projection operator:*

$$\mathcal{P}_{\mathbb{M}} \in \mathbb{F} \to \mathbb{F}_{\mathbb{M}}$$
$$\mathcal{P}_{\mathbb{M}}[f](\mathbf{x}) \equiv (\mathcal{C}_{\mathbb{M}}(\mathcal{C}_{\mathbb{M}}^{-1}[f]))(\mathbf{x}) = \sum_{\mathbf{n}\in\mathbb{M}} \phi_{\mathbf{n}} \int \mathrm{d}\mathbf{x}'\, \phi_{\mathbf{n}}'^{*} f'.$$

*Obviously, $\mathcal{P}_{\mathbb{B}} \equiv \mathbb{1}$.*

When applied to the delta function, the projection operator produces a restricted delta function:

**Definition B.4.** *The restricted delta function $\delta_{\mathbb{M}} \in \mathbb{F}_{\mathbb{M}}$ is a projected form of the standard delta function:*

$$\delta_{\mathbb{M}}(\mathbf{x}', \mathbf{x}) = \mathcal{P}_{\mathbb{M}}[\delta] = \sum_{\mathbf{n}\in\mathbb{M}} \phi_{\mathbf{n}}'^{*} \phi_{\mathbf{n}}.$$

*Note that in general $\delta_{\mathbb{M}}^{*}(\mathbf{x}', \mathbf{x}) = \delta_{\mathbb{M}}(\mathbf{x}, \mathbf{x}')$, so the order of variables is important. For a full basis, this definition coincides with the standard delta function: $\delta_{\mathbb{B}}(\mathbf{x}', \mathbf{x}) \equiv \delta(\mathbf{x}' - \mathbf{x})$.*

The projection transformation can be, in turn, expressed using the restricted delta function:

$$\mathcal{P}_{\mathbb{M}}[f](\mathbf{x}) = \int \mathrm{d}\mathbf{x}'\, \delta_{\mathbb{M}}(\mathbf{x}', \mathbf{x}) f'. \tag{B.4}$$

The conjugate of $\mathcal{P}_{\mathbb{M}}$ is, therefore,

$$(\mathcal{P}_{\mathbb{M}}[f](\mathbf{x}))^{*} = \int \mathrm{d}\mathbf{x}'\, \delta_{\mathbb{M}}^{*}(\mathbf{x}', \mathbf{x}) f'^{*} = \mathcal{P}_{\mathbb{M}}^{*}[f^{*}](\mathbf{x}). \tag{B.5}$$

## B.2. Functional differentiation

Let $\mathcal{F}[f] \in \mathbb{F}_{\mathbb{M}} \to \mathbb{F}$ be some arbitrary functional operator (not to be confused with quantum mechanical operators) acting on functions from a restricted basis. Such an operator can be as simple as an algebraic function of $f$, for example, $\mathcal{F}[f] = f^2$, but it can also be more complicated. Note that in general this operator is not linear; therefore, its result is not guaranteed to belong to the same restricted basis as its argument. Also,

since $\mathbb{C}$ is a specific case of $\mathbb{F}$ (a constant function of coordinates), a specific case of a functional operator is a functional $\mathcal{F}[f] \in \mathbb{F}_{\mathbb{M}} \to \mathbb{C}$. This means that the calculus described in this section applies to functionals as well.

The composition and decomposition transformations from Definition B.1 define a bijection between a restricted function space $\mathbb{F}_{\mathbb{M}}$ and a vector space of dimensionality $\mathbb{C}^{|\mathbb{M}|}$ (where $|\mathbb{M}|$ denotes the cardinality of $\mathbb{M}$). Therefore any functional operator $\mathcal{F}$ can be alternatively treated as a function of a vector of mode populations and a coordinate vector:

$$\begin{aligned} &F \in \mathbb{C}^{|\mathbb{M}|} \to \mathbb{F} \equiv \mathbb{C}^{|\mathbb{M}|} \to \mathbb{R}^D \to \mathbb{C} \\ &F(\boldsymbol{\alpha}, \mathbf{x}) \equiv \mathcal{F}[\mathcal{C}_{\mathbb{M}}(\boldsymbol{\alpha})](\mathbf{x}). \end{aligned} \tag{B.6}$$

Since the operator is not linear, this correspondence in general cannot be expressed in the form of a matrix.

Using this correspondence, we can define the differentiation in the space of functional operators:

**Definition B.5.** *The derivative of a functional operator is*

$$\begin{aligned} &\frac{\delta}{\delta f'} \in (\mathbb{F}_{\mathbb{M}} \to \mathbb{F}) \to \left(\mathbb{R}^D \to \mathbb{F}_{\mathbb{M}} \to \mathbb{F}\right) \\ &\frac{\delta \mathcal{F}[f]}{\delta f'} = \sum_{\mathbf{n} \in \mathbb{M}} \phi'^{*}_{\mathbf{n}} \frac{\partial \mathcal{F}[\mathcal{C}_{\mathbb{M}}(\boldsymbol{\alpha})]}{\partial \alpha_{\mathbf{n}}}\bigg|_{\boldsymbol{\alpha} = \mathcal{C}_{\mathbb{M}}^{-1}[f]}. \end{aligned}$$

Note that the type of the returned operator differs from its argument type: the result depends on two coordinates, not just one. The second coordinate ($\mathbf{x}'$) comes from the function $f' \equiv f(\mathbf{x}')$ by which we are differentiating.

This definition may look too elaborate at first, but later in this section we will see that it leads to intuitive consequences, making the functional derivative behave very similarly to the Wirtinger derivative from Appendix A. Let us first demonstrate that the definition obeys standard differentiation rules.

**Theorem B.1.** *The functional differentiation from Definition B.5 obeys sum, product, quotient, and chain differentiation rules. The latter one is applied as if $\mathcal{F}[f]$ were a function of*

*two independent variables $f$ and $f^*$:*

$$\frac{\delta\mathcal{F}[\mathcal{G}[f]]}{\delta f'} = \int \mathrm{d}\mathbf{x}'' \left( \frac{\delta\mathcal{F}}{\delta\mathcal{G}''} \frac{\delta\mathcal{G}}{\delta f'} + \frac{\delta\mathcal{F}}{\delta\mathcal{G}''^*} \frac{\delta\mathcal{G}^*}{\delta f'} \right).$$

*Proof.* The first three rules are proved straightforwardly by substituting $\mathcal{F}+\mathcal{G}$, $\mathcal{F}\mathcal{G}$ and $\mathcal{F}/\mathcal{G}$ into Definition B.5. To prove the chain differentiation rule, let us substitute $\mathcal{F}[\mathcal{G}]$ into the definition:

$$\begin{aligned} \frac{\delta\mathcal{F}[\mathcal{G}[f]]}{\delta f'} &= \sum_{\mathbf{n}\in\mathbb{M}} \phi'^*_{\mathbf{n}} \frac{\partial\mathcal{F}[\mathcal{G}[\mathcal{C}_{\mathbb{M}}(\boldsymbol{\alpha})]]}{\partial\alpha_{\mathbf{n}}}\bigg|_{\boldsymbol{\alpha}=\mathcal{C}^{-1}_{\mathbb{M}}[f]} \\ &= \sum_{\mathbf{n}\in\mathbb{M}} \phi'^*_{\mathbf{n}} \frac{\partial\mathcal{F}[\mathcal{C}(\boldsymbol{\beta})]}{\partial\alpha_{\mathbf{n}}}\bigg|_{\boldsymbol{\beta}=\mathcal{C}^{-1}[\mathcal{G}[\mathcal{C}_{\mathbb{M}}(\boldsymbol{\alpha})]]}. \end{aligned} \tag{B.7}$$

Applying the chain rule for Wirtinger derivatives, and recalling the definition of the decomposition transformation:

$$\frac{\partial\mathcal{F}[\mathcal{C}(\boldsymbol{\beta})]}{\partial\alpha_{\mathbf{n}}} = \sum_{\mathbf{m}\in\mathbb{B}} \left( \frac{\partial\mathcal{F}[\mathcal{C}(\boldsymbol{\beta})]}{\partial\beta_{\mathbf{m}}} \frac{\partial\beta_{\mathbf{m}}}{\partial\alpha_{\mathbf{n}}} + \frac{\partial\mathcal{F}[\mathcal{C}(\boldsymbol{\beta})]}{\partial\beta^*_{\mathbf{m}}} \frac{\partial\beta^*_{\mathbf{m}}}{\partial\alpha_{\mathbf{n}}} \right), \tag{B.8}$$

where the nested differentials are calculated as

$$\frac{\partial\beta_{\mathbf{m}}}{\partial\alpha_{\mathbf{n}}} = \frac{\partial(\mathcal{C}^{-1}[G(\boldsymbol{\alpha},\mathbf{x})])_{\mathbf{m}}}{\partial\alpha_{\mathbf{n}}} = \int \mathrm{d}\mathbf{x}'' \phi''^*_{\mathbf{m}} \frac{\partial G(\boldsymbol{\alpha},\mathbf{x})}{\partial\alpha_{\mathbf{n}}}, \tag{B.9}$$

and

$$\frac{\partial\beta^*_{\mathbf{m}}}{\partial\alpha_{\mathbf{n}}} = \int \mathrm{d}\mathbf{x}'' \phi''_{\mathbf{m}} \frac{\partial G^*(\boldsymbol{\alpha},\mathbf{x})}{\partial\alpha_{\mathbf{n}}}. \tag{B.10}$$

Substituting this into (B.7), we get

$$\begin{aligned} \frac{\delta\mathcal{F}[\mathcal{G}[f]]}{\delta f'} = \int \mathrm{d}\mathbf{x}'' \Bigg( &\sum_{\mathbf{m}\in\mathbb{B}} \phi''^*_{\mathbf{m}} \frac{\partial\mathcal{F}[\mathcal{C}(\boldsymbol{\beta})]}{\partial\beta_{\mathbf{m}}}\bigg|_{\boldsymbol{\beta}=\mathcal{C}^{-1}[\mathcal{G}[f]]} \sum_{\mathbf{n}\in\mathbb{M}} \phi'^*_{\mathbf{n}} \frac{\partial\mathcal{G}[\mathcal{C}(\boldsymbol{\alpha})]}{\partial\alpha_{\mathbf{n}}}\bigg|_{\boldsymbol{\alpha}=\mathcal{C}^{-1}_{\mathbb{M}}[f]} \\ &+ \sum_{\mathbf{m}\in\mathbb{B}} \phi''_{\mathbf{m}} \frac{\partial\mathcal{F}[\mathcal{C}(\boldsymbol{\beta})]}{\partial\beta^*_{\mathbf{m}}}\bigg|_{\boldsymbol{\beta}=\mathcal{C}^{-1}[\mathcal{G}[f]]} \sum_{\mathbf{n}\in\mathbb{M}} \phi'^*_{\mathbf{n}} \frac{\partial\mathcal{G}^*[\mathcal{C}(\boldsymbol{\alpha})]}{\partial\alpha_{\mathbf{n}}}\bigg|_{\boldsymbol{\alpha}=\mathcal{C}^{-1}_{\mathbb{M}}[f]} \Bigg). \end{aligned} \tag{B.11}$$

Recognising Definition B.5 for $\delta\mathcal{F}/\delta\mathcal{G}$ and $\delta\mathcal{G}/\delta f$, we obtain the statement of the theorem. □

The above theorem demonstrates that, with respect to the functional differentiation,

functional operators behave as if they depend on two independent functions, $f$ and $f^*$ — just like complex-valued functions with respect to the Wirtinger differentiation.

Most of the time we will deal with functional operators in a particular form, namely an algebraic expression of their arguments. It turns out that for this subset, functional differentiation behaves almost exactly like the Wirtinger differentiation and allows one to circumvent Definition B.5, calculating derivatives based on well-known symbolic rules.

**Theorem B.2.** *If a functional operator $\mathcal{F} \in \mathbb{F}_{\mathbb{M}} \to \mathbb{F}$ has the form $\mathcal{F}[f] \equiv g(f)$, where $g(z)$ is a function that can be expanded into the power series of $z^r(z^*)^s$, then $\delta\mathcal{F}/\delta f'$ and $\delta\mathcal{F}/\delta f'^*$ can be calculated as derivatives of $g(f)$ over $f$ and $f^*$, respectively, times the restricted delta function:*

$$\frac{\delta\mathcal{F}}{\delta f'} = \delta_{\mathbb{M}}(\mathbf{x}', \mathbf{x}) \left.\frac{\partial g(z)}{\partial z}\right|_{z=f(\mathbf{x})}, \quad \frac{\delta\mathcal{F}}{\delta f'^*} = \delta^*_{\mathbb{M}}(\mathbf{x}', \mathbf{x}) \left.\frac{\partial g(z)}{\partial z^*}\right|_{z=f(\mathbf{x})}.$$

*Proof.* We will prove the first identity. Without loss of generality, we can consider $\mathcal{F} = f^r(f^*)^s$. Substituting this into Definition B.5, differentiating the composition according to Definition B.1 and recognising the restricted delta function, we get:

$$\begin{aligned}
\frac{\delta\mathcal{F}}{\delta f'} &= \sum_{\mathbf{n}\in\mathbb{M}} \phi'^*_{\mathbf{n}} \left.\frac{\partial\left(\mathcal{C}^r_{\mathbb{M}}(\boldsymbol{\alpha})(\mathcal{C}^*_{\mathbb{M}}(\boldsymbol{\alpha}))^s\right)}{\partial\alpha_{\mathbf{n}}}\right|_{\boldsymbol{\alpha}=\mathcal{C}^{-1}_{\mathbb{M}}[f]} \\
&= \sum_{\mathbf{n}\in\mathbb{M}} \phi'^*_{\mathbf{n}} r\phi_{\mathbf{n}}\, \mathcal{C}^{r-1}_{\mathbb{M}}(\boldsymbol{\alpha})(\mathcal{C}^*_{\mathbb{M}}(\boldsymbol{\alpha}))^s\big|_{\boldsymbol{\alpha}=\mathcal{C}^{-1}_{\mathbb{M}}[f]} \qquad \text{(B.12)} \\
&= r\delta_{\mathbb{M}}(\mathbf{x}', \mathbf{x}) f^{r-1}(f^*)^s = \delta_{\mathbb{M}}(\mathbf{x}', \mathbf{x}) \left.\frac{\partial g(z)}{\partial z}\right|_{z=f(\mathbf{x})}.
\end{aligned}$$

The second identity is proved in the same way. □

## B.3. Functional integration

In this section we will only postulate the expression for the integral of a functional operator. For the rationale behind this definition one can refer to the detailed explanation by Dalton [130]. Just as in the differentiation case, we will make use of the equivalence between a functional operator and a function of two vectors.

**Definition B.6.** *An integral of a functional operator $\mathcal{F} \in \mathbb{F}_{\mathbb{M}} \to \mathbb{F}$ is an integral of the*

*corresponding function over mode variables:*

$$\int \delta^2 f \in (\mathbb{F}_{\mathbb{M}} \to \mathbb{F}) \to (\mathbb{R}^D \to \mathbb{C})$$
$$\int \delta^2 f \mathcal{F}[f] = \int \mathrm{d}^2\boldsymbol{\alpha}\, \mathcal{F}[\mathcal{C}_{\mathbb{M}}(\boldsymbol{\alpha})] = \left(\prod_{\mathbf{n}\in\mathbb{M}} \int \mathrm{d}^2\alpha_{\mathbf{n}}\right) \mathcal{F}[\mathcal{C}_{\mathbb{M}}(\boldsymbol{\alpha})],$$

*where the product of integrals stands for their successive application. If the restricted basis contains an infinite number of modes, the integral is treated as a limit* $|\mathbb{M}| \to \infty$.

The functional integration has a Fourier-like property analogous to Lemma A.1, but its statement requires the definition of the delta functional:

**Definition B.7.** *For a restricted basis* $\mathbb{M}$*, the delta functional is*

$$\Delta_{\mathbb{M}} \in \mathbb{F}_{\mathbb{M}} \to \mathbb{R}$$
$$\Delta_{\mathbb{M}}[f] \equiv \prod_{\mathbf{n}\in\mathbb{M}} \delta(\operatorname{Re}\alpha_{\mathbf{n}})\delta(\operatorname{Im}\alpha_{\mathbf{n}}),$$

*where* $\boldsymbol{\alpha} = \mathcal{C}_{\mathbb{M}}^{-1}[f]$.

The delta functional has the sifting property in functional integrals:

$$\begin{aligned}\int \delta^2 f \mathcal{F}[f]\Delta_{\mathbb{M}}[f] &= \int \mathrm{d}^2\boldsymbol{\alpha}\, \mathcal{F}(\mathcal{C}_{\mathbb{M}}[\boldsymbol{\alpha}]) \prod_{\mathbf{n}\in\mathbb{M}} \delta(\operatorname{Re}\alpha_{\mathbf{n}})\delta(\operatorname{Im}\alpha_{\mathbf{n}}) \\ &= \mathcal{F}(\mathcal{C}_{\mathbb{M}}[\boldsymbol{\alpha}])\big|_{\forall \mathbf{n}\in\mathbb{M}\ \alpha_{\mathbf{n}}=0} \\ &= \mathcal{F}[f]\big|_{f\equiv 0}.\end{aligned} \tag{B.13}$$

By analogy with the field displacement operator from Definition 3.1, we can define a displacement functional, which will often appear in the formulation of functional Wigner transformation (Definition 3.2) and accompanying proofs:

**Definition B.8.** *The displacement functional takes two functions as arguments and returns a complex result:*

$$D \in \mathbb{F} \to \mathbb{F} \to \mathbb{C}$$
$$D[g,f] = \exp \int \mathrm{d}\mathbf{x}\, (-gf^* + g^*f).$$

The displacement functional exhibits Fourier-like properties in functional integrals.

**Lemma B.1** (functional extension of Lemma A.1)**.** *For $f \in \mathbb{F}_{\mathbb{M}}$ and $g \in \mathbb{F}_{\mathbb{M}}$, and for any non-negative integers $r$ and $s$:*

$$\int \delta^2 f f^r (f^*)^s D[g,f] = \pi^{2|\mathbb{M}|} \left(-\frac{\delta}{\delta g^*}\right)^r \left(\frac{\delta}{\delta g}\right)^s \Delta_{\mathbb{M}}[g].$$

*Proof.* We will start by representing the functional integral and the integrand in mode form:

$$\begin{aligned} &\int \delta^2 f f^r (f^*)^s \exp \int \mathrm{d}\mathbf{x}\, (-g f^* + g^* f) \\ &= \int \mathrm{d}^2\boldsymbol{\alpha} \left(\sum_{\mathbf{n}\in\mathbb{M}} \phi_{\mathbf{n}}\alpha_{\mathbf{n}}\right)^r \left(\sum_{\mathbf{n}\in\mathbb{M}} \phi^*_{\mathbf{n}}\alpha^*_{\mathbf{n}}\right)^s \prod_{\mathbf{n}\in\mathbb{M}} \exp(-\beta_{\mathbf{n}}\alpha^*_{\mathbf{n}} + \beta^*_{\mathbf{n}}\alpha_{\mathbf{n}}) \\ &= (*), \end{aligned} \tag{B.14}$$

where $\boldsymbol{\alpha} = \mathcal{C}^{-1}_{\mathbb{M}}[f]$ and $\boldsymbol{\beta} = \mathcal{C}^{-1}_{\mathbb{M}}[g]$. Expanding powers of $f$ and $f^*$ using the multinomial theorem:

$$\begin{aligned} (*) = \int \mathrm{d}^2\boldsymbol{\alpha} &\left(\sum_{\sum u_{\mathbf{m}}=r} \binom{r}{\{u_{\mathbf{m}}\}} \prod_{\mathbf{n}\in\mathbb{M}} \phi^{u_{\mathbf{n}}}_{\mathbf{n}} \alpha^{u_{\mathbf{n}}}_{\mathbf{n}}\right) \\ &\times \left(\sum_{\sum v_{\mathbf{m}}=s} \binom{s}{\{v_{\mathbf{m}}\}} \prod_{\mathbf{n}\in\mathbb{M}} (\phi^*_{\mathbf{n}})^{v_{\mathbf{n}}} (\alpha^*_{\mathbf{n}})^{v_{\mathbf{n}}}\right) \prod_{\mathbf{n}\in\mathbb{M}} \exp(-\beta_{\mathbf{n}}\alpha^*_{\mathbf{n}} + \beta^*_{\mathbf{n}}\alpha_{\mathbf{n}}), \end{aligned} \tag{B.15}$$

where $\binom{r}{\{u_{\mathbf{m}}\}} \equiv r!\,/(\prod u_{\mathbf{m}}!)$ are multinomial coefficients. Splitting variables:

$$\begin{aligned} (*) = &\sum_{\sum u_{\mathbf{m}}=r,\, \sum v_{\mathbf{m}}=s} \binom{r}{\{u_{\mathbf{m}}\}} \binom{s}{\{v_{\mathbf{m}}\}} \\ &\prod_{\mathbf{n}\in\mathbb{M}} \phi^{u_{\mathbf{n}}}_{\mathbf{n}} (\phi^*_{\mathbf{n}})^{v_{\mathbf{n}}} \int d^2\alpha_{\mathbf{n}} \alpha^{u_{\mathbf{n}}}_{\mathbf{n}} (\alpha^*_{\mathbf{n}})^{v_{\mathbf{n}}} \exp(-\beta_{\mathbf{n}}\alpha^*_{\mathbf{n}} + \beta^*_{\mathbf{n}}\alpha_{\mathbf{n}}). \end{aligned} \tag{B.16}$$

Applying Lemma A.1 to evaluate the integrals over $\alpha_{\mathbf{n}}$:

$$\begin{aligned} (*) = &\sum_{\sum u_{\mathbf{m}}=r,\, \sum v_{\mathbf{m}}=s} \binom{r}{\{u_{\mathbf{m}}\}} \binom{s}{\{v_{\mathbf{m}}\}} \pi^{2|\mathbb{M}|} \\ &\times \prod_{\mathbf{n}\in\mathbb{M}} \phi^{u_{\mathbf{n}}}_{\mathbf{n}} (\phi^*_{\mathbf{n}})^{v_{\mathbf{n}}} \left(-\frac{\partial}{\partial\beta^*_{\mathbf{n}}}\right)^{u_{\mathbf{n}}} \left(\frac{\partial}{\partial\beta_{\mathbf{n}}}\right)^{v_{\mathbf{n}}} \delta(\mathrm{Re}\,\beta_{\mathbf{n}})\delta(\mathrm{Im}\,\beta_{\mathbf{n}}). \end{aligned} \tag{B.17}$$

Collapsing sums, and recognising functional derivatives (Definition B.5) and the delta

functional (Definition B.7):

$$\begin{aligned}(*) &= \pi^{2|\mathbb{M}|}\left(-\sum_{\mathbf{n}\in\mathbb{M}}\phi_{\mathbf{n}}\frac{\partial}{\partial\beta^*_{\mathbf{n}}}\right)^r\left(\sum_{\mathbf{n}\in\mathbb{M}}\phi^*_{\mathbf{n}}\frac{\partial}{\partial\beta_{\mathbf{n}}}\right)^s\prod_{\mathbf{n}\in\mathbb{M}}\delta(\operatorname{Re}\beta_{\mathbf{n}})\delta(\operatorname{Im}\beta_{\mathbf{n}})\\ &= \pi^{2|\mathbb{M}|}\left(-\frac{\delta}{\delta g^*}\right)^r\left(\frac{\delta}{\delta g}\right)^s\Delta_{\mathbb{M}}[g].\end{aligned}$$ □

It is easy to show that functional integration has the same integration by parts property as regular integration:

$$\int\delta^2 f\frac{\delta\mathcal{F}[f]}{\delta f'}\mathcal{G}[f] = \int\delta^2 f\frac{\delta(\mathcal{F}[f]\mathcal{G}[f])}{\delta f'} - \int\delta^2 f\frac{\delta\mathcal{G}[f]}{\delta f'}\mathcal{F}[f]. \tag{B.18}$$

Functional integration by parts serves as the foundation of several theorems from Chapter 3. These theorems additionally need several lemmas that help us eliminate the first term in the right-hand part of the above expression. These are extensions of Lemma A.2 and Lemma A.3 in terms of functional operators, with an addition of one more functional-specific lemma.

**Lemma B.2** (functional extension of Lemma A.2)**.** *For a square-integrable functional operator $\mathcal{F}$ (i.e., a functional operator that produces only square-integrable functions),*

$$\int\delta^2 g\frac{\delta}{\delta g'}\left(D[g,f]\mathcal{F}[g]\right) = 0,$$
$$\int\delta^2 g\frac{\delta}{\delta g'^*}\left(D[g,f]\mathcal{F}[g]\right) = 0.$$

*Proof.* We will prove the first equation. Let $\boldsymbol{\alpha} = \mathcal{C}^{-1}_{\mathbb{M}}[f]$ and $\boldsymbol{\beta} = \mathcal{C}^{-1}_{\mathbb{M}}[g]$. The displacement functional can be represented as a function of mode vectors:

$$\begin{aligned}D[g,f] &= \exp\int\mathrm{d}x\sum_{\mathbf{n}\in\mathbb{M},\mathbf{m}\in\mathbb{M}}\left(-\phi_{\mathbf{n}}\phi^*_{\mathbf{m}}\beta_{\mathbf{n}}\alpha^*_{\mathbf{m}} + \phi^*_{\mathbf{n}}\phi_{\mathbf{m}}\beta^*_{\mathbf{n}}\alpha_{\mathbf{m}}\right)\\ &= \exp\sum_{\mathbf{n}\in\mathbb{M},\mathbf{m}\in\mathbb{M}}\left(-\delta_{\mathbf{nm}}\beta_{\mathbf{n}}\alpha^*_{\mathbf{n}} + \delta_{\mathbf{nm}}\beta^*_{\mathbf{n}}\alpha_{\mathbf{n}}\right)\\ &= \exp\sum_{\mathbf{n}\in\mathbb{M}}\left(-\beta_{\mathbf{n}}\alpha^*_{\mathbf{n}} + \beta^*_{\mathbf{n}}\alpha_{\mathbf{n}}\right).\end{aligned}\tag{B.19}$$

We introduce a special notation for this lemma to indicate the subset of $\mathbb{M}$ used by

operators and functionals. With this notation, for fixed $\mathbf{n}$:

$$\begin{aligned} D[g,f] &= \prod_{\mathbf{m}\in\mathbb{M}} \exp\left(-\beta_{\mathbf{m}}\alpha^*_{\mathbf{m}} + \beta^*_{\mathbf{m}}\alpha_{\mathbf{m}}\right) \\ &= \exp\left(-\beta_{\mathbf{n}}\alpha^*_{\mathbf{n}} + \beta^*_{\mathbf{n}}\alpha_{\mathbf{n}}\right) \prod_{\mathbf{m}\in\mathbb{M},\mathbf{m}\neq\mathbf{n}} \exp\left(-\beta_{\mathbf{m}}\alpha^*_{\mathbf{m}} + \beta^*_{\mathbf{m}}\alpha_{\mathbf{m}}\right) \\ &= D_{\neg\mathbf{n}} D_{\mathbf{n}}, \end{aligned} \tag{B.20}$$

and, similarly,

$$\begin{aligned} g &= g_{\neg\mathbf{n}} + g_{\mathbf{n}}, \\ \int \mathrm{d}^2\boldsymbol{\beta} &= \int \mathrm{d}^2\boldsymbol{\beta}_{\neg\mathbf{n}} \int \mathrm{d}^2\beta_{\mathbf{n}}. \end{aligned} \tag{B.21}$$

Separating variables in the integral using the introduced notation:

$$\begin{aligned} \int \delta^2 g \frac{\delta}{\delta g'} \left(D[g,f]\mathcal{F}[g]\right) &= \int \mathrm{d}^2\boldsymbol{\beta} \sum_{\mathbf{n}\in\mathbb{M}} \phi'^*_{\mathbf{n}} \frac{\partial}{\partial\beta_{\mathbf{n}}} D_{\neg\mathbf{n}} D_{\mathbf{n}} \mathcal{F}[g] \\ &= \sum_{\mathbf{n}\in\mathbb{M}} \phi'^*_{\mathbf{n}} \int \mathrm{d}^2\boldsymbol{\beta}_{\neg\mathbf{n}} D_{\neg\mathbf{n}} \int \mathrm{d}^2\beta_{\mathbf{n}} \frac{\partial}{\partial\beta_{\mathbf{n}}} D_{\mathbf{n}} \mathcal{F}[\mathcal{C}_{\mathbb{M}}(\boldsymbol{\beta})]. \end{aligned} \tag{B.22}$$

For each term the internal integral is equal to zero because of Lemma A.2, and therefore the whole sum is zero. □

**Lemma B.3** (functional extension of Lemma A.3)**.** *For a square-integrable functional operator $\mathcal{F}$, restricted function $f \in \mathbb{F}_{\mathbb{M}}$, and non-negative integers $r$ and $s$,*

$$\begin{aligned} \int \delta^2 f \frac{\delta}{\delta f} \left( \mathcal{F}[f] \left(\frac{\delta}{\delta f}\right)^s \left(-\frac{\delta}{\delta f^*}\right)^r \Delta_{\mathbb{M}}[f] \right) = 0, \\ \int \delta^2 f \frac{\delta}{\delta f^*} \left( \mathcal{F}[f] \left(\frac{\delta}{\delta f}\right)^s \left(-\frac{\delta}{\delta f^*}\right)^r \Delta_{\mathbb{M}}[f] \right) = 0. \end{aligned}$$

*Proof.* Proved by expanding the functional integral and differentials into modes and applying Lemma A.3. □

In order to perform transformations of a master equation in the future, we will need a lemma which justifies a certain operation with the Laplacian (which is a part of the kinetic term in a Hamiltonian).

**Lemma B.4.** *Let mode functions in a restricted basis $\mathbb{M}$ satisfy the condition that for any*

*pair of modes* $\mathbf{m}, \mathbf{n} \in \mathbb{M}$

$$\oint_{\partial A} \phi_{\mathbf{m}} (\nabla \phi^*_{\mathbf{n}} \cdot \mathbf{v}) \mathrm{d}S = 0,$$

*where $A$ is the integration area associated with the basis, $\partial A$ is its boundary, and $\mathbf{v}$ is the outward-pointing unit normal of a surface element* $\mathrm{d}S$. *Then for any* $\mathcal{F} \in \mathbb{F}_{\mathbb{M}} \to \mathbb{F}$,

$$\int_A \mathrm{d}\mathbf{x} \left( \nabla^2 \frac{\delta}{\delta f} \right) f \mathcal{F}[f] = \int_A \mathrm{d}\mathbf{x} \frac{\delta}{\delta f} (\nabla^2 f) \mathcal{F}[f]$$

*Proof.* Integration limits play an important role in this proof, so we will write them explicitly. The components of the integral are expanded using the basis functions as

$$\int_A \mathrm{d}\mathbf{x} \left( \nabla^2 \frac{\delta}{\delta f} \right) f \mathcal{F}[f] = \sum_{\mathbf{n} \in \mathbb{M}, \mathbf{m} \in \mathbb{M}} \left( \int_A \mathrm{d}\mathbf{x} (\nabla^2 \phi^*_{\mathbf{n}}) \phi_{\mathbf{m}} \right) \frac{\partial}{\partial \alpha_{\mathbf{n}}} \alpha_{\mathbf{m}} \mathcal{F}[\mathcal{C}_{\mathbb{M}}(\boldsymbol{\alpha})], \tag{B.23}$$

where $\boldsymbol{\alpha} = \mathcal{C}^{-1}_{\mathbb{M}}[f]$. Using Green's first identity and the condition for the integrals over the boundary of $A$:

$$\begin{aligned} \int_A \mathrm{d}\mathbf{x} (\nabla^2 \phi^*_{\mathbf{n}}) \phi_{\mathbf{m}} &= \oint_{\partial A} \phi_{\mathbf{m}} (\nabla \phi^*_{\mathbf{n}} \cdot \mathbf{v}) \mathrm{d}S - \int_A \mathrm{d}\mathbf{x} (\nabla \phi^*_{\mathbf{n}}) (\nabla \phi_{\mathbf{m}}) \\ &= 0 - \int_A \mathrm{d}\mathbf{x} (\nabla \phi^*_{\mathbf{n}}) (\nabla \phi_{\mathbf{m}}) \\ &= \oint_{\partial A} \phi^*_{\mathbf{n}} (\nabla \phi_{\mathbf{m}} \cdot \mathbf{v}) \mathrm{d}S - \int_A \mathrm{d}\mathbf{x} (\nabla \phi^*_{\mathbf{n}}) (\nabla \phi_{\mathbf{m}}) \\ &= \int_A \mathrm{d}\mathbf{x} \phi^*_{\mathbf{n}} (\nabla^2 \phi_{\mathbf{m}}), \end{aligned} \tag{B.24}$$

Substituting this back into (B.23):

$$\begin{aligned} \int_A \mathrm{d}\mathbf{x} \left( \nabla^2 \frac{\delta}{\delta f} \right) f \mathcal{F}[f] &= \sum_{\mathbf{n} \in \mathbb{M}, \mathbf{m} \in \mathbb{M}} \left( \int_A \mathrm{d}\mathbf{x} \phi^*_{\mathbf{n}} (\nabla^2 \phi_{\mathbf{m}}) \right) \frac{\partial}{\partial \alpha_{\mathbf{n}}} \alpha_{\mathbf{m}} \mathcal{F}(\boldsymbol{\alpha}) \\ &= \int_A \mathrm{d}\mathbf{x} \frac{\delta}{\delta f} (\nabla^2 f) \mathcal{F}[f]. \end{aligned}$$

□

Note that this lemma imposes an additional requirement on basis functions, which is, essentially, a generalised form of periodicity in the zeroth and the first derivative over $A$. In this work we use two bases: plane waves and harmonic modes (see Appendix D for details).

For the harmonic basis the condition is obviously satisfied, since the boundary of $A$ is

on the infinity, and both zeroth and first derivatives (or any other order, for that matter) of any mode function (D.6) are equal to zero there.

For the plane wave basis the area $A$ is a box (let us suppose for definiteness that it spans from 0 to $L_j$ in every dimension $j$), and the mode functions are separable ($\phi_{\mathbf{n}}(\mathbf{x}) \equiv \prod_{j=1}^{D} \phi_{n_j}^{(j)}(x_j)$) so the variables in the integral from the condition can be easily separated too:

$$\oint_{\partial A} \phi_{\mathbf{m}}(\nabla\phi_{\mathbf{n}}^* \cdot \mathbf{v})\mathrm{d}S = \sum_{j=1}^{D} \phi_{m_j}^{(j)} \frac{\mathrm{d}\phi_{n_j}^{(j)*}}{\mathrm{d}x_j}\bigg|_{x_j=0}^{L_j} \prod_{k=1,k\neq j}^{D} \int_0^{L_k} \mathrm{d}x_k \phi_{m_k}^{(k)} \phi_{n_k}^{(k)*}. \tag{B.25}$$

It is obvious from (D.2) that for any mode $\mathbf{n}$

$$\phi_{n_j}^{(j)}(0) = \phi_{n_j}^{(j)}(L_j), \quad \frac{\mathrm{d}\phi_{n_j}^{(j)}}{\mathrm{d}x_j}\bigg|_{x_j=0} = \frac{\mathrm{d}\phi_{n_j}^{(j)}}{\mathrm{d}x_j}\bigg|_{x_j=L_j}, \tag{B.26}$$

which makes the integral above zero.

In this thesis we will assume that this condition is satisfied for any basis we work with.

# Appendix C.

# Functional FPE to SDE correspondences

Wigner transformation, to which the majority of this thesis is dedicated, produces an FPE, or its functional equivalent, from a given master equation. An FPE is an equation in partial derivatives, and, in general, is not easy to solve — even numerically. The major part of the usefulness of the Wigner transformation (paired with the Wigner truncation) is that it produces an FPE in a special form, which can be further transformed to a set of SDEs, with the Wigner function playing the role of a probability distribution. The algorithms for solving such equations numerically are much more straightforward.

The actual correspondence between FPE and SDEs has been formulated and proved for real-valued coefficients in literature [131]. In this thesis we need to transform FPEs with complex coefficients, or even functional operator ones. While it is always possible to express them in the real-valued form, it is much more convenient to derive correspondence theorems that work directly on such FPEs. In this Appendix we will do that by proceeding successively from the initial real-valued theorem to complex-valued and functional correspondences.

In addition, we will do the same for the Itô formula, which provides an expression for the time derivative of any function of stochastic variables. This formula is useful, among other cases, if one wants to derive the time dependence of some integral observable (for instance, population), without solving SDEs themselves. Alternatively, it can serve as an additional test of a numerical algorithm used to propagate SDEs in time.

## C.1. Correspondences

We will start by formulating the known real-valued correspondence in a form which is more convenient for further proofs in this section, and is also closer to the results one obtains from the Wigner transformation.

**Lemma C.1** (real-valued FPE–SDEs correspondence in a convenient form.)**.** *Let* $\mathbf{z}^T \equiv (z_1 \dots z_M)$ *be a set of real variables. Then the FPE*

$$\frac{\mathrm{d}W}{\mathrm{d}t} = -\boldsymbol{\partial}_{\mathbf{z}}^T \cdot \mathbf{a}W + \frac{1}{2}\operatorname{Tr}\left\{\boldsymbol{\partial}_{\mathbf{z}}\boldsymbol{\partial}_{\mathbf{z}}^T BB^T\right\} W$$

*is equivalent to the set of SDEs in the Itô form*

$$\mathrm{d}\mathbf{z} = \mathbf{a}\mathrm{d}t + B\mathrm{d}\mathbf{Z}$$

*and to the set of SDEs in the Stratonovich form*

$$\mathrm{d}\mathbf{z} = (\mathbf{a} - \mathbf{s})\mathrm{d}t + B\mathrm{d}\mathbf{Z},$$

*where the noise-induced (Stratonovich) drift vector* $\mathbf{s}$ *has elements*

$$s_j = \frac{1}{2}\sum_{k,i} B_{ki}\frac{\partial}{\partial z_k}B_{ji} = \frac{1}{2}\operatorname{Tr}\left\{B^T\boldsymbol{\partial}_{\mathbf{z}}\mathbf{e}_j^T B\right\},$$

*with* $\mathbf{e}_j$ *being a unit vector with elements* $(\mathbf{e}_j)_i = \delta_{ij}$*. Here* $W \equiv W(\mathbf{z})$ *is a probability distribution,* $\mathbf{a} \equiv \mathbf{a}(\mathbf{z})$ *is a vector function,* $B \equiv B(\mathbf{z})$ *is a matrix function (*$B$ *having the size* $M \times L$*, where* $L$ *is the number of noise sources),* $\boldsymbol{\partial}_{\mathbf{z}}^T \equiv (\mathrm{d}/\mathrm{d}z_1 \dots \mathrm{d}/\mathrm{d}z_M)$ *is a cogradient vector, and* $\mathbf{Z}$ *is a standard* $L$*-dimensional Wiener process with* $\langle \mathrm{d}Z_j^2 \rangle = \mathrm{d}t$*.*

*Proof.* For the detailed proof see Risken [131], sections 3.3 and 3.4. □

The above theorem can be extended to work with complex Wirtinger derivatives and complex-valued coefficients. Of course, in order to produce a real-valued $\mathrm{d}W/\mathrm{d}t$ in the left-hand part, an FPE must have a particular form.

**Theorem C.1.** *Let* $\boldsymbol{\alpha}^T \equiv (\alpha_1 \dots \alpha_M)$ *be a set of complex variables. Then the FPE*

$$\frac{\mathrm{d}W}{\mathrm{d}t} = -\boldsymbol{\partial}_{\boldsymbol{\alpha}}^T\mathbf{a}W - \boldsymbol{\partial}_{\boldsymbol{\alpha}^*}^T\mathbf{a}^*W + \operatorname{Tr}\left\{\boldsymbol{\partial}_{\boldsymbol{\alpha}^*}\boldsymbol{\partial}_{\boldsymbol{\alpha}}^T BB^H\right\} W$$

*is equivalent to the set of SDEs in the Itô form*

$$\mathrm{d}\boldsymbol{\alpha} = \mathbf{a}\mathrm{d}t + B\mathrm{d}\mathbf{Z},$$

*and to the set of SDEs in the Stratonovich form*

$$\mathrm{d}\boldsymbol{\alpha} = (\mathbf{a} - \mathbf{s})\mathrm{d}t + B\mathrm{d}\mathbf{Z},$$

*where the Stratonovich term has elements*

$$s_j = \frac{1}{2}\operatorname{Tr}\left\{B^H \boldsymbol{\partial}_{\boldsymbol{\alpha}^*} \mathbf{e}_j^T B\right\},$$

*and* $\mathbf{Z} = (\mathbf{X} + i\mathbf{Y})/\sqrt{2}$ *is an* $L$*-dimensional standard complex-valued Wiener process (with* $\langle \mathrm{d}Z_j \mathrm{d}Z_k^* \rangle = \delta_{jk}\mathrm{d}t$*), containing two standard* $L$*-dimensional Wiener processes* $\mathbf{X}$ *and* $\mathbf{Y}$*.*

*Proof.* Let us expand the FPE using real variables: $\boldsymbol{\alpha} = \mathbf{x} + i\mathbf{y}$, $\mathbf{a} = \mathbf{u} + i\mathbf{v}$, $B = F + iG$, $\boldsymbol{\partial}_{\boldsymbol{\alpha}} = (\boldsymbol{\partial}_{\mathbf{x}} - i\boldsymbol{\partial}_{\mathbf{y}})/2$. This results in

$$\begin{aligned}\frac{\mathrm{d}W}{\mathrm{d}t} = & -\boldsymbol{\partial}_{\mathbf{x}}^T \mathbf{u} W - \boldsymbol{\partial}_{\mathbf{y}}^T \mathbf{v} W + \frac{1}{4}\operatorname{Tr}\left\{(\boldsymbol{\partial}_{\mathbf{x}}\boldsymbol{\partial}_{\mathbf{x}}^T + \boldsymbol{\partial}_{\mathbf{y}}\boldsymbol{\partial}_{\mathbf{y}}^T)(FF^T + GG^T)\right. \\ & \left.-(\boldsymbol{\partial}_{\mathbf{x}}\boldsymbol{\partial}_{\mathbf{y}}^T - \boldsymbol{\partial}_{\mathbf{y}}\boldsymbol{\partial}_{\mathbf{x}}^T)(FG^T - GF^T)\right\} W \\ & + \frac{i}{4}\operatorname{Tr}\left\{(\boldsymbol{\partial}_{\mathbf{x}}\boldsymbol{\partial}_{\mathbf{x}}^T + \boldsymbol{\partial}_{\mathbf{y}}\boldsymbol{\partial}_{\mathbf{y}}^T)(FG^T - GF^T)\right\} W \\ & + \frac{i}{4}\operatorname{Tr}\left\{(\boldsymbol{\partial}_{\mathbf{x}}\boldsymbol{\partial}_{\mathbf{y}}^T - \boldsymbol{\partial}_{\mathbf{y}}\boldsymbol{\partial}_{\mathbf{x}}^T)(FF^T + GG^T)\right\} W.\end{aligned} \tag{C.1}$$

Since $FF^T + GG^T$ and $\boldsymbol{\partial}_{\mathbf{x}}\boldsymbol{\partial}_{\mathbf{x}}^T + \boldsymbol{\partial}_{\mathbf{y}}\boldsymbol{\partial}_{\mathbf{y}}^T$ are symmetric matrices, and $FG^T - GF^T$ and $\boldsymbol{\partial}_{\mathbf{x}}\boldsymbol{\partial}_{\mathbf{y}}^T - \boldsymbol{\partial}_{\mathbf{y}}\boldsymbol{\partial}_{\mathbf{x}}^T$ are antisymmetric ones, the corresponding traces are equal to zero, which gives us the FPE in real variables

$$\begin{aligned}\frac{\mathrm{d}W}{\mathrm{d}t} = & -\boldsymbol{\partial}_{\mathbf{x}}^T \mathbf{u} W - \boldsymbol{\partial}_{\mathbf{y}}^T \mathbf{v} W + \frac{1}{4}\operatorname{Tr}\left\{(\boldsymbol{\partial}_{\mathbf{x}}\boldsymbol{\partial}_{\mathbf{x}}^T + \boldsymbol{\partial}_{\mathbf{y}}\boldsymbol{\partial}_{\mathbf{y}}^T)(FF^T + GG^T)\right. \\ & \left.-(\boldsymbol{\partial}_{\mathbf{x}}\boldsymbol{\partial}_{\mathbf{y}}^T - \boldsymbol{\partial}_{\mathbf{y}}\boldsymbol{\partial}_{\mathbf{x}}^T)(FG^T - GF^T)\right\} W.\end{aligned} \tag{C.2}$$

In order to use Lemma C.1, we need to merge variables $\mathbf{x}$ and $\mathbf{y}$ into one variable vector $\mathbf{z} \equiv \mathbf{x} \oplus \mathbf{y}$. This will give us an equation in the form identical to that from the lemma,

with drift vector $\tilde{\mathbf{a}} \equiv \mathbf{u} \oplus \mathbf{v}$ and diffusion matrix

$$\tilde{B}\tilde{B}^T \equiv \frac{1}{2}\begin{pmatrix} FF^T + GG^T & FG^T - GF^T \\ GF^T - FG^T & FF^T + GG^T \end{pmatrix}, \tag{C.3}$$

which gives the noise matrix

$$\tilde{B} = \frac{1}{\sqrt{2}}\begin{pmatrix} F & -G \\ G & F \end{pmatrix}. \tag{C.4}$$

Therefore, the equivalent SDEs in the Itô form are

$$d\mathbf{z} = \tilde{\mathbf{a}}dt + \tilde{B}d\tilde{\mathbf{Z}}, \tag{C.5}$$

where $d\tilde{\mathbf{Z}} \equiv d\mathbf{X} \oplus d\mathbf{Y}$. Returning to the previous variables:

$$\begin{aligned} \mathrm{d}\mathbf{x} &= \mathbf{u}dt + \frac{1}{\sqrt{2}}Fd\mathbf{X} - \frac{1}{\sqrt{2}}Gd\mathbf{Y}, \\ \mathrm{d}\mathbf{y} &= \mathbf{v}dt + \frac{1}{\sqrt{2}}Gd\mathbf{X} + \frac{1}{\sqrt{2}}Fd\mathbf{Y}. \end{aligned} \tag{C.6}$$

Multiplying the second equation by $i$ and adding it to the first one:

$$d\boldsymbol{\alpha} = \mathbf{a}dt + \frac{1}{\sqrt{2}}(F + iG)(d\mathbf{X} + id\mathbf{Y}), \tag{C.7}$$

which leads to the Itô part of the theorem statement

$$d\boldsymbol{\alpha} = \mathbf{a}dt + Bd\mathbf{Z}. \tag{C.8}$$

The noise-induced drift term in the Stratonovich case can be calculated by substituting $\tilde{B}$ into the expression for $s_j$ from Lemma C.1. We will calculate $s_j$ with $j$ belonging to the $\mathbf{x}$ and the $\mathbf{y}$ part of the coordinate space separately. Starting from the $\mathbf{x}$ part:

$$s_j^{(x)} = \frac{1}{4}\mathrm{Tr}\left\{\begin{pmatrix} F^T & G^T \\ -G^T & F^T \end{pmatrix}\begin{pmatrix} \boldsymbol{\partial}_{\mathbf{x}} \\ \boldsymbol{\partial}_{\mathbf{y}} \end{pmatrix}\begin{pmatrix} \mathbf{e}_j^T & 0 \end{pmatrix}\begin{pmatrix} F & -G \\ G & F \end{pmatrix}\right\}. \tag{C.9}$$

Multiplying the matrices, we get:

$$\begin{aligned}
&= \frac{1}{4}\operatorname{Tr}\left\{\begin{pmatrix} F^T & G^T \\ -G^T & F^T \end{pmatrix}\begin{pmatrix} \partial_{\mathbf{x}} \\ \partial_{\mathbf{y}} \end{pmatrix}\begin{pmatrix} \mathbf{e}_j^T F & -\mathbf{e}_j^T G \end{pmatrix}\right\} \\
&= \frac{1}{4}\operatorname{Tr}\left\{\begin{pmatrix} F^T & G^T \\ -G^T & F^T \end{pmatrix}\begin{pmatrix} \partial_{\mathbf{x}}\mathbf{e}_j^T F & -\partial_{\mathbf{x}}\mathbf{e}_j^T G \\ \partial_{\mathbf{y}}\mathbf{e}_j^T F & -\partial_{\mathbf{y}}\mathbf{e}_j^T G \end{pmatrix}\right\} \\
&= \frac{1}{4}\left(\operatorname{Tr}\left\{F^T\partial_{\mathbf{x}}\mathbf{e}_j^T F\right\} + \operatorname{Tr}\left\{G^T\partial_{\mathbf{y}}\mathbf{e}_j^T F\right\}\right. \\
&\quad \left. + \operatorname{Tr}\left\{G^T\partial_{\mathbf{x}}\mathbf{e}_j^T G\right\} - \operatorname{Tr}\left\{F^T\partial_{\mathbf{y}}\mathbf{e}_j^T G\right\}\right).
\end{aligned} \tag{C.10}$$

Similarly for the $\mathbf{y}$ part,

$$\begin{aligned}
s_j^{(y)} = \frac{1}{4}&\left(\operatorname{Tr}\left\{F^T\partial_{\mathbf{x}}\mathbf{e}_j^T G\right\} + \operatorname{Tr}\left\{G^T\partial_{\mathbf{y}}\mathbf{e}_j^T G\right\}\right. \\
&\left. - \operatorname{Tr}\left\{G^T\partial_{\mathbf{x}}\mathbf{e}_j^T F\right\} + \operatorname{Tr}\left\{F^T\partial_{\mathbf{y}}\mathbf{e}_j^T F\right\}\right).
\end{aligned} \tag{C.11}$$

Therefore, the final term in the complex-valued SDEs is

$$s_j = s_j^{(x)} + i s_j^{(y)} = \frac{1}{2}\operatorname{Tr}\left\{B^H\partial_{\boldsymbol{\alpha}^*}\mathbf{e}_j^T B\right\}, \tag{C.12}$$

which finishes the proof. □

Note the asymmetry in the expression for the Stratonovich term: if $B = B(\alpha)$, then $\mathbf{s} \equiv 0$. This is initially caused by the asymmetry in the target SDEs. A truly general form of an FPE would be

$$\begin{aligned}
\frac{\mathrm{d}W}{\mathrm{d}t} = &-2\operatorname{Re}\left(\partial_{\boldsymbol{\alpha}}^T\mathbf{a}\right)W + \operatorname{Tr}\left\{\partial_{\boldsymbol{\alpha}^*}\partial_{\boldsymbol{\alpha}}^T B_1 B_1^H\right\}W + \operatorname{Tr}\left\{\partial_{\boldsymbol{\alpha}^*}\partial_{\boldsymbol{\alpha}}^T B_2 B_2^H\right\}W \\
&+ 2\operatorname{Re}\left(\operatorname{Tr}\left\{\partial_{\boldsymbol{\alpha}}\partial_{\boldsymbol{\alpha}}^T B_1 B_2^T\right\} + \operatorname{Tr}\left\{\partial_{\boldsymbol{\alpha}}\partial_{\boldsymbol{\alpha}}^T B_2 B_1^T\right\}\right)W,
\end{aligned} \tag{C.13}$$

which corresponds to the system of SDEs

$$\mathrm{d}\boldsymbol{\alpha} = (\mathbf{a} - \mathbf{s})\mathrm{d}t + B_1\mathrm{d}\mathbf{Z} + B_2\mathrm{d}\mathbf{Z}^*, \tag{C.14}$$

where the Stratonovich term has elements

$$\begin{aligned} s_j = \frac{1}{2}\Big(&\mathrm{Tr}\left\{B_1^H \boldsymbol{\partial}_{\boldsymbol{\alpha}^*} \mathbf{e}_j^T B_1\right\} + \mathrm{Tr}\left\{B_2^H \boldsymbol{\partial}_{\boldsymbol{\alpha}^*} \mathbf{e}_j^T B_2\right\} \\ &+ \mathrm{Tr}\left\{B_1^T \boldsymbol{\partial}_{\boldsymbol{\alpha}} \mathbf{e}_j^T B_2\right\} + \mathrm{Tr}\left\{B_2^T \boldsymbol{\partial}_{\boldsymbol{\alpha}} \mathbf{e}_j^T B_1\right\}\Big). \end{aligned} \tag{C.15}$$

In the theorem above we limited the space of possible SDEs to those with $B_2 \equiv 0$, leading to the observed asymmetry.

In many applications (some of which are discussed in this thesis), it is advantageous to enumerate the state vector of a system using two variables instead of one, namely the mode identifier and the component number. This helps to describe particles which can occupy the same set of modes, but are otherwise distinguishable. We will now reformulate the previous theorem, including this component distinction.

**Theorem C.2** (multi-component reformulation of Theorem C.1)**.** *Let $\boldsymbol{\alpha}^{(j)}$, $j = 1 \dots C$ be $C$ sets of complex variables $\boldsymbol{\alpha}^{(j)} \equiv (\alpha_1^{(j)} \dots \alpha_{M_j}^{(j)})$. Then the FPE*

$$\begin{aligned} \frac{\mathrm{d}W}{\mathrm{d}t} = &-\sum_{j=1}^{C} \boldsymbol{\partial}_{\boldsymbol{\alpha}^{(j)}}^T \mathbf{a}^{(j)} W - \sum_{j=1}^{C} \boldsymbol{\partial}_{(\boldsymbol{\alpha}^{(j)})^*}^T (\mathbf{a}^{(j)})^* W \\ &+ \sum_{j=1}^{C}\sum_{k=1}^{C} \mathrm{Tr}\left\{\boldsymbol{\partial}_{(\boldsymbol{\alpha}^{(j)})^*} \boldsymbol{\partial}_{\boldsymbol{\alpha}^{(k)}}^T B^{(k)} (B^{(j)})^H\right\} W \end{aligned}$$

*is equivalent to the set of SDEs in the Itô form*

$$\mathrm{d}\boldsymbol{\alpha}^{(j)} = \mathbf{a}^{(j)}\mathrm{d}t + B^{(j)}\mathrm{d}\mathbf{Z},$$

*or to the set of SDEs in the Stratonovich form*

$$\mathrm{d}\boldsymbol{\alpha}^{(j)} = (\mathbf{a}^{(j)} - \mathbf{s}^{(j)})\mathrm{d}t + B^{(j)}\mathrm{d}\mathbf{Z},$$

*where the Stratonovich term has elements*

$$s_i^{(j)} = \frac{1}{2}\sum_{k=1}^{C} \mathrm{Tr}\left\{(B^{(k)})^H \boldsymbol{\partial}_{(\boldsymbol{\alpha}^{(k)})^*} \mathbf{e}_i^T B^{(j)}\right\}.$$

*Here $\mathbf{Z}$ is an $L$-dimensional standard complex-valued Wiener process, and the noise matrices $B^{(j)}$ have sizes $M_j \times L$.*

*Proof.* Let us join all variable sets $\boldsymbol{\alpha}^{(j)}$ into a single set

$$\boldsymbol{\alpha} \equiv \bigoplus_{j=1}^{C} \boldsymbol{\alpha}^{(j)}. \tag{C.16}$$

Then we can use Theorem C.1 with the drift vector

$$\mathbf{a} = \bigoplus_{j=1}^{C} \mathbf{a}^{(j)}, \tag{C.17}$$

the cogradient vector

$$\boldsymbol{\partial}_{\boldsymbol{\alpha}} = \bigoplus_{j=1}^{C} \boldsymbol{\partial}_{\boldsymbol{\alpha}^{(j)}}, \tag{C.18}$$

and the noise matrix

$$B = \begin{pmatrix} B^{(1)} \\ \vdots \\ B^{(C)} \end{pmatrix}. \tag{C.19}$$

This gives us SDEs in the Itô form

$$\mathrm{d}\boldsymbol{\alpha} = \mathbf{a}\mathrm{d}t + B\mathrm{d}\mathbf{Z}, \tag{C.20}$$

where $d\mathbf{Z}$ is an $L$-dimensional standard complex-valued Wiener process. Splitting this equation for different components, we get the Itô part of the theorem statement. Substituting $B$ into the expression for the Stratonovich term:

$$s_i^{(j)} = \frac{1}{2} \operatorname{Tr} \left\{ \begin{pmatrix} (B^{(1)})^H & \cdots & (B^{(C)})^H \end{pmatrix} \begin{pmatrix} \boldsymbol{\partial}_{(\boldsymbol{\alpha}^{(1)})^*} \\ \vdots \\ \boldsymbol{\partial}_{(\boldsymbol{\alpha}^{(C)})^*} \end{pmatrix} \begin{pmatrix} 0 & \cdots & \mathbf{e}_i^T & \cdots & 0 \end{pmatrix} \begin{pmatrix} B^{(1)} \\ \vdots \\ B^{(C)} \end{pmatrix} \right\}. \tag{C.21}$$

Multiplying the matrices successively, we get

$$
\begin{aligned}
&= \frac{1}{2}\operatorname{Tr}\left\{\begin{pmatrix}(B^{(1)})^H & \cdots & (B^{(C)})^H\end{pmatrix}\begin{pmatrix}\boldsymbol{\partial}_{(\boldsymbol{\alpha}^{(1)})^*}\mathbf{e}_i^T B^{(j)} \\ \vdots \\ \boldsymbol{\partial}_{(\boldsymbol{\alpha}^{(C)})^*}\mathbf{e}_i^T B^{(j)}\end{pmatrix}\right\} \\
&= \frac{1}{2}\sum_{k=1}^{C}\operatorname{Tr}\left\{(B^{(k)})^H\boldsymbol{\partial}_{(\boldsymbol{\alpha}^{(k)})^*}\mathbf{e}_i^T B^{(j)}\right\},
\end{aligned}
\tag{C.22}
$$

which is the expression from the theorem statement. □

Most of the time we will deal with FPEs in a functional form, so we will reformulate the correspondence once again, now using functional derivatives.

**Theorem C.3.** *The FPE in a functional form*

$$
\begin{aligned}
\frac{\mathrm{d}W}{\mathrm{d}t} = \int \mathrm{d}\mathbf{x}\Bigg(&-\sum_{j=1}^{C}\frac{\delta}{\delta f_j}\mathcal{A}_j W - \sum_{j=1}^{C}\frac{\delta}{\delta f_j^*}\mathcal{A}_j^* W \\
&+\sum_{j=1}^{C}\sum_{k=1}^{C}\frac{\delta^2}{\delta f_j^*\delta f_k}\sum_{l=1}^{L}\mathcal{B}_{kl}\mathcal{B}_{jl}^* W\Bigg)
\end{aligned}
$$

*is equivalent to the set of SDEs in the Itô form*

$$
\mathrm{d}f_j = \mathcal{P}_{\mathbb{M}_j}\left[\mathcal{A}_j\mathrm{d}t + \sum_{l=1}^{L}\mathcal{B}_{jl}\mathrm{d}Q_l\right],
$$

*or the set of SDEs in the Stratonovich form*

$$
\mathrm{d}f_j = \mathcal{P}_{\mathbb{M}_j}\left[(\mathcal{A}_j - \mathcal{S}_j)\mathrm{d}t + \sum_{l=1}^{L}\mathcal{B}_{jl}\mathrm{d}Q_l\right],
$$

*where*

$$
\mathcal{S}_j = \frac{1}{2}\sum_{k=1}^{C}\sum_{l=1}^{L}\mathcal{B}_{kl}^*\frac{\delta}{\delta f_k^*}\mathcal{B}_{jl}.
$$

*Here $f_j \in \mathbb{F}_{\mathbb{M}_j}$, $\mathcal{A}_j \equiv \mathcal{A}_j[\mathbf{f}]$ and $\mathcal{B}_{jl} \equiv \mathcal{B}_{jl}[\mathbf{f}]$ are functional operators, $W \equiv W[\mathbf{f}]$ is a probability functional, and $L$ is the number of noise sources. The standard functional Wiener processes $Q_l$ are the compositions of standard complex-valued Wiener processes:*

$$
Q_l = \sum_{\mathbf{n}\in\mathbb{B}}\phi_{\mathbf{n}}Z_{l,\mathbf{n}}.
$$

*Proof.* Expanding the functional derivatives according to Definition B.5 with $f_j = \sum_{\mathbf{n}\in\mathbb{M}_j} \phi_{j,\mathbf{n}}\alpha_{j,\mathbf{n}}$:

$$\begin{aligned}\frac{\mathrm{d}W}{\mathrm{d}t} = \Bigg( &-\sum_{j=1}^{C}\sum_{\mathbf{n}\in\mathbb{M}_j}\frac{\partial}{\partial\alpha_{j,\mathbf{n}}}\int \mathrm{d}\mathbf{x}\,\phi^*_{j,\mathbf{n}}\mathcal{A}_j W - \sum_{j=1}^{C}\sum_{\mathbf{n}\in\mathbb{M}_j}\frac{\partial}{\partial\alpha^*_{j,\mathbf{n}}}\int \mathrm{d}\mathbf{x}\,\phi_{j,\mathbf{n}}\mathcal{A}^*_j W \\ &+\sum_{j=1}^{C}\sum_{k=1}^{C}\sum_{\mathbf{m}\in\mathbb{M}_j,\mathbf{n}\in\mathbb{M}_k}\frac{\partial}{\partial\alpha^*_{j,\mathbf{m}}}\frac{\partial}{\partial\alpha_{k,\mathbf{n}}}\int \mathrm{d}\mathbf{x}\phi_{j,\mathbf{m}}\phi^*_{k,\mathbf{n}}\sum_{l=1}^{L}\mathcal{B}^*_{jl}\mathcal{B}_{kl}W\Bigg).\end{aligned} \tag{C.23}$$

The diffusion term has to be transformed in order to conform to Theorem C.2:

$$\begin{aligned}\int \mathrm{d}\mathbf{x}\phi_{j,\mathbf{m}}\phi^*_{k,\mathbf{n}}\sum_{l=1}^{L}\mathcal{B}_{kl}\mathcal{B}^*_{jl} &= \iint \mathrm{d}\mathbf{x}\,\mathrm{d}\mathbf{x}'\,\phi'_{j,\mathbf{m}}\phi^*_{k,\mathbf{n}}\sum_{l=1}^{L}\mathcal{B}'^*_{jl}\mathcal{B}_{kl}\delta(\mathbf{x}-\mathbf{x}') \\ &= \iint \mathrm{d}\mathbf{x}\,\mathrm{d}\mathbf{x}'\,\phi'_{j,\mathbf{m}}\phi^*_{k,\mathbf{n}}\sum_{l=1}^{L}\mathcal{B}'^*_{jl}\mathcal{B}_{kl}\sum_{\mathbf{p}\in\mathbb{B}}\phi'^*_{\mathbf{p}}\phi_{\mathbf{p}} \\ &= \sum_{l=1}^{L}\sum_{\mathbf{p}\in\mathbb{B}}\int \mathrm{d}\mathbf{x}\,\phi_{j,\mathbf{m}}\mathcal{B}^*_{jl}\phi^*_{\mathbf{p}}\int \mathrm{d}\mathbf{x}\,\phi^*_{k,\mathbf{n}}\mathcal{B}_{kl}\phi_{\mathbf{p}}.\end{aligned} \tag{C.24}$$

Note that we did not specify the index of the full basis used to expand the delta function. It can be any orthonormal and complete basis, in particular one of $\mathbb{B}_j$ — this will not change the result.

Now we have the FPE in the form required by Theorem C.2 with

$$a^{(j)}_{\mathbf{m}} = \int \mathrm{d}\mathbf{x}\,\phi^*_{j,\mathbf{m}}\mathcal{A}_j,\ \mathbf{m}\in\mathbb{M}_j, \tag{C.25}$$

and

$$B^{(j)}_{\mathbf{m},(\mathbf{p},l)} = \int \mathrm{d}\mathbf{x}\,\phi^*_{j,\mathbf{m}}\mathcal{B}_{jl}\phi_{\mathbf{p}},\ \mathbf{m}\in\mathbb{M}_j, \mathbf{p}\in\mathbb{B}, l\in[1\ldots L]. \tag{C.26}$$

Note that the columns of $B$ are enumerated using the compound index $\mathbf{p}, l$.

Therefore, the initial FPE is equivalent to the set of SDEs in the Itô form

$$\mathrm{d}\alpha^{(j)}_{\mathbf{m}} = \int \mathrm{d}\mathbf{x}\,\phi^*_{j,\mathbf{m}}\mathcal{A}_j\mathrm{d}t + \sum_{\mathbf{p}\in\mathbb{B},l\in[1\ldots L]}\int \mathrm{d}\mathbf{x}\,\phi^*_{j,\mathbf{m}}\mathcal{B}_{jl}\phi_{\mathbf{p}}\mathrm{d}Z_{\mathbf{p},l}. \tag{C.27}$$

Multiplying by $\phi'_{j,\mathbf{m}}$ and grouping by component:

$$\begin{aligned}\sum_{\mathbf{m}\in\mathbb{M}_j}\phi'_{j,\mathbf{m}}\mathrm{d}\alpha^{(j)}_{\mathbf{m}} = &\sum_{\mathbf{m}\in\mathbb{M}_j}\phi'_{j,\mathbf{m}}\int \mathrm{d}\mathbf{x}\,\phi^*_{j,\mathbf{m}}\mathcal{A}_j\mathrm{d}t \\ &+\sum_{\mathbf{m}\in\mathbb{M}_j}\phi'_{j,\mathbf{m}}\int \mathrm{d}\mathbf{x}\,\phi^*_{j,\mathbf{m}}\sum_{l=1}^{L}\sum_{\mathbf{p}\in\mathbb{B}}\mathcal{B}_{jl}\phi_{\mathbf{p}}\mathrm{d}Z_{\mathbf{p},l}.\end{aligned} \tag{C.28}$$

Recognising Definition B.3 of the projection operator:

$$\mathrm{d}f_j = \mathcal{P}_{\mathbb{M}_j}\left[\mathcal{A}_j\mathrm{d}t + \sum_{l=1}^{L}\mathcal{B}_{jl}\sum_{\mathbf{p}\in\mathbb{B}}\phi_{\mathbf{p}}\mathrm{d}Z_{\mathbf{p},l}\right]. \tag{C.29}$$

Defining the standard functional Wiener process as $Q_l = \sum_{\mathbf{p}\in\mathbb{B}}\phi_{\mathbf{p}}Z_{\mathbf{p},l}$:

$$\mathrm{d}f_c = \mathcal{P}_{\mathbb{M}_j}\left[\mathcal{A}_j\mathrm{d}t + \sum_{l=1}^{L}\mathcal{B}_{jl}\mathrm{d}Q_l\right]. \tag{C.30}$$

Performing the same multiplication and summation on the Stratonovich term from Theorem C.2:

$$\mathcal{S}_j = \sum_{\mathbf{m}\in\mathbb{M}_j}\phi'_{j,\mathbf{m}}s^{(j)}_{\mathbf{m}} = \frac{1}{2}\sum_{\mathbf{m}\in\mathbb{M}_j}\phi'_{j,\mathbf{m}}\sum_{k=1}^{C}\mathrm{Tr}\left\{(B^{(k)})^H\boldsymbol{\partial}_{(\boldsymbol{\alpha}^{(k)})^*}\mathbf{e}^T_{\mathbf{m}}B^{(j)}\right\}. \tag{C.31}$$

Transforming the trace to a summation:

$$\mathcal{S}_j = \frac{1}{2}\sum_{\mathbf{m}\in\mathbb{M}_c}\phi'_{j,\mathbf{m}}\sum_{k=1}^{C}\sum_{\mathbf{n}\in\mathbb{M}_k}\sum_{l=1}^{L}\sum_{\mathbf{p}\in\mathbb{B}}(B^{(k)}_{\mathbf{n}(\mathbf{p},l)})^*\frac{\partial}{\partial(\alpha^{(k)}_{\mathbf{n}})^*}B^{(j)}_{\mathbf{m}(\mathbf{p},l)}. \tag{C.32}$$

Using the multimode form (C.26) of the noise matrix:

$$\mathcal{S}_j = \frac{1}{2}\sum_{\mathbf{m}\in\mathbb{M}_j}\phi'_{j,\mathbf{m}}\sum_{k=1}^{C}\sum_{\mathbf{n}\in\mathbb{M}_k}\sum_{l=1}^{L}\sum_{\mathbf{p}\in\mathbb{B}}\int \mathrm{d}\mathbf{x}\,\phi_{k,\mathbf{n}}\mathcal{B}^*_{kl}\phi^*_{\mathbf{p}}\int \mathrm{d}\mathbf{x}\,\phi^*_{j,\mathbf{m}}\frac{\partial}{\partial(\alpha^{(k)}_{\mathbf{n}})^*}\mathcal{B}_{jl}\phi_{\mathbf{p}}. \tag{C.33}$$

Substituting $\sum_{\mathbf{p}\in\mathbb{B}}\phi^*_{\mathbf{p}}\phi_{\mathbf{p}} = \delta(\mathbf{x}-\mathbf{x}')$:

$$\mathcal{S}_j = \frac{1}{2}\sum_{\mathbf{m}\in\mathbb{M}_j}\phi'_{j,\mathbf{m}}\sum_{k=1}^{C}\sum_{\mathbf{n}\in\mathbb{M}_k}\sum_{l=1}^{L}\int \mathrm{d}\mathbf{x}\,\phi_{k,\mathbf{n}}\mathcal{B}^*_{kl}\phi^*_{j,\mathbf{m}}\frac{\partial}{\partial(\alpha^{(k)}_{\mathbf{n}})^*}\mathcal{B}_{jl}. \tag{C.34}$$

Recognising the projection transformation and the functional differential:

$$\begin{aligned}\mathcal{S}_j &= \mathcal{P}_{\mathbb{M}_j}\left[\frac{1}{2}\sum_{k=1}^{C}\sum_{\mathbf{n}\in\mathbb{M}_k}\sum_{l=1}^{L}\phi_{k,\mathbf{n}}\mathcal{B}^*_{kl}\frac{\partial}{\partial(\alpha^{(k)}_{\mathbf{n}})^*}\mathcal{B}_{jl}\right]\\ &= \mathcal{P}_{\mathbb{M}_j}\left[\frac{1}{2}\sum_{k=1}^{C}\sum_{l=1}^{L}\mathcal{B}^*_{kl}\frac{\delta}{\delta f^*_k}\mathcal{B}_{jl}\right].\end{aligned}$$ □

Alternatively, the FPE from the above theorem can be expressed in a short matrix form. The FPE in this case is

$$\frac{dW}{dt} = \int \mathrm{d}\mathbf{x}\left(-\delta_{\mathbf{f}}\cdot\boldsymbol{\mathcal{A}}W - \delta_{\mathbf{f}^*}\cdot\boldsymbol{\mathcal{A}}^*W + \mathrm{Tr}\left\{\delta_{\mathbf{f}^*}\delta^T_{\mathbf{f}}\mathcal{B}\mathcal{B}^H\right\}W\right), \tag{C.35}$$

where the functional cogradient $\delta_{\mathbf{f}} = (\delta/\delta f_1 \dots \delta/\delta f_C)$, $\mathcal{A}$ is a vector of $C$ functional operators, and $\mathcal{B}$ is a matrix of $C \times L$ functional operators. Such FPE is equivalent to the matrix SDE in the Stratonovich form:

$$\mathrm{d}\mathbf{f} = \boldsymbol{\mathcal{P}}\left[(\boldsymbol{\mathcal{A}} - \boldsymbol{\mathcal{S}})\,\mathrm{d}t + \mathcal{B}\mathrm{d}\mathbf{Q}\right], \tag{C.36}$$

with the Stratonovich term

$$\boldsymbol{\mathcal{S}}_j = \frac{1}{2}\,\mathrm{Tr}\left\{\mathcal{B}^H\delta_{\mathbf{f}^*}\mathbf{e}_j^T\mathcal{B}\right\}, \tag{C.37}$$

where $\boldsymbol{\mathcal{P}}^T \equiv (\mathcal{P}_{\mathbb{M}_1} \dots \mathcal{P}_{\mathbb{M}_C})$ is a vector of projection operators, and $\mathbf{Q}^T \equiv (Q_1 \dots Q_C)$ is a vector of standard functional Wiener processes.

## C.2. Itô formula

In this section we will follow a procedure similar to the one in the previous section and derive the Itô formula for the differential of a functional, based on the standard definition for the multi-variable real-valued case. Again, we will formulate the real-valued correspondence in a way that is convenient for future proofs.

**Lemma C.2.** *Let $\mathbf{z}^T \equiv (z_1 \dots z_M)$ be a set of real variables, and $\mathbf{Z}(t)$ be a standard $L$-dimensional Wiener process. For the set of SDEs in the Itô form*

$$\mathrm{d}\mathbf{z} = \mathbf{a}(\mathbf{z},t)\mathrm{d}t + B(\mathbf{z},t)\mathrm{d}\mathbf{Z}(t),$$

*the differential of a function $f(\mathbf{z})$ is*

$$\mathrm{d}f(\mathbf{z}) = \mathbf{a}\cdot\boldsymbol{\partial}_{\mathbf{z}} f(\mathbf{z})\mathrm{d}t + \frac{1}{2}\operatorname{Tr}\left\{BB^T\boldsymbol{\partial}_{\mathbf{z}}\boldsymbol{\partial}_{\mathbf{z}}^T\right\} f(\mathbf{z})\mathrm{d}t + \operatorname{Tr}\left\{B\mathrm{d}\mathbf{Z}\boldsymbol{\partial}_{\mathbf{z}}^T\right\} f(\mathbf{z}).$$

*Proof.* For the detailed proof see Gardiner [132], section 4.3.3. □

As a next step, we will extend this lemma to operate on vectors of complex variables and SDEs with complex-valued coefficients from Theorem C.1.

**Theorem C.4.** *Let $\boldsymbol{\alpha}^T \equiv (\alpha_1 \ldots \alpha_M)$ be a set of complex variables, and $\mathbf{Z} = (\mathbf{X} + i\mathbf{Y})/\sqrt{2}$ be an $L$-dimensional standard complex-valued Wiener process, containing two standard $L$-dimensional Wiener processes $\mathbf{X}$ and $\mathbf{Y}$. For the set of SDEs in the Itô form*

$$\mathrm{d}\boldsymbol{\alpha} = \mathbf{a}(\boldsymbol{\alpha}, t)\mathrm{d}t + B(\boldsymbol{\alpha}, t)\mathrm{d}\mathbf{Z}(t),$$

*the differential of a function $f(\boldsymbol{\alpha})$ is*

$$\mathrm{d}f(\boldsymbol{\alpha}) = 2\operatorname{Re}(\mathbf{a}\cdot\boldsymbol{\partial}_{\boldsymbol{\alpha}})f(\boldsymbol{\alpha})\mathrm{d}t + \operatorname{Tr}\left\{BB^H\boldsymbol{\partial}_{\boldsymbol{\alpha}^*}\boldsymbol{\partial}_{\boldsymbol{\alpha}}^T\right\} f(\boldsymbol{\alpha})\mathrm{d}t + 2\operatorname{Re}\operatorname{Tr}\left\{B\mathrm{d}\mathbf{Z}\boldsymbol{\partial}_{\boldsymbol{\alpha}}^T\right\} f(\boldsymbol{\alpha}).$$

*Proof.* The proof follows the same scheme as Theorem C.1, just in the opposite direction. Let $f = g + ih$, $\boldsymbol{\alpha} = \mathbf{x} + i\mathbf{y}$, $\mathbf{a} = \mathbf{u} + i\mathbf{v}$, $B = F + iG$, $\boldsymbol{\partial}_{\boldsymbol{\alpha}} = (\boldsymbol{\partial}_{\mathbf{x}} - i\boldsymbol{\partial}_{\mathbf{y}})/2$. Then the set of SDEs from the statement is equivalent to

$$\mathrm{d}\begin{pmatrix}\mathbf{x}\\ \mathbf{y}\end{pmatrix} = \begin{pmatrix}\mathbf{u}\\ \mathbf{v}\end{pmatrix}\mathrm{d}t + \frac{1}{\sqrt{2}}\begin{pmatrix}F & -G\\ G & F\end{pmatrix}\begin{pmatrix}\mathrm{d}\mathbf{X}\\ \mathrm{d}\mathbf{Y}\end{pmatrix}. \tag{C.38}$$

Applying Lemma C.2 for real-valued functions $g(\mathbf{x}, \mathbf{y})$ and $h(\mathbf{x}, \mathbf{y})$ and combining them into $f = g + ih$, we get

$$\begin{aligned}\mathrm{d}f = &\begin{pmatrix}\mathbf{x}\\ \mathbf{y}\end{pmatrix}\cdot\begin{pmatrix}\boldsymbol{\partial}_{\mathbf{x}}\\ \boldsymbol{\partial}_{\mathbf{y}}\end{pmatrix} f\mathrm{d}t + \frac{1}{4}\operatorname{Tr}\left\{\begin{pmatrix}F & -G\\ G & F\end{pmatrix}\begin{pmatrix}F^T & G^T\\ -G^T & F^T\end{pmatrix}\begin{pmatrix}\boldsymbol{\partial}_{\mathbf{x}}\\ \boldsymbol{\partial}_{\mathbf{y}}\end{pmatrix}\begin{pmatrix}\boldsymbol{\partial}_{\mathbf{x}}\\ \boldsymbol{\partial}_{\mathbf{y}}\end{pmatrix}^T\right\} f\mathrm{d}t\\ &+ \frac{1}{\sqrt{2}}\operatorname{Tr}\left\{\begin{pmatrix}F & -G\\ G & F\end{pmatrix}\begin{pmatrix}\mathrm{d}\mathbf{X}\\ \mathrm{d}\mathbf{Y}\end{pmatrix}\begin{pmatrix}\boldsymbol{\partial}_{\mathbf{x}}\\ \boldsymbol{\partial}_{\mathbf{y}}\end{pmatrix}^T\right\} f.\end{aligned} \tag{C.39}$$

Now let us match this equation and the lemma statement term by term.

The first term:

$$\begin{aligned} 2\,\mathrm{Re}(\mathbf{a}\cdot\boldsymbol{\partial}_{\alpha}) &= \mathrm{Re}\left((\mathbf{u}+i\mathbf{v})\cdot\left(\boldsymbol{\partial}_{\mathbf{x}}-i\boldsymbol{\partial}_{\mathbf{y}}\right)\right) \\ &= \mathbf{u}\cdot\boldsymbol{\partial}_{\mathbf{x}}+\mathbf{v}\cdot\boldsymbol{\partial}_{\mathbf{y}} \\ &= \begin{pmatrix}\mathbf{x}\\ \mathbf{y}\end{pmatrix}\cdot\begin{pmatrix}\boldsymbol{\partial}_{\mathbf{x}}\\ \boldsymbol{\partial}_{\mathbf{y}}\end{pmatrix}. \end{aligned} \tag{C.40}$$

The second term:

$$\begin{aligned} \mathrm{Tr}\left\{BB^{H}\boldsymbol{\partial}_{\alpha^*}\boldsymbol{\partial}_{\alpha}^{T}\right\} = \frac{1}{4}\mathrm{Tr}\left\{(FF^{T}+GG^{T})(\boldsymbol{\partial}_{\mathbf{x}}\boldsymbol{\partial}_{\mathbf{x}}^{T}+\boldsymbol{\partial}_{\mathbf{y}}\boldsymbol{\partial}_{\mathbf{y}}^{T})\right\} \\ -\frac{1}{4}\mathrm{Tr}\left\{(FG^{T}-GF^{T})(\boldsymbol{\partial}_{\mathbf{x}}\boldsymbol{\partial}_{\mathbf{y}}^{T}-\boldsymbol{\partial}_{\mathbf{y}}\boldsymbol{\partial}_{\mathbf{x}}^{T})\right\} \\ +\frac{i}{4}\mathrm{Tr}\left\{(FG^{T}-GF^{T})(\boldsymbol{\partial}_{\mathbf{x}}\boldsymbol{\partial}_{\mathbf{x}}^{T}+\boldsymbol{\partial}_{\mathbf{y}}\boldsymbol{\partial}_{\mathbf{y}}^{T})\right\} \\ +\frac{i}{4}\mathrm{Tr}\left\{(GG^{T}+FF^{T})(\boldsymbol{\partial}_{\mathbf{x}}\boldsymbol{\partial}_{\mathbf{y}}^{T}-\boldsymbol{\partial}_{\mathbf{y}}\boldsymbol{\partial}_{\mathbf{x}}^{T})\right\}. \end{aligned} \tag{C.41}$$

Same as in Theorem C.1, we notice that $FF^{T}+GG^{T}$ and $\boldsymbol{\partial}_{\mathbf{x}}\boldsymbol{\partial}_{\mathbf{x}}^{T}+\boldsymbol{\partial}_{\mathbf{y}}\boldsymbol{\partial}_{\mathbf{y}}^{T}$ are symmetric matrices, and $FG^{T}-GF^{T}$ and $\boldsymbol{\partial}_{\mathbf{x}}\boldsymbol{\partial}_{\mathbf{y}}^{T}-\boldsymbol{\partial}_{\mathbf{y}}\boldsymbol{\partial}_{\mathbf{x}}^{T}$ are antisymmetric ones. Therefore, the last two terms contain traces of antisymmetric matrices and are, consequently, equal to zero:

$$\begin{aligned} &= \frac{1}{4}\mathrm{Tr}\left\{(FF^{T}+GG^{T})\boldsymbol{\partial}_{\mathbf{x}}\boldsymbol{\partial}_{\mathbf{x}}^{T}+(FG^{T}-GF^{T})\boldsymbol{\partial}_{\mathbf{y}}\boldsymbol{\partial}_{\mathbf{x}}^{T})\right\} \\ &\quad+\frac{1}{4}\mathrm{Tr}\left\{(GF^{T}-FG^{T})\boldsymbol{\partial}_{\mathbf{x}}\boldsymbol{\partial}_{\mathbf{y}}^{T}+(FF^{T}+GG^{T})\boldsymbol{\partial}_{\mathbf{y}}\boldsymbol{\partial}_{\mathbf{y}}^{T})\right\} \\ &= \frac{1}{4}\mathrm{Tr}\left\{\begin{pmatrix}FF^{T}+GG^{T} & FG^{T}-GF^{T}\\ GF^{T}-FG^{T} & FF^{T}+GG^{T}\end{pmatrix}\begin{pmatrix}\boldsymbol{\partial}_{\mathbf{x}}\boldsymbol{\partial}_{\mathbf{x}}^{T} & \boldsymbol{\partial}_{\mathbf{x}}\boldsymbol{\partial}_{\mathbf{y}}^{T}\\ \boldsymbol{\partial}_{\mathbf{y}}\boldsymbol{\partial}_{\mathbf{x}}^{T} & \boldsymbol{\partial}_{\mathbf{y}}\boldsymbol{\partial}_{\mathbf{y}}^{T}\end{pmatrix}\right\} \\ &= \frac{1}{4}\mathrm{Tr}\left\{\begin{pmatrix}F & -G\\ G & F\end{pmatrix}\begin{pmatrix}F^{T} & G^{T}\\ -G^{T} & F^{T}\end{pmatrix}\begin{pmatrix}\boldsymbol{\partial}_{\mathbf{x}}\\ \boldsymbol{\partial}_{\mathbf{y}}\end{pmatrix}\begin{pmatrix}\boldsymbol{\partial}_{\mathbf{x}}\\ \boldsymbol{\partial}_{\mathbf{y}}\end{pmatrix}^{T}\right\}. \end{aligned} \tag{C.42}$$

The third term:

$$\begin{aligned} 2\,\mathrm{Re}\,\mathrm{Tr}\left\{B\mathrm{d}\mathbf{Z}\boldsymbol{\partial}_{\alpha}^{T}\right\} &= \frac{1}{\sqrt{2}}\mathrm{Re}\,\mathrm{Tr}\left\{(F+iG)(\mathrm{d}\mathbf{X}+i\mathrm{d}\mathbf{Y})(\boldsymbol{\partial}_{\mathbf{x}}-i\boldsymbol{\partial}_{\mathbf{y}})\right\} \\ &= \frac{1}{\sqrt{2}}\mathrm{Tr}\left\{F\mathrm{d}\mathbf{X}\boldsymbol{\partial}_{\mathbf{x}}+F\mathrm{d}\mathbf{Y}\boldsymbol{\partial}_{\mathbf{y}}-G\mathrm{d}\mathbf{Y}\boldsymbol{\partial}_{\mathbf{x}}+G\mathrm{d}\mathbf{X}\boldsymbol{\partial}_{\mathbf{y}}\right\} \\ &= \frac{1}{\sqrt{2}}\mathrm{Tr}\left\{\begin{pmatrix}F & -G\\ G & F\end{pmatrix}\begin{pmatrix}\mathrm{d}\mathbf{X}\\ \mathrm{d}\mathbf{Y}\end{pmatrix}\begin{pmatrix}\boldsymbol{\partial}_{\mathbf{x}}\\ \boldsymbol{\partial}_{\mathbf{y}}\end{pmatrix}^{T}\right\}. \end{aligned} \tag{C.43}$$

All terms are matched, thus proving the theorem. □

The above theorem can be reformulated for the multi-component SDEs from Theorem C.2.

**Theorem C.5.** *Let $\boldsymbol{\alpha}^{(j)}$, $j = 1 \dots C$ be $C$ sets of complex variables $\boldsymbol{\alpha}^{(j)} \equiv (\alpha_1^{(j)} \dots \alpha_{M_j}^{(j)})$. For the SDE in the Itô form*

$$\mathrm{d}\boldsymbol{\alpha}^{(j)} = \mathbf{a}^{(j)}\mathrm{d}t + B^{(j)}\mathrm{d}\mathbf{Z},$$

*the differential of a function $f(\boldsymbol{\alpha}^{(1)}, \dots, \boldsymbol{\alpha}^{(C)})$ is*

$$\begin{aligned}\mathrm{d}f = 2\sum_{j=1}^{C}\mathrm{Re}(\mathbf{a}^{(j)} \cdot \boldsymbol{\partial}_{\boldsymbol{\alpha}^{(j)}})f\,\mathrm{d}t + \sum_{j=1}^{C}\sum_{k=1}^{C}\mathrm{Tr}\left\{B^{(j)}(B^{(k)})^H\boldsymbol{\partial}_{(\boldsymbol{\alpha}^{(k)})^*}\boldsymbol{\partial}^T_{\boldsymbol{\alpha}^{(j)}}\right\}f\,\mathrm{d}t \\ + 2\sum_{j=1}^{C}\mathrm{Re}\,\mathrm{Tr}\left\{B^{(j)}\mathrm{d}\mathbf{Z}\boldsymbol{\partial}^T_{\boldsymbol{\alpha}^{(j)}}\right\}f.\end{aligned}$$

*Proof.* Proved analogously to Theorem C.2, by combining $\boldsymbol{\alpha}^{(j)}$ into a single vector and applying Theorem C.4. □

Finally, we can use the multi-component reformulation to derive the Itô formula in a functional form for the set of SDEs from Theorem C.3.

**Theorem C.6.** *Given the set of functional SDEs in the Itô form*

$$\mathrm{d}f_j = \mathcal{P}_{\mathbb{M}j}\left[\mathcal{A}_j\mathrm{d}t + \sum_{l=1}^{L}\mathcal{B}_{jl}\mathrm{d}Q_l\right],$$

*the differential of a functional operator $\mathcal{F}[\mathbf{f}]$ is*

$$\begin{aligned}\mathrm{d}\mathcal{F}[\mathbf{f}] = \int \mathrm{d}\mathbf{x}'\Bigg(2\sum_{j=1}^{C}\mathrm{Re}\left(\mathcal{A}'_j\frac{\delta}{\delta f'_j}\right)\mathcal{F}[\mathbf{f}]\mathrm{d}t \\ + \sum_{j=1}^{C}\sum_{k=1}^{C}\sum_{l=1}^{L}\mathcal{B}'_{jl}\mathcal{B}'^{*}_{kl}\frac{\delta}{\delta f'_j}\frac{\delta}{\delta f'^{*}_k}\mathcal{F}[\mathbf{f}]\mathrm{d}t \\ +2\sum_{j=1}^{C}\sum_{l=1}^{L}\mathrm{Re}\left(\mathcal{B}'_{jl}\mathrm{d}Q'_l\frac{\delta}{\delta f'_j}\right)\mathcal{F}[\mathbf{f}]\Bigg).\end{aligned}$$

*Here $f_j$, $\mathcal{A}_j$, $\mathcal{B}_{jl}$, $L$, and $Q_l$ are defined in the same way as in Theorem C.3.*

*Proof.* The set of SDEs can be rewritten in terms of complex vectors as

$$\mathrm{d}\alpha^{(j)}_{\mathbf{m}} = \int \mathrm{d}\mathbf{x}\, \phi^*_{j,\mathbf{m}} \mathcal{A}_j \mathrm{d}t + \sum_{l=1}^{L} \sum_{\mathbf{p}\in\mathbb{B}} \int \mathrm{d}\mathbf{x}\, \phi^*_{j,\mathbf{m}} \mathcal{B}_{jl} \phi_{\mathbf{p}} \mathrm{d}Z_{\mathbf{p},l}, \quad \mathbf{m} \in \mathbb{M}_j. \tag{C.44}$$

Now, treating the functional operator as a function of $C$ complex vectors

$$\mathcal{F} \equiv \mathcal{F}[\mathcal{C}_{\mathbb{M}_1}(\boldsymbol{\alpha}^{(1)}), \ldots, \mathcal{C}_{\mathbb{M}_C}(\boldsymbol{\alpha}^{(C)})], \tag{C.45}$$

we can use Theorem C.5 with the drift vectors

$$a^{(j)}_{\mathbf{m}} = \int \mathrm{d}\mathbf{x}\, \phi^*_{j,\mathbf{m}} \mathcal{A}_j, \tag{C.46}$$

and the noise matrices

$$B^{(j)}_{\mathbf{m},(\mathbf{p},l)} = \int \mathrm{d}\mathbf{x}\, \phi^*_{j,\mathbf{m}} \mathcal{B}_{jl} \phi_{\mathbf{p}}. \tag{C.47}$$

Applying Theorem C.5:

$$\begin{aligned}
\mathrm{d}\mathcal{F} = {} & 2\sum_{j=1}^{C} \sum_{\mathbf{m}\in\mathbb{M}_j} \mathrm{Re}\left( \int \mathrm{d}\mathbf{x}'\, \phi'^*_{j,\mathbf{m}} \mathcal{A}'_j \frac{\partial}{\partial \alpha_{j,\mathbf{m}}} \right) \mathcal{F}\, \mathrm{d}t \\
& + \sum_{j=1}^{C}\sum_{k=1}^{C} \sum_{\mathbf{m}\in\mathbb{M}_j} \sum_{\mathbf{n}\in\mathbb{M}_k} \sum_{l=1}^{L}\sum_{\mathbf{p}\in\mathbb{B}} \int \mathrm{d}\mathbf{x}'\, \phi'^*_{j,\mathbf{m}} \mathcal{B}'_{jl} \phi'_{\mathbf{p}} \int \mathrm{d}\mathbf{x}''\, \phi''_{k,\mathbf{n}} \mathcal{B}''^*_{kl} \phi''^*_{\mathbf{p}} \frac{\partial^2 \mathcal{F}}{\partial \alpha^*_{k,\mathbf{n}} \partial \alpha_{j,\mathbf{m}}} \mathrm{d}t \\
& + 2\sum_{j=1}^{C} \mathrm{Re}\left( \sum_{\mathbf{m}\in\mathbb{M}_j} \sum_{l=1}^{L}\sum_{\mathbf{p}\in\mathbb{B}} \int \mathrm{d}\mathbf{x}'\, \phi'^*_{j,\mathbf{m}} \mathcal{B}'_{jl} \phi'_{\mathbf{p}} \mathrm{d}Z_{\mathbf{p},l} \frac{\partial}{\partial \alpha_{j,\mathbf{m}}} \mathcal{F} \right).
\end{aligned} \tag{C.48}$$

Recognising definitions of the functional differentials, the functional Wiener process, and the delta function, we get

$$\begin{aligned}
= {} & 2\sum_{j=1}^{C} \mathrm{Re}\left( \int \mathrm{d}\mathbf{x}'\, \mathcal{A}'_j \frac{\delta}{\delta f'_j} \right) \mathcal{F}\, \mathrm{d}t + \sum_{j=1}^{C}\sum_{k=1}^{C}\sum_{l=1}^{L} \int \mathrm{d}\mathbf{x}'\, \mathcal{B}'_{jl} \mathcal{B}'^*_{kl} \frac{\delta}{\delta f'_j} \frac{\delta}{\delta f'^*_k} \mathcal{F}\, \mathrm{d}t \\
& + 2\sum_{j=1}^{C}\sum_{l=1}^{L} \mathrm{Re}\left( \int \mathrm{d}\mathbf{x}'\, \mathcal{B}'_{jl} \mathrm{d}Q'_l \frac{\delta}{\delta f'_j} \right) \mathcal{F},
\end{aligned} \tag{C.49}$$

which leads to the statement of the theorem. □

Alternatively, the functional Itô formula can be written in a matrix form as

$$\begin{aligned} \mathrm{d}\mathcal{F}[\mathbf{f}] = \int \mathrm{d}\mathbf{x}' \Big( & 2\,\mathrm{Re}\,(\boldsymbol{\mathcal{A}}' \cdot \boldsymbol{\delta}_{\boldsymbol{\Psi}'})\,\mathcal{F}[\mathbf{f}]\mathrm{d}t + \mathrm{Tr}\left\{\mathcal{B}'(\mathcal{B}')^H \boldsymbol{\delta}_{\mathbf{f}'^*}\boldsymbol{\delta}_{\mathbf{f}'}^T\right\}\mathcal{F}[\mathbf{f}]\mathrm{d}t \\ & + 2\,\mathrm{Re}\,\mathrm{Tr}\left\{\mathcal{B}'\mathrm{d}\mathbf{Q}'\boldsymbol{\delta}_{\mathbf{f}'}^T\right\}\mathcal{F}[\mathbf{f}]\Big)\,. \end{aligned} \tag{C.50}$$

# Appendix D.

# Basis sets

While it is possible to apply the central theorems from this thesis to many different basis sets satisfying the orthonormality and completeness conditions (B.1), other factors restrict the choice in practical applications. Ideally, one would want the following to be true:

- the basis modes are natural to the physical problem in question (e.g., plain waves for a freely expanding BEC);
- decomposition of a function defined on a discrete spatial grid in the basis is computationally effective; and
- the generalised periodicity condition from Lemma B.4 applies.

For the applications discussed in this thesis, the first condition is the hardest to satisfy since the equations we use are nonlinear, which makes ground and excited states of the system inexpressible algebraically (with some exceptions, e.g. when the nonlinearity is negligible). The advantage of this condition being satisfied is that fewer modes will be required to describe the dynamics of a system, thus making it easier to satisfy the Wigner truncation condition (see Section 5.4 for details).

Taking this into account, we have settled on two basis sets to use in the calculations. The plane wave basis was used as the primary one, and the harmonic oscillator basis was used as the backup. In practice, the latter was not very useful for the simulations considered in this thesis since it required roughly the same number of modes as the plane wave basis, and was more difficult to work with from the computational point of view. Nevertheless, we are including its description in this Appendix as it may still be useful for different (e.g. one-dimensional) systems.

## D.1. Plane wave basis

The plane wave basis consists of eigenfunctions of the kinetic term of a Hamiltonian:

$$\left(-\frac{\hbar^2}{2m}\nabla^2\right)\phi_{\mathbf{n}} = E_{\mathbf{n}}\phi_{\mathbf{n}}. \tag{D.1}$$

The eigenfunctions are defined in a $D$-dimensional box with the shape $(L_1, \dots, L_D)$ with $\prod_{d=1}^{D} L_d \equiv V$ (which corresponds to the integration area $A$ introduced in Appendix B):

$$\phi_{\mathbf{n}}(\mathbf{x}) = e^{i\mathbf{k}_{\mathbf{n}}\mathbf{x}}/\sqrt{V}, \tag{D.2}$$

and have the corresponding eigenvalues (energies)

$$E_{\mathbf{n}} = \frac{\hbar^2|\mathbf{k}_{\mathbf{n}}|^2}{2m}. \tag{D.3}$$

Because of the periodic boundary conditions at the edges of the box, possible values of the components of the spatial frequency vector $\mathbf{k}$ are

$$(\mathbf{k}_{\mathbf{n}})_d = \frac{2\pi n_d}{L_d}. \tag{D.4}$$

This basis set is the most computationally effective. Functions defined on the discrete grid $x_d = 0, h, \dots, L_d - h$ (the step $d = L_d/M_d$, where $M_d$ is the number of modes in the dimension $d$) can be decomposed into this basis using the Fast Fourier transform (FFT), which is available for a wide range of platforms and programming languages, and has the asymptotical complexity $\mathcal{O}(M \log_2 M)$ (where the total number of modes $M = \prod_{d=1}^{D} M_d$).

While this basis is far from being natural for a harmonically confined BEC with nonlinear interactions, its effectiveness overweighs all the disadvantages; plane wave modes can be viewed as pixels for the mode space.

## D.2. Harmonic oscillator basis

It often happens that, for a pseudo-1D BEC, the confinement in transverse dimensions is strong enough to make the nonlinear interaction negligible. In these cases, it can

be advantageous to use the harmonic oscillator basis for these dimensions despite its computational drawbacks.

The harmonic basis consists of eigenfunctions of the kinetic and potential terms of a Hamiltonian:

$$\left(-\frac{\hbar^2}{2m}\nabla^2 + \frac{m\sum_{d=1}^{D}\omega_d^2 x_d^2}{2}\right)\phi_{\mathbf{n}} = E_{\mathbf{n}}\phi_{\mathbf{n}}. \tag{D.5}$$

The eigenfunctions are

$$\phi_{\mathbf{n}} = \prod_{d=1}^{D}\phi_{n_d}^{(d)}(x_d) = \prod_{d=1}^{D}\frac{1}{\sqrt{2^{n_d}n_d!\,l_d\sqrt[4]{\pi}}}H_{n_d}\left(\frac{x_d}{l_d}\right)\exp\left(-\frac{x_d^2}{2l_d^2}\right), \tag{D.6}$$

where $H_{n_d}$ is the "physicists' " Hermite polynomial of order $n_d$, and $l_d = \sqrt{\hbar/(m\omega_d)}$ is the characteristic length. The corresponding eigenvalues are

$$E_{\mathbf{n}} = \hbar\sum_{d=1}^{D}\omega_d(n_d + \frac{1}{2}). \tag{D.7}$$

Decomposition into this basis is less computationally effective than FFT in terms of speed, memory, and even precision (due to extremely large range of weight coefficients needed for the decomposition). There are even some restrictions on the function being transformed. The next section describes the algorithm and these restrictions in detail.

## D.3. Discrete harmonic transformation

The numerical algorithm for the decomposition of a function defined on a discrete grid in the harmonic basis [133] is much less known than the FFT and has some unusual properties, so it is worth describing in brief.

Given some function $f(\mathbf{x})$, one can expand it into the harmonic oscillator basis as

$$\alpha_{\mathbf{n}} = (\mathcal{C}^{-1}[f])_{\mathbf{n}} \equiv \int f(x)\phi_{\mathbf{n}}^*(\mathbf{x})\mathrm{d}\mathbf{x}, \tag{D.8}$$

where we have used the terminology from Appendix B. The corresponding backward

transformation is

$$f(\mathbf{x}) = \mathcal{C}[f](\boldsymbol{\alpha}) \equiv \sum_{\mathbf{n}\in\mathbb{B}} \alpha_{\mathbf{n}}\phi_{\mathbf{n}}(\mathbf{x}). \tag{D.9}$$

In general, when we do not know anything about $f(\mathbf{x})$, and only have its value sampled at some set of points, the value of the integral can be calculated only approximately. However, we can obtain exact results for functions of a certain kind if we are allowed to choose the sampling points.

The method is based on the Gauss-Hermite quadrature [134], which states that the value of a Gaussian weighted integral can be approximated as a weighted sum:

$$\int_{-\infty}^{\infty} g(x)e^{-x^2}\mathrm{d}x = \sum_{i=1}^{N} w_i g(r_i) + E, \tag{D.10}$$

where $N$ is the number of sample points. The weights $w_i$ are calculated as

$$w_i = \frac{2^{N-1}N!\sqrt{\pi}}{N^2(H_{N-1}(r_i))^2}, \tag{D.11}$$

and the sample points $r_i$ are the roots of the Hermite polynomial $H_N$. The error term is

$$E = \frac{N!\sqrt{\pi}}{2^N(2N)!}g^{(2N)}(\xi). \tag{D.12}$$

Therefore if $g(x)$ is a polynomial of order $Q$, one can eliminate the error term by choosing $N$ so that $2N \geq Q + 1$, thus making the quadrature exact.

In practical applications, we are dealing with restricted bases. Without loss of generality, we can consider a restricted basis to be consisting of the first several low-energy modes. If the modes are actually sparse, it will only reduce the effectiveness of the method because we can always assume that we are dealing with sequential modes up to the maximum one and then drop all the superfluous components from the result.

### D.3.1. One-dimensional case

Let us consider a one-dimensional case first, with a function $\Psi(x) \in \mathbb{F}_{\mathbb{M}}$, where $|\mathbb{M}| = M$. We want to find the population of the first $M'$ modes for the decomposition of $f(x) = \Psi^s(x)$, where $s$ is a natural number (note that, despite the original function $\Psi$

having non-zero population only in a finite number of modes, $\Psi^s$ may, in general, have an infinite number of modes in its decomposition). This means that we need to calculate

$$\alpha_m = \int \Psi^s(x)\phi_m^*(x)\mathrm{d}x. \tag{D.13}$$

By definition of the mode functions (D.6),

$$\Psi^s(x)\phi_m^*(x) = P(x/l_x)\exp\left(-\frac{(s+1)x^2}{2l_x^2}\right), \tag{D.14}$$

where $P(x)$ is a polynomial of order less than or equal to $(M-1)s+m$. Since we want to have the same set of sample points for any $m \in [0, M'-1]$, we will consider the worst case $m = M'-1$, which makes the order of $P(x)$ limited by $(M-1)s+M'-1$. Changing variables in the integral to make it comply to the form (D.10) and applying the quadrature, we get:

$$\begin{aligned}\alpha_m &= \int P(x/l_x)\exp\left(-\frac{(s+1)x^2}{2l_x^2}\right)dx \\ &= l_x\sqrt{\frac{2}{s+1}}\int P\left(y\sqrt{\frac{2}{s+1}}\right)e^{-y^2}dy \\ &= l_x\sqrt{\frac{2}{s+1}}\sum_{i=1}^{N} w_i P\left(r_i\sqrt{\frac{2}{s+1}}\right),\end{aligned} \tag{D.15}$$

where the number of sampling points necessary to make the quadrature exact is determined by the order of $P(x)$:

$$N \geq \frac{(M-1)s+M'}{2}. \tag{D.16}$$

Replacing $P$ with $\Psi$ and $\phi$ using (D.14):

$$\begin{aligned}\alpha_m &= l_x\sqrt{\frac{2}{s+1}}\sum_{i=1}^{N} w_i\Psi^s\left(l_x r_i\sqrt{\frac{2}{s+1}}\right)\phi_m^*\left(l_x r_i\sqrt{\frac{2}{s+1}}\right)\exp(r_i^2) \\ &= \sum_{i=1}^{N}\tilde{w}_i\phi_m(\tilde{x}_i)f(\tilde{x}_i),\end{aligned} \tag{D.17}$$

where the modified sampling points are

$$\tilde{x}_i = l_x r_i \sqrt{\frac{2}{s+1}}, \tag{D.18}$$

and the modified weights are

$$\tilde{w}_i = w_i l_x \sqrt{\frac{2}{s+1}} \exp(r_i^2). \tag{D.19}$$

Since we usually need the population of all modes at once, it is more convenient to use the matrix form of the discrete harmonic transformation (DHT):

$$\boldsymbol{\alpha} = G(\mathbf{f}) \equiv \Phi^T \operatorname{diag}(\tilde{\mathbf{w}})\mathbf{f} \equiv \Phi^T(\tilde{\mathbf{w}} \circ \mathbf{f}), \tag{D.20}$$

where $\Phi_{im} = \phi_m(\tilde{x}_i)$ is an $N \times M'$ matrix, $\tilde{\mathbf{w}}$ is an $N$-vector of elements $\tilde{w}_i$, $\mathbf{f}$ is an $N$-vector of elements $f(\tilde{x}_i)$, and the symbol $\circ$ stands for the Hadamard (element wise) product. The corresponding backward transformation is then expressed as

$$\mathbf{f} = G^{-1}(\boldsymbol{\alpha}) \equiv \Phi\boldsymbol{\alpha}. \tag{D.21}$$

There are a few catches in the practical implementation of this algorithm. First, there can be significant round-off errors during the expansion for the large $N$ due to the exponential term in the expression for weights (D.19). Second, note that $G^{-1}(G(\mathbf{f})) \neq \mathbf{f}$ for $s > 1$, since during the expansion we are effectively discarding the higher-order modes of $\Psi^s$ and are thus losing some information. For $s = 1$ and $M' \geq M$ though the transformation is reversible.

Lastly, since the known order $s$ is hard-coded into the algorithm, including the values of the sampling points, one has to transform different orders of the known function from $\mathbb{F}_{\mathbb{M}}$ separately. This is a usual case when the DHT is used to solve a nonlinear Schrödinger equation in momentum space. For a concrete example, consider an equation

$$i\hbar\frac{\mathrm{d}\Psi}{\mathrm{d}t} = -\frac{\hbar^2}{2m}\nabla^2\Psi + \frac{m\omega^2x^2}{2}\Psi + g\Psi|\Psi|^2 - i\gamma\Psi|\Psi|^4. \tag{D.22}$$

If this equation is propagated in momentum space, the last two terms have to be transformed using different transformations because the first one has the order $s = 3$, and the

second one has the order $s = 5$:

$$i\hbar\frac{\mathrm{d}\boldsymbol{\alpha}}{\mathrm{d}t} = \mathbf{E}\cdot\boldsymbol{\alpha} + gG_{s=3}(G^{-1}_{s=3}(\boldsymbol{\alpha})|G^{-1}_{s=3}(\boldsymbol{\alpha})|^2) - i\gamma G_{s=5}(G^{-1}_{s=5}(\boldsymbol{\alpha})|G^{-1}_{s=5}(\boldsymbol{\alpha})|^4). \quad \text{(D.23)}$$

### D.3.2. Multi-dimensional case

The DHT can be easily generalized to operate in several dimensions. Basically, we need to apply the 1D transformation for each dimension successively. If $F_{ij\ldots} = f(\tilde{x}^{(1)}_i, \tilde{x}^{(2)}_j, \ldots)$ is a $D$-dimensional matrix of shape $N_1 \times N_2 \times \ldots \times N_D$ consisting of samples of $f$ taken on the discrete grid

$$\tilde{x}^{(d)}_i = l^{(d)}_x r^{(d)}_i \sqrt{\frac{2}{s+1}}, \quad \text{(D.24)}$$

then for every dimension $d$ we want to perform the transformation, we need to:

- perform the multidimensional transposition $F' = T_{1\leftrightarrow d}[F]$, which changes the shape of $F$ to $N_d \times N_2 \times \ldots \times N_1 \times \ldots \times N_D$ (i.e., makes the $d$-th dimension major);
- calculate the dot product $C' = (\Phi^{(d)})^T \operatorname{diag}(\tilde{\mathbf{w}}^{(d)})F'$, where $\Phi^{(d)}_{im} = \phi^{(d)}_m(\tilde{x}^{(d)}_i)$ is an $N_d \times M'_d$ matrix, $\tilde{\mathbf{w}}^{(d)}$ is an $N_d$-vector of weights

  $$\tilde{w}^{(d)}_i = w^{(d)}_i l^{(d)}_x \sqrt{\frac{2}{s+1}} \exp((r^{(d)}_i)^2), \quad \text{(D.25)}$$

  and $F'$ is treated as a 2-dimensional matrix of shape $N_d \times N_2 \ldots N_1 \ldots N_D$;
- perform the backward transposition $C = T_{1\leftrightarrow d}[C']$.

In a single expression, it is a composition of two transpositions and one dot product:

$$G_d \equiv T_{1\leftrightarrow d}((\Phi^{(d)})^T \operatorname{diag}(\tilde{\mathbf{w}}^{(d)})\cdot)T_{1\leftrightarrow d}, \quad \text{(D.26)}$$

with backward transformation

$$G^{-1}_d \equiv T_{1\leftrightarrow d}(\Phi^{(d)}\cdot)T_{1\leftrightarrow d}, \quad \text{(D.27)}$$

These 1D transformations can be applied in an arbitrary order for all the required dimensions.

# Appendix E.

# Numerical methods

This Appendix outlines the approach to numerical simulations performed for this thesis. While full texts of the programs used are too long to include verbatim in the text, the main choices made will be described here.

## E.1. Parallel calculations

The phase space methods described in this thesis are inherently parallel. Such algorithms are suitable to run on modern graphical processing units (GPUs), as long as the data being processed fits the video memory (which was our case). We chose nVidia's CUDA as the general purpose GPU (GPGPU) platform because of its maturity and the included set of libraries with effective implementations of the FFT, random number generators, and other useful algorithms. In practice, OpenCL could be used as well: at the moment it is just as fast as CUDA on nVidia video cards, and has an additional benefit of supporting AMD cards.

Furthermore, in order to speed up prototyping we did not use the CUDA language itself (which is, essentially, a superset of C++), but Python bindings to it. Python is a general-purpose dynamically typed language with a rich set of third-party libraries. It is quite popular in the academic community owing to the excellent NumPy and SciPy packages [135], which provide an extensive toolset for numerical calculations. PyCUDA [136] augments it with a convenient access to CUDA and its libraries, significantly reducing the amount of boilerplate code and making metaprogramming possible. Of course, the dynamical facilities of Python make it slower than C++, but this was negligible in our

simulations since the majority of calculations was done on GPU, and the Python language overhead was masked by their asynchronous execution.

The use of GPU hardware allowed us to reach a hundredfold speedup of calculations on a single nVidia Tesla C2050 as compared to MatLab implementations. This was improved even further by combining the results calculated on several video cards, such as we did for the calculations in Section 9.2, where we used seven nVidia Tesla M2090.

## E.2. XMDS

For cases where the raw speed of calculations was less important, and a custom GPGPU program was not required, we used the XMDS package [137, 138]. XMDS is a code generator for numerical simulation problems, written in Python. It creates and compiles a C++ program that performs the integration, based on a brief XML description of the simulation problem. The strength of XMDS lies in highly optimized integration algorithms it uses (which is improved even more by on-demand compilation), and in its transparent usage of multi-processor interface (MPI), which allows it to take advantage of multiple cores of a CPU, or multiple nodes in a cluster. We used XMDS to integrate the SDEs in Chapter 6.

## E.3. Stochastic integration

The problem of integrating SDEs is well-studied; for some general information, one can refer to a book by Kloeden and Platen [139], or to extensive reviews by Drummond and Mortimer [140], and by Werner and Drummond [141].

Convergence properties of stochastic integration algorithms may depend on the equation being integrated, so we tested several widely used algorithms with our target system. The first one is the semi-implicit central difference method (CD) [141], which is robust and simple to implement. We tried it both in its general form, and in the interaction picture (denoted CDIP in the figures below), which is commonly referred to as "split-step". Unfortunately, CD and CDIP have only second order convergence in time.

The methods from the Runge-Kutta family can be applied without changes to a set of SDEs in the Stratonovich form [142, 143] and are able to achieve higher orders of convergence for the deterministic part of the equations. It is even possible to employ

variable-stepsize methods, which are strongly convergent, provided that stochastic differentials on the subintervals are sampled correctly [143]. Since our target problems have relatively uniform characteristic time over the whole range of interest, there was no particular need in variable stepsize methods. We have implemented two fixed stepsize RK methods: the RK4 interaction picture method (RK4IP) [144], and a low dissipation, low dispersion and low storage RK46NL method [145], which both have fourth order convergence in the drift part.

As Burrage *et al* correctly point out in their comment [146], the major drawback of RK methods when applied to SDEs is that convergence for the stochastic part for these methods is, in general, only of the first order. Nevertheless, when the evolution is dominated by the deterministic part, as in our case, high order methods can still demonstrate maximum achievable overall convergence for a certain range of time steps. This means that while asymptotically CD and CDIP methods may perform better, a satisfactory accuracy can be achieved with RK4IP and RK46NL using a much lower number of time steps.

To test that we have applied the four methods described above to a typical simulation problem from Chapter 7, the Ramsey interferometry sequence, with the parameters described in Section 7.4. This includes nonlinear elastic interactions and three sources of nonlinear losses (and corresponding noises in the stochastic part of SDEs). The test consisted of integrating the equations used to plot Fig. 7.4 for a shorter time $t_e = 0.1$ s.

The convergence was estimated as the relative difference in a quantity of interest between the reference results obtained with $S$ time steps, and auxiliary results obtained with $S/2$ time steps. We initialized the random number generator with the same seed for all tests and sampled the noise for the auxiliary integration as two sequential noises, so the total noise for two steps of the reference integration was exactly the same as the noise for a single step of the auxiliary integration. This allowed us to test strong convergence in addition to weak convergence (i.e., convergence of a quantity averaged over simulation trajectories). In addition, we always started from the same noises in the initial state for all tests, so all the tests which had the same number of steps used exactly the same noises.

The quantities used to estimate convergence are:

- The "full" error $E_{\boldsymbol{\Psi}} = \|\boldsymbol{\Psi}^S(t_e) - \boldsymbol{\Psi}^{S/2}(t_e)\|_2 / \|\boldsymbol{\Psi}^S(t_e)\|_2$, where $\|\ldots\|_2$ is the 2-norm, and $\boldsymbol{\Psi}^S(t)$ is the full solution vector at time $t$ for the total number of steps $S$,

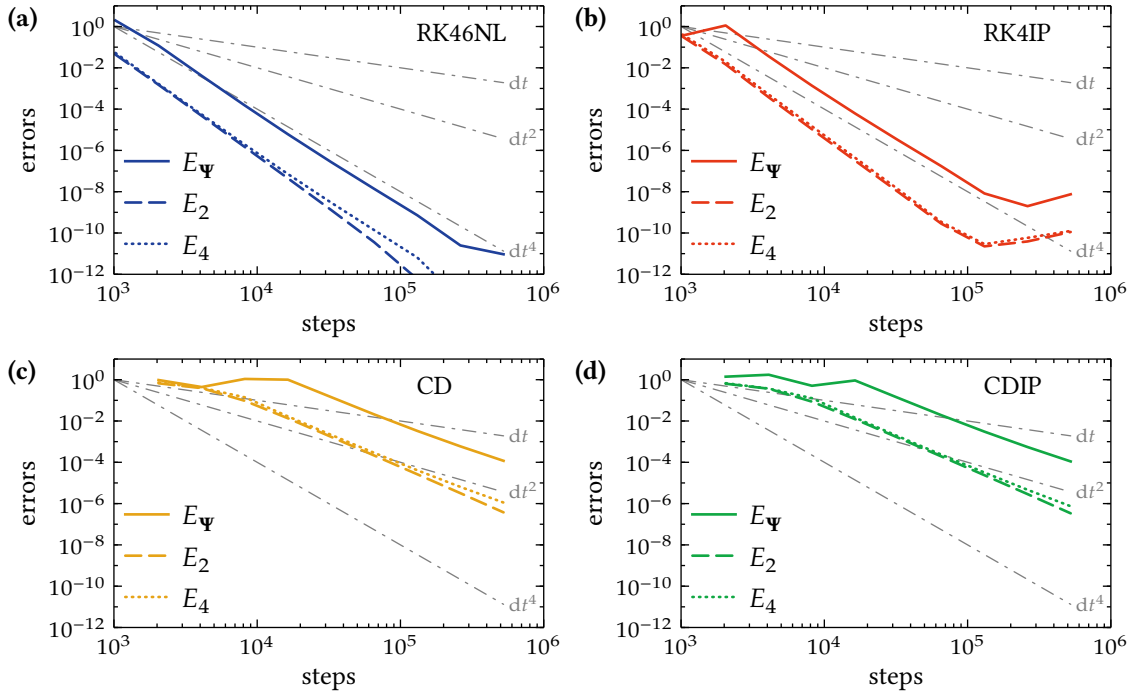


FIGURE E.1.: Convergence tests for classical CGPEs with **(a)** RK46NL, **(b)** RK4IP, **(c)** CD and **(d)** CDIP integration algorithms. The plots show full errors $E_\Psi$ (solid lines), errors for a second order correlation $E_2$ (dashed lines), and errors for a fourth order correlation $E_4$ (dotted lines). Slopes corresponding to first, second and fourth order convergence are given for reference (dash-dotted grey lines).

consisting of solution vectors for all trajectories. This quantity was used to estimate the strong convergence.

- The error in the total population $E_2 = |N^S(t_e) - N^{S/2}(t_e)|/|N^S(t_e)|$, where $N = \langle \tilde{\Psi}_1^\dagger \tilde{\Psi}_1 + \tilde{\Psi}_2^\dagger \tilde{\Psi}_2 \rangle$ is a second order correlation. The total population $N$ is averaged over trajectories and therefore the behavior of its error corresponds to the weak convergence.

- The error in the square of the $z$-component of the total spin operator $E_4 = |Z^S(t_e) - Z^{S/2}(t_e)|/|Z^S(t_e)|$, where $Z = \langle \hat{S}_z^2 \rangle$ is a fourth order correlation (8.12).

To check the order of convergence in the deterministic part only, we executed our tests for the classical CGPEs (7.7). The results are plotted in Fig. E.1, with $\mathrm{d}t$, $\mathrm{d}t^2$ and $\mathrm{d}t^4$ lines given for reference. It is evident that RK4IP and RK46NL have fourth order convergence, while CD and CDIP have only second order, as expected.

The tests for the Wigner representation SDEs (7.28), plotted in Fig. E.2, which include stochastic terms, show a different picture. The RK algorithms behave as fourth order

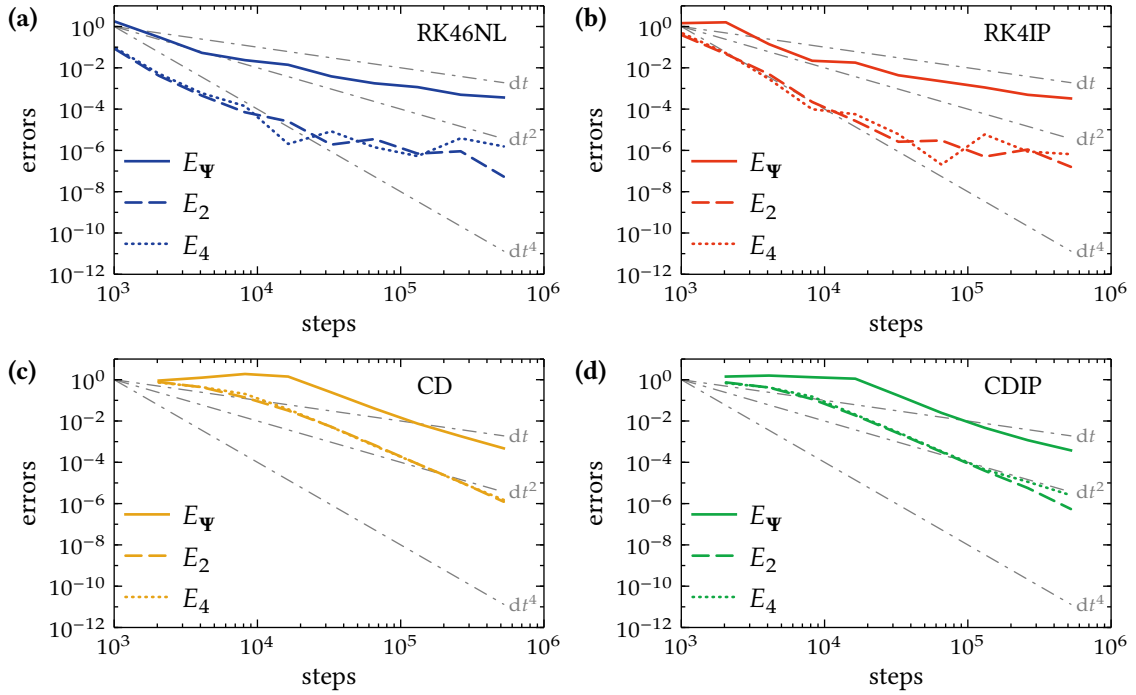


FIGURE E.2.: Convergence tests for the Wigner representation SDEs, 64 trajectories. The meaning of the lines is the same as in Fig. E.1.

ones for larger time steps, and then deteriorate to the first order. On the other hand, the CD algorithms show steady second order behavior for all time steps. This is in agreement with the Burrage *et al* predictions.

While the CD algorithms clearly outperform the RK ones on the infinity, we do not need much accuracy in the simulations from Chapter 7 and Chapter 8, as the errors in the experimental results are quite large. It is enough to have $10^{-3} - 10^{-4}$ relative weak convergence in the quantities of interest for integration times of the order of $t = 1\,\mathrm{s}$, which approximately corresponds to the range $10^{-4} - 10^{-5}$ in our tests (which were only executed for 0.1 s).

In order to compare the methods, we have plotted errors in the total population as a function of time spent for integration in Fig. E.3, with the target accuracy area marked with the grey band. It is apparent that the RK methods achieve the target accuracy about one order of magnitude faster than the CD methods. That is why for our simulations we decided to pick one of the RK algorithms.

Since the problem is not stiff (notice that CD and CDIP show almost identical results in Fig. E.1 and Fig. E.2), the RK4IP method does not have much advantage over RK46NL, while the latter has a low-storage property, which means that in each substep of the RK

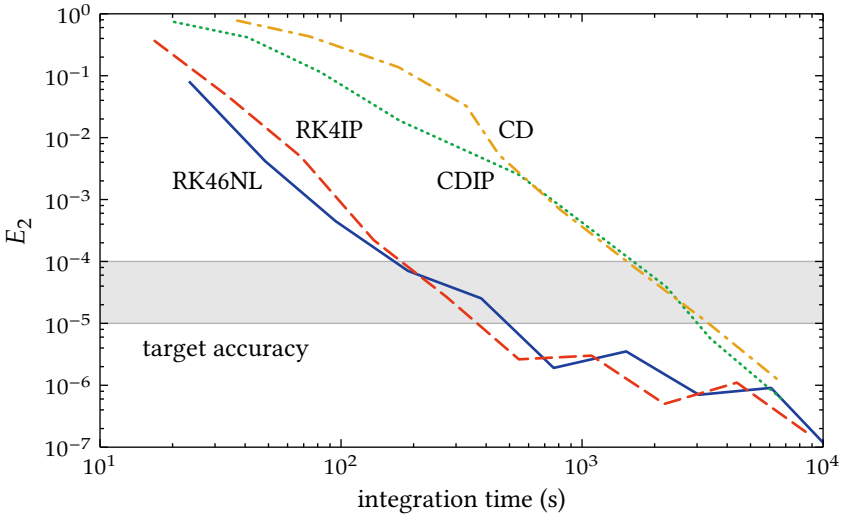


Figure E.3.: Comparison of the weak error in total population $E_2$ for RK46NL (blue solid line), RK4IP (red dashed line), CD (yellow dash-dotted line) and CDIP (green dotted line). The errors are plotted against the time taken by the corresponding integration algorithm to achieve them. The approximate target range of errors is shown as the grey band.

propagation the result depends only on the output of the previous step. It is quite important in the GPGPU world, where one has to keep whole arrays of intermediate results in video memory. Finally, the RK46NL algorithm was picked and used for simulations in this thesis.

The number of time steps for each simulation in this thesis was chosen so that the total error in plotted quantities was indistinguishable in the plots (quantitatively, this corresponds to a relative error of at most $10^{-3}$, estimated using auxiliary integration with a halved number of time steps, as described above). Consequently, in the body of the thesis the time convergence errors are omitted in figures for clarity.

## E.4. Software developed for this thesis

In the process of writing this thesis we have created several libraries used by our simulation programs. While usefulness of these libraries may decrease with time quickly (in case we choose not to maintain them), and many of the sources are not very well documented, we still feel that it is necessary to reference them here.

The programs used to obtain and process the numerical results in this thesis can be found in the Git repository github.com/Manticore/thesis, along with the sources of the thesis itself. This includes both Python programs and several XMDS scripts used in

Chapter 6.

The processing code for the XMDS scripts was generated by a symbolic calculation library github.com/Manticore/wigner, written in Haskell. This library is able to perform the Wigner transformation of arbitrary operator expressions (including the ones with field operators) and conversions between normally and symmetrically ordered operator products. In addition to Chapter 6, it was used to test the theorems from Chapter 4 and also in several other places in the thesis where ordering conversions of complex operator expressions were needed.

To obtain the results in Chapter 7 and Chapter 8 we created github.com/Manticore/beclab, a framework in Python and CUDA for simulating the dynamics of trapped BECs. The low-level part of this library later gave rise to github.com/Manticore/reikna, a code generator for GPGPU algorithms written in Python, which can work both with CUDA and OpenCL.

# Bibliography


[1] K. Sakmann, A. I. Streltsov, O. E. Alon, and L. S. Cederbaum, *Exact Quantum Dynamics of a Bosonic Josephson Junction*, Phys. Rev. Lett. **103**, 220601 (2009). [p 1]

[2] M. H. Anderson, J. R. Ensher, M. R. Matthews, C. E. Wieman, and E. A. Cornell, *Observation of bose-einstein condensation in a dilute atomic vapor.*, Science **269**, 198 (1995). [p 1]

[3] K. Davis *et al.*, *Bose-Einstein Condensation in a Gas of Sodium Atoms*, Phys. Rev. Lett. **75**, 3969 (1995). [p 1]

[4] S. N. Bose, *Plancks Gesetz und Lichtquantenhypothese*, Z. Phys. **26**, 178 (1924). [p 1]

[5] A. Einstein, *Quantentheorie des einatomigen idealen Gases*, Sitzber. Preuss. Akad. **1**, 261 (1924). [p 1]

[6] A. Einstein, *Quantentheorie des einatomigen idealen Gases. Zweite Abhandlung.*, Sitzber. Preuss. Akad. **1**, 3 (1925). [p 1]

[7] R. P. Feynman, *Simulating physics with computers*, Int. J. Theor. Phys. **21**, 467 (1982). [pp 2, 3, and 101]

[8] B. P. Lanyon *et al.*, *Universal digital quantum simulation with trapped ions.*, Science **334**, 57 (2011). [pp 2 and 115]

[9] N. Xu *et al.*, *Quantum Factorization of 143 on a Dipolar-Coupling Nuclear Magnetic Resonance System*, Phys. Rev. Lett. **108**, 130501 (2012). [p 2]

[10] E. P. Wigner, *On the Quantum Correction For Thermodynamic Equilibrium*, Phys. Rev. **40**, 749 (1932). [pp 2 and 7]

[11] P. A. M. Dirac, *On the Analogy Between Classical and Quantum Mechanics*, Rev. Mod. Phys. **17**, 195 (1945). [pp 2 and 7]

[12] J. E. Moyal, *Quantum mechanics as a statistical theory*, Math. Proc. Cambridge **45**, 99 (1947). [pp 2 and 7]

[13] K. Husimi, *Some Formal Properties of the Density Matrix*, Proc. Phys. Math. Soc. Jpn. **22**, 264 (1940). [pp 2, 101, and 111]

[14] E. Sudarshan, *Equivalence of Semiclassical and Quantum Mechanical Descriptions of Statistical Light Beams*, Phys. Rev. Lett. **10**, 277 (1963). [p 2]

[15] R. Glauber, *Photon Correlations*, Phys. Rev. Lett. **10**, 84 (1963). [p 2]

[16] R. Glauber, *Coherent and Incoherent States of the Radiation Field*, Phys. Rev. **131**, 2766 (1963). [p 2]

[17] P. D. Drummond and C. W. Gardiner, *Generalised P-representations in quantum optics*, J. Phys. A: Math. Gen. **13**, 2353 (1980). [pp 3, 101, 104, and 110]

[18] P. D. Drummond, C. W. Gardiner, and D. F. Walls, *Quasiprobability methods for nonlinear chemical and optical systems*, Phys. Rev. A **24**, 914 (1981). [p 3]

[19] J. S. Bell, *On the Einstein-Podolsky-Rosen paradox*, Physics **1**, 195 (1964). [pp 3, 101, and 102]

[20] B. Opanchuk, M. D. Reid, L. E. C. Rosales-Zárate, and P. D. Drummond, *Probabilistic simulation of mesoscopic quantum paradoxes*, arXiv:1301.6305 (2013). [p 3]

[21] P. D. Drummond, B. Opanchuk, L. E. C. Rosales-Zárate, and M. D. Reid, *Simulating Bell violations without quantum computers*, arXiv:1310.0668 (2013). [p 3]

[22] P. P. Deuar and P. D. Drummond, *Gauge P representations for quantum-dynamical problems: Removal of boundary terms*, Phys. Rev. A **66**, 033812 (2002). [pp 3 and 119]

[23] Y. Li, Y. Castin, and A. Sinatra, *Optimum Spin Squeezing in Bose-Einstein Condensates with Particle Losses*, Phys. Rev. Lett. **100**, 210401 (2008). [p 3]

[24] Y. Li, P. Treutlein, J. Reichel, and A. Sinatra, *Spin squeezing in a bimodal condensate: spatial dynamics and particle losses*, Eur. Phys. J. B **68**, 365 (2009). [pp 3, 90, and 94]

[25] A. Sinatra, E. Witkowska, J.-C. Dornstetter, Y. Li, and Y. Castin, *Limit of Spin Squeezing in Finite-Temperature Bose-Einstein Condensates*, Phys. Rev. Lett. **107**, 060404 (2011). [p 3]

[26] A. A. Norrie, R. J. Ballagh, and C. W. Gardiner, *Quantum Turbulence in Condensate Collisions: An Application of the Classical Field Method*, Phys. Rev. Lett. **94**, 040401 (2005). [pp 3 and 4]

[27] P. P. Deuar and P. D. Drummond, *Correlations in a BEC Collision: First-Principles Quantum Dynamics with 150 000 Atoms*, Phys. Rev. Lett. **98**, 120402 (2007). [pp 3, 4, 47, and 115]

[28] P. D. Drummond and A. D. Hardman, *Simulation of Quantum Effects in Raman-Active Waveguides*, Europhys. Lett. **21**, 279 (1993). [pp 4, 45, 47, 64, and 114]

[29] P. D. Drummond, R. M. Shelby, S. R. Friberg, and Y. Yamamoto, *Quantum solitons in optical fibres*, Nature **365**, 307 (1993). [pp 4, 99, and 115]

[30] J. F. Corney *et al.*, *Many-Body Quantum Dynamics of Polarization Squeezing in Optical Fibers*, Phys. Rev. Lett. **97**, 023606 (2006). [pp 4 and 114]

[31] J. F. Corney *et al.*, *Simulations and experiments on polarization squeezing in optical fiber*, Phys. Rev. A **78**, 023831 (2008). [pp 4 and 114]

[32] L. Isella and J. Ruostekoski, *Nonadiabatic dynamics of a Bose-Einstein condensate in an optical lattice*, Phys. Rev. A **72**, 011601 (2005). [p 4]

[33] L. Isella and J. Ruostekoski, *Quantum dynamics in splitting a harmonically trapped Bose-Einstein condensate by an optical lattice: Truncated Wigner approximation*, Phys. Rev. A **74**, 063625 (2006). [pp 4 and 118]

[34] C. Gross, J. Estève, M. K. Oberthaler, A. D. Martin, and J. Ruostekoski, *Local and spatially extended sub-Poisson atom-number fluctuations in optical lattices*, Phys. Rev. A **84**, 011609 (2011). [p 4]

[35] J. Ruostekoski and L. Isella, *Dissipative Quantum Dynamics of Bosonic Atoms in a Shallow 1D Optical Lattice*, Phys. Rev. Lett. **95**, 110403 (2005). [pp 4, 46, and 118]

[36] U. Shrestha, J. Javanainen, and J. Ruostekoski, *Quantum dynamics of instability-induced pulsations of a Bose-Einstein condensate in an optical lattice*, Phys. Rev. A **79**, 043617 (2009). [p 4]

[37] A. D. Martin and J. Ruostekoski, *Quantum and Thermal Effects of Dark Solitons in a One-Dimensional Bose Gas*, Phys. Rev. Lett. **104**, 194102 (2010). [p 4]

[38] A. D. Martin and J. Ruostekoski, *Nonequilibrium quantum dynamics of atomic dark solitons*, New J. Phys. **12**, 055018 (2010). [p 4]

[39] A. A. Norrie, R. J. Ballagh, and C. W. Gardiner, *Quantum turbulence and correlations in Bose-Einstein condensate collisions*, Phys. Rev. A **73**, 043617 (2006). [pp 4, 46, 85, and 94]

[40] M. Steel *et al.*, *Dynamical quantum noise in trapped Bose-Einstein condensates*, Phys. Rev. A **58**, 4824 (1998). [pp 4 and 118]

[41] A. A. Norrie, R. J. Ballagh, C. W. Gardiner, and A. S. Bradley, *Three-body recombination of ultracold Bose gases using the truncated Wigner method*, Phys. Rev. A **73**, 043618 (2006). [pp 4, 54, and 55]

[42] M. Egorov *et al.*, *Long-lived periodic revivals of coherence in an interacting Bose-Einstein condensate*, Phys. Rev. A **84**, 021605(R) (2011). [pp 4, 66, 75, 77, 78, 81, 85, and 87]

[43] B. Opanchuk, M. Egorov, S. E. Hoffmann, A. I. Sidorov, and P. D. Drummond, *Quantum noise in three-dimensional BEC interferometry*, Europhys. Lett. **97**, 50003 (2012). [p 4]

[44] B. Opanchuk, Q.-Y. He, M. D. Reid, and P. D. Drummond, *Dynamical preparation of Einstein-Podolsky-Rosen entanglement in two-well Bose-Einstein condensates*, Phys. Rev. A **86**, 023625 (2012). [pp 4, 59, 60, 61, 62, and 64]

[45] S. J. Carter, P. D. Drummond, M. D. Reid, and R. M. Shelby, *Squeezing of quantum solitons*, Phys. Rev. Lett. **58**, 1841 (1987). [pp 4, 99, and 114]

[46] S. E. Hoffmann, J. F. Corney, and P. D. Drummond, *Hybrid phase-space simulation method for interacting Bose fields*, Phys. Rev. A **78**, 013622 (2008). [p 4]

[47] S. Chaturvedi, K. Dechoum, and P. D. Drummond, *Limits to squeezing in the degenerate optical parametric oscillator*, Phys. Rev. A **65**, 033805 (2002). [pp 4 and 64]

[48] K. Dechoum, P. D. Drummond, S. Chaturvedi, and M. D. Reid, *Critical fluctuations and entanglement in the nondegenerate parametric oscillator*, Phys. Rev. A **70**, 53807 (2004). [pp 4 and 64]

[49] P. D. Drummond and P. Kinsler, *Quantum tunneling and thermal activation in the parametric oscillator*, Phys. Rev. A **40**, 4813 (1989). [p 4]

[50] P. Kinsler and P. D. Drummond, *Quantum dynamics of the parametric oscillator*, Phys. Rev. A **43**, 6194 (1991). [p 4]

[51] Q.-Y. He *et al.*, *Quantum dynamics in ultracold atomic physics*, Front. Phys. **7**, 16 (2012). [p 4]

[52] R. Graham and H. Haken, *Functional Fokker-Planck treatment of electromagnetic field propagation in a thermal medium*, Z. Phys. **234**, 193 (1970). [p 4]

[53] R. Graham and H. Haken, *Functional quantum statistics of light propagation in a two-level system*, Z. Phys. **235**, 166 (1970). [p 4]

[54] C. W. Gardiner and M. J. Davis, *The stochastic Gross–Pitaevskii equation: II*, J. Phys. B **36**, 4731 (2003). [p 4]

[55] P. B. Blakie, A. S. Bradley, M. J. Davis, R. J. Ballagh, and C. W. Gardiner, *Dynamics and statistical mechanics of ultra-cold Bose gases using c-field techniques*, Adv. Phys. **57**, 363 (2008). [pp 4, 57, 77, and 118]

[56] A. Polkovnikov, *Phase space representation of quantum dynamics*, Ann. Phys. **325**, 1790 (2010). [pp 4, 47, and 118]

[57] A. Sinatra, C. Lobo, and Y. Castin, *The truncated Wigner method for Bose-condensed gases: limits of validity and applications*, J. Phys. B **35**, 3599 (2002). [pp 4, 40, 46, 57, 64, 66, 77, and 118]

[58] B. Opanchuk and P. D. Drummond, *Functional Wigner representation of quantum dynamics of Bose-Einstein condensate*, J. Math. Phys. **54**, 042107 (2013). [p 5]

[59] K. Cahill and R. Glauber, *Ordered Expansions in Boson Amplitude Operators*, Phys. Rev. **177**, 1857 (1969). [pp 7, 8, 9, 11, 53, and 56]

[60] M. Hillery, R. F. O'Connell, M. O. Scully, and E. P. Wigner, *Distribution functions in physics: Fundamentals*, Phys. Rep. **106**, 121 (1984). [pp 7 and 101]

[61] C. W. Gardiner and P. Zoller, *Quantum Noise*, Springer, 4th edition, 2004. [pp 7, 10, 101, and 104]

[62] H. Weyl, *The Theory of Groups and Quantum Mechanics*, Dover Publications, 1950. [p 8]

[63] W. H. Louisell, *Quantum Statistical Properties of Radiation*, Wiley, John & Sons, Incorporated, 1990. [p 19]

[64] S. A. Morgan, *A gapless theory of Bose-Einstein condensation in dilute gases at finite temperature*, J. Phys. B **33**, 3847 (2000). [p 40]

[65] S. Kokkelmans, J. N. Milstein, M. L. Chiofalo, R. Walser, and M. J. Holland, *Resonance superfluidity: Renormalization of resonance scattering theory*, Phys. Rev. A **65**, 053617 (2002). [p 40]

[66] M. W. Jack, *Decoherence due to Three-Body Loss and its Effect on the State of a Bose-Einstein Condensate*, Phys. Rev. Lett. **89**, 140402 (2002). [p 41]

[67] A. Polkovnikov, *Quantum corrections to the dynamics of interacting bosons: Beyond the truncated Wigner approximation*, Phys. Rev. A **68**, 053604 (2003). [p 45]

[68] J. Javanainen and J. Ruostekoski, *Emergent classicality in continuous quantum measurements*, New J. Phys. **15**, 013005 (2013). [p 46]

[69] Y. Kagan, B. V. Svistunov, and G. V. Shlyapnikov, *Effect of Bose condensation on inelastic processes in gases*, JETP Lett. **42**, 209 (1985). [p 53]

[70] E. A. Burt *et al.*, *Coherence, Correlations, and Collisions: What One Learns about Bose-Einstein Condensates from Their Decay*, Phys. Rev. Lett. **79**, 337 (1997). [pp 53 and 68]

[71] M. K. Olsen and A. S. Bradley, *Numerical representation of quantum states in the positive-P and Wigner representations*, Opt. Commun. **282**, 3924 (2009). [p 57]

[72] J. Ruostekoski and A. D. Martin, *Truncated Wigner method for Bose gases*, arXiv:1009.1073 (2010). [pp 57 and 77]

[73] M. F. Riedel *et al.*, *Atom-chip-based generation of entanglement for quantum metrology.*, Nature **464**, 1170 (2010). [pp 63, 66, 89, 93, 94, and 95]

[74] L. Pitaevskii and S. Stringari, *Bose-Einstein Condensation*, Oxford University Press, 2003. [pp 65, 67, and 71]

[75] M. Egorov *et al.*, *Measurement of s-wave scattering lengths in a two-component Bose-Einstein condensate*, Phys. Rev. A **87**, 053614 (2013). [pp 66 and 77]

[76] H. Zeng, W. Zhang, and F. Lin, *Nonclassical Bose-Einstein condensate*, Phys. Rev. A **52**, 2155 (1995). [p 67]

[77] T.-L. Ho and V. B. Shenoy, *Binary Mixtures of Bose Condensates of Alkali Atoms*, Phys. Rev. Lett. **77**, 3276 (1996). [p 67]

[78] R. J. Ballagh, K. Burnett, and T. F. Scott, *Theory of an Output Coupler for Bose-Einstein Condensed Atoms*, Phys. Rev. Lett. **78**, 1607 (1997). [p 67]

[79] V. A. Yurovsky, A. Ben-Reuven, P. S. Julienne, and C. J. Williams, *Atom loss from Bose-Einstein condensates due to Feshbach resonance*, Phys. Rev. A **60**, R765 (1999). [p 67]

[80] K. M. Mertes *et al.*, *Nonequilibrium Dynamics and Superfluid Ring Excitations in Binary Bose-Einstein Condensates*, Phys. Rev. Lett. **99**, 190402 (2007). [pp 68, 75, 77, and 78]

[81] M. L. Chiofalo, S. Succi, and M. P. Tosi, *Ground state of trapped interacting Bose-Einstein condensates by an explicit imaginary-time algorithm*, Phys. Rev. E **62**, 7438 (2000). [p 69]

[82] W. Bao and Q. Du, *Computing the Ground State Solution of Bose-Einstein Condensates by a Normalized Gradient Flow*, SIAM J. Sci. Comput. **25**, 1674 (2004). [pp 69 and 70]

[83] F. Dalfovo, S. Giorgini, and S. Stringari, *Theory of Bose-Einstein condensation in trapped gases*, Rev. Mod. Phys. **71**, 463 (1999). [p 74]

[84] R. P. Anderson, *Nonequilibrium dynamics and relative phase evolution of two-component Bose-Einstein condensates*, PhD thesis, Swinburne University, 2010. [p 74]

[85] A. Widera *et al.*, *Precision measurement of spin-dependent interaction strengths for spin-1 and spin-2 87 Rb atoms*, New J. Phys. **8**, 152 (2006). [p 77]

[86] D. S. Hall, M. R. Matthews, C. E. Wieman, and E. A. Cornell, *Measurements of Relative Phase in Two-Component Bose-Einstein Condensates*, Phys. Rev. Lett. **81**, 4532(E) (1998). [p 77]

[87] M. Egorov, *Coherence and collective oscillations of a two-component Bose-Einstein condensate*, PhD thesis, Swinburne University of Technology, 2012. [pp 78, 85, and 87]

[88] M. Kitagawa and M. Ueda, *Squeezed spin states*, Phys. Rev. A **47**, 5138 (1993). [pp 89 and 94]

[89] D. J. Wineland, J. J. Bollinger, W. M. Itano, and D. Heinzen, *Squeezed atomic states and projection noise in spectroscopy*, Phys. Rev. A **50**, 67 (1994). [p 89]

[90] J. Hald, J. L. Sørensen, C. Schori, and E. S. Polzik, *Spin Squeezed Atoms: A Macroscopic Entangled Ensemble Created by Light*, Phys. Rev. Lett. **83**, 1319 (1999). [p 89]

[91] A. Kuzmich, L. Mandel, and N. P. Bigelow, *Generation of spin squeezing via continuous quantum nondemolition measurement*, Phys. Rev. Lett. **85**, 1594 (2000). [p 89]

[92] C. Gross, T. Zibold, E. Nicklas, J. Estève, and M. K. Oberthaler, *Nonlinear atom interferometer surpasses classical precision limit.*, Nature **464**, 1165 (2010). [pp 89 and 96]

[93] A. Sørensen, L.-M. Duan, J. I. Cirac, and P. Zoller, *Many-particle entanglement with Bose-Einstein condensates.*, Nature **409**, 63 (2001). [pp 89 and 90]

[94] Q.-Y. He, T. G. Vaughan, P. D. Drummond, and M. D. Reid, *Entanglement, number fluctuations and optimized interferometric phase measurement*, New J. Phys. **14**, 093012 (2012). [pp 89 and 95]

[95] Q.-Y. He, S.-G. Peng, P. D. Drummond, and M. D. Reid, *Planar quantum squeezing and atom interferometry*, Phys. Rev. A **84**, 022107 (2011). [p 90]

[96] A. M. Kaufman *et al.*, *Radio-frequency dressing of multiple Feshbach resonances*, Phys. Rev. A **80**, 050701 (2009). [p 97]

[97] A. Einstein, B. Podolsky, and N. Rosen, *Can Quantum-Mechanical Description of Physical Reality Be Considered Complete?*, Phys. Rev. **47**, 777 (1935). [p 101]

[98] M. D. Reid and D. F. Walls, *Violations of classical inequalities in quantum optics*, Phys. Rev. A **34**, 1260 (1986). [p 101]

[99] Y. Aharonov, D. Z. Albert, and L. Vaidman, *How the result of a measurement of a component of the spin of a spin-1/2 particle can turn out to be 100*, Phys. Rev. Lett. **60**, 1351 (1988). [pp 101 and 104]

[100] M. E. Goggin *et al.*, *Violation of the Leggett-Garg inequality with weak measurements of photons.*, P. Natl. Acad. Sci. USA **108**, 1256 (2011). [p 101]

[101] J. F. Clauser, M. Horne, A. Shimony, and R. Holt, *Proposed Experiment to Test Local Hidden-Variable Theories*, Phys. Rev. Lett. **23**, 880 (1969). [pp 102 and 103]

[102] A. Aspect, J. Dalibard, and G. Roger, *Experimental Test of Bell's Inequalities Using Time- Varying Analyzers*, Phys. Rev. Lett. **49**, 1804 (1982). [p 102]

[103] G. Weihs, T. Jennewein, C. Simon, H. Weinfurter, and A. Zeilinger, *Violation of Bell's Inequality under Strict Einstein Locality Conditions*, Phys. Rev. Lett. **81**, 5039 (1998). [p 102]

[104] A. Cabello, *Minimum Detection Efficiency for a Loophole-Free Atom-Photon Bell Experiment*, Phys. Rev. Lett. **98**, 220402 (2007). [p 102]

[105] J.-Å. Larsson, *Bell's inequality and detector inefficiency*, Phys. Rev. A **57**, 3304 (1998). [p 102]

[106] J.-Å. Larsson and J. Semitecolos, *Strict detector-efficiency bounds for n-site Clauser-Horne inequalities*, Phys. Rev. A **63**, 022117 (2001). [p 102]

[107] M. Giustina *et al.*, *Bell violation using entangled photons without the fair-sampling assumption*, Nature **497**, 227 (2013). [p 102]

[108] P. D. Drummond, *Violations of Bell's Inequality in Cooperative States*, Phys. Rev. Lett. **50**, 1407 (1983). [pp 103 and 104]

[109] G. S. Agarwal and S. Chaturvedi, *Scheme to measure the positive P distribution*, Phys. Rev. A **49**, R665 (1994). [p 104]

[110] A. K. Gupta and D. Song, *Lp-norm spherical distribution*, J. Stat. Plan. Infer. **60**, 241 (1997). [p 106]

[111] G. Marsaglia, *Choosing a Point from the Surface of a Sphere*, Ann. Math. Statist. **43**, 645 (1972). [p 106]

[112] G. Marsaglia and W. W. Tsang, *A simple method for generating gamma variables*, ACM T. Math. Software **26**, 363 (2000). [p 107]

[113] J. Howell, A. Lamas-Linares, and D. Bouwmeester, *Experimental Violation of a Spin-1 Bell Inequality Using Maximally Entangled Four-Photon States*, Phys. Rev. Lett. **88**, 030401 (2002). [p 107]

[114] D. M. Greenberger, M. Horne, and A. Zeilinger, *Bell's Theorem, Quantum Theory and Conceptions of the Universe*, Springer, 1989. [p 108]

[115] N. D. Mermin, *Extreme quantum entanglement in a superposition of macroscopically distinct states*, Phys. Rev. Lett. **65**, 1838 (1990). [pp 108 and 109]

[116] M. A. Rowe *et al.*, *Experimental violation of a Bell's inequality with efficient detection.*, Nature **409**, 791 (2001). [p 108]

[117] D. Leibfried *et al.*, *Creation of a six-atom 'Schrödinger cat' state.*, Nature **438**, 639 (2005). [p 108]

[118] T. Monz *et al.*, *14-Qubit Entanglement: Creation and Coherence*, Phys. Rev. Lett. **106**, 130506 (2011). [p 108]

[119] M. Ardehali, *Bell inequalities with a magnitude of violation that grows exponentially with the number of particles*, Phys. Rev. A **46**, 5375 (1992). [p 109]

[120] F. Arecchi, E. Courtens, R. Gilmore, and H. Thomas, *Atomic Coherent States in Quantum Optics*, Phys. Rev. A **6**, 2211 (1972). [p 111]

[121] W.-M. Zhang, D. H. Feng, and R. Gilmore, *Coherent states: Theory and some applications*, Rev. Mod. Phys. **62**, 867 (1990). [p 111]

[122] S. Lloyd, *Universal Quantum Simulators*, Science **273**, 1073 (1996). [p 115]

[123] A. Altland and F. Haake, *Equilibration and macroscopic quantum fluctuations in the Dicke model*, New J. Phys. **14**, 073011 (2012). [p 115]

[124] J.-C. Jaskula *et al.*, *Sub-Poissonian Number Differences in Four-Wave Mixing of Matter Waves*, Phys. Rev. Lett. **105**, 190402 (2010). [p 115]

[125] P. P. Deuar, *First-principles quantum simulations of many-mode open interacting Bose gases using stochastic gauge methods*, PhD thesis, The University of Queensland, 2005. [p 119]

[126] L. I. Plimak, M. K. Olsen, M. Fleischhauer, and M. J. Collett, *Beyond the Fokker-Planck equation: Stochastic simulation of complete Wigner representation for the optical parametric oscillator*, Europhys. Lett. **56**, 372 (2001). [p 119]

[127] W. Wirtinger, *Zur formalen Theorie der Funktionen von mehr komplexen Veränderlichen*, Math. Ann. **97**, 357 (1927). [p 121]

[128] A. Hjørungnes and D. Gesbert, *Complex-Valued Matrix Differentiation: Techniques and Key Results*, IEEE T. Signal Proces. **55**, 2740 (2007). [p 121]

[129] K. Kreutz-Delgado, *The Complex Gradient Operator and the CR-Calculus*, arXiv:0906.4835 (2009). [p 121]

[130] B. J. Dalton, *Phase space theory of Bose–Einstein condensates and time-dependent modes*, Ann. Phys. **327**, 2432 (2012). [pp 127 and 132]

[131] H. Risken, *The Fokker-Planck Equation*, Springer-Verlag, Berlin, 2nd edition, 1996. [pp 139 and 140]

[132] C. W. Gardiner, *Handbook of Stochastic Methods*, Springer-Verlag, Berlin, 2nd edition, 1997. [p 150]

[133] C. Dion and E. Cancès, *Spectral method for the time-dependent Gross-Pitaevskii equation with a harmonic trap*, Phys. Rev. E **67**, 046706 (2003). [p 157]

[134] M. Abramowitz and I. Stegun, *Handbook of Mathematical Functions*, Dover Publications, 1972. [p 158]

[135] T. E. Oliphant, *Python for Scientific Computing*, Comput. Sci. Eng. **9**, 10 (2007). [p 163]

[136] A. Klöckner *et al.*, *PyCUDA and PyOpenCL: A scripting-based approach to GPU run-time code generation*, Parallel Comput. **38**, 157 (2012). [p 163]

[137] G. Collecutt and P. D. Drummond, *XMDS: eXtensible Multi-Dimensional Simulator*, Comput. Phys. Commun. **142**, 219 (2001). [p 164]

[138] G. R. Dennis, J. J. Hope, and M. T. Johnsson, *XMDS2: Fast, scalable simulation of coupled stochastic partial differential equations*, Comput. Phys. Commun. **184**, 201 (2013). [p 164]

[139] P. E. Kloeden and E. Platen, *Numerical Solution of Stochastic Differential Equations*, Springer-Verlag, Berlin, 1992. [p 164]

[140] P. D. Drummond and I. K. Mortimer, *Computer simulations of multiplicative stochastic differential equations*, J. Comput. Phys. **93**, 144 (1991). [p 164]

[141] M. J. Werner and P. D. Drummond, *Robust Algorithms for Solving Stochastic Partial Differential Equations*, J. Comput. Phys. **132**, 312 (1997). [p 164]

[142] J. Wilkie, *Numerical methods for stochastic differential equations*, Phys. Rev. E **70**, 017701 (2004). [p 164]

[143] J. Wilkie and M. Cetinbas, *Variable-stepsize Runge-Kutta methods for stochastic Schrodinger equations*, Phys. Lett. A **337**, 166 (2005). [pp 164 and 165]

[144] B. M. Caradoc-Davies, *Vortex Dynamics in Bose-Einstein Condensates*, PhD thesis, University of Otago, 2000. [p 165]

[145] J. Berland, C. Bogey, and C. Bailly, *Low-dissipation and low-dispersion fourth-order Runge–Kutta algorithm*, Comput. Fluids **35**, 1459 (2006). [p 165]

[146] K. Burrage, P. Burrage, D. Higham, P. Kloeden, and E. Platen, *Comment on "Numerical methods for stochastic differential equations"*, Phys. Rev. E **74**, 068701 (2006). [p 165]